Adaptative hp-finite elements with guaranteed error contraction and inexact multilevel solvers

Patrik Daniel

THÈSE

PRÉSENTÉE À

SORBONNE UNIVERSITÉ

ÉCOLE DOCTORALE: Sciences Mathématiques de Paris Centre (ED 386)

Par **Patrik DANIEL**

POUR OBTENIR LE GRADE DE

DOCTEUR

SPÉCIALITÉ: Mathématiques Appliquées

Éléments finis *hp* adaptatifs avec contraction d'erreur garantie et solveurs multi-niveaux inexacts

---

Directeur de thèse: Martin Vohralík

Co-directeur de thèse: Alexandre Ern

Soutenue le: 22 mars 2019

Devant la commission d'examen formée de:

Roland BECKER	Université de Pau et des Pays de l'Adour	Examinateur
Emmanuel CREUSÉ	Université Polytechnique des Hauts-de-France	Rapporteur
Alexandre ERN	Université Paris-Est & Inria Paris	Co-directeur de thése
Cindy GUICHARD	Sorbonne Université	Examinatrice
Frédéric HECHT	Sorbonne Université	Examinateur
Dirk PRAETORIUS	Université technique de Vienne	Examinateur
Martin VOHRALÍK	Inria Paris & Université Paris-Est	Directeur de thése
Thomas P. WIHLER	Université de Berne	Rapporteur

SORBONNE UNIVERSITÉ
CRÉATEURS DE FUTURS DEPUIS 1257

informatics mathematics

A THESIS

PRESENTED AT

SORBONNE UNIVERSITY

DOCTORAL SCHOOL: Mathematical Sciences of Central Paris (ED 386)

By **Patrik DANIEL**

TO OBTAIN THE DEGREE OF DOCTOR OF PHILOSOPHY
SPECIALITY: Applied Mathematics

Adaptive *hp*-finite elements with guaranteed error contraction and inexact multilevel solvers

---

Thesis advisor: Martin Vohralík
Thesis co-advisor: Alexandre Ern

Defended on: March 22, 2019

In front of the examination committee consisting of:

Roland BECKER	University of Pau and Pays de l'Adour	Examiner
Emmanuel CREUSÉ	Polytechnic University of Hauts-de-France	Reviewer
Alexandre ERN	University of Paris-Est & Inria Paris	Thesis co-advisor
Cindy GUICHARD	Sorbonne University	Examiner
Frédéric HECHT	Sorbonne University	Examiner
Dirk PRAETORIUS	Vienna University of Technology	Examiner
Martin VOHRALÍK	Inria Paris & University of Paris-Est	Thesis advisor
Thomas P. WIHLER	University of Bern	Reviewer

To my parents and my friends
for always being there for me.

SERENA

This thesis has been carried out within the research team SERENA, a joint project-team between **Inria** and **Ecole des Ponts ParisTech**.

INRIA Paris
2 rue Simone Iff
75589 Paris, France

CERMICS (ENPC)
Université Paris-Est
77455 Marne-la-Vallée, France

Team's website: https://team.inria.fr/serena/

Résumé

Nous proposons de nouveaux algorithmes de raffinement adaptatif pour l'approximation des problèmes elliptiques par la méthode des éléments finis *hp*. Nous considérons des solveurs algébriques exacts puis inexacts au sein du cadre générique des méthodes adaptatives consistant en quatre modules concaténés: `RESOLUTION`, `ESTIMATION`, `MARQUAGE`, `RAFFINEMENT`. Les stratégies reposent sur la construction d'estimateurs d'erreur *a posteriori* par flux équilibrés. Notamment, pour une approximation inexacte obtenue par un solveur algébrique itératif (arbitraire), nous prouvons une borne sur l'erreur totale ainsi que sur l'erreur algébrique et l'erreur de discrétisation. La structure hiérarchique des espaces d'éléments finis *hp* est cruciale pour obtenir la borne supérieure sur l'erreur algébrique, ce qui nous permet de formuler des critères d'arrêt précis pour le solveur algébrique. Notre critère de raffinement *hp* repose sur la résolution de deux problèmes résiduels locaux, posés sur les macro-éléments autour des sommets du maillage qui ont été marqués. Ces derniers sont sélectionnés par un critère de type bulk-chasing. Ces deux problèmes résiduels imitent l'effet du raffinement h et p. Une caractéristique de notre approche est que nous obtenons une quantité calculable qui donne une borne garantie sur le rapport entre l'erreur d'énergie (inconnue) à la prochaine étape de la boucle adaptative et l'erreur actuelle (i.e. sur le facteur de réduction d'erreur). Des simulations numériques sont présentées afin de valider les stratégies adaptatives. Nous examinons la précision de notre borne sur le facteur de réduction d'erreur qui s'avère être excellente, avec des indices d'efficacité proches de la valeur optimale de 1. En pratique, nous observons des taux de convergence asymptotiquement exponentiels, aussi bien dans le cadre de la résolution algébrique exacte que dans celui de la résolution inexacte. Enfin, nous menons une analyse théorique des stratégies proposées. Sous certaines hypothèses supplémentaires sur les raffinements h et p, y compris la propriété de nœud intérieur et des raffinements suffisants en p, nous prouvons que les facteurs calculables de réduction sont bornés par une constante générique strictement inférieure à 1. Ceci implique la convergence des stratégies adaptatives.

Mots-clés: problème elliptique, méthode des éléments finis, adaptativité *hp*, flux equilibré, estimation d'erreur *a posteriori*, erreur algébrique, erreur de discrétisation, réduction d'erreur, convergence

Abstract

We propose new practical adaptive refinement algorithms for conforming hp-finite element approximations of elliptic problems. We consider the use of both exact and inexact solvers within the established framework of adaptive methods consisting of four concatenated modules: `SOLVE`, `ESTIMATE`, `MARK`, `REFINE`. The strategies are driven by guaranteed equilibrated flux a posteriori error estimators. Namely, for an inexact approximation obtained by an (arbitrary) iterative algebraic solver, the bounds for the total, the algebraic, and the discretization errors are provided. The nested hierarchy of hp-finite element spaces is crucially exploited for the algebraic error upper bound which in turn allows us to formulate sharp stopping criteria for the algebraic solver. Our hp-refinement criterion hinges on from solving two local residual problems posed on patches of elements around marked vertices selected by a bulk-chasing criterion. They respectively emulate h-refinement and p-refinement. One particular feature of our approach is that we derive a computable real number which gives a guaranteed bound on the ratio of the (unknown) energy error in the next adaptive loop step with respect to the present one (i.e. on the error reduction factor). Numerical experiments are presented to validate the proposed adaptive strategies. We investigate the accuracy of our bound on the error reduction factor which turns out to be excellent, with effectivity indices close to the optimal value of one. In practice, we observe asymptotic exponential convergence rates, in both the exact and inexact algebraic solver settings. Finally, we also provide a theoretical analysis of the proposed strategies. We prove that under some additional assumptions on the h- and p-refinements, including the interior node property and sufficient p-refinements, the computable reduction factors are indeed bounded by a generic constant strictly smaller than one. This implies the convergence of the adaptive strategies.

Keywords: elliptic problem, finite element method, hp-adaptivity, equilibrated flux, a posteriori error estimate, algebraic error, discretization error, stopping criteria, error reduction, convergence

Acknowledgements

I would like to express my deep thanks and appreciation to both of my supervisors Martin Vohralík and Alexandre Ern. First of all, thank you for taking the risk and accepting my application, even though we hadn't had a chance to meet in person before the actual start of my Ph.D. studies. I must admit that these past three years have been quite a roller coaster ride for me, so I am eternally grateful for all the time you dedicated to my work, your encouragement and your outstanding guidance in the field of numerical analysis. I wish to thank also Iain Smears for his help and valuable comments and advices he always provided us with.

Besides my advisors, I would like to thank the rest of the examination committee, starting with Emmanuel Creusé and Thomas P. Wihler, who kindly accepted to review this thesis, and also Roland Becker, Cindy Guichard, Frédéric Hecht and Dirk Praetorius for participating and providing interesting remarks, questions and insights.

Big thanks goes to all the researchers, post-docs, and Ph.D. students of the SERENA project-team and their warm welcome back in October 2015. It has been my pleasure to get to know you and to work in such an inspiring and stimulating research environment with a friendly atmosphere. I owe a special thanks to my office buddies Sarah, Jad and Ani with whom I was lucky to spend most of the time during these past three years. I sincerely hope that our friendship will continue beyond the scope of our "Ph.D. lives". I would also like to thank Jan Papež for sharing his impressive finite elements' MATLAB code with me in the beginning of my studies in France, it was indeed a great source of knowledge and served as a perfect base for my own *hp*-AFEM implementation.

And last but not least, I would like to thank my family and my friends, the old ones back in Slovakia, as well as the new ones I was lucky to meet in Paris, without your support I would not have made it here. Ďakujem!

> "*If you are lucky enough to have lived in Paris as a young man, then wherever you go for the rest of your life, it stays with you, for Paris is a movable feast.*"
>
> - Ernest Hemingway, 1950

Contents

List of Figures

List of Tables

Introduction

"The book of nature is written in the language of mathematics."

Galileo Galilei, 1623

Nowadays, mathematics and computational science are used in almost every discipline of science, engineering, industry, and technology. Researchers and engineers all around the world employ mathematical tools to gain insight and better understanding of complex environmental and physical phenomena. A broad range of these physical phenomena can be described by means of partial differential equations (PDEs). Unfortunately, only for a few toy examples of PDEs, we are able to find explicit analytical solutions. In most cases one must resort to seeking (only) numerical approximations by the aid of computers. Hence, there is a continual need to develop *efficient*, *accurate*, *reliable*, and *robust* numerical techniques.

Finite element method and the concept of adaptivity

In the industrial context, namely in the fields of mechanical, structural, automotive, and civil engineering, the *finite element method* (FEM) (see Courant (1943), Ciarlet (1978), Ern and Guermond (2004), Brenner and Scott (2008)) has been established as one of the most powerful and flexible techniques for the numerical solution of PDEs and is widely used as a tool in engineering decision-making process.

The fundamental concepts of the FEM include partitioning of the computational domain Ω into a mesh (also called a partition) $\mathcal{T}$, a finite set of smaller, simpler elements (also called cells), and the approximation of the analytical solution by a piecewise polynomial on that mesh. This is done in the form of a linear combination of basis functions from a discrete function space V, called the finite element space, see Figure 1 for illustration. The construction of this space is directly linked to the domain partitioning; the finite element basis functions have a local support consisting of several mesh elements only. Finally, the approximation is obtained by solving the system of algebraic equations arising from employing the basis of the discrete finite element space in the weak formulation of the PDE.

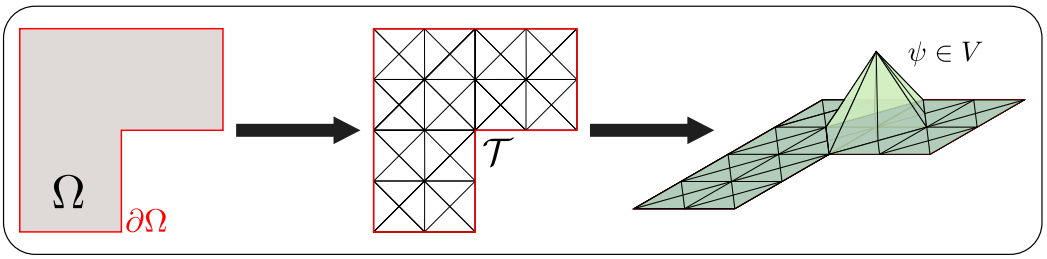

Figure 1: An example of a computational domain Ω (*left*), its partitioning $\mathcal{T}$ into mesh elements (triangles) denoted by black lines (*center*), and a particular piecewise affine basis function from the corresponding finite element space (*right*).

In this thesis, the linear elliptic model problem we examine is the homogeneous Poisson problem for the Laplace equation in dimension $d = 2, 3$, where one looks for $u : \Omega \to \mathbb{R}$, $\Omega \subset \mathbb{R}^d$ being a polygon/polyhedron, such that

$$-\Delta u = f \quad \text{in } \Omega, \qquad u = 0 \quad \text{on } \partial\Omega. \tag{1}$$

h-adaptivity

The quality of the finite element approximation of the unknown solution u of (1) is strongly related to the resolution of the used mesh, usually represented by the symbol h. Following the classical approach, finer meshes, with *uniformly* decreasing element size, will lead to better, more accurate approximations. However, there are two main drawbacks of such an approach in practical applications: **(i)** solutions of the practical problems in physics or engineering are usually not uniformly complex throughout the computational domain – they may contain local singularities or special features restricted just to a small region of the domain which deteriorate the accuracy of the numerical approximation overall; **(ii)** in case of high-resolution three-dimensional simulations, uniformly-refined meshes result in massive algebraic problems. Such huge problems require too much computational time to obtain a solution, assuming that it is possible to store the necessary amount of data within the memory of the computer hardware at use. These two observations led to the natural remedy of using meshes with elements of different sizes throughout the domain, refined in the vicinity of the local features. This is the principle of the *mesh-adaptive* finite element method (h-AFEM), cf. e.g. Babuška and Rheinboldt (1978), Ainsworth and Oden (2000) or Verfürth (2013).

p-adaptivity

Alternatively to adapting the size of the elements, to improve the quality of a numerical approximation, one can also choose to locally adjust the polynomial degree p of the local finite element basis functions used for approximating the solution (p-AFEM). Nevertheless, as suggested by classical interpolation

theory, cf. Babuška et al. (1981), Babuška and Suri (1987), Schwab (1998), one needs to keep in mind that high order interpolating functions produce more accurate results than lower order functions, e.g. piecewise linear, only if the original function is locally smooth. The required regularity cannot be guaranteed in the vicinity of the boundaries, corners, or in regions where the coefficients are discontinuous; in such regions, the desired error reduction can be obtained solely by h-refinement.

hp-adaptivity

The merge of the two above approaches has led to the notion of hp-adaptive finite element method (hp-AFEM), where the approximate solution is improved by a combination of h- and p-refinement: one refines the mesh and increases the polynomial degree at the same time, cf. Babuška and Guo (1986a,b). We illustrate the different types of refinements in Figure 2.

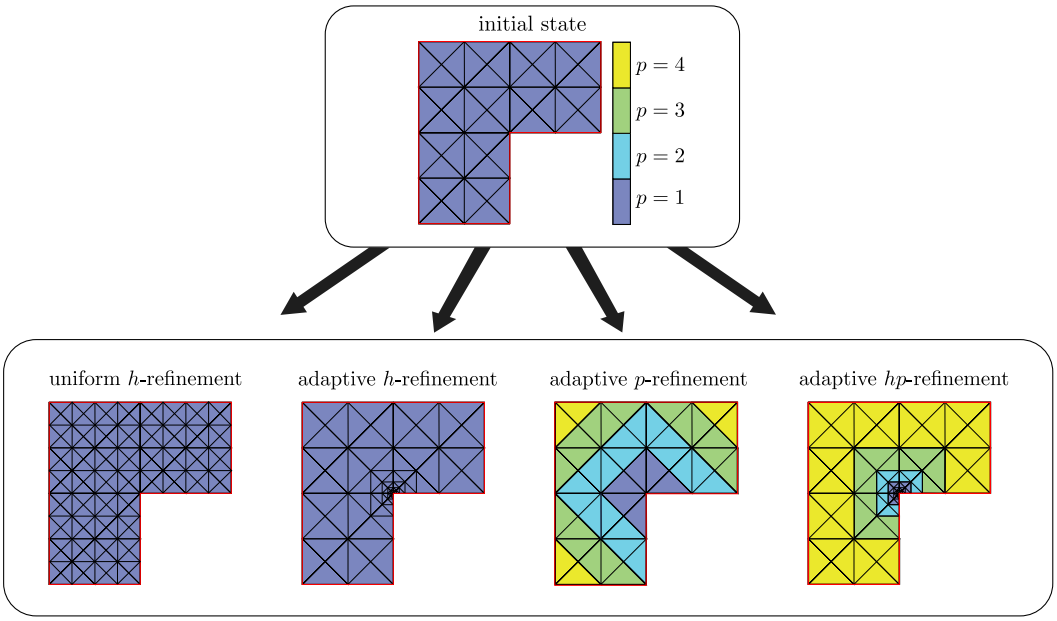

Figure 2: Different types of refinements applied to an example mesh from Figure 1, where a singularity is present in the re-entrant corner. Colours indicate the polynomial degree p of the finite element approximation used on the element.

r-adaptivity

For completeness, we mention here also the so-called r-adaptation of the mesh, cf. Díaz et al. (1983), Zienkiewicz and Zhu (1991), Mackenzie and Robertson (2002). This corresponds to *re*-distribution of nodes defining an initial mesh without adding any new nodes and preserving the element connectivity and possibly also the logical tensor product structure; adding or deleting degrees

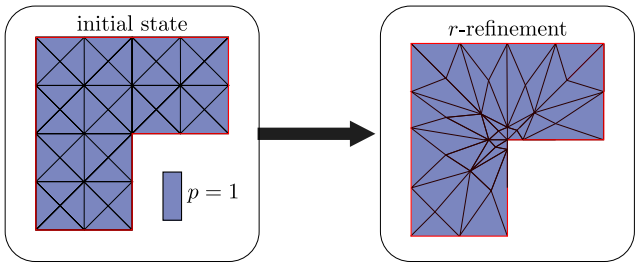

Figure 3: An example of r-adaptation of a mesh from Figure 1.

of freedom (including change of polynomial degree) is prohibited, cf. Figure 3. The r-adaptivity aims at an optimal use of a given mesh topology, which can be seen as a fixed amount of available computational effort in terms of memory resources. The best precision of a pure r-adaptive algorithm clearly has a certain limit. However, a combination of h-, p-, and hp-refinements with r-adaptive redistribution of the fixed mesh at certain steps of refinement could lead to even more efficient methods. We do not consider this technique here, as it leads to non-nested finite element spaces, which limits the theoretical results that can be proved.

A-posteriori-driven AFEM

Already in the mid-1980's, it was proved by Gui and Babuška (1986b) that when a reasonable combination of mesh adaptation together with appropriate polynomial degree distribution is used, consisting in decreasing the size of the mesh elements in the vicinity of singularities and using high-order polynomials as basis functions in the parts of domain where the solution is smooth, the hp–AFEM can lead to exponentially-fast convergence with respect to the number of degrees of freedom. In their subsequent work (Gui and Babuška (1986a)), they also showed a priori rules for the hp-adaptation for special cases with known solutions.

However, in practice, one is mainly interested in hp-adaptive algorithms which adapt the employed finite element spaces purely on the basis of *a posteriori* knowledge. Since the late-1980's, a siginificant amount of research has been dedicated to the development of a posteriori error estimators. We mention a few possibilities for the choice of energy-norm a posteriori error estimates in the finite element setting: (explicit) residual estimates, cf. Babuška and Rheinboldt (1978), Verfürth (2013), Dari et al. (1996), (implicit) estimates based on solving auxiliary local residual problems, cf. Bank and Weiser (1985), Durán and Rodríguez (1992), estimates employing hierarchical basis, cf. Bank and Smith (1993), Deuflhard et al. (1989), estimates derived by purely functional methods, cf. Neittaanmäki and Repin (2004), Repin (2003), averaging (recovery-based) estimates, cf. Zienkiewicz and Zhu (1987), Carstensen and Bartels (2002), Bartels and Carstensen (2002), Creusé and

Nicaise (2010, 2013), and the equilibrated flux estimates (employed in this work), cf. Destuynder and Métivet (1999), Luce and Wohlmuth (2004), Braess et al. (2009), Ern and Vohralík (2015). For a general overview, we refer to the survey books by Ainsworth and Oden (2000), Repin (2008), and Verfürth (2013) and the references therein. It is the estimation of the magnitude of the error and its distribution within the computational domain which provides the guidance for the self-adaptive numerical methods such as the AFEM.

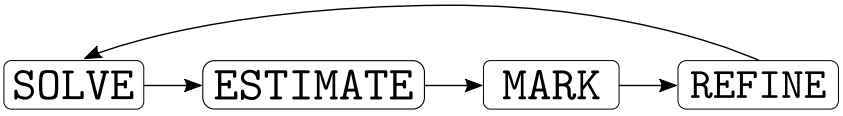

Scheme 1: A general form of an adaptive algorithm driven by a posteriori estimation.

The well-established framework of an a-posteriori-driven adaptive algorithm can be stated in a form of an adaptive loop presented in Scheme 1. In general, the algorithm first computes the solution using the initial coarse mesh and a corresponding low polynomial degree finite element space. Subsequently, the error distribution is estimated and used to mark the critical region with the highest local error indicators. The error is then reduced by means of h-, p-, or hp-refinements of the marked elements. A new approximation of the solution is then computed at the next iteration of the adaptive loop. The algorithm terminates when the estimated error drops below a prescribed tolerance.

Some theoretical results in the context of h-AFEM

Let us for a moment restrict ourselves to the context of h-AFEM, where the refinement is done solely by means of h-refinement.

The theoretical study of h-AFEM is already well developed and rather complete. A decade after the pioneering works of Gui and Babuška (1986b,a) and Babuška and Guo (1986a,b) in the one-dimensional case, Dörfler (1996) proved the convergence of the adaptive algorithm of the form described in Scheme 1 for the model problem (1) in two space dimensions. This was then extended by Morin et al. (2000). Binev et al. (2004) followed with a modification of the method by Morin et al. (2000), amounting to adding a coarsening routine, which they proved to have not only optimal convergence rate, but also optimal computational complexity. Namely, whenever for some $s > 0$, it is possible to approximate (in the energy norm) the exact solution u with accuracy $\mathcal{O}(n^{-s})$ by a continuous piecewise affine function on a triangulation consisting of n triangles, then the a-posteriori-driven adaptive algorithm of Binev et al. (2004) leads to an approximation of the same type while using only $\mathcal{O}(n)$ arithmetic computations. The optimality result of Binev et al. (2004) represented a breakthrough in the theoretical analysis of the adaptive

methods. Nevertheless, it has been further improved by Stevenson (2007) who was able to bypass the necessity of the coarsening routine. An extension of these prior results to the case of general second-order linear, symmetric elliptic operators in any space dimension $d \geq 2$ is contained in the work of Cascón et al. (2008). Finally, Cohen et al. (2012) achieved the results on convergence rates for general right-hand side $f \in H^{-1}(\Omega)$, for $d = 2$. Let us also note that most of the above convergence results are formulated for h-AFEM driven by residual-type a posteriori error estimators; other estimators have in particular been addressed by Cascón and Nochetto (2012) and Kreuzer and Siebert (2011). Other important results are to be found in Morin et al. (2003, 2008), Mekchay and Nochetto (2005), Aurada et al. (2013), Feischl et al. (2014) and Diening et al. (2016). In particular, Carstensen et al. (2014) provide an abstract framework with identification of axioms implying optimal convergence rates for h-AFEM. For further insight, we refer to the survey by Nochetto et al. (2009).

State-of-the-art in the context of hp-AFEM

The theoretical results are much less developed for the hp-AFEM. The hardship still remains even in the automatic decision on which refinements should be performed in order to improve the obtained numerical approximation effectively and without any a priori knowledge about the exact solution. The decision-making process is usually referred to as an *hp-adaptive refinement strategy*. Various strategies have been proposed in the literature over the past decades. For an excellent review of the state of the art with computational comparison of thirteen different strategies, we refer to Mitchell and McClain (2011). Below, we provide a brief review of some of the available strategies:

Texas 3-step. An approach introduced by Oden et al. (1992) combines the power of h- and p-refinement rather separately. The simplest version proceeds in 3 steps: (i) two tolerances $\epsilon_1 > 0$ and $\epsilon_2 > 0$ are set and several steps of uniform h-refinement are applied to the initial coarse mesh; (ii) adaptive h-refinement is applied until the first error tolerance ϵ_1 is reached; (iii) adaptive p-refinement is then performed in order to reduce the error below the second error tolerance ϵ_2, see also Bey (1994) and Bey et al. (1995).

Type parameter. Gui and Babuška (1986a) use the ratio of the local error estimators for the approximations of order p_K and $p_K - 1$. If this ratio is greater than a user-predefined *type-parameter*, one shall apply h-refinement, otherwise p-refinement is suggested. This strategy was also used by Adjerid et al. (1999).

Estimating the regularity of the solution. The strategy proposed by Mavriplis (1994) uses the decay rate of the Legendre expansion coefficients of the solution to estimate its local regularity. Other strate-

gies exploiting the idea of estimating the local regularity include those by Houston et al. (2003), Houston and Süli (2005), Wihler (2011), and Fankhauser et al. (2014). We refer to Amrein et al. (2017) and Houston and Wihler (2018) for an application of such strategies in the context of *hp*-adaptive linearization by the Newton method.

Predicted error reduction. Melenk and Wohlmuth (2001) exploit the refinement history of the marked elements and compare the current local error estimator with its predicted value from the previous step of refinement. Afterwards, the comparison with a priori expected error reduction steers the *hp*-refinement decision. In the first iteration, when the refinement history is not yet available, all the elements are *h*-refined.

Reference solution. A strategy described e.g. in Rachowicz et al. (1989) relies on the so-called reference solution which is computed using a globally refined finite element space with all the elements uniformly *h*-refined and their local polynomial degrees increased by one. Local projections of this reference solution into suitable locally refined spaces then lead to the choice for local refinement yielding the greatest error reduction. For details, we refer to Demkowicz et al. (2002), Demkowicz (2007), and Šolín and Demkowicz (2004).

Optimization and nonlinear programming. The choice of an optimal *hp*-refinement is by its very nature an optimization problem. Patra and Gupta (2001) formally stated the problem of *hp*-mesh design in the language of optimization as a nonlinear programming problem and derived its optimality criteria, see also Novotný et al. (2000).

Despite the significant interest in *hp*-adaptivity, for the majority of the available *hp*-adaptive refinement strategies, there are almost no results concerning convergence of the adaptive algorithms employing them. It is the work of Dörfler and Heuveline (2007) which contained the first result showing the contraction property for one-dimensional *hp*-AFEM in the form

$$\|(u - u_{\ell+1}^{\mathrm{ex}})'\| \leq C_{\mathrm{red}} \|(u - u_{\ell}^{\mathrm{ex}})'\| \quad \text{with } C_{\mathrm{red}} < 1, \tag{2}$$

with $u_{\ell+1}$ and u_ℓ being the approximate solutions obtained by two consecutive steps of the adaptive loop of Scheme 1 employing the *hp*-adaptive refinement strategy inspired by Schmidt and Siebert (2000) (with exact algebraic solver). This refinement strategy is based on estimating the error reduction corresponding to an *h*- or *p*-refinement of elements based on the solution of local problems. The results of Dörfler and Heuveline (2007) have been later extended to higher dimensions by Bürg and Dörfler (2011). In Bank et al. (2013) the authors refer to (2) as saturation property and prove it in the setting of a general second-order elliptic problem. Their adaptive algorithm is driven

by residual a posteriori error estimates and their *hp*-refinement strategy follows Bank and Nguyen (2012). We note that (2) does not imply optimal complexity of the resulting adaptive algorithm.

The state-of-the-art optimality result is (to our knowledge) given in the work of Canuto et al. (2017a), where one iteration of their abstract *hp*-AFEM algorithm consists of M iterations of the adaptive loop of Scheme 1 in combination with a coarsening routine by Binev (2013, 2018). Due to the choice of p-robust error estimator in one-dimensional setting, the number of iterations M necessary to achieve the error reduction by a fixed factor C_{red} is bounded and does not depend on the maximal polynomial degree employed. Owing to the inclusion of the coarsening routine, it is consequently shown that the method leads to an instance optimal reducer of the corresponding error function in one dimension. However, in two and more dimensions, the situation is more complex and the number of necessary iterations M grows more than quadratically with the maximal polynomial degree. The same authors then continued in the study of the two-dimensional case in Canuto et al. (2017b). They replaced the error estimator of Melenk and Wohlmuth (2001) by the solution of local problems inspired by the p-robust equilibrated flux estimator of Braess et al. (2009) and investigated which increase of the local polynomial degree leads to the p-robust error reduction such as (2) where C_{red} is independent of p. They provided numerical evidence that the increase of local polynomial degree by a quantity $\lceil \lambda p \rceil$, where $\lambda > 0$, ensures the so-called local saturation property on each marked patch of elements, which is a sufficient condition to prove the p-robust error reduction. The question of (optimal) convergence of the *hp*-AFEM algorithms still remains a subject of active research.

Contents of this thesis

Chapter 1

In Chapter 1 of this thesis, we devise a new practical *hp*-refinement strategy for the conforming *hp*-finite element approximation of second-order elliptic problems in the spirit of Scheme 1. The salient feature of this work is a *computable* guaranteed bound on the error reduction factor. In particular, we derive a computable number $C_{\ell,\mathrm{red}} \in [0,1]$ such that the following contraction property holds true:

$$\|\nabla(u - u_{\ell+1}^{\mathrm{ex}})\| \leq C_{\ell,\mathrm{red}} \|\nabla(u - u_{\ell}^{\mathrm{ex}})\|, \tag{3}$$

with u_ℓ^{ex} the available discrete solution obtained on the ℓ-th iteration of the adaptive loop and $u_{\ell+1}^{\mathrm{ex}}$ the discrete solution that will be obtained at the next step but is not available yet (with exact algebraic solvers), see (1.23). For the definition of $C_{\ell,\mathrm{red}}$, it is essential to bound from below the incremental

error $\|\nabla(u_{\ell+1}^{\mathrm{ex}} - u_{\ell}^{\mathrm{ex}})\|$ in terms of $\|\nabla(u - u_{\ell}^{\mathrm{ex}})\|$. In our case, such a bound hinges on the following lower bound, cf. Lemma 1.5.1:

$$\|\nabla(u_{\ell+1}^{\mathrm{ex}} - u_{\ell}^{\mathrm{ex}})\|_{\omega_\ell} \geq \underline{\eta}_{\mathcal{M}_\ell^\theta}, \tag{4}$$

where the quantity $\underline{\eta}_{\mathcal{M}_\ell^\theta}$ is fully computable. We note that in Chapter 1 we do not prove that the reduction factor $C_{\ell,\mathrm{red}}$ is bounded by a generic constant strictly smaller than one. However, the numerical experiments provided therein are more than satisfactory, showing that indeed in practice $C_{\ell,\mathrm{red}} \leq C < 1$. More precisely, in a series of numerical experiments featuring test cases with known smooth and singular solutions u, we examine the accuracy of our bound on the reduction factor $C_{\ell,\mathrm{red}}$ by means of the effectivity index

$$I_{\ell,\mathrm{red}}^{\mathrm{eff}} = \frac{C_{\ell,\mathrm{red}}}{\frac{\|\nabla(u-u_{\ell+1}^{\mathrm{ex}})\|}{\|\nabla(u-u_{\ell}^{\mathrm{ex}})\|}}, \tag{5}$$

i.e. the ratio of the predicted reduction factor over the actual reduction factor. We find the effectivity index $I_{\ell,\mathrm{red}}^{\mathrm{eff}}$ in general quite close to the optimal value of one. This can be appreciated in the left panel of Figure 4, where we plot the values of $I_{\ell,\mathrm{red}}^{\mathrm{eff}}$ throughout all the iterations of the adaptive algorithm employed to solve the model problem (1) posed on the L-shape domain depicted previously in Figures 1–3. The analogous effectivity indices of the corresponding lower bounds $\underline{\eta}_{\mathcal{M}_\ell^\theta}$ used in (4) are also presented in the right panel of Figure 4.

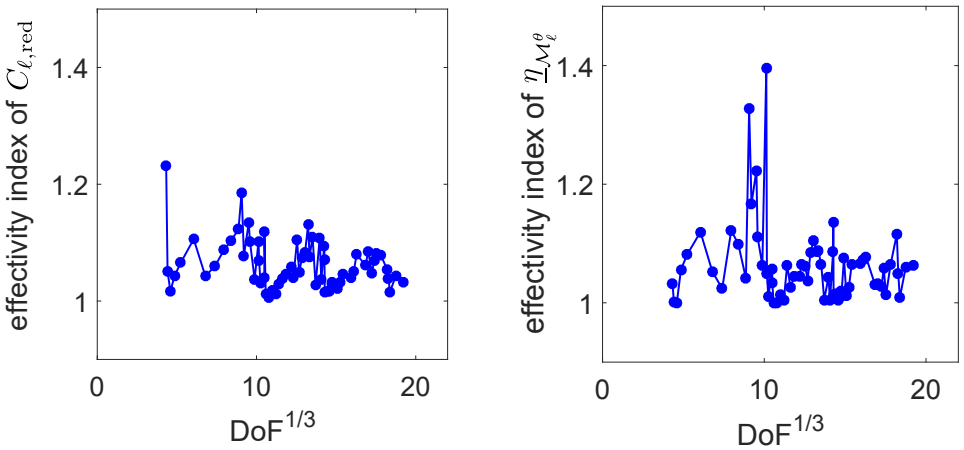

Figure 4: [Model problem (1) posed on the L-shape domain, exact solver] Effectivity indices $I_{\ell,\mathrm{red}}^{\mathrm{eff}}$ defined by (5) for the computed error reduction factor from (3) (*left*) and effectivity indices of the discrete lower bound $\underline{\eta}_{\mathcal{M}_\ell^\theta}$ computed as the ratio $\|\nabla(u_{\ell+1}^{\mathrm{ex}} - u_{\ell}^{\mathrm{ex}})\|_{\omega_\ell}/\underline{\eta}_{\mathcal{M}_\ell^\theta}$ (*right*) corresponding to (4) throughout the iterations of our *hp*-adaptive algorithm.

Moreover, in all our numerical experiments, our *hp*-adaptive strategy leads to asymptotic *exponential* convergence rates with respect to the total number

of degrees of freedom used to compute the discrete solution, cf. Figure 5.

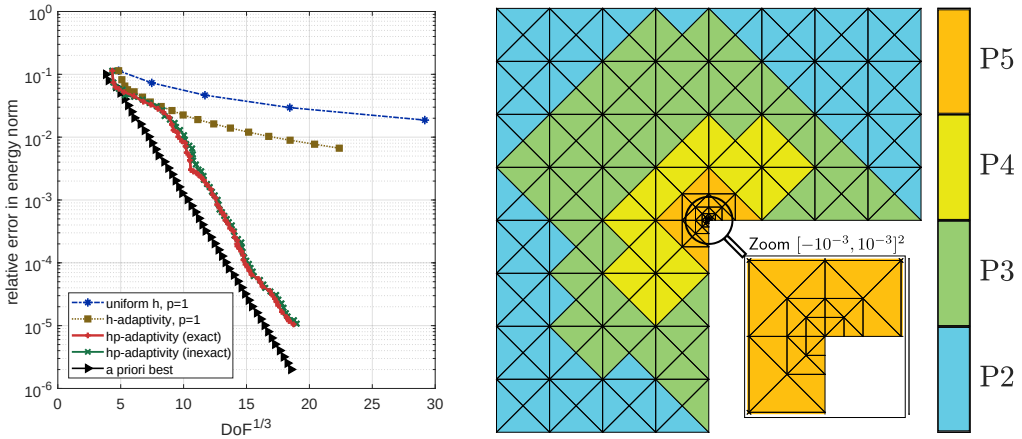

Figure 5: [Model problem (1) posed on the L-shape domain] Relative energy errors $\|\nabla(u - u_\ell^{\mathrm{ex}})\|/\|\nabla u\|$ and $\|\nabla(u - u_\ell)\|/\|\nabla u\|$ as a function of $\mathrm{DoF}_\ell^{\frac{1}{3}}$, obtained using our *hp*-adaptive algorithm with exact and inexact solvers in comparison with simpler approaches (uniform mesh refinement, only using *h*-adaptivity) and the a priori best possible adaptive method relying on the knowledge of the exact solution (*left*) and an example of mesh and polynomial degree distribution obtained after 34 iterations of our *hp*-adaptive algorithm (*right*).

With some similarities to Canuto et al. (2017b), our *hp*-adaptive algorithm relies crucially on the *equilibrated flux* a posteriori error estimate $\eta(\mathcal{T}_\ell)$ on the energy error $\|\nabla(u - u_\ell^{\mathrm{ex}})\| \leq \eta(\mathcal{T}_\ell)$, see Theorem 1.3.2. The roots of this approach can be traced back to the ideas of Prager and Synge (1947) and the hyper-circle method, see e.g. Neittaanmäki and Repin (2004). The reconstructed flux has been used as a tool for deriving a posteriori error estimators in many publications, e.g. the pioneering PhD. thesis of Ladevèze (1975), works by Kelly (1984), Destuynder and Métivet (1999), Ainsworth and Babuška (1999), Braess and Schöberl (2008), and the references therein. For a more recent unifying framework for (potential and) equilibrated flux reconstructions relying on the solution of local mixed finite element problems and leading to guaranteed and polynomial-degree robust error estimators for most of the standard discretization schemes, we refer to Ern and Vohralík (2015). Reconstruction of fluxes done by local postprocessing of the approximate solution avoiding the solution of local mixed finite element problems was also proposed by Becker et al. (2016). The equilibrated flux error estimators have been used also in other contexts, see e.g. Ainsworth (2007), Kim (2007a,b), Cochez-Dhondt and Nicaise (2008), Creusé and Nicaise (2008), Becker et al. (2012), and Creusé et al. (2011, 2017).

The local error estimators are then exploited to mark mesh vertices via Dörfler's marking criterion, cf. Dörfler (1996). On the corresponding patches of elements $\omega_\ell^{\mathbf{a}}$, defined as the subset of elements sharing the marked vertex $\mathbf{a}$,

we then solve two separate local residual problems

$$(\nabla r^{\mathbf{a},\star}, \nabla v^{\mathbf{a},\star})_{\omega_\ell^{\mathbf{a}}} = (f, v^{\mathbf{a},\star})_{\omega_\ell^{\mathbf{a}}} - (\nabla u_\ell, \nabla v^{\mathbf{a},\star})_{\omega_\ell^{\mathbf{a}}} \quad \forall\, v^{\mathbf{a},\star} \in V_\ell^{\mathbf{a},\star}, \quad \text{and } \star \in \{h, p\},$$

with the local finite element spaces $V_\ell^{\mathbf{a},h}$ and $V_\ell^{\mathbf{a},p}$, see (1.14) and (1.15) below, emulating the application of the corresponding type of refinement. This look-ahead idea quantifying the potential benefits of h- and p-refinement then leads to the final local refinement-decision based on the comparison of energy norms of the residual liftings $r^{\mathbf{a},\star}$. Several other hp-refinement strategies also suggest solving auxiliary local problems to forecast the error reduction obtained by performing h- or p-refinement. We refer, in particular, to the works of Dörfler and Heuveline (2007) and Bürg and Dörfler (2011), where the local problems associated with various refinement patterns are considered on single elements only, and an additional minimization problem is solved to make the final refinement decision, as opposed to the local problems posed on patches of elements and a simple comparing procedure yielding the refinement decision in our case. The comparison of performance of our strategy with respect to some other selected approaches is also provided within the numerics section of Chapter 1. The details concerning our implementation of the conforming hp-AFEM with varying polynomial degrees among the mesh elements are given in Appendix A.

This chapter is based on the article Daniel et al. (2018a) published in the journal *Computers & Mathematics with Applications*, vol. 76 (2018) pp. 967-983, written in collaboration with Alexandre Ern, Iain Smears, and Martin Vohralík.

Chapter 2

We consider in this part an extension of the hp-adaptive strategy for the model problem (1) proposed in Chapter 1 in an inexact algebraic solver setting. We avoid the unrealistic exact (up to machine precision) solution of the underlying linear algebraic system and rather take into account the use of an *inexact algebraic solver* within the adaptive algorithm. This type of analysis is still relatively rare in the context of AFEM. To name a few exceptions, this issue has been addressed by Stevenson (2005a, 2007), Becker and Mao (2009), Becker et al. (2010), Arioli et al. (2013a,b) for linear elliptic problems and by Holst et al. (2013), Carstensen et al. (2014), Gantner et al. (2017) for nonlinear elliptic problems, and Carstensen and Gedicke (2012) for eigenvalue problems, all in the context of the h-AFEM, and most recently in Führer et al. (2018) in the context of adaptive BEM.

We focus our attention on recovering the contraction property (3) also in the inexact setting. In particular, we show that while using a properly designed *stopping criterion* for the algebraic solver, see Section 2.4.3, the error reduction between the inexact discrete solution u_ℓ, available at the current

step ℓ of the adaptive loop, and the next inexact approximation $u_{\ell+1}$, still to be computed in the next step of the adaptive loop, verifies a contraction property analogous to (3). More precisely, the following holds true:

$$\|\nabla(u-u_{\ell+1})\| \leq C_{\ell,\mathrm{red}}\|\nabla(u-u_\ell)\| \quad \text{with} \quad 0 \leq C_{\ell,\mathrm{red}} := \frac{\sqrt{1-\frac{\underline{\eta}^2_{\mathcal{M}^\theta_\ell}}{\eta^2(u_\ell,\mathcal{T}_\ell)}}}{(1-\gamma_{\ell+1})} \leq 1, \tag{6}$$

where $\gamma_{\ell+1}$ is a parameter of the adaptive stopping criterion (2.71), $\theta \in (0,1]$ is the fixed parameter of Dörfler's marking procedure, $\eta(u_\ell,\mathcal{T}_\ell)$ denotes the guaranteed total error upper bound further distinguishing the discretization and algebraic error components, see Theorem 2.3.3, and $\underline{\eta}_{\mathcal{M}^\theta_\ell}$ is the guaranteed lower bound on the incremental error between the current inexact approximation u_ℓ and the (unavailable) exact solution $u^{\mathrm{ex}}_{\ell+1}$ at the next level

$$\|\nabla(u^{\mathrm{ex}}_{\ell+1}-u_\ell)\|_{\omega_\ell} \geq \underline{\eta}_{\mathcal{M}^\theta_\ell}, \tag{7}$$

following the spirit of (4). In Figure 6, we give a preview of the accuracy study of the predicted error reduction $C_{\ell,\mathrm{red}}$ and the lower bound $\underline{\eta}_{\mathcal{M}^\theta_\ell}$ by means of their effectivity indices which we find in both cases close to the optimal value of one.

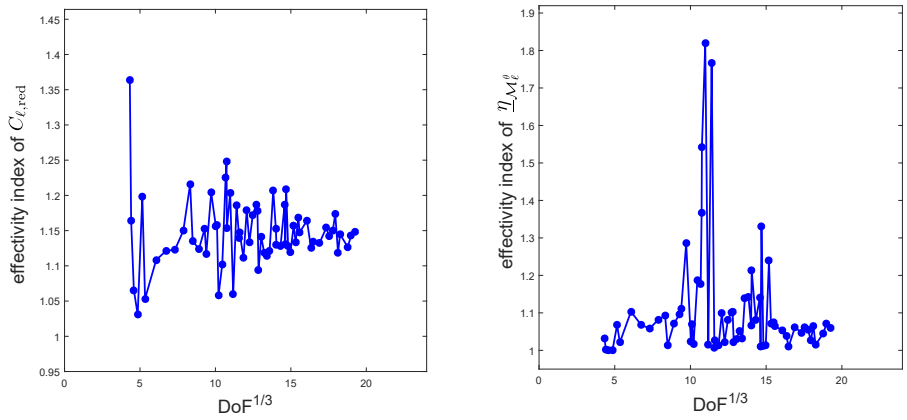

Figure 6: [Model problem (1) posed on the L-shape domain, inexact solver] Effectivity indices for the error reduction factor estimate $C_{\ell,\mathrm{red}}$ of (6) defined by $\frac{C_{\ell,\mathrm{red}}}{\|\nabla(u-u_{\ell+1})\|/\|\nabla(u-u_\ell)\|}$ (*left*) and for the lower bound $\underline{\eta}_{\mathcal{M}^\theta_\ell}$ from (7) computed as the ratio $\|\nabla(u^{\mathrm{ex}}_{\ell+1}-u_\ell)\|_{\omega_\ell}/\underline{\eta}_{\mathcal{M}^\theta_\ell}$ (*right*).

Following Jiránek et al. (2010), Ern and Vohralík (2013), Rey et al. (2014), Becker et al. (2015), and Papež et al. (2017), we construct guaranteed equilibrated flux a posteriori error bounds on the algebraic and the total errors in energy norm, see Theorem 2.3.3. Namely, for the algebraic error upper bound, we adapted the results of Papež et al. (2017), formulated in the context of h- and p-FEM, to the present hp-AFEM setting. We focus on a specific construction of the algebraic error flux reconstruction exploiting the nested hierarchy

of *hp*-finite element spaces created throughout the adaptive algorithm. The possibility to distinguish and estimate separately the different error components is a remarkable feature of the equilibrated flux error estimators.

In terms of algebraic solver, we opted in our numerical experiments for a geometric multigrid employing the sequence of nested *hp*-finite element spaces (cf. Bramble and Pasciak (1993), Wu and Chen (2006), and the books by Hackbusch (1985) and Trottenberg et al. (2001)). We note, however, that our results remain valid for an arbitrary choice of the algebraic solver. The a posteriori knowledge of the algebraic and total errors enables us to design adaptive stopping criteria tailored to ensure that the algebraic error does not significantly contribute to the total error. We refer to the pioneering work of Becker et al. (1995) and Becker (1998), where for a multigrid iterative solver, the authors also investigate an objective stopping criterion taking into account the finite element discretization instead of a usual ad-hoc stopping criterion designed from a pure numerical algebra point of view. Among others, Ern and Vohralík (2013), elaborating on Jiránek et al. (2010), devise a posteriori stopping criteria for inexact Newton methods and iterative linear solvers in the context of nonlinear diffusion PDEs. The control of the algebraic error can be performed also by means of goal-oriented adaptivity based on duality techniques, see e.g. Becker and Rannacher (2001), Patera and Rønquist (2001), or Meidner et al. (2009).

In a series of numerical experiments in Section 2.6, we present the results illustrating the savings in terms of number of necessary iterations of the algebraic solver and time spent on algebraic computations while employing the proposed adaptive stopping criterion in comparison with the use of more classical criteria based on the relative algebraic residual. Moreover, for all the test cases, the obtained meshes and polynomial degree distributions lead to asymptotic exponential convergence even in the presence of an inexact solver, as highlighted by the results depicted in Figure 5.

This chapter is based on the results of the article Daniel et al. (2018b), submitted for publication, written in collaboration with Alexandre Ern and Martin Vohralík.

Chapter 3

In the final chapter, we elaborate a theoretical analysis of the *hp*-refinement strategies for the model problem (1) proposed in Chapters 1 and 2. We aim, in particular, at providing rigorous convergence proofs. We proceed along the lines of the works by Dörfler (1996) and Morin et al. (2000, 2002), where the solution of the resulting linear systems on each level is assumed to be exact, and Binev et al. (2004), Stevenson (2005b, 2007), Becker and Mao (2009), Becker et al. (2010) and Arioli et al. (2013a) where the authors considered the potential effect of the use of iterative linear solvers on the convergence of the adaptive algorithm. In contrast to the previous results in the inexact

algebraic solver setting, one important advantage of the present work is that our bounds on algebraic, discretization, and total error do not contain any generic constant and remain fully computable.

In order to ensure error reduction on each adaptive loop step and convergence of the *hp*-adaptive algorithm, we show that the computable reduction factor $C_{\ell,\mathrm{red}}$ of the contraction properties (3) and (6) can be bounded by a generic constant strictly smaller than one. Namely, this constant depends only on the marking parameter θ, the space dimension d, the mesh shape-regularity $\kappa_{\mathcal{T}}$, the user-defined maximal polynomial degree $p_{\max}$, and, in the inexact setting, also on the coefficient $\widetilde{\gamma}_\ell$ of the adaptive stopping criterion employed to terminate the iterations of the algebraic solver.

For this, we first slightly modify the marking procedure by appending an extra layer of elements to the marked set obtained by Dörfler's marking criterion. Afterwards, we introduce additional assumptions on the used *h*- and *p*-refinements. On the one hand, the *h*-refinement must now ensure the interior node property, see e.g. the full refinement of triangle elements in Binev et al. (2004), Stevenson (2007), or Morin et al. (2002), where tetrahedral elements were considered as well. On the other hand, the *p*-refinement has to be more significant: once the element is selected to be *p*-refined, its polynomial degree shall be increased by at least d. Such assumptions, in particular, allow us to use the bubble function technique, see e.g. Verfürth (2013), in order to show the discrete stability of the local flux equilibration in Propositions 3.4.1 and 3.7.1. This local stability then serves as the main tool in the present convergence proofs. An example of the convergence proof avoiding the inner node property can be found in Cascón et al. (2008), where the contraction property is provided for a sum of the energy error and the scaled error estimate, or Carstensen et al. (2014), where the contraction is only obtained after a certain number of steps of the adaptive loop.

This chapter sums up the results of the article Daniel and Vohralík (2018), currently in preparation.

Future perspectives

Several extensions of the current work can be made. Based on numerical observations, we believe that a *p*-robust version of the convergence proofs presented in Chapter 3 could be achieved. Taking into account more general right-hand side terms within the theoretical analysis can be considered as well. From a practical point of view, an improvement of our approach can be achieved by incorporating a coarsening routine correcting the unnecessary degrees of freedom possibly produced in the early stages of the *hp*-adaptation. Another improvement of the strategy could be obtained by additionally taking into account, within the refinement-decision criterion, the number of newly created degrees of freedom resulting from either *h*- or *p*-refinement. A general second-order elliptic model problem could also be examined in order to assess

more thoroughly the practicality of our approach. In this case, incorporating also anisotropic h- and p-refinements within the proposed methodology may be required. Finally, the theoretical analysis concerning the computational (quasi-)optimality of the proposed adaptive algorithms would be interesting but would require further research.

Chapter 1

An adaptive *hp*-refinement strategy with computable guaranteed bound on the error reduction factor

This chapter consists of the article Daniel et al. (2018a) published in the journal *Computers & Mathematics with Applications*, vol. 76 (2018) pp. 967-983, written with Alexandre Ern, Iain Smears and Martin Vohralík.

Contents

Abstract

We propose a new practical adaptive refinement strategy for *hp*-finite element approximations of elliptic problems. Following recent theoretical developments in polynomial-degree-robust a posteriori error analysis, we solve two types of discrete local problems on vertex-based patches. The first type involves the solution on each patch of a mixed finite element problem with homogeneous Neumann boundary conditions, which leads to an $\mathbf{H}(\mathrm{div}, \Omega)$-conforming equilibrated flux. This, in turn, yields a guaranteed upper bound on the error and serves to mark mesh vertices for refinement via Dörfler's bulk-chasing criterion. The second type of local problems involves the solution, on patches associated with marked vertices only, of two separate primal finite element problems with homogeneous Dirichlet boundary conditions, which serve to decide between *h*-, *p*-, or *hp*-refinement. Altogether, we show that these ingredients lead to a computable guaranteed bound on the ratio of the errors between successive refinements (error reduction factor). In a series of numerical experiments featuring smooth and singular solutions, we study the performance of the proposed *hp*-adaptive strategy and observe exponential convergence rates. We also investigate the accuracy of our bound on the reduction factor by evaluating the ratio of the predicted reduction factor relative to the true error reduction, and we find that this ratio is in general quite close to the optimal value of one.

1.1 Introduction

Adaptive discretization methods constitute an important tool in computational science and engineering. Since the pioneering works on the *hp*-finite element method by Gui and Babuška (1986b,a) and Babuška and Guo (1986a,b) in the 1980s, where it was shown that for one-dimensional problems *hp*-refinement leads to exponential convergence with respect to the number of degrees of freedom on *a priori* adapted meshes, there has been a great amount of work devoted to developing *adaptive hp-refinement* strategies based on *a posteriori error estimates*. Convergence of *hp*-adaptive finite element approximations for elliptic problems, has, though, been addressed only very recently in Dörfler and Heuveline (2007), Bürg and Dörfler (2011), and Bank et al. (2013). The first optimality result we are aware of is by *et al.* Canuto et al. (2017a), where an important ingredient is the *hp*-coarsening routine by Binev (2013, 2018). These works extend to the *hp*-context the previous *h*-convergence and optimality results by Dörfler (1996), Morin et al. (2002, 2003), Stevenson (2007), Cascón et al. (2008), Carstensen et al. (2014), see

also Nochetto et al. (2009) and the references therein. It is worth mentioning that most of the available convergence results are formulated for adaptive methods driven by residual-type a posteriori error estimators; other estimators have in particular been addressed by Cascón and Nochetto (2012) and Kreuzer and Siebert (2011).

A key ingredient for adaptive *hp*-refinement is a local criterion in each mesh cell marked for refinement that allows one to decide whether *h*-, *p*-, or *hp*-refinement should be performed. There is a substantial amount of such criteria proposed in the literature; a computational overview can be found in Mitchell and McClain (2014, 2011). Some of the mathematically motivated *hp*-decision criteria include, among others, those proposed by Eibner and Melenk (2007), Houston and Süli (2005) which both estimate the local regularity of the exact weak solution. Our proposed strategy fits into the group of algorithms based on solving local boundary value problems allowing us to forecast the benefits of performing *h*- or *p*-refinement, as recently considered in, e.g., Bürg and Dörfler (2011), Dörfler and Heuveline (2007). Similarly to Dörfler and Heuveline (2007), we use the *local* finite element spaces associated with a specific type of refinement to perform the above forecast and to take the local *hp*-refinement decision. We also mention the work of Demkowicz et al. (2002) for an earlier, yet more expensive, version of the look-ahead idea, where it is proposed to solve an auxiliary problem on a *global* finite element space corresponding to a mesh refined uniformly either in h or in p.

In the present work, we focus on the Poisson model problem with (homogeneous) Dirichlet boundary conditions. In weak form, the model problem reads as follows: Find $u \in H^1_0(\Omega)$ such that

$$(\nabla u, \nabla v) = (f, v) \qquad \forall v \in H^1_0(\Omega), \tag{1.1}$$

where $\Omega \subset \mathbb{R}^d$, $d = 2, 3$, is a polygonal/polyhedral domain (open, bounded, and connected set) with a Lipschitz boundary, $f \in L^2(\Omega)$, $H^1_0(\Omega)$ denotes the Sobolev space of all functions in $L^2(\Omega)$ which have all their first-order weak derivatives in $L^2(\Omega)$ and a zero trace on $\partial\Omega$, and $(\cdot, \cdot)$ stands for the $L^2(\Omega)$ or $[L^2(\Omega)]^d$ inner product. Our first goal is to propose a reliable and computationally-efficient *hp-adaptive strategy* to approximate the model problem (1.1) that hinges on the recent theoretical developments on polynomial-degree-robust a posteriori error estimates due to Braess et al. (2009) and Ern and Vohralík (2015, 2016). The present *hp*-adaptive algorithm follows the well-established paradigm based on an iterative loop where each step consists of the following four modules:

$$\texttt{SOLVE} \to \texttt{ESTIMATE} \to \texttt{MARK} \to \texttt{REFINE}. \tag{1.2}$$

Here, `SOLVE` stands for application of the conforming finite element method on a matching (no hanging nodes) simplicial mesh to approximate the model problem (1.1); spatially-varying polynomial degree is allowed. The module

`ESTIMATE` is based on an equilibrated flux a posteriori error estimate, obtained by solving, for each mesh vertex, a local mixed finite element problem with a (homogeneous) Neumann boundary condition on the patch of cells sharing the given vertex. The module `MARK` is based on a bulk-chasing criterion inspired by the well-known Dörfler's marking proposed in Dörfler (1996); here we mark mesh vertices and not simplices since we observe a smoother performance in practice and since we later work with some vertex-based auxiliary quantities.

The module `REFINE`, where we include our *hp*-decision criterion, is organized into three steps. First, we solve two local finite element problems on each patch of simplices attached to a mesh vertex marked for refinement, with either the mesh refined or the polynomial degree increased. This is inspired by the key observation from (Ern and Vohralík, 2015, Lemma 3.23) that guaranteed local efficiency can be materialized by some local conforming finite element solves. These conforming residual liftings allow us, in particular, to estimate the effect of applying h- or p-refinement, and lead to a partition of the set of marked vertices into two disjoint subsets, one collecting the mesh vertices flagged for h-refinement and the other collecting the mesh vertices flagged for p-refinement. The second step of the module `REFINE` uses these two subsets to flag the simplices for h-, p, or hp-refinement. Finally, the third step of the module `REFINE` uses the above sets of flagged simplices to build the next simplicial mesh and the next polynomial-degree distribution. Let us mention that recently, Dolejší et al. (2016) also devised an *hp*-adaptive algorithm driven by polynomial-degree-robust a posteriori error estimates based on the equilibrated fluxes from Braess et al. (2009), Ern and Vohralík (2015, 2016). The differences with the present work are that the interior penalty discontinuous Galerkin method is considered in Dolejší et al. (2016), and more importantly, that the present *hp*-decision criterion hinges on local primal solves on patches around marked vertices.

The second goal of the present work is to show that the proposed *hp*-adaptive strategy automatically leads to a *computable guaranteed bound* on the *error reduction factor* between two consecutive steps of the adaptive loop (1.2). More precisely, we show how to compute explicitly a real number $C_{\mathrm{red}} \in [0,1]$ so that

$$\|\nabla(u-u_{\ell+1})\| \leq C_{\mathrm{red}}\|\nabla(u-u_\ell)\|, \tag{1.3}$$

where u_ℓ denotes the discrete solution on ℓ-th iteration of the adaptive loop, see Theorem 1.5.2. Thus the number C_{red} gives a guaranteed (constant-free) bound on the ratio of the errors between successive refinements. This must not be confused with saying that the error is guaranteed to be reduced, since the case $C_{\mathrm{red}} = 1$ cannot be ruled out in general without additional assumptions (e.g. an interior node property, see Morin et al. (2002) for further details). The computation of C_{red} crucially relies on a combined use of the equilibrated fluxes and of the conforming residual liftings, which were already used for the error estimation and *hp*-refinement decision criterion respectively. It is worth noting that we consider a homogeneous Dirichlet boundary condition for the

local residual liftings in order to obtain an estimate on the error reduction factor that is as sharp as possible.

The rest of this chapter is organized as follows. Section 1.2 describes the discrete setting and introduces some useful notation. Section 1.3 presents the modules `SOLVE`, `ESTIMATE`, and `MARK`, whereas Section 1.4 presents the module `REFINE`. Section 1.5 contains our main result on a guaranteed bound on the error reduction factor. Finally, numerical experiments on two-dimensional test cases featuring smooth and singular solutions are discussed in Section 1.6, and conclusions are drawn in Section 1.7.

1.2 Discrete setting

The main purpose of the adaptive loop (1.2) is to generate a sequence of finite-dimensional H^1_0-conforming finite element spaces $(V_\ell)_{\ell\geq 0}$, where the integer $\ell \geq 0$ stands for the iteration counter in (1.2). H^1_0-conformity means that $V_\ell \subset H^1_0(\Omega)$ for all $\ell \geq 0$. In this work, we shall make the following nestedness assumption:

$$V_\ell \subset V_{\ell+1}, \qquad \forall \ell \geq 0. \tag{1.4}$$

The space V_ℓ is built from two ingredients: (i) a matching simplicial mesh $\mathcal{T}_\ell$ of the computational domain Ω, that is, a finite collection of (closed) non-overlapping simplices $K \in \mathcal{T}_\ell$ covering $\overline{\Omega}$ exactly and such that the intersection of two different simplices is either empty, a common vertex, a common edge, or a common face; (ii) a polynomial-degree distribution described by the vector $\mathbf{p}_\ell := (p_{\ell,K})_{K\in\mathcal{T}_\ell}$ that assigns a polynomial degree to each simplex $K \in \mathcal{T}_\ell$. The conforming finite element space V_ℓ is then defined as

$$V_\ell := \mathbb{P}_{\mathbf{p}_\ell}(\mathcal{T}_\ell) \cap H^1_0(\Omega), \qquad \forall \ell \geq 0,$$

where $\mathbb{P}_{\mathbf{p}_\ell}(\mathcal{T}_\ell)$ denotes the space of piecewise polynomials of total degree $p_{\ell,K} \geq 1$ on each simplex $K \in \mathcal{T}_\ell$. In other words, any function $v_\ell \in V_\ell$ satisfies $v_\ell \in H^1_0(\Omega)$ and $v_\ell|_K \in \mathbb{P}_{p_{\ell,K}}(K)$ for all $K \in \mathcal{T}_\ell$, where for an integer $p \geq 1$, $\mathbb{P}_p(K)$ stands for the space of polynomials of total degree at most p on the simplex K.

The initial mesh $\mathcal{T}_0$ and the initial polynomial-degree distribution $\mathbf{p}_0$ are given, and the purpose of each step $\ell \geq 0$ of the adaptive loop (1.2) is to produce the next mesh $\mathcal{T}_{\ell+1}$ and the next polynomial-degree distribution $\mathbf{p}_{\ell+1}$. In order to ensure the nestedness property (1.4), the following two properties are to be satisfied: (i) The sequence $(\mathcal{T}_\ell)_{\ell\geq 0}$ is hierarchical, i.e., for all $\ell \geq 0$ and all $\widetilde{K} \in \mathcal{T}_{\ell+1}$, there is a unique simplex $K \in \mathcal{T}_\ell$, called the parent of $\widetilde{K}$ so that $\widetilde{K} \subseteq K$; (ii) The local polynomial degree is locally increasing, i.e., for all $\ell \geq 0$ and all $\widetilde{K} \in \mathcal{T}_{\ell+1}$, $p_{\ell+1,\widetilde{K}} \geq p_{\ell,K}$ where $K \in \mathcal{T}_\ell$ is the parent of $\widetilde{K}$. Moreover, we assume the following shape-regularity property: There exists a constant $\kappa_{\mathcal{T}} > 0$ such that $\max_{K\in\mathcal{T}_\ell} h_K/\rho_K \leq \kappa_{\mathcal{T}}$ for all $\ell \geq 0$, where h_K is

the diameter of K and ρ_K is the diameter of the largest ball inscribed in K.

Before closing this section, we introduce some further useful notation. The set of vertices $\mathcal{V}_\ell$ of each mesh $\mathcal{T}_\ell$ is decomposed into $\mathcal{V}_\ell^{\rm int}$ and $\mathcal{V}_\ell^{\rm ext}$, the set of inner and boundary vertices, respectively. For each vertex $\mathbf{a} \in \mathcal{V}_\ell$, the so-called hat function $\psi_\ell^{\mathbf{a}}$ is the continuous, piecewise affine function that takes the value 1 at the vertex $\mathbf{a}$ and the value 0 at all the other vertices of $\mathcal{V}_\ell$; the function $\psi_\ell^{\mathbf{a}}$ is in V_ℓ for all $\mathbf{a} \in \mathcal{V}_\ell^{\rm int}$. Moreover, we consider the simplex patch $\mathcal{T}_\ell^{\mathbf{a}} \subset \mathcal{T}_\ell$ which is the collection of the simplices in $\mathcal{T}_\ell$ sharing the vertex $\mathbf{a} \in \mathcal{V}_\ell$, and we denote by $\omega_\ell^{\mathbf{a}}$ the corresponding open subdomain. Finally, for each simplex $K \in \mathcal{T}_\ell$, $\mathcal{V}_K$ denotes the set of vertices of K.

1.3 The modules SOLVE, ESTIMATE, and MARK

In this section we present the modules SOLVE, ESTIMATE, and MARK from the adaptive loop (1.2). Let $\ell \geq 0$ denote the current iteration number.

1.3.1 The module SOLVE

The module SOLVE takes as input the H^1_0-conforming finite element space V_ℓ and outputs the discrete function $u_\ell \in V_\ell$ which is the unique solution of

$$(\nabla u_\ell, \nabla v_\ell) = (f, v_\ell) \qquad \forall v_\ell \in V_\ell. \tag{1.5}$$

1.3.2 The module ESTIMATE

Following Destuynder and Métivet (1999), Braess et al. (2009), Ern and Vohralík (2015), Dolejší et al. (2016), Ern and Vohralík (2016), see also the references therein, the module ESTIMATE relies on an equilibrated flux a posteriori error estimate on the energy error $\|\nabla(u - u_\ell)\|$. The module ESTIMATE takes as input the finite element solution u_ℓ and outputs a collection of local error indicators $\{\eta_K\}_{K\in\mathcal{T}_\ell}$. The equilibrated flux is constructed locally from mixed finite element solves on the simplex patches $\mathcal{T}_\ell^{\mathbf{a}}$ attached to each vertex $\mathbf{a} \in \mathcal{V}_\ell$. For this construction, we consider as in Dolejší et al. (2016) the local polynomial degree $p_{\mathbf{a}}^{\rm est} := \max_{K\in\mathcal{T}_\ell^{\mathbf{a}}} p_{\ell,K}$ (any other choice so that $p_{\mathbf{a}}^{\rm est} \geq \max_{K\in\mathcal{T}_\ell^{\mathbf{a}}} p_{\ell,K}$ can also be employed). We consider the local Raviart–Thomas–Nédélec mixed finite element spaces $(\mathbf{V}_\ell^{\mathbf{a}}, Q_\ell^{\mathbf{a}})$ which are defined for all $\mathbf{a} \in \mathcal{V}_\ell^{\rm int}$ by

$$\mathbf{V}_\ell^{\mathbf{a}} := \{\mathbf{v}_\ell \in \mathbf{H}(\mathrm{div}, \omega_\ell^{\mathbf{a}});\ \mathbf{v}_\ell|_K \in \mathbf{RTN}_{p_{\mathbf{a}}^{\rm est}}(K),\ \forall K \in \mathcal{T}_\ell^{\mathbf{a}},\ \mathbf{v}_\ell\cdot\mathbf{n}_{\omega_\ell^{\mathbf{a}}} = 0 \text{ on } \partial\omega_\ell^{\mathbf{a}}\},$$

$$Q_\ell^{\mathbf{a}} := \{q_\ell \in \mathbb{P}_{p_{\mathbf{a}}^{\rm est}}(\mathcal{T}_\ell^{\mathbf{a}});\ (q_\ell, 1)_{\omega_\ell^{\mathbf{a}}} = 0\},$$

and, for all $\mathbf{a} \in \mathcal{V}_\ell^{\mathrm{ext}}$,

$$\mathbf{V}_\ell^{\mathbf{a}} := \{\mathbf{v}_\ell \in \mathbf{H}(\mathrm{div}, \omega_\ell^{\mathbf{a}});\ \mathbf{v}_\ell|_K \in \mathbf{RTN}_{p_{\mathbf{a}}^{\mathrm{est}}}(K),\ \forall K \in \mathcal{T}_\ell^{\mathbf{a}},\ \mathbf{v}_\ell \cdot \mathbf{n}_{\omega_\ell^{\mathbf{a}}} = 0 \text{ on } \partial\omega_\ell^{\mathbf{a}} \backslash \partial\Omega\},$$
$$Q_\ell^{\mathbf{a}} := \mathbb{P}_{p_{\mathbf{a}}^{\mathrm{est}}}(\mathcal{T}_\ell^{\mathbf{a}}),$$

where $\mathbf{RTN}_{p_{\mathbf{a}}^{\mathrm{est}}}(K) := [\mathbb{P}_{p_{\mathbf{a}}^{\mathrm{est}}}(K)]^d + \mathbb{P}_{p_{\mathbf{a}}^{\mathrm{est}}}(K)\mathbf{x}$, and $\mathbf{n}_{\omega_\ell^{\mathbf{a}}}$ denotes the unit outward-pointing normal to $\omega_\ell^{\mathbf{a}}$.

Definition 1.3.1 (Flux reconstruction $\boldsymbol{\sigma}_\ell$)**.** *Let u_ℓ solve (1.5). The global equilibrated flux $\boldsymbol{\sigma}_\ell$ is constructed as $\boldsymbol{\sigma}_\ell := \sum_{\mathbf{a} \in \mathcal{V}_\ell} \boldsymbol{\sigma}_\ell^{\mathbf{a}}$, where, for each vertex $\mathbf{a} \in \mathcal{V}_\ell$, $(\boldsymbol{\sigma}_\ell^{\mathbf{a}}, \gamma_\ell^{\mathbf{a}}) \in \mathbf{V}_\ell^{\mathbf{a}} \times Q_\ell^{\mathbf{a}}$ solves*

$$(\boldsymbol{\sigma}_\ell^{\mathbf{a}}, \mathbf{v}_\ell)_{\omega_\ell^{\mathbf{a}}} - (\gamma_\ell^{\mathbf{a}}, \nabla\cdot\mathbf{v}_\ell)_{\omega_\ell^{\mathbf{a}}} = -(\psi_\ell^{\mathbf{a}} \nabla u_\ell, \mathbf{v}_\ell)_{\omega_\ell^{\mathbf{a}}} \qquad \forall \mathbf{v}_\ell \in \mathbf{V}_\ell^{\mathbf{a}}, \tag{1.6a}$$
$$(\nabla\cdot\boldsymbol{\sigma}_\ell^{\mathbf{a}}, q_\ell)_{\omega_\ell^{\mathbf{a}}} = (f\psi_\ell^{\mathbf{a}} - \nabla u_\ell \cdot \nabla\psi_\ell^{\mathbf{a}}, q_\ell)_{\omega_\ell^{\mathbf{a}}} \quad \forall q_\ell \in Q_\ell^{\mathbf{a}}; \tag{1.6b}$$

or, equivalently,

$$\boldsymbol{\sigma}_\ell^{\mathbf{a}} := \operatorname*{arg\,min}_{\mathbf{v}_\ell \in \mathbf{V}_\ell^{\mathbf{a}},\, \nabla\cdot\mathbf{v}_\ell = \Pi_{Q_\ell^{\mathbf{a}}}(f\psi_\ell^{\mathbf{a}} - \nabla u_\ell \cdot \nabla\psi_\ell^{\mathbf{a}})} \|\psi_\ell^{\mathbf{a}} \nabla u_\ell + \mathbf{v}_\ell\|_{\omega_\ell^{\mathbf{a}}},$$

and where $\boldsymbol{\sigma}_\ell^{\mathbf{a}}$ is extended by zero outside $\omega_\ell^{\mathbf{a}}$.

Note that the Neumann compatibility condition for the problem (1.6) is satisfied for all $\mathbf{a} \in \mathcal{V}_\ell^{\mathrm{int}}$ (take $v_\ell = \psi_\ell^{\mathbf{a}}$ as a test function in (1.5)). Moreover, Definition 1.3.1 yields a globally $\mathbf{H}(\mathrm{div}, \Omega)$-conforming flux reconstruction $\boldsymbol{\sigma}_\ell$ such that

$$(\nabla\cdot\boldsymbol{\sigma}_\ell, v_\ell)_K = (f, v_\ell)_K \quad \forall v_\ell \in \mathbb{P}_{\min_{\mathbf{a} \in \mathcal{V}_K} p_{\mathbf{a}}^{\mathrm{est}}}(K), \text{ for all } K \in \mathcal{T}_\ell, \tag{1.7}$$

see (Dolejší et al., 2016, Lemma 3.6).

A possible "best" choice for a flux reconstruction would actually be

$$\boldsymbol{\sigma}_\ell := \arg \min_{\mathbf{v}_\ell \in \mathbf{V}_\ell,\, \nabla\cdot\mathbf{v}_\ell = \Pi_{\mathbb{P}_{\mathbf{p}_\ell}(\mathcal{T}_\ell)} f} \|\nabla u_\ell + \mathbf{v}_\ell\|,$$

with $\mathbf{V}_\ell$ a discrete subspace of $\mathbf{H}(\mathrm{div}, \Omega)$. However, this *global minimization* would be too expensive to compute; its cost is comparable to the cost required to obtain the approximate solution u_ℓ itself. This is the reason why we rely on the *local* partition-of-unity-based versions of the above global minimization problem in the Definition 1.3.1. We provide an illustration of the exact flux $-\nabla u$ in Figure 1.1 (right) and an illustration of the approximate flux $-\nabla u_2$ and the resulting flux reconstruction $\boldsymbol{\sigma}_2$ in Figure 1.2. The functions are plotted on a subdomain $\omega_2^{\mathbf{a}} \subset \Omega$, $\mathbf{a} \in \mathcal{V}_2$, with the corresponding pair $(\mathcal{T}_2^{\mathbf{a}}, \mathbf{p}_2^{\mathbf{a}})$.

Using the current notation, (Dolejší et al., 2016, Theorem 3.3) states the following result:

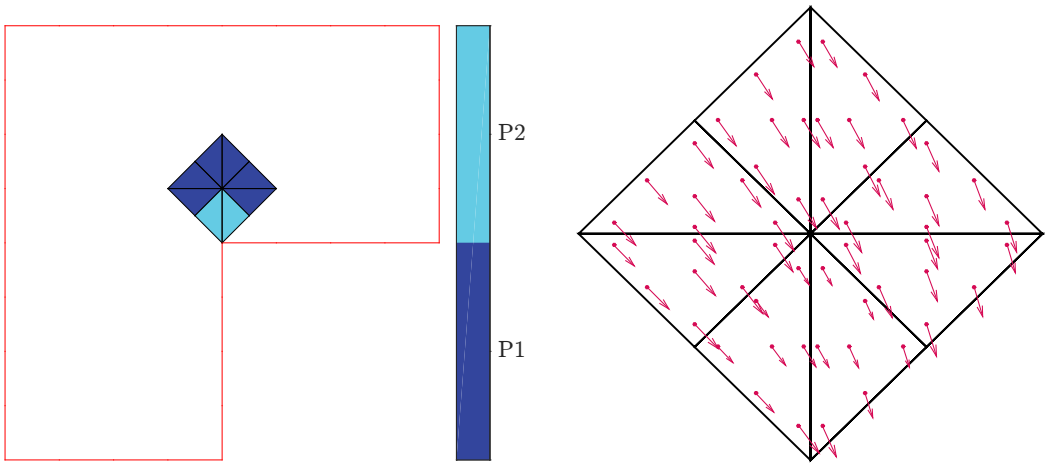

Figure 1.1: [L-shape domain of Section 1.6.2] The illustration of flux reconstruction on a single patch $\omega_2^{\mathbf{a}}$, $\mathbf{a} \in \mathcal{V}_2$; global position of the patch $\omega_2^{\mathbf{a}}$ (*left*) and the exact flux $-\nabla u \in \mathbf{H}(\mathrm{div}, \Omega)$ on the patch $\omega_2^{\mathbf{a}}$ (*right*).

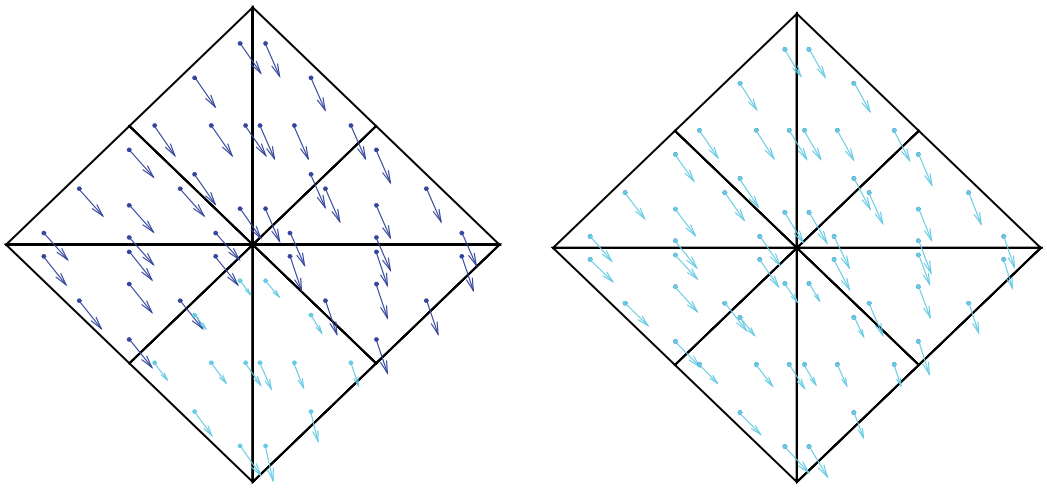

Figure 1.2: [L-shape domain of Section 1.6.2] The illustration of flux reconstruction on a single patch $\omega_2^{\mathbf{a}}$, $\mathbf{a} \in \mathcal{V}_2$; approximate flux $-\nabla u_2 \notin \mathbf{H}(\mathrm{div}, \Omega)$ (*left*) and the flux reconstruction $\boldsymbol{\sigma}_2 \in \mathbf{V}_2 \subset \mathbf{H}(\mathrm{div}, \Omega)$ on the patch $\omega^{\mathbf{a}}$ (*right*).

Theorem 1.3.2 (Guaranteed upper bound on the error)**.** *Let u solve (1.1) and u_ℓ solve (1.5). Let $\boldsymbol{\sigma}_\ell$ be the equilibrated flux reconstruction of Definition 1.3.1. Then*

$$\|\nabla(u-u_\ell)\| \le \eta(\mathcal{T}_\ell) := \left\{ \sum_{K\in\mathcal{T}_\ell} \eta_K^2 \right\}^{\frac{1}{2}}, \quad \eta_K := \|\nabla u_\ell + \boldsymbol{\sigma}_\ell\|_K + \frac{h_K}{\pi}\|f - \nabla\cdot\boldsymbol{\sigma}_\ell\|_K. \tag{1.8}$$

Proof. From the definitions of the weak solution u and its finite element approximation u_ℓ we have $(u - u_\ell) \in H_0^1(\Omega)$. Then the energy norm of the error

$(u - u_\ell)$ can be characterized as a dual norm

$$\|\nabla(u - u_\ell)\| = \sup_{v \in H^1_0(\Omega), \|\nabla v\| = 1} (\nabla(u - u_\ell), \nabla v).$$

Fix $v \in H^1_0(\Omega)$ with $\|\nabla v\| = 1$. We proceed with using the weak solution characterization (3.1), adding and subtracting $(\boldsymbol{\sigma}_\ell, \nabla v)$,

$$(\nabla(u - u_\ell), \nabla v) = (f, v) - (\nabla u_\ell, \nabla v) = (f - \nabla{\cdot}\boldsymbol{\sigma}_\ell, v) - (\nabla u_\ell + \boldsymbol{\sigma}_\ell, \nabla v),$$

where we have also employed the Green theorem $(\boldsymbol{\sigma}_\ell, \nabla v) = -(\nabla{\cdot}\boldsymbol{\sigma}_\ell, v)$. We will proceed with bounding the two terms on the above right-hand side separately.

Namely, we obtain the following upper bound

$$\begin{aligned}(f - \nabla{\cdot}\boldsymbol{\sigma}_\ell, v) &= \sum_{K \in \mathcal{T}_\ell} (f - \nabla{\cdot}\boldsymbol{\sigma}_\ell, v - \Pi_{\mathbb{P}_0(K)} v)_K \\ &\leq \sum_{K \in \mathcal{T}_\ell} \|f - \nabla{\cdot}\boldsymbol{\sigma}_\ell\|_K \|v - \Pi_{\mathbb{P}_0(K) v}\|_K,\end{aligned}$$

where we crucially employed the equilibration property (1.7) of the flux reconstruction $\boldsymbol{\sigma}_\ell$ together with the definition of L^2-orthogonal projection to enforce the zero mean value of test function inside the scalar product. The Cauchy–Schwarz inequality was also used. We finish by using the Poincaré inequality

$$\sum_{K \in \mathcal{T}_\ell} \|f - \nabla{\cdot}\boldsymbol{\sigma}_\ell\|_K \|v - \Pi_{\mathbb{P}_0(K) v}\|_K \leq \sum_{K \in \mathcal{T}_\ell} \frac{h_K}{\pi} \|f - \nabla{\cdot}\boldsymbol{\sigma}_\ell\|_K \|\nabla v\|_K. \tag{1.10}$$

For the second term the Cauchy–Schwarz inequality yields

$$-(\nabla u_\ell + \boldsymbol{\sigma}_\ell, \nabla v) \leq \sum_{K \in \mathcal{T}_\ell} \|\nabla u_\ell + \boldsymbol{\sigma}_\ell\|_K \|\nabla v\|_K. \tag{1.11}$$

The estimate (1.8) then follows from combining (1.10) and (1.11) with the Cauchy–Schwarz inequality once again and using the property $\|\nabla v\| = 1$. □

As discussed in, e.g., (Ern and Vohralík, 2015, Remark 3.6), the term $\frac{h_K}{\pi}\|f - \nabla{\cdot}\boldsymbol{\sigma}_\ell\|_K$ represents, for all $K \in \mathcal{T}_\ell$, a local oscillation in the source datum f that, under suitable smoothness assumptions, converges to zero two orders faster than the error. To cover the whole computational range in our numerical experiments, this term is kept in the error indicator η_K.

1.3.3 The module MARK

The module MARK takes as input the local error estimators $\{\eta_K\}_{K \in \mathcal{T}_\ell}$ from Theorem 1.3.2 and outputs a set of marked vertices $\widetilde{\mathcal{V}}_\ell^\theta \subset \mathcal{V}_\ell$ using a bulk-chasing

criterion inspired by the well-known Dörfler's marking criterion, cf. Dörfler (1996). The reason why we mark vertices and not simplices is that our *hp*-decision criterion in the module REFINE (see Section 1.4) hinges on the solution of local primal solves posed on the patches $\mathcal{T}_\ell^{\mathbf{a}}$ associated with the marked vertices $\mathbf{a} \in \widetilde{\mathcal{V}}_\ell^\theta$; we also observe in practice a smoother performance of the overall *hp*-adaptive procedure when marking vertices than when marking elements. Vertex-marking strategies are also considered, among others, in Morin et al. (2002), Canuto et al. (2017b).

For a subset $\mathcal{S} \subset \mathcal{T}_\ell$, we use the notation $\eta(\mathcal{S}) := \{\sum_{K\in\mathcal{S}} \eta_K^2\}^{1/2}$. In the module MARK, the set of marked vertices $\widetilde{\mathcal{V}}_\ell^\theta$ is selected in such a way that

$$\eta\Big(\bigcup_{\mathbf{a}\in\widetilde{\mathcal{V}}_\ell^\theta} \mathcal{T}_\ell^{\mathbf{a}}\Big) \geq \theta\, \eta(\mathcal{T}_\ell), \tag{1.12}$$

where $\theta \in (0, 1]$ is a fixed threshold. Letting

$$\mathcal{M}_\ell^\theta := \bigcup_{\mathbf{a}\in\widetilde{\mathcal{V}}_\ell^\theta} \mathcal{T}_\ell^{\mathbf{a}} \subset \mathcal{T}_\ell \tag{1.13}$$

be the collection of all the simplices that belong to a patch associated with a marked vertex, we observe that (1.12) means that $\eta(\mathcal{M}_\ell^\theta) \geq \theta\, \eta(\mathcal{T}_\ell)$. To select a set $\widetilde{\mathcal{V}}_\ell^\theta$ of minimal cardinality, the mesh vertices in $\mathcal{V}_\ell$ are sorted by comparing the vertex-based error estimators $\eta(\mathcal{T}_\ell^{\mathbf{a}})$ for all $\mathbf{a} \in \mathcal{V}_\ell$, and a greedy algorithm is employed to build the set $\widetilde{\mathcal{V}}_\ell^\theta$. The module MARK is summarized in Algorithm 1. A possibly slightly larger set $\widetilde{\mathcal{V}}_\ell^\theta$ can be constructed with linear cost in terms of the number of mesh vertices by using the algorithm proposed in (Dörfler, 1996, Section 5.2).

Algorithm 1 (**module** MARK)

procedure MARK($\{\eta_K\}_{K\in\mathcal{T}_\ell}$, θ)
  ▷ **Input:** error indicators $\{\eta_K\}_{K\in\mathcal{T}_\ell}$, marking parameter $\theta \in (0, 1]$
  ▷ **Output:** set of marked vertices $\widetilde{\mathcal{V}}_\ell^\theta$
  for all $\mathbf{a} \in \mathcal{V}_\ell$ **do**
    Compute the vertex-based error estimator $\eta(\mathcal{T}_\ell^{\mathbf{a}})$
  end for
  Sort the vertices according to $\eta(\mathcal{T}_\ell^{\mathbf{a}})$
  Set $\widetilde{\mathcal{V}}_\ell^\theta := \emptyset$
  while $\eta(\bigcup_{\mathbf{a}\in\widetilde{\mathcal{V}}_\ell^\theta} \mathcal{T}_\ell^{\mathbf{a}}) < \theta\, \eta(\mathcal{T}_\ell)$ **do**
    Add to $\widetilde{\mathcal{V}}_\ell^\theta$ the next sorted vertex $\mathbf{a} \in \mathcal{V}_\ell \setminus \widetilde{\mathcal{V}}_\ell^\theta$
  end while
end procedure

1.4 The module REFINE

The module REFINE takes as input the set of marked vertices $\widetilde{\mathcal{V}}_\ell^\theta$ and outputs the mesh $\mathcal{T}_{\ell+1}$ and the polynomial-degree distribution $\mathbf{p}_{\ell+1}$ to be used at the next step of the adaptive loop (1.2); the integer $\ell \geq 0$ is the current iteration number therein. This module is organized into three steps. First, an *hp*-decision is made on all the marked vertices so that each marked vertex $\mathbf{a} \in \widetilde{\mathcal{V}}_\ell^\theta$ is flagged either for *h*-refinement or for *p*-refinement. This means that the set $\widetilde{\mathcal{V}}_\ell^\theta$ is split into two disjoint subsets $\widetilde{\mathcal{V}}_\ell^\theta = \widetilde{\mathcal{V}}_\ell^h \cup \widetilde{\mathcal{V}}_\ell^p$ with obvious notation (here we drop the superscript θ to simplify the notation). Then, in the second step, the subsets $\widetilde{\mathcal{V}}_\ell^h$ and $\widetilde{\mathcal{V}}_\ell^p$ are used to define subsets $\mathcal{M}_\ell^h$ and $\mathcal{M}_\ell^p$ of the set of marked simplices $\mathcal{M}_\ell^\theta$ (see (1.13)). The subsets $\mathcal{M}_\ell^h$ and $\mathcal{M}_\ell^p$ are not necessarily disjoint which means that some simplices can be flagged for *hp*-refinement. Finally, the two subsets $\mathcal{M}_\ell^h$ and $\mathcal{M}_\ell^p$ are used to construct $\mathcal{T}_{\ell+1}$ and $\mathbf{p}_{\ell+1}$.

1.4.1 *hp*-decision on vertices

Our *hp*-decision on marked vertices is made on the basis of two local primal solves on the patch $\mathcal{T}_\ell^{\mathbf{a}}$ attached to each marked vertex $\mathbf{a} \in \widetilde{\mathcal{V}}_\ell^\theta$. The idea is to construct two distinct local patch-based spaces in order to emulate separately the effects of *h*- and *p*-refinement. Let us denote the polynomial-degree distribution in the patch $\mathcal{T}_\ell^{\mathbf{a}}$ by the vector $\mathbf{p}_\ell^{\mathbf{a}} := (p_{\ell,K})_{K \in \mathcal{T}_\ell^{\mathbf{a}}}$.

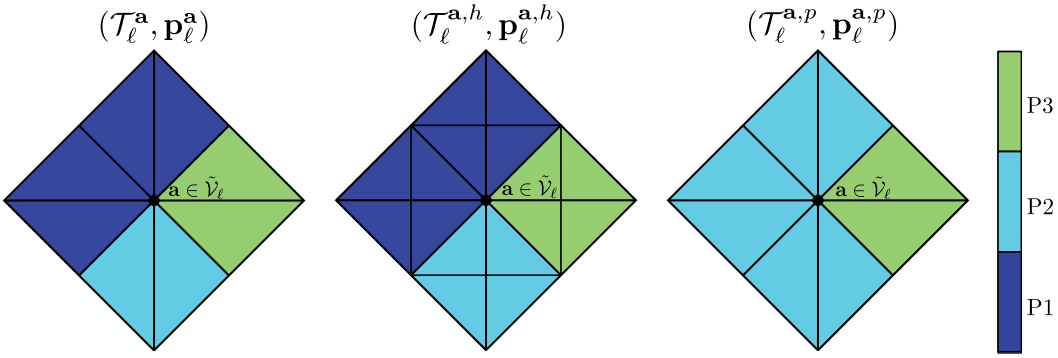

Figure 1.3: An example of patch $\mathcal{T}_\ell^{\mathbf{a}}$ together with its polynomial-degree distribution $\mathbf{p}_\ell^{\mathbf{a}}$ (*left*) and its *h*-refined (*center*) and *p*-refined versions (*right*) from Definitions 1.4.1 and 1.4.2 respectively.

Definition 1.4.1 (***h*-refinement residual**). *Let $\mathbf{a} \in \widetilde{\mathcal{V}}_\ell^\theta$ be a marked vertex with associated patch $\mathcal{T}_\ell^{\mathbf{a}}$ and polynomial-degree distribution $\mathbf{p}_\ell^{\mathbf{a}}$. We set*

$$V_\ell^{\mathbf{a},h} := \mathbb{P}_{\mathbf{p}_\ell^{\mathbf{a},h}}(\mathcal{T}_\ell^{\mathbf{a},h}) \cap H_0^1(\omega_\ell^{\mathbf{a}}), \tag{1.14}$$

where $\mathcal{T}_\ell^{\mathbf{a},h}$ is obtained as a matching simplicial refinement of $\mathcal{T}_\ell^{\mathbf{a}}$ by dividing each simplex $K \in \mathcal{T}_\ell^{\mathbf{a}}$ into at least two children simplices, and the polynomial-degree distribution $\mathbf{p}_\ell^{\mathbf{a},h}$ is obtained from $\mathbf{p}_\ell^{\mathbf{a}}$ by assigning to each newly-created

simplex the same polynomial degree as its parent. Then, we let $r^{\mathbf{a},h} \in V_\ell^{\mathbf{a},h}$ *solve*

$$(\nabla r^{\mathbf{a},h}, \nabla v^{\mathbf{a},h})_{\omega_\ell^{\mathbf{a}}} = (f, v^{\mathbf{a},h})_{\omega_\ell^{\mathbf{a}}} - (\nabla u_\ell, \nabla v^{\mathbf{a},h})_{\omega_\ell^{\mathbf{a}}} \qquad \forall\, v^{\mathbf{a},h} \in V_\ell^{\mathbf{a},h}.$$

Definition 1.4.2 (*p*-**refinement residual**)**.** *Let* $\mathbf{a} \in \widetilde{\mathcal{V}}_\ell^\theta$ *be a marked vertex with associated patch* $\mathcal{T}_\ell^{\mathbf{a}}$ *and polynomial-degree distribution* $\mathbf{p}_\ell^{\mathbf{a}}$*. We set*

$$V_\ell^{\mathbf{a},p} := \mathbb{P}_{\mathbf{p}_\ell^{\mathbf{a},p}}(\mathcal{T}_\ell^{\mathbf{a},p}) \cap H_0^1(\omega_\ell^{\mathbf{a}}), \tag{1.15}$$

where $\mathcal{T}_\ell^{\mathbf{a},p} := \mathcal{T}_\ell^{\mathbf{a}}$*, and the polynomial-degree distribution* $\mathbf{p}_\ell^{\mathbf{a},p}$ *is obtained from* $\mathbf{p}_\ell^{\mathbf{a}}$ *by assigning to each simplex* $K \in \mathcal{T}_\ell^{\mathbf{a},p} = \mathcal{T}_\ell^{\mathbf{a}}$ *the polynomial degree* $p_{\ell,K} + \delta_K^{\mathbf{a}}$ *where*

$$\delta_K^{\mathbf{a}} := \begin{cases} 1 & \text{if } p_{\ell,K} = \min_{K' \in \mathcal{T}_\ell^{\mathbf{a}}} p_{\ell,K'}, \\ 0 & \text{otherwise.} \end{cases} \tag{1.16}$$

Then, we let $r^{\mathbf{a},p} \in V_\ell^{\mathbf{a},p}$ *solve*

$$(\nabla r^{\mathbf{a},p}, \nabla v^{\mathbf{a},p})_{\omega_\ell^{\mathbf{a}}} = (f, v^{\mathbf{a},p})_{\omega_\ell^{\mathbf{a}}} - (\nabla u_\ell, \nabla v^{\mathbf{a},p})_{\omega_\ell^{\mathbf{a}}} \qquad \forall\, v^{\mathbf{a},p} \in V_\ell^{\mathbf{a},p}.$$

The local residual liftings $r^{\mathbf{a},h}$ and $r^{\mathbf{a},p}$ from Definitions 1.4.1 and 1.4.2, respectively, are used to define the following two disjoint subsets of the set of marked vertices $\widetilde{\mathcal{V}}_\ell^\theta$:

$$\widetilde{\mathcal{V}}_\ell^h := \{\mathbf{a} \in \widetilde{\mathcal{V}}_\ell^\theta \mid \|\nabla r^{\mathbf{a},h}\|_{\omega_\ell^{\mathbf{a}}} \geq \|\nabla r^{\mathbf{a},p}\|_{\omega_\ell^{\mathbf{a}}}\}, \tag{1.17a}$$

$$\widetilde{\mathcal{V}}_\ell^p := \{\mathbf{a} \in \widetilde{\mathcal{V}}_\ell^\theta \mid \|\nabla r^{\mathbf{a},h}\|_{\omega_\ell^{\mathbf{a}}} < \|\nabla r^{\mathbf{a},p}\|_{\omega_\ell^{\mathbf{a}}}\}, \tag{1.17b}$$

in such a way that

$$\widetilde{\mathcal{V}}_\ell^\theta = \widetilde{\mathcal{V}}_\ell^h \cup \widetilde{\mathcal{V}}_\ell^p, \qquad \widetilde{\mathcal{V}}_\ell^h \cap \widetilde{\mathcal{V}}_\ell^p = \emptyset.$$

The above *hp*-decision criterion on vertices means that a marked vertex is flagged for *h*-refinement if the local residual norm $\|\nabla r^{\mathbf{a},h}\|_{\omega_\ell^{\mathbf{a}}}$ is larger than $\|\nabla r^{\mathbf{a},p}\|_{\omega_\ell^{\mathbf{a}}}$; otherwise, this vertex is flagged for *p*-refinement. Further motivation for this choice is discussed in Remark 1.5.3.

Remark 1.4.3 (*p*-refinement)**.** *Other choices are possible for the polynomial-degree increment defined in* (1.16)*. One possibility is to set* $\delta_K^{\mathbf{a}} = 1$ *for all* $K \in \mathcal{T}_\ell^{\mathbf{a}}$*. However, in our numerical experiments, we observe that this choice leads to rather scattered polynomial-degree distributions over the whole computational domain. The choice* (1.16) *is more conservative and leads to a smoother overall polynomial-degree distribution. We believe that this choice is preferable, at least as long as a polynomial-degree coarsening procedure is not included in the adaptive loop. Another possibility is to use* $\lceil \alpha p_{\ell,K} \rceil$ *with* $\alpha > 1$ *instead of* $p_{\ell,K} + \delta_K^{\mathbf{a}}$*, which corresponds to the theoretical developments in* Canuto et al. (2017b).

1.4.2 hp-decision on simplices

The second step in the module `REFINE` is to use the subsets $\widetilde{\mathcal{V}}_\ell^h$ and $\widetilde{\mathcal{V}}_\ell^p$ to decide whether h-, p- , or hp-refinement should be performed on each simplex having at least one flagged vertex. To this purpose, we define the following subsets:

$$\mathcal{M}_\ell^h := \{K \in \mathcal{T}_\ell \mid \mathcal{V}_K \cap \widetilde{\mathcal{V}}_\ell^h \neq \emptyset\} \subset \mathcal{M}_\ell^\theta, \tag{1.18a}$$

$$\mathcal{M}_\ell^p := \{K \in \mathcal{T}_\ell \mid \mathcal{V}_K \cap \widetilde{\mathcal{V}}_\ell^p \neq \emptyset\} \subset \mathcal{M}_\ell^\theta. \tag{1.18b}$$

In other words, a simplex $K \in \mathcal{T}_\ell$ is flagged for h-refinement (resp., p-refinement) if it has at least one vertex flagged for h-refinement (resp., p-refinement). Note that the subsets $\mathcal{M}_\ell^h$ and $\mathcal{M}_\ell^p$ are not necessarily disjoint since a simplex can have some vertices flagged for h-refinement and others flagged for p-refinement; such simplices are then flagged for hp-refinement. Note also that $\mathcal{M}_\ell^h \cup \mathcal{M}_\ell^p = \cup_{\mathbf{a}\in\widetilde{\mathcal{V}}_\ell^\theta} \mathcal{T}_\ell^{\mathbf{a}} = \mathcal{M}_\ell^\theta$ is indeed the set of marked simplices considered in the module `MARK`.

1.4.3 hp-refinement

In this last and final step, the subsets $\mathcal{M}_\ell^h$ and $\mathcal{M}_\ell^p$ are used to produce first the next mesh $\mathcal{T}_{\ell+1}$ and then the next polynomial-degree distribution $\mathbf{p}_{\ell+1}$ on the mesh $\mathcal{T}_{\ell+1}$.

The next mesh $\mathcal{T}_{\ell+1}$ is a matching simplicial refinement of $\mathcal{T}_\ell$ obtained by dividing each flagged simplex $K \in \mathcal{M}_\ell^h$ into at least two simplices in a way that is consistent with the matching simplicial refinement of $\mathcal{T}_\ell^{\mathbf{a}}$ considered in Definition 1.4.1 to build $\mathcal{T}_\ell^{\mathbf{a},h}$, i.e., such that $\mathcal{T}_\ell^{\mathbf{a},h} \subset \mathcal{T}_{\ell+1}$ for all $\mathbf{a} \in \widetilde{\mathcal{V}}_\ell^h$. Note that to preserve the conformity of the mesh, additional refinements beyond the set of flagged simplices $\mathcal{M}_\ell^h$ may be carried out when building $\mathcal{T}_{\ell+1}$. Several algorithms can be considered to refine the mesh. In our numerical experiments, we used the newest vertex bisection algorithm, see Sewell (1972).

After having constructed the next mesh $\mathcal{T}_{\ell+1}$, we assign the next polynomial-degree distribution $\mathbf{p}_{\ell+1}$ as follows. For all $\widetilde{K} \in \mathcal{T}_{\ell+1}$, let K denote its parent simplex in $\mathcal{T}_\ell$. We then set

$$p_{\ell+1,\widetilde{K}} := p_{\ell,K} \qquad \text{if } K \notin \mathcal{M}_\ell^p, \tag{1.19}$$

that is, we assign the same polynomial degree to the children of a simplex that is not flagged for p-refinement, whereas we set

$$p_{\ell+1,\widetilde{K}} := \max_{\mathbf{a}\in\mathcal{V}_K\cap\widetilde{\mathcal{V}}_\ell^p} \left(p_{\ell,K} + \delta_K^{\mathbf{a}}\right) \qquad \text{if } K \in \mathcal{M}_\ell^p, \tag{1.20}$$

that is, we assign to the children of a simplex $K \in \mathcal{M}_\ell^p$ flagged for p-refinement the largest of the polynomial degrees considered in Definition 1.4.2 to build the local residual liftings associated with the vertices of K flagged for p-refinement.

1.4.4 Summary of the module REFINE

The module REFINE is summarized in Algorithm 2.

Algorithm 2 (**module** REFINE)

module REFINE($\widetilde{\mathcal{V}}_\ell^\theta$)
  ▷ **Input:** set of marked vertices $\widetilde{\mathcal{V}}_\ell^\theta$
  ▷ **Output:** next level mesh $\mathcal{T}_{\ell+1}$, polynomial-degree distribution $\mathbf{p}_{\ell+1}$
  for all $\mathbf{a} \in \widetilde{\mathcal{V}}_\ell^\theta$ **do**
    Compute the h-refinement residual lifting $r^{\mathbf{a},h}$ from Definition 1.4.1
    Compute the p-refinement residual lifting $r^{\mathbf{a},p}$ from Definition 1.4.2
  end for
  hp-decision on vertices: build the subsets $\widetilde{\mathcal{V}}_\ell^h$ and $\widetilde{\mathcal{V}}_\ell^p$ from (1.17)
  hp-decision on simplices: build the subsets $\mathcal{M}_\ell^h$ and $\mathcal{M}_\ell^p$ from (1.18)
  Build $\mathcal{T}_{\ell+1}$ from $\mathcal{T}_\ell$ and $\mathcal{M}_\ell^h$
  Build $\mathbf{p}_{\ell+1}$ on $\mathcal{T}_{\ell+1}$ from $\mathbf{p}_\ell$, $\{\delta_K^{\mathbf{a}}\}_{\mathbf{a}\in\widetilde{\mathcal{V}}_\ell^p, K\in\mathcal{T}_\ell^{\mathbf{a}}}$, and $\mathcal{M}_\ell^p$ using (1.19) and (1.20)
end module

To illustrate Algorithm 2, we examine in detail a particular situation with three marked vertices as encountered on the 6th iteration ($\ell = 6$) of the adaptive loop applied to the L-shape problem described in Section 1.6.2. In Figure 1.4 (left panel), we display the mesh $\mathcal{T}_6$ and the polynomial-degree distribution $\mathbf{p}_6$. There are three marked vertices in $\widetilde{\mathcal{V}}_6^\theta$. In Figure 1.5, for the three marked vertices, we visualize the norms $\|\nabla r^{\mathbf{a},h}\|_{\omega_6^{\mathbf{a}}}$ and $\|\nabla r^{\mathbf{a},p}\|_{\omega_6^{\mathbf{a}}}$ which are the key ingredients for the hp-decision on vertices. The resulting simplices flagged for h- and p-refinement are shown in the central panel of Figure 1.4, whereas the right panel of Figure 1.4 displays the next mesh $\mathcal{T}_7$ and the next polynomial-degree distribution $\mathbf{p}_7$.

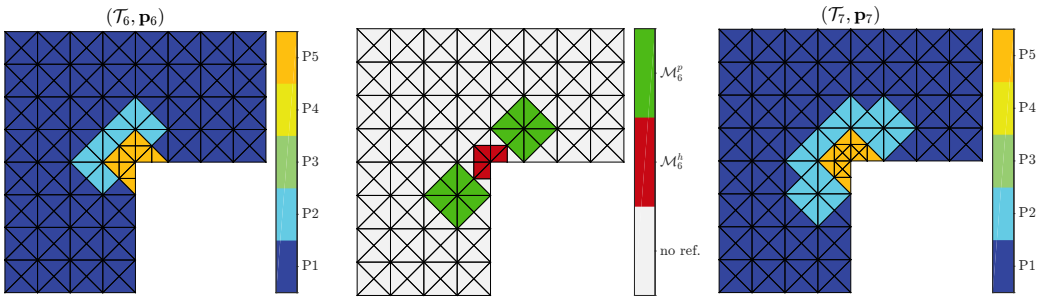

Figure 1.4: [L-shape problem from Section 1.6.2] The mesh and the polynomial degree distribution on the 6th iteration of the adaptive procedure (*left*). Result of the hp-decision: simplices in $\mathcal{M}_6^h$ are shown in red and simplices in $\mathcal{M}_6^p$ are shown in green, the two subsets $\mathcal{M}_6^h$ and $\mathcal{M}_6^p$ being here disjoint (*center*). The resulting mesh $\mathcal{T}_7$ and polynomial-degree distribution $\mathbf{p}_7$ (*right*).

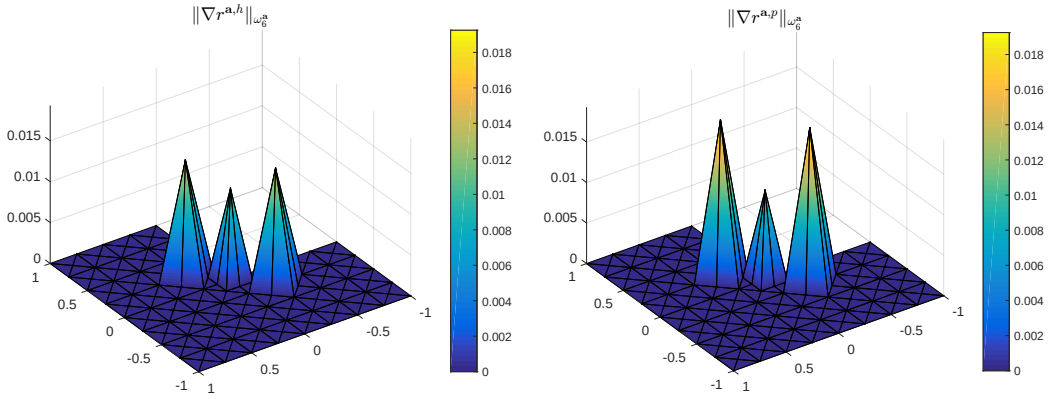

Figure 1.5: [L-shape problem from Section 1.6.2] For the three marked vertices in $\widetilde{\mathcal{V}}_6^\theta$, we display the piecewise $\mathbb{P}_1$ functions which take the value $\|\nabla r^{\mathbf{a},h}\|_{\omega_6^{\mathbf{a}}}$ in the vertex $\mathbf{a}$ and 0 elsewhere (*left*) and the value $\|\nabla r^{\mathbf{a},p}\|_{\omega_6^{\mathbf{a}}}$ in the vertex $\mathbf{a}$ and 0 elsewhere (*right*).

1.5 Guaranteed bound on the error reduction factor

In this section we show that it is possible to compute, at marginal additional costs, a guaranteed bound on the energy error reduction factor $C_{\rm red}$ from (1.3) on each iteration ℓ of the adaptive loop (1.2). This bound can be computed right after the end of module `REFINE` at the modest price of one additional primal solve in each patch $\mathcal{T}_\ell^{\mathbf{a}}$ associated with each marked vertex $\mathbf{a} \in \widetilde{\mathcal{V}}_\ell^\theta$. Recall the set of marked simplices $\mathcal{M}_\ell^\theta = \cup_{\mathbf{a}\in\widetilde{\mathcal{V}}_\ell^\theta}\mathcal{T}_\ell^{\mathbf{a}}$. Let us denote by $\omega_\ell := \cup_{\mathbf{a}\in\widetilde{\mathcal{V}}_\ell^\theta}\omega_\ell^{\mathbf{a}}$ the corresponding open subdomain; notice that a point $\mathbf{x}$ is in $\overline{\omega_\ell}$ if and only if there is $K \in \mathcal{M}_\ell^\theta$ so that $\mathbf{x} \in K$. We start with the following discrete lower bound result:

Lemma 1.5.1 (Guaranteed lower bound on the incremental error on marked simplices)**.** *Let the mesh $\mathcal{T}_{\ell+1}$ and the polynomial-degree distribution $\mathbf{p}_{\ell+1}$ result from Algorithm 2, and recall that $V_{\ell+1} = \mathbb{P}_{\mathbf{p}_{\ell+1}}(\mathcal{T}_{\ell+1}) \cap H_0^1(\Omega)$ is the finite element space to be used on iteration $(\ell+1)$ of the adaptive loop (1.2). For all the marked vertices $\mathbf{a} \in \widetilde{\mathcal{V}}_\ell^\theta$, let us set, in extension of (1.14), (1.15),*

$$V_\ell^{\mathbf{a},hp} := V_{\ell+1}|_{\omega_\ell^{\mathbf{a}}} \cap H_0^1(\omega_\ell^{\mathbf{a}}),$$

and construct the residual lifting $r^{\mathbf{a},hp} \in V_\ell^{\mathbf{a},hp}$ by solving

$$(\nabla r^{\mathbf{a},hp}, \nabla v^{\mathbf{a},hp})_{\omega_\ell^{\mathbf{a}}} = (f, v^{\mathbf{a},hp})_{\omega_\ell^{\mathbf{a}}} - (\nabla u_\ell, \nabla v^{\mathbf{a},hp})_{\omega_\ell^{\mathbf{a}}} \qquad \forall\, v^{\mathbf{a},hp} \in V_\ell^{\mathbf{a},hp}. \quad (1.21)$$

Then, extending $r^{\mathbf{a},hp}$ *by zero outside* $\omega_\ell^{\mathbf{a}}$*, the following holds true:*

$$\|\nabla(u_{\ell+1}-u_\ell)\|_{\omega_\ell} \geq \underline{\eta}_{\mathcal{M}_\ell^\theta}, \quad \underline{\eta}_{\mathcal{M}_\ell^\theta} := \begin{cases} \dfrac{\sum_{\mathbf{a}\in\widetilde{\mathcal{V}}_\ell^\theta} \left\|\nabla r^{\mathbf{a},hp}\right\|_{\omega_\ell^{\mathbf{a}}}^2}{\left\|\nabla\left(\sum_{\mathbf{a}\in\widetilde{\mathcal{V}}_\ell^\theta} r^{\mathbf{a},hp}\right)\right\|_{\omega_\ell}} & \text{if } \sum_{\mathbf{a}\in\widetilde{\mathcal{V}}_\ell^\theta} r^{\mathbf{a},hp} \neq 0, \\ 0 & \text{otherwise.} \end{cases} \tag{1.22}$$

Proof. Let $V_{\ell+1}(\omega_\ell)$ stand for the restriction of the space $V_{\ell+1}$ to the subdomain ω_ℓ and let $V_{\ell+1}^0(\omega_\ell) := V_{\ell+1}(\omega_\ell) \cap H_0^1(\omega_\ell)$ stand for the corresponding homogeneous Dirichlet subspace. Note that $(u_{\ell+1}-u_\ell)$ is a member of $V_{\ell+1}(\omega_\ell)$, but not necessarily of $V_{\ell+1}^0(\omega_\ell)$. Then, the following holds true:

$$\begin{aligned} \|\nabla(u_{\ell+1}-u_\ell)\|_{\omega_\ell} &= \sup_{v_{\ell+1}\in V_{\ell+1}(\omega_\ell)} \frac{(\nabla(u_{\ell+1}-u_\ell),\nabla v_{\ell+1})_{\omega_\ell}}{\|\nabla v_{\ell+1}\|_{\omega_\ell}} \\ &\geq \sup_{v_{\ell+1}\in V_{\ell+1}^0(\omega_\ell)} \frac{(\nabla(u_{\ell+1}-u_\ell),\nabla v_{\ell+1})_{\omega_\ell}}{\|\nabla v_{\ell+1}\|_{\omega_\ell}} \\ &= \sup_{v_{\ell+1}\in V_{\ell+1}^0(\omega_\ell)} \frac{(f,v_{\ell+1})_{\omega_\ell} - (\nabla u_\ell,\nabla v_{\ell+1})_{\omega_\ell}}{\|\nabla v_{\ell+1}\|_{\omega_\ell}}, \end{aligned}$$

where we have used the definition (1.5) of $u_{\ell+1}$ on the mesh $\mathcal{T}_{\ell+1}$, since $v_{\ell+1}$ extended by zero outside of ω_ℓ belongs to the space $V_{\ell+1}$ whenever $v_{\ell+1} \in V_{\ell+1}^0(\omega_\ell)$. Now, choosing $v_{\ell+1} = \sum_{\mathbf{a}\in\widetilde{\mathcal{V}}_\ell^\theta} r^{\mathbf{a},hp}$ (note that this function indeed belongs to $V_{\ell+1}^0(\omega_\ell)$), we infer that

$$\begin{aligned} &\left(f, \sum_{\mathbf{a}\in\widetilde{\mathcal{V}}_\ell^\theta} r^{\mathbf{a},hp}\right)_{\omega_\ell} - \left(\nabla u_\ell, \nabla\left(\sum_{\mathbf{a}\in\widetilde{\mathcal{V}}_\ell^\theta} r^{\mathbf{a},hp}\right)\right)_{\omega_\ell} \\ &\qquad = \sum_{\mathbf{a}\in\widetilde{\mathcal{V}}_\ell^\theta} \left\{\left(f, r^{\mathbf{a},hp}\right)_{\omega_\ell^{\mathbf{a}}} - \left(\nabla u_\ell, \nabla r^{\mathbf{a},hp}\right)_{\omega_\ell^{\mathbf{a}}}\right\} = \sum_{\mathbf{a}\in\widetilde{\mathcal{V}}_\ell^\theta} \left\|\nabla r^{\mathbf{a},hp}\right\|_{\omega_\ell^{\mathbf{a}}}^2, \end{aligned}$$

where we have employed $r^{\mathbf{a},hp}$ as a test function in (1.21). This finishes the proof. □

Our main result is summarized in the following contraction property in the spirit of (Cascón and Nochetto, 2012, Theorem 5.1), (Canuto et al., 2017b, Proposition 4.1), and the references therein. The specificity of the present work is that we obtain a guaranteed and computable bound on the error reduction factor. In contrast to these references, however, we do not prove here that C_{red} is strictly smaller than one, although we observe it numerically in Section 1.6. We believe that one could show $C_{\mathrm{red}} < 1$ under additional assumptions on the refinements, such as the interior node property, see Morin et al. (2002), but we will not pursue this consideration further here.

Theorem 1.5.2 (Guaranteed bound on the energy error reduction factor)**.** *Let the mesh $\mathcal{T}_{\ell+1}$ and the polynomial-degree distribution $\mathbf{p}_{\ell+1}$ result from Algorithm 2, and let $V_{\ell+1} = \mathbb{P}_{\mathbf{p}_{\ell+1}}(\mathcal{T}_{\ell+1}) \cap H^1_0(\Omega)$ be the finite element space to be used on iteration $(\ell+1)$ of the adaptive loop (1.2). Let $\underline{\eta}_{\mathcal{M}^\theta_\ell}$ be defined by (1.22). Then, unless $\eta(\mathcal{M}^\theta_\ell) = 0$ in which case $u_\ell = u$ and the adaptive loop terminates, the new numerical solution $u_{\ell+1} \in V_{\ell+1}$ satisfies*

$$\|\nabla(u-u_{\ell+1})\| \le C_{\mathrm{red}}\|\nabla(u-u_\ell)\| \quad \text{with} \quad 0 \le C_{\mathrm{red}} := \sqrt{1-\theta^2\frac{\underline{\eta}^2_{\mathcal{M}^\theta_\ell}}{\eta^2(\mathcal{M}^\theta_\ell)}} \le 1. \tag{1.23}$$

Proof. We first observe that $\eta(\mathcal{M}^\theta_\ell) = 0$ implies using (1.12) and (1.8) that the error is zero on iteration ℓ, i.e., $u = u_\ell$, so that the adaptive loop (1.2) terminates. Let us now assume that $\eta(\mathcal{M}^\theta_\ell) \neq 0$. Since the spaces $\{V_\ell\}_{\ell\ge0}$ are nested, cf. (1.4), Galerkin's orthogonality implies the following Pythagorean identity:

$$\|\nabla(u-u_{\ell+1})\|^2 = \|\nabla(u-u_\ell)\|^2 - \|\nabla(u_{\ell+1}-u_\ell)\|^2.$$

Moreover, owing to Lemma 1.5.1, we infer that

$$\|\nabla(u_{\ell+1}-u_\ell)\| \ge \|\nabla(u_{\ell+1}-u_\ell)\|_{\omega_\ell} \ge \underline{\eta}_{\mathcal{M}^\theta_\ell} = \frac{\underline{\eta}_{\mathcal{M}^\theta_\ell}}{\eta(\mathcal{M}^\theta_\ell)}\eta(\mathcal{M}^\theta_\ell).$$

Using the marking criterion (1.12) and the definition of $\mathcal{M}^\theta_\ell$, we next see that

$$\begin{aligned}\|\nabla(u-u_{\ell+1})\|^2 &\le \|\nabla(u-u_\ell)\|^2 - \frac{\underline{\eta}^2_{\mathcal{M}^\theta_\ell}}{\eta^2(\mathcal{M}^\theta_\ell)}\eta^2(\mathcal{M}^\theta_\ell)\\ &\le \|\nabla(u-u_\ell)\|^2 - \theta^2\frac{\underline{\eta}^2_{\mathcal{M}^\theta_\ell}}{\eta^2(\mathcal{M}^\theta_\ell)}\eta^2(\mathcal{T}_\ell).\end{aligned}$$

The assertion (1.23) follows from the error estimate (1.8) and taking the square root. □

Remark 1.5.3 (Local residual optimization)**.** *The use of the local residual liftings $r^{\mathbf{a},h}$ and $r^{\mathbf{a},p}$ from Definitions 1.4.1 and 1.4.2 respectively in the hp-decision criterion (1.17) on marked vertices is motivated by the result of Theorem 1.5.2. Indeed, suppose that $r^{\mathbf{a},h}$ is larger than $r^{\mathbf{a},p}$ in norm, and that only h-refinement is performed in the subdomain $\omega^{\mathbf{a}}_\ell$ at the end of Algorithm 2. Then, the local residual $r^{\mathbf{a},hp}$ from Lemma 1.5.1 coincides with $r^{\mathbf{a},h}$ which means that by flagging the marked vertex $\mathbf{a}$ for h-refinement, one maximizes the contribution $\|\nabla r^{\mathbf{a},hp}\|^2_{\omega^{\mathbf{a}}_\ell}$ in the numerator of (1.22) defining $\underline{\eta}_{\mathcal{M}^\theta_\ell}$. It is also possible to design a more complex hp-refinement strategy exploiting directly (1.23). Here we simply stick to Algorithm 2 which in our numerical experiments reported in Section 1.6 leads to exponential convergence rates.*

Remark 1.5.4 (Sharper bound)**.** *Theorem 1.5.2 obviously also holds true with the slightly sharper constant* $C_{\mathrm{red}} = \sqrt{1 - \frac{\eta^2_{\mathcal{M}_\ell^\theta}}{\eta^2(\mathcal{T}_\ell)}}$*. This is equivalent to considering in (1.23)* θ_ℓ *such that* $\eta(\mathcal{M}_\ell^\theta) = \theta_\ell\, \eta(\mathcal{T}_\ell)$ *in place of* θ*, a strategy adopted in the numerical experiments in Section 1.6 below. We note that* $\theta_\ell \geq \theta$*, however employing* θ_ℓ *in Algorithm 1 would lead to the same set of marked simplices* $\mathcal{M}_\ell^{\theta_\ell} = \mathcal{M}_\ell^\theta$*.*

1.6 Numerical experiments

We consider two test cases for the model problem (1.1), both in two space dimensions, one with a (relatively) smooth weak solution and one with a singular weak solution. Our main goal with the numerical experiments is to verify that the *hp*-refinement strategy of Algorithm 2 leads to an exponential rate of convergence with respect to the number of degrees of freedom DoF_ℓ of the finite element spaces V_ℓ in the form

$$\|\nabla(u - u_\ell)\| \leq C_1 \exp\left(-C_2 \mathrm{DoF}_\ell^{\frac{1}{3}}\right), \tag{1.24}$$

with positive constants C_1, C_2 independent of DoF_ℓ. In addition, we assess the sharpness of the guaranteed bound on the reduction factor C_{red} from Theorem 1.5.2 by means of the effectivity index defined as

$$I_{\mathrm{red}}^{\mathrm{eff}} = \frac{C_{\mathrm{red}}}{\frac{\|\nabla(u-u_{\ell+1})\|}{\|\nabla(u-u_\ell)\|}}. \tag{1.25}$$

We always consider the (well-established) choice $\theta = 0.5$ for the marking parameter, fine-tuning it on each step to θ_ℓ as described in Remark 1.5.4. As mentioned above, we apply the newest vertex bisection algorithm (Sewell (1972)) to perform *h*-refinement and we use the polynomial-degree increment (1.16) to perform *p*-refinement.

We compare the performance of our *hp*-refinement algorithm to two other algorithms based on a different *hp*-decision criteria, namely the PARAM and PRIOR criteria from the survey paper by Mitchell and McClain (2014) which are both based on a local smoothness estimation. These criteria hinge on the local L^2-orthogonal projection u_ℓ^{p-1} of the numerical solution u_ℓ onto the local lower-polynomial-degree space $\mathbb{P}_{p_{\ell,K}-1}(K)$ for all the marked simplices $K \in \mathcal{M}_\ell^\theta$. This leads to the local quantity $\eta_K^{p-1} := \|\nabla(u_\ell - u_\ell^{p-1})\|_K$; in case of $p_{\ell,K} = 1$, when the quantity η_K^{p-1} is not available, for both criteria, the marked simplex K is *p*-refined. The criterion PARAM, proposed in Gui and Babuška (1986a), relies on the local smoothness indicator $g_K := \eta_K/\eta_K^{p-1}$ and a user-defined parameter $\gamma > 0$; the marked simplex K is *h*-refined if $g_K > \gamma$, and otherwise it is *p*-refined. The presence of the parameter γ is a drawback of this criterion; in our experiments we use the values $\gamma = 0.3$ and $\gamma = 0.6$,

as suggested in Mitchell and McClain (2014). The criterion PRIOR, which is a simplified version of the one proposed in Süli et al. (2000), relies on the quantity $s_K := 1 - \log(\eta_K/\eta_K^{p-1})/\log(p_{\ell,K}/(p_{\ell,K}-1))$; the marked simplex K is h-refined if $p_{\ell,K} > s_K - 1$, and otherwise it is p-refined. To make the comparison with our approach more objective, we apply for both criteria the suggested p-refinement only to those simplices such that $p_{\ell,K} = \min_{K' \in \mathcal{T}_\mathtt{a}} p_{\ell,K'}$.

1.6.1 Smooth solution (sharp Gaussian)

We consider a square domain $\Omega = (-1,1) \times (-1,1)$ and a weak solution that is smooth but has a rather sharp peak

$$u(x,y) = (x^2-1)(y^2-1)\exp\left(-100(x^2+y^2)\right).$$

We start from a criss-cross initial mesh $\mathcal{T}_0$ with $\max_{K\in\mathcal{T}_0} h_K = 0.25$ and a uniform polynomial-degree distribution equal to 1 on all triangles.

Figure 1.6 presents the final mesh and polynomial-degree distribution obtained after 30 steps of the hp-adaptive procedure (1.2) (left panel) along with the obtained numerical solution (right panel). Figure 1.7 displays the relative error $\|\nabla(u-u_\ell)\|/\|\nabla u\|$ as a function of $\mathrm{DoF}_\ell^{\frac{1}{3}}$ in logarithmic-linear scale to illustrate that the present hp-adaptive procedure leads to an asymptotic exponential rate of convergence. The values of the constants C_1 and C_2 from (1.24) given by the 2-parameter least squares fit are 3.97 and 0.70, respectively. The value of C_2 indicates the slope steepness of the fitted line in logarithmic-linear scale, in particular, the higher value of C_2, the steeper slope. For comparison, we also plot the relative error obtained when using the hp-decision criteria PRIOR and PARAM described above and also for the pure h-version of the adaptive loop. The quality of the a posteriori error estimators of Theorem 1.3.2 throughout the whole hp-adaptive process can be appreciated in Figure 1.8 where the effectivity indices, defined as the ratio of the error estimator $\eta(\mathcal{T}_\ell)$ and the actual error $\|\nabla(u-u_\ell)\|$, are presented. Then, in Figure 1.9 we compare the actual and estimated error distributions on iteration $\ell = 20$ of the adaptive loop, showing excellent agreement. Figure 1.10 (left panel) presents the effectivity index for the reduction factor C_{red}, see (1.25), throughout the adaptive process. Overall, values quite close to one are obtained, except at some of the first iterations where the values are larger but do not exceed 2.5. Moreover, all the values are larger than one, confirming that the bound on the reduction factor C_{red} is indeed guaranteed. Figure 1.10 (right panel) examines the quality of the lower bound $\underline{\eta}_{\mathcal{M}_\ell^\theta}$ from Lemma 1.5.1 by plotting the ratio of the left-hand side to the right-hand side of the lower bound in (1.22). Except for one iteration where this ratio takes a larger value close to 4.5, we observe that this ratio takes always values quite close to, and larger than, one, indicating that $\underline{\eta}_{\mathcal{M}_\ell^\theta}$ delivers a sharp and guaranteed lower bound on the energy error decrease. To give some further insight into the pro-

posed *hp*-adaptive process, we present in Tables 1.1 and 1.2 some details on the *hp*-refinement decisions throughout the first 10 and the last 10 iterations of the adaptive loop. Finally, Table 1.5 (top) compares the different strategies namely in terms of the number of iterations of the adaptive loop (1.2); here our strategy is a clear winner.

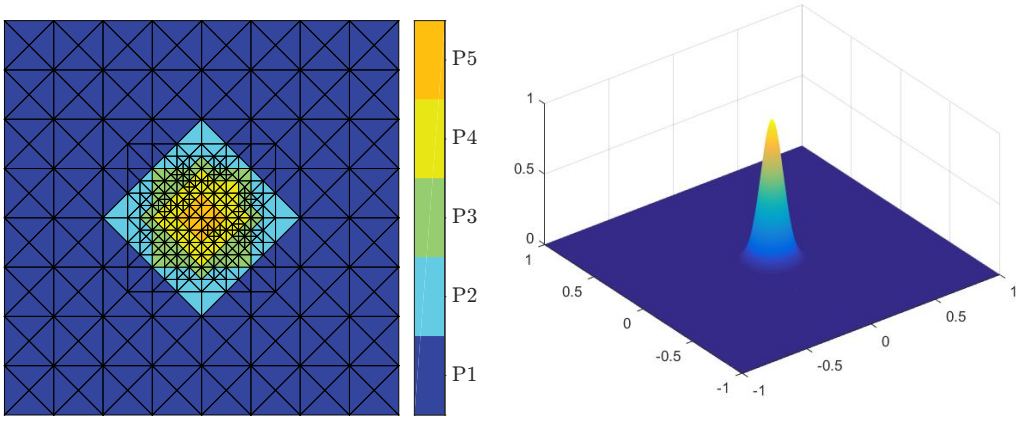

Figure 1.6: [Sharp-Gaussian of Section 1.6.1] The final mesh and polynomial-degree distribution obtained after 30 iterations of the *hp*-adaptive procedure (*left*) and the obtained numerical solution u_{30} (*right*).

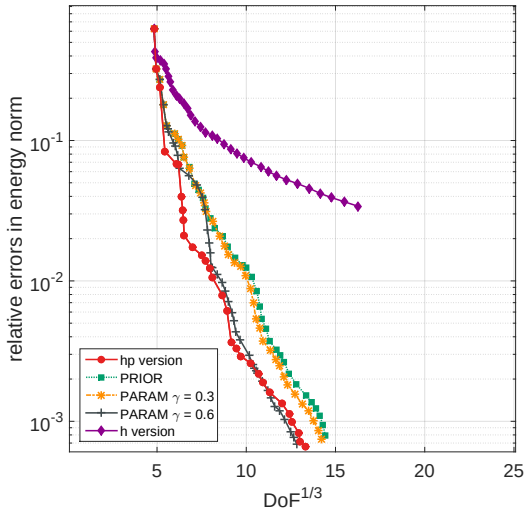

Figure 1.7: [Sharp-Gaussian of Section 1.6.1] Relative energy error $\|\nabla(u-u_\ell)\|/\|\nabla u\|$ as a function of $\mathrm{DoF}_\ell^{\frac{1}{3}}$, obtained using the present *hp*-decision criterion, the criteria PRIOR and PARAM ($\gamma = 0.3$, $\gamma = 0.6$), and using only *h*-refinement.

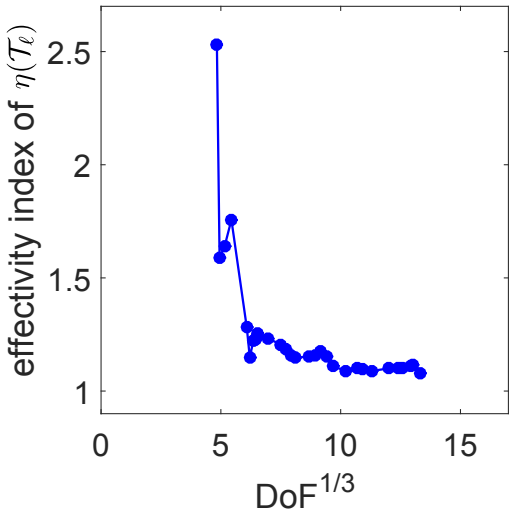

Figure 1.8: [Sharp-Gaussian of Section 1.6.1] Effectivity indices of the error estimators $\eta(\mathcal{T}_\ell)$ from Theorem 1.3.2, defined as the ratio $\eta(\mathcal{T}_\ell)/\|\nabla(u-u_\ell)\|$, throughout the hp-adaptive procedure.

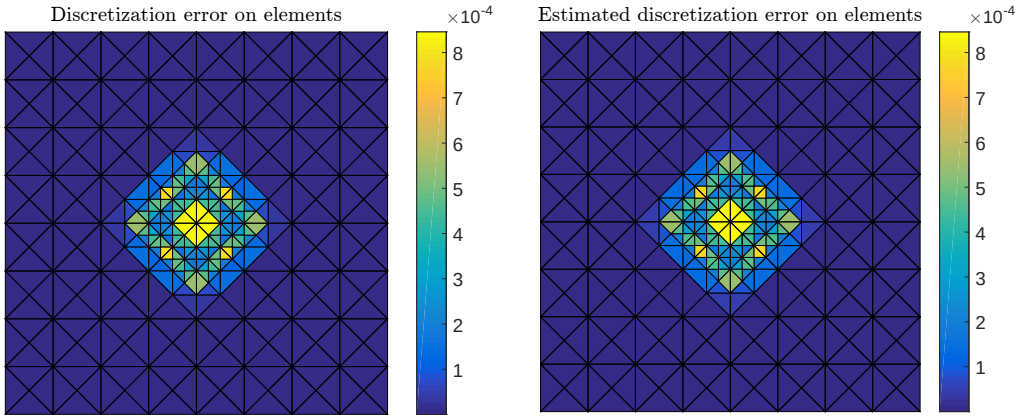

Figure 1.9: [Sharp-Gaussian of Section 1.6.1] The distribution of the energy error $\|\nabla(u-u_\ell)\|_K$ (*left*) and of the error estimators η_K from Theorem 1.3.2 (*right*), $\ell = 20$. The effectivity index of the estimate defined as $\eta(\mathcal{T}_{20})/\|\nabla(u-u_{20})\|$ is 1.1108.

Iteration	1	2	3	4	5	6	7	8	9	10
Triangles	256	256	256	256	264	264	264	264	264	264
Maximal polynomial degree	1	2	3	4	4	4	4	4	4	4
Marked vertices	1	1	1	1	2	2	2	1	1	1
Triangles flagged for h-refinement	0	0	0	8	0	0	0	0	0	8
Triangles flagged for p-refinement	8	8	8	0	12	12	4	2	2	0
Triangles flagged for hp-refinement	0	0	0	0	0	0	0	0	0	0

Table 1.1: [Sharp-Gaussian of Section 1.6.1] Refinement decisions in Algorithm 2 during the first 10 iterations of the adaptive loop (1.2).

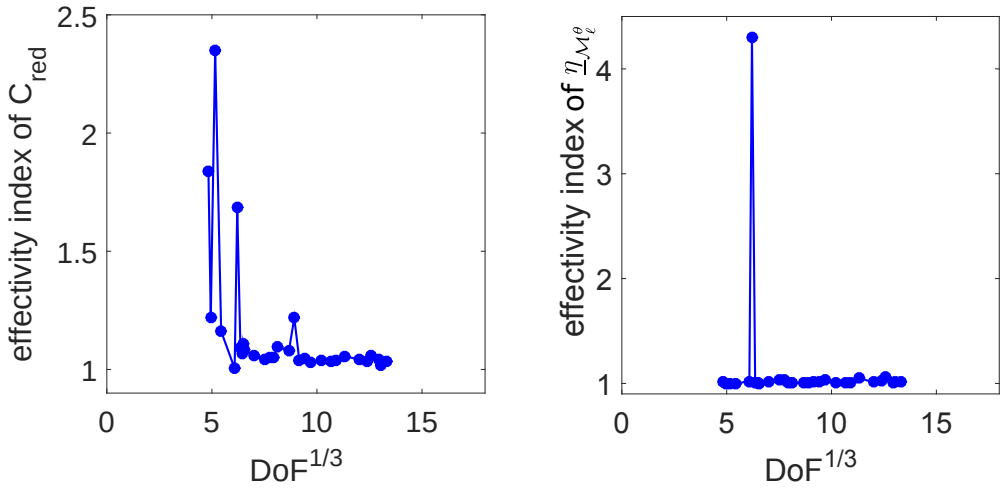

Figure 1.10: [Sharp-Gaussian of Section 1.6.1] Effectivity indices (1.25) for the error reduction factor C_{red} from Theorem 1.5.2 (*left*) and effectivity indices for the lower bound $\underline{\eta}_{\mathcal{M}_\ell^\theta}$ from Lemma 1.5.1 defined as the ratio $\|\nabla(u_{\ell+1}-u_\ell)\|_{\omega_\ell}/\underline{\eta}_{\mathcal{M}_\ell^\theta}$ (*right*).

Iteration	20	21	22	23	24	25	26	27	28	29
Triangles	392	406	430	450	478	514	552	580	612	612
Maximal polynomial degree	5	5	5	5	5	5	5	5	5	5
Marked vertices	2	3	3	3	4	3	2	3	4	4
Triangles flagged for h-refinement	12	24	16	24	30	23	14	21	0	28
Triangles flagged for p-refinement	0	0	4	0	0	0	0	0	16	0
Triangles flagged for hp-refinement	0	0	0	0	0	0	0	0	0	0

Table 1.2: [Sharp-Gaussian of Section 1.6.1] Refinement decisions in Algorithm 2 during the last 10 iterations of the adaptive loop (1.2).

1.6.2 Singular solution (L-shape domain)

In our second test case, we consider the L-shape domain $\Omega = (-1,1)\times(-1,1)\setminus[0,1]\times[-1,0]$ with $f=0$ and the exact solution (in polar coordinates)

$$u(r,\varphi) = r^{\frac{2}{3}}\sin\left(\frac{2\varphi}{3}\right).$$

For this test case, following (Dolejší et al., 2016, Theorem 3.3) and the references therein, the error estimator $\eta(\mathcal{T}_\ell)$ employed within the adaptive procedure takes into account also the error from the approximation of the inhomogeneous Dirichlet boundary condition prescribed by the exact solution on $\partial\Omega$. We start the computation on a criss-cross grid $\mathcal{T}_0$ with $\max_{K\in\mathcal{T}_0} h_K = 0.25$ and all the polynomial degrees set uniformly to 1.

Figure 1.11 presents the final mesh and polynomial-degree distribution after 65 steps of the hp-adaptive procedure (1.2) (left panel) along with a zoom

in the window $[-10^{-6}, 10^{-6}] \times [-10^{-6}, 10^{-6}]$ near the re-entrant corner (right panel). Figure 1.12 (left panel) displays the relative error $\|\nabla(u - u_\ell)\|/\|\nabla u\|$ as a function of $\mathrm{DoF}_\ell^{1/3}$ in logarithmic-linear scale to illustrate that, as in the previous test case, the present *hp*-adaptive procedure leads to an asymptotic exponential rate of convergence. The corresponding values of constants C_1 and C_2 in expression (1.24) obtained by the 2-parameter least squares fit are 4.73 and 0.69, respectively. For the direct comparison with other methods, we refer to the long version (Mitchell and McClain, 2011, Table 15) of the survey paper Mitchell and McClain (2014). However, note that data sets of greater sizes than in our case have been used for the least squares fitting therein. A detailed view when the error takes lower values is provided in the right panel of Figure 1.12. We also plot the relative errors obtained when using the *hp*-decision criteria PRIOR and PARAM, as well as those obtained using APRIORI criterion exploiting the a priori knowledge of the exact solution (marked simplices are *h*-refined only if they touch the corner singularity, otherwise they are *p*-refined). In addition, we provide also the relative errors obtained by employing the (non-adaptive) strategy which we refer to as LINEAR, inspired by the theoretical results for the one-dimensional problem with singular solution Gui and Babuška (1986b,a), Szabó and Babuška (1991). When employing this strategy, we start from a coarse grid $\mathcal{T}_0$ with $\max_{K\in\mathcal{T}_0} h_K = 0.5$. At each iteration, only the patch containing the re-entrant corner is *h*-refined. Thus, the elements of each mesh $\mathcal{T}_\ell$, $\ell \geq 1$, decrease in size in geometric progression (in our case with factor 0.5) toward the re-entrant corner. For each $\mathcal{T}_\ell$, $\ell \geq 1$, we group the elements in layers $\mathcal{L}_1, \mathcal{L}_2, \ldots, \mathcal{L}_{m(\ell)}$ depending on their distance from the origin ($\mathcal{L}_1$ containing the singularity), such that $\mathcal{T}_\ell = \bigcup_{i=1}^{m(\ell)} \mathcal{L}_i$. The total number of layers $m(\ell)$ depends on how many times the current mesh $\mathcal{T}_\ell$ has been refined. Each element $K \in \mathcal{T}_\ell$ is then assigned a polynomial degree $p_{\ell,K}$ layer-wise, increasing linearly away from the singularity, in the way

$$p_{\ell,K} := \left\lceil 1 + \frac{(i-1)}{3} \right\rceil,$$

where i is the index of the layer $\mathcal{L}_i$ containing the element K. For the strategy APRIORI (Figure 1.13) and the strategy LINEAR (Figure 1.14), we illustrate also the resulting polynomial-degree distribution at the step when the relative error reaches 10^{-5}. As for the previous test case, in Figure 1.15 we illustrate the quality of the error estimator from Theorem 1.3.2 in terms of the effectivity index $\eta(\mathcal{T}_\ell)/\|\nabla(u - u_\ell)\|$ throughout all the iterations of the present *hp*-adaptive process. Figure 1.16 then compares the actual and estimated error distributions on iteration $\ell = 45$ of the adaptive loop, showing excellent agreement. Figure 1.17 (left panel) presents the effectivity index for the reduction factor C_{red}, see (1.25), throughout the adaptive process, whereas the right panel of Figure 1.17 examines the quality of the lower bound $\underline{\eta}_{\mathcal{M}_\ell^\theta}$ from Lemma 1.5.1 by plotting the ratio of the left-hand side to the right-hand

side of the lower bound in (1.22). For both quantities, we can draw similar conclusions to the previous test case, thereby confirming that sharp estimates on the error reduction factor are available. Additional numerical experiments (not shown here) indicate that the lower bound estimate can be made even sharper by performing h-refinement so as to satisfy the interior node property. Finally, to give some further insight into the hp-adaptive process, we present in Tables 1.3 and 1.4 some details on the hp-refinement decisions made by the proposed hp-refinement criterion during the first 10 and the last 10 iterations of the adaptive loop. We observe that in the initial iterations, where the underlying mesh is still rather coarse, the polynomial degree is increased also on the simplices touching the re-entrant corner. Nevertheless, this decision does not occur anymore later when the mesh around the singularity is already more strongly refined than in the rest of the domain. Therefore, an improvement of our approach is expected, as suggested in Canuto et al. (2017a), in conjunction with an appropriate coarsening strategy correcting the excessive p-refinement in the early stages. Table 1.5 (bottom) again brings some additional comparisons with other strategies in terms of number of iterations and number of degrees of freedom necessary to reach relative error 10^{-5}. We observe that the results achieved using the present strategy are comparable with those achieved by other (established) strategies.

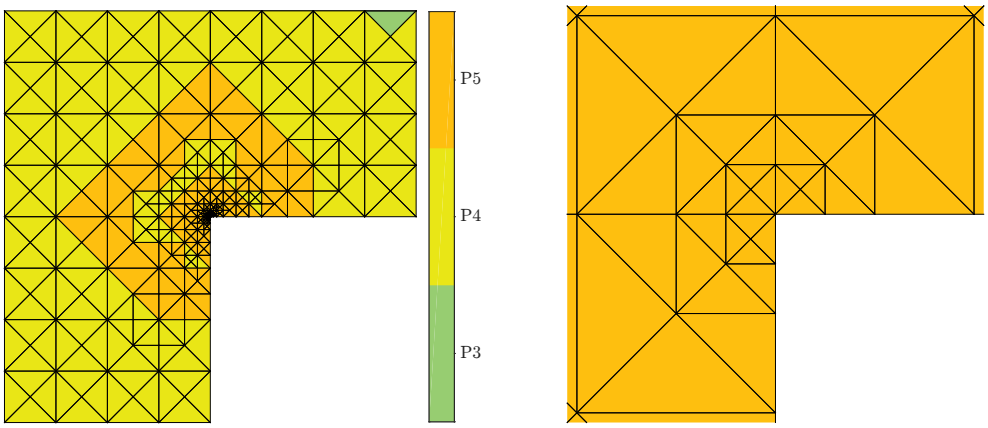

Figure 1.11: [L-shape domain of Section 1.6.2] The final mesh and polynomial-degree distribution obtained after 65 iterations of the hp-adaptive procedure (*left*) and a zoom in $[-10^{-6}, 10^{-6}] \times [-10^{-6}, 10^{-6}]$ near the re-entrant corner (*right*).

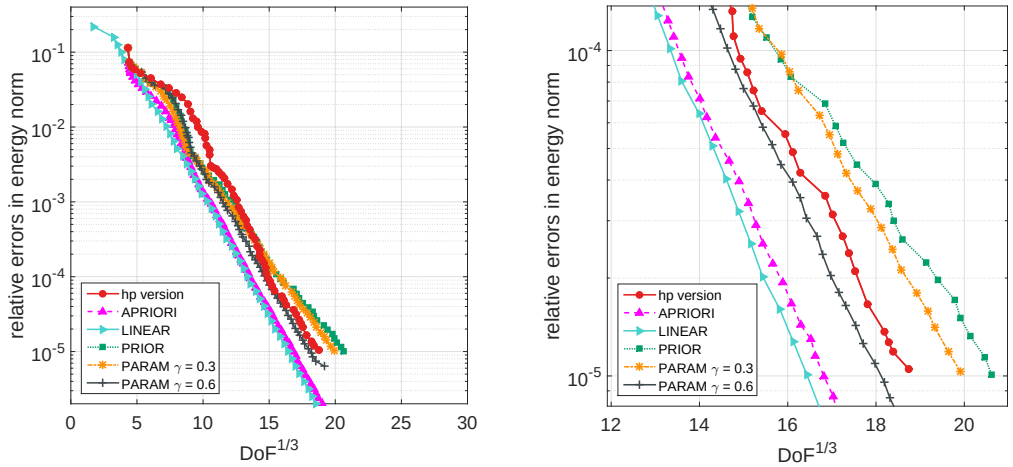

Figure 1.12: [L-shape domain of Section 1.6.2] Relative energy error $\|\nabla(u-u_\ell)\|/\|\nabla u\|$ as a function of $\mathrm{DoF}_\ell^{\frac{1}{3}}$, obtained using the present *hp*-decision criterion, the criteria PRIOR and PARAM ($\gamma = 0.3$ and $\gamma = 0.6$), the APRIORI, and LINEAR strategy (*left*) and a detailed view (*right*).

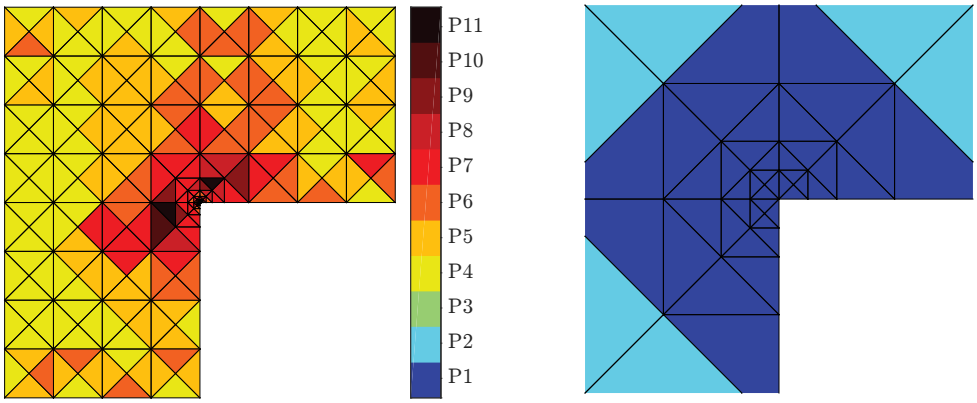

Figure 1.13: [L-shape domain of Section 1.6.2] Mesh and polynomial-degree distribution obtained after 70 iterations (when the relative error reaches 10^{-5}) of the adaptive procedure employing the APRIORI *hp*-strategy (*left*) and a zoom in $[-10^{-7}, 10^{-7}] \times [-10^{-7}, 10^{-7}]$ near the re-entrant corner (*right*).

Iteration	1	2	3	4	5	6	7	8	9	10
Triangles	192	192	192	192	192	198	204	210	216	222
Maximal polynomial degree	1	2	3	4	5	5	5	5	5	5
Marked vertices	1	1	1	2	2	3	4	4	6	6
Triangles flagged for *h*-refinement	0	0	0	0	6	6	6	6	6	6
Triangles flagged for *p*-refinement	6	6	6	12	6	12	16	18	16	18
Triangles flagged for *hp*-refinement	0	0	0	0	2	0	0	0	0	0

Table 1.3: [L-shape domain of Section 1.6.2] Refinement decisions in Algorithm 2 during the first 10 iterations of the adaptive loop (1.2).

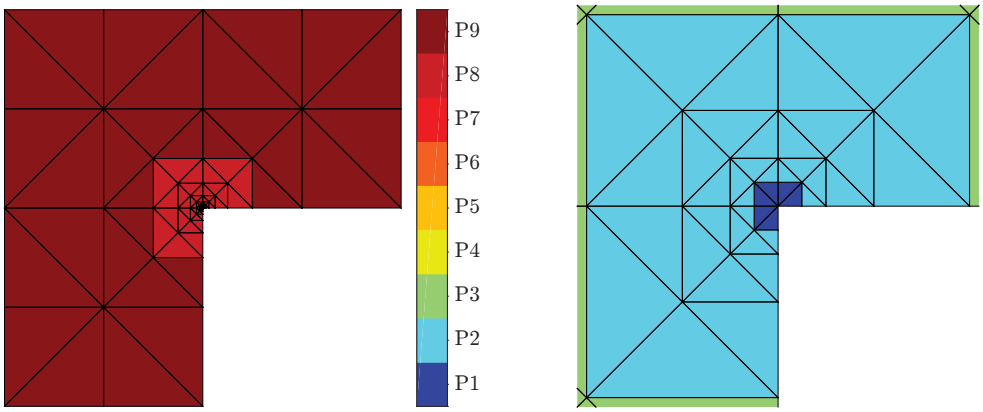

Figure 1.14: [L-shape domain of Section 1.6.2] Mesh and polynomial-degree distribution obtained after 45 iterations (when the relative error reaches 10^{-5}) of the procedure employing the refinement strategy LINEAR (*left*) and a zoom in $[-10^{-6}, 10^{-6}] \times [-10^{-6}, 10^{-6}]$ near the re-entrant corner (*right*).

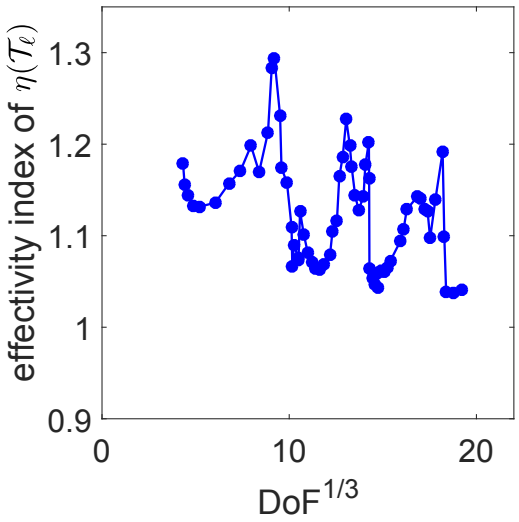

Figure 1.15: [L-shape domain of Section 1.6.2] The effectivity indices of the error estimate $\eta(\mathcal{T}_\ell)$, defined as $\eta(\mathcal{T}_\ell)/\|\nabla(u - u_\ell)\|$, throughout the 65 iterations of the present *hp*-adaptive procedure.

Iteration	56	57	58	59	60	61	62	63	64	65
Triangles	492	512	518	524	538	568	574	580	614	660
Maximal polynomial degree	5	5	5	5	5	5	5	5	5	5
Marked vertices	4	4	5	4	3	3	3	4	5	5
Triangles flagged for *h*-refinement	16	6	6	6	18	6	6	28	30	32
Triangles flagged for *p*-refinement	8	16	13	22	0	6	6	0	0	8
Triangles flagged for *hp*-refinement	0	0	0	0	0	0	0	0	0	4

Table 1.4: [L-shape domain of Section 1.6.2] Refinement decisions in Algorithm 2 during the last 10 iterations of the adaptive loop (1.2).

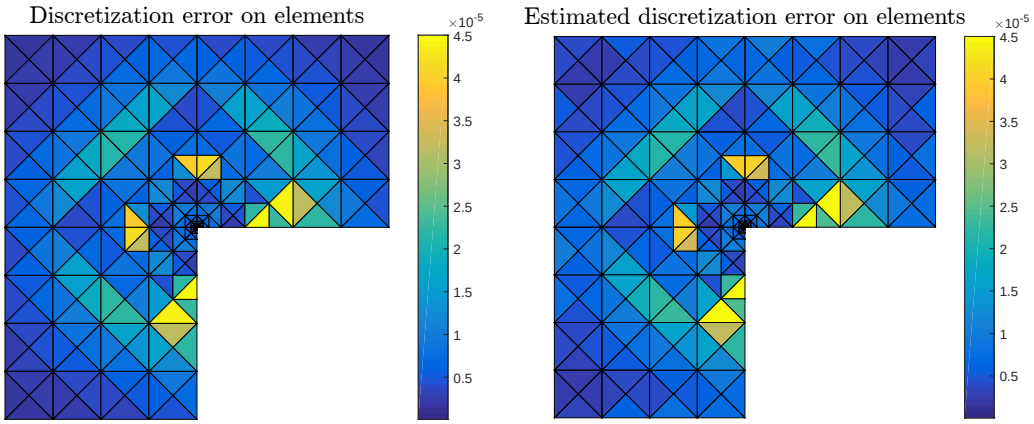

Figure 1.16: [L-shape domain of Section 1.6.2] Distribution of the energy error $\|\nabla(u-u_\ell)\|_K$ (*left*) and of the local error estimators η_K from Theorem 1.3.2 (*right*), $\ell = 45$. The effectivity index of the estimate defined as $\eta(\mathcal{T}_{45})/\|\nabla(u-u_{45})\|$ is 1.0468.

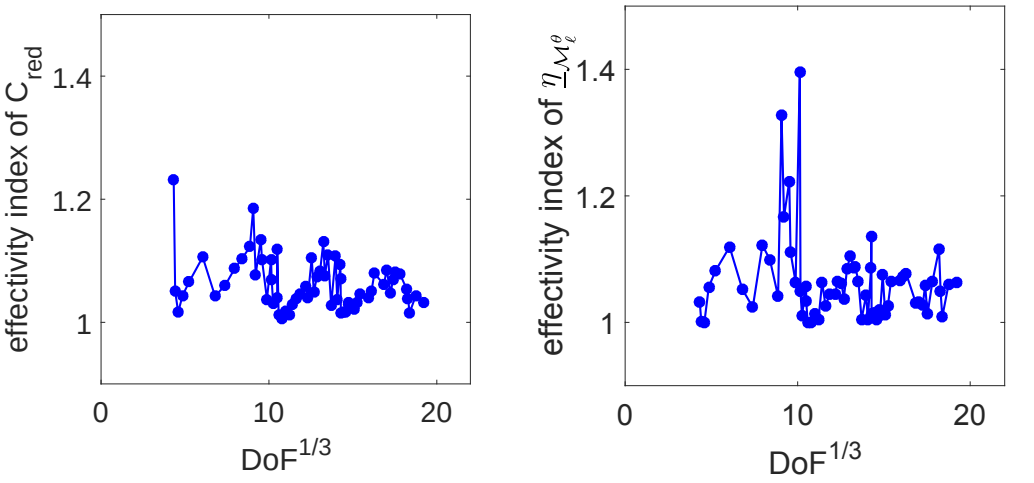

Figure 1.17: [L-shape domain of Section 1.6.2] Effectivity indices (1.25) for the error reduction factor $C_{\rm red}$ from Theorem 1.5.2 (*left*) and effectivity indices for the lower bound $\underline{\eta}_{\mathcal{M}_\ell^\theta}$ from Lemma 1.5.1 defined as the ratio $\|\nabla(u_{\ell+1}-u_\ell)\|_{\omega_\ell} \,/\, \underline{\eta}_{\mathcal{M}_\ell^\theta}$ (*right*).

1.7 Conclusions

In this work, we have devised an hp-adaptive strategy to approximate model elliptic problems using conforming finite elements. Mesh vertices are marked using polynomial-degree-robust a posteriori error estimates based on equilibrated fluxes. Then marked vertices are flagged either for h- or for p-refinement based on the solution of two local finite element problems where local residual liftings are computed. Moreover, by solving a third local finite element problem once the hp-decision has been taken and the next mesh and polynomial-degree distribution have been determined, it is possible to compute

		our	APRIORI	PRIOR	PARAM 0.3	PARAM 0.6
Sharp Gaussian	iter	27	–	37	36	40
(relative error 10^{-3})	$\mathrm{DoF}^{1/3}$	12.56	–	14.29	14.06	12.49
L-shape domain	iter	65	70	68	67	68
(relative error 10^{-5})	$\mathrm{DoF}^{1/3}$	19.24	17.35	20.82	20.07	18.18

Table 1.5: Comparison of the different adaptive *hp*-strategies in terms of the number of iterations of the loop (1.2) and of the number of degrees of freedom necessary to reach the given relative error for model problems of Sections 1.6.1 and 1.6.2.

a guaranteed bound on the error reduction factor. Our numerical experiments featuring two-dimensional smooth and singular weak solutions indicate that the present *hp*-adaptive strategy leads to asymptotic exponential convergence rates with respect to the total number of degrees of freedom employed to compute the discrete solution. Moreover, our bound on the error reduction factor appears to be, in most cases, quite sharp. Several extensions of the present work can be considered. On the theoretical side, it is important to prove that our bound on the reduction factor C_{red} is smaller than one and to study how it depends on the mesh-size and especially on the polynomial degree. On the numerical side, three-dimensional test cases and taking into account an inexact algebraic solver are on the agenda. We note that the use of anisotropic *h*- and *p*-refinements may become mandatory while applying the proposed methodology to three-dimensional problems or more general two-dimensional problems, such as, for instance, convection-dominated problems.

Chapter 2

An adaptive *hp*-refinement strategy with inexact solvers and computable guaranteed bound on the error reduction factor

We expose in this chapter the results of the article Daniel et al. (2018b), submitted for publication. This work was done in collaboration with Alexandre Ern and Martin Vohralík.

Contents

Abstract

In this work we extend our recently proposed adaptive refinement strategy for *hp*-finite element approximations of elliptic problems by taking into account an inexact algebraic solver. Namely, on each level of refinement and on each iteration of an (arbitrary) iterative algebraic solver, we compute guaranteed a posteriori error bounds on the algebraic and the total errors in energy norm. For the algebraic error upper bound, we crucially exploit the nested hierarchy of *hp*-finite element spaces created throughout the adaptive algorithm, whereas the rest of the components of the total error upper and lower bounds are computed using the finest space only. These error bounds allow us to formulate adaptive stopping criteria for the algebraic solver ensuring that the algebraic error does not significantly contribute to the total error. Next, we use the total error bound to mark mesh vertices for refinement via Dörfler's bulk-chasing criterion. On patches associated with marked vertices only, we solve two separate primal finite element problems with homogeneous Dirichlet (Neumann) boundary conditions, which serve to decide between *h*-, *p*-, or *hp*-refinement. Altogether, we show that these ingredients lead to a computable guaranteed bound on the ratio of the total errors of the inexact approximations between successive refinements (the error reduction factor), when the stopping criteria are satisfied. Finally, in a series of numerical experiments, we investigate the practicality of the proposed adaptive solver, the accuracy of our bound on the reduction factor, and show that exponential convergence rates are also achieved even in the presence of an inexact algebraic solver.

2.1 Introduction

The adaptive finite element method (AFEM), developed back in the 1980s (see e.g. Gui and Babuška (1986b,a), Babuška and Guo (1986a,b)), is still one of the fundamental and widely used numerical methods for solving the boundary value problems arising in physics or engineering sciences. In short, it can be described as a numerical method which automatically, in an iterative fashion, adapts the employed finite element space until a sufficiently accurate approximation of the solution is obtained. For an overview and further insight, we refer the reader to work of Nochetto et al. (2009), and the references therein.

In the vast majority of the publications, the resulting linear systems are assumed to be solved *exactly*. However, in practical applications, including large scale numerical computations, the exact solve is not feasible in most cases; it may actually be greatly advantageous to employ an *inexact* (iterative) algebraic solver. The incorporation of an inexact algebraic solver, as an alternative to the use of (sparse) direct solvers, within the AFEM framework and its rigorous analysis is rather an exception. It has been addressed by Stevenson (2005a, 2007), Becker and Mao (2009), Becker et al. (2010), Arioli et al. (2013a,b) for linear elliptic problems and by Holst et al. (2013), Carstensen et al. (2014) and Gantner et al. (2017) for nonlinear elliptic problems, all in the context of the *h*-AFEM. We also mention the work of Becker et al. (1995), where the authors deal with the issue of settling an objective stopping criterion for a multigrid iterative solver, and the work of Ern and Vohralík (2013) where the authors devise a posteriori stopping criteria for inexact Newton methods and iterative linear solvers in the context of diffusion PDEs.

The main goal of this chapter is to extend the *hp*-adaptive refinement strategy with *computable guaranteed bound on the error reduction factor* recently proposed by Daniel et al. (2018a) to approximate elliptic problems by taking into account an inexact algebraic iterative solver inside the adaptive loop. In this work, we consider as a model problem the Poisson equation with homogeneous Dirichlet boundary conditions. Let $\Omega \subset \mathbb{R}^d$, $d = 2, 3$, be a polytopal domain (open, bounded and connected set) with a Lipschitz boundary $\partial\Omega$. The model problem in its weak form reads as follows: Seek $u \in H_0^1(\Omega)$, such that

$$(\nabla u, \nabla v) = (f, v) \qquad \forall v \in H_0^1(\Omega), \tag{2.1}$$

where $H_0^1(\Omega)$ denotes the Sobolev space of all functions in $L^2(\Omega)$ which have all their first-order weak derivatives in $L^2(\Omega)$ and a vanishing trace on $\partial\Omega$, and $(\cdot, \cdot)$ stands for the $L^2(\Omega)$ or $[L^2(\Omega)]^d$ inner product. We employ the conforming *hp*-finite element method to discretize the model problem (2.1) on a matching (no hanging nodes) simplicial mesh. The well-established paradigm of the adaptive iterative procedures, used by Daniel et al. (2018a) as well, comprises at each step the four independent, but concatenated, modules, see Scheme 2.1. The module `SOLVE`, as already mentioned, usually stands for rather unrealistic

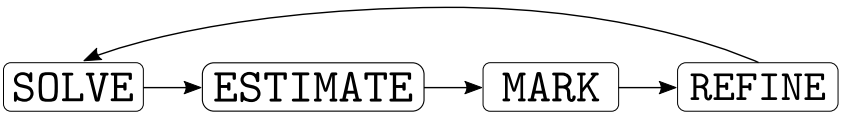

Scheme 2.1: Paradigm of an adaptive loop with exact algebraic solver.

exact (up to machine precision) solution of the underlying, possibly very large and/or ill-conditioned, linear algebraic problem. Thus, we opt to replace the module `SOLVE` in Scheme 2.1 by the module `ONE_SOLVER_STEP` coupled directly together with the module `ESTIMATE` in an adaptive sub-loop. This is

conceptually described in Scheme 2.2.

Scheme 2.2: Paradigm of an adaptive loop employing an inexact algebraic solver.

The ONE_SOLVER_STEP in Scheme 2.2 stands for performing only one (or a certain small number of) iteration(s) of the iterative solver to the resulting algebraic system. The obtained inexact solution is then immediately analyzed within the ESTIMATE module which now distinguishes the *algebraic error* and the *total error*. The interplay between the modules ONE_SOLVER_STEP and ESTIMATE, which is indicated by the forward and backward arrows between them in Scheme 2.2, corresponds to the progressive improvement of the current approximate solution by performing additional iteration(s) of the algebraic solver within module ONE_SOLVER_STEP with the immediate calls of module ESTIMATE. Our present choice of the module ESTIMATE amounts to a natural extension of the developments of algebraic a posteriori error bounds via a *multilevel approach* by Papež et al. (2017) to the present setting with variable polynomial degree. The adaptive sub-loop is piloted by a tailored *adaptive stopping criterion*, namely, we stop at the moment when we are sure that the algebraic error lies below the total error.

The remaining two modules extend the workflow of the strategy proposed by Daniel et al. (2018a). The module MARK refers to applying a bulk-chasing criterion inspired by the well-known Dörfler's marking (see Dörfler (1996)); we mark mesh vertices and not simplices since we observe a smoother performance in practice and since we later work with some vertex-based auxiliary quantities. The module REFINE, including our *hp*-decision criterion, then proceeds in three steps. First, we solve two local finite element problems on each patch of simplices attached to a mesh vertex marked for refinement, with either the mesh refined or the polynomial degree increased. These conforming residual liftings allow us, in particular, to estimate the effect of applying *h*- or *p*-refinement, and lead to a partition of the set of marked vertices into two disjoint subsets, one collecting the mesh vertices flagged for *h*-refinement and the other collecting the mesh vertices flagged for *p*-refinement. The second step of the module REFINE uses these two subsets to flag the simplices for *h*-, *p*-, or *hp*-refinement. Finally, the third step of the module REFINE uses the above sets of flagged simplices to build the next simplicial mesh and the next polynomial-degree distribution.

We are particularly interested in recovering the computable guaranteed bound on the error reduction factor introduced in Daniel et al. (2018a) also in the inexact setting described in Scheme 2.2, and for this reason our bounds are

derived using various equilibrated flux reconstructions in the spirit of Ern and Vohralík (2013). One of the main contributions of the present work is to show that using a properly designed stopping criterion for the algebraic solver, see Section 2.4.3, it is possible, at the end of each iteration of the inexact adaptive loop given in Scheme 2.2, to compute a real number $C_{\mathrm{red}} \in [0,1]$ such that

$$\|\nabla(u - u_{\ell+1})\| \leq C_{\mathrm{red}} \|\nabla(u - u_\ell)\|, \tag{2.2}$$

where u is the unknown weak solution of (2.1), u_ℓ and $u_{\ell+1}$ are its discrete inexact approximations on step ℓ, and $\ell+1$ respectively, of the adaptive loop of Scheme 2.2. Note that in (2.2), the inexact solution u_ℓ on the ℓ-th iteration is at our disposal while the weak solution u and the next level's inexact solution $u_{\ell+1}$ are unknown. The number C_{red} is fully computable, giving a guaranteed upper bound on the ratio of the total errors of the *inexact approximations* between two successive refinements.

The rest of this chapter is organized as follows: in Section 2.2 we specify the discrete setting and some useful notation, in particular, concerning the inexact finite element approximation. In Section 2.3, we introduce the theoretical background of the a posteriori error bounds computed later within our `ESTIMATE` module. The overall description of all the modules of the proposed inexact *hp*-adaptive algorithm follows in Section 2.4. The result on a computable guaranteed bound on the reduction factor in the inexact setting is given in Section 2.5. Section 2.6 illustrates our theoretical findings and applicability of the proposed strategy with numerical experiments carried out on two-dimensional test cases. Finally, conclusions are drawn in Section 2.7.

2.2 Setting and notation

While using the adaptive loop of Scheme 2.2 a sequence of discrete finite element spaces $\{V_\ell\}_{\ell\geq 0}$, with $\ell \geq 0$ the iteration counter, is generated. We enforce the H_0^1-conformity $V_\ell \subset H_0^1(\Omega)$ for all $\ell \geq 0$ and make the following nestedness assumption:

$$V_\ell \subset V_{\ell+1}, \qquad \forall \ell \geq 0. \tag{2.3}$$

Each space V_ℓ is built up on the pair $(\mathcal{T}_\ell, \mathbf{p}_\ell)$, where $\mathcal{T}_\ell$ denotes a matching simplicial mesh of the computational domain Ω, i.e. a finite collection of (closed) non-overlapping simplices $K \in \mathcal{T}_\ell$ covering $\overline{\Omega}$ exactly and such that the intersection of two different simplices is either empty, a common vertex, a common edge, or a common face, and where the polynomial-degree distribution vector $\mathbf{p}_\ell := \{p_{\ell,K}\}_{K\in\mathcal{T}_\ell}$ assigns a degree $p_{\ell,K} \in \mathbb{N}_{\geq 1}$ to each simplex $K \in \mathcal{T}_\ell$. The conforming finite element space V_ℓ is then defined as

$$V_\ell := \mathbb{P}_{\mathbf{p}_\ell}(\mathcal{T}_\ell) \cap H_0^1(\Omega), \qquad \forall \ell \geq 0, \tag{2.4}$$

where $\mathbb{P}_{\mathbf{p}_\ell}(\mathcal{T}_\ell)$ denotes the space of piece-wise polynomials of total degree at most $p_{\ell,K}$ on each simplex $K \in \mathcal{T}_\ell$. In other words, any function $v_\ell \in V_\ell$ satisfies $v_\ell \in H^1_0(\Omega)$ and $v_\ell|_K \in \mathbb{P}_{p_{\ell,K}}(K)$ for all $K \in \mathcal{T}_\ell$, where $\mathbb{P}_p(K)$ stands for the space of all polynomials of total degree at most p on the simplex K. Let us denote by N_ℓ the dimension of the ℓ-th level space V_ℓ.

The initial coarse mesh and the initial polynomial-degree distribution $(\mathcal{T}_0, \mathbf{p}_0)$ are assumed to be given. The purpose of each step $\ell \geq 0$ of the adaptive loop of Scheme 2.2 is to produce the next pair $(\mathcal{T}_{\ell+1}, \mathbf{p}_{\ell+1})$. The nestedness property (2.3) gives us two restrictions on the meshes and polynomial-degree distributions defining the spaces V_ℓ: (i) the sequence of meshes $\{\mathcal{T}_\ell\}_{\ell\geq 0}$ needs to be *hierarchically nested*, i.e., for all $\ell \geq 1$ the mesh $\mathcal{T}_\ell$ is a refinement of $\mathcal{T}_{\ell-1}$ such that for all $K \in \mathcal{T}_\ell$, there is a unique simplex $\widetilde{K} \in \mathcal{T}_{\ell-1}$, called the parent of K, satisfying $K \subseteq \widetilde{K}$; (ii) The local polynomial degree is *locally increasing*, i.e., for all $\ell \geq 1$ and all $K \in \mathcal{T}_\ell$, $p_{\ell,K} \geq p_{\ell-1,\widetilde{K}}$, where $\widetilde{K} \in \mathcal{T}_{\ell-1}$ is the parent of K. Moreover, we assume the following standard shape-regularity property: There exists a constant $\kappa_\mathcal{T} > 0$ such that $\max_{K\in\mathcal{T}_\ell} h_K/\rho_K \leq \kappa_\mathcal{T}$ for all $\ell \geq 0$, where h_K is the diameter of K and ρ_K is the diameter of the largest ball inscribed in K.

Let us now introduce some additional useful notation. We denote by $\mathcal{V}_\ell$ the set of vertices of $\mathcal{T}_\ell$ decomposed into interior vertices $\mathcal{V}_\ell^{\text{int}}$ and vertices on the boundary $\mathcal{V}_\ell^{\text{ext}}$. For each vertex $\mathbf{a} \in \mathcal{V}_\ell$, $\ell \geq 0$, the so-called hat function $\psi_\ell^{\mathbf{a}}$ is the continuous, piecewise affine function that takes the value 1 at the vertex $\mathbf{a}$ and the value 0 at all the other vertices of $\mathcal{V}_\ell$; the function $\psi_\ell^{\mathbf{a}}$ is in V_ℓ for all $\mathbf{a} \in \mathcal{V}_\ell^{\text{int}}$. Furthermore, we consider the simplex patch $\mathcal{T}_\ell^{\mathbf{a}} \subset \mathcal{T}_\ell$ which is the collection of the simplices sharing the vertex $\mathbf{a} \in \mathcal{V}_\ell$, with $\omega_\ell^{\mathbf{a}}$ the corresponding open subdomain coinciding with the support of $\psi_\ell^{\mathbf{a}}$. Finally, for each simplex $K \in \mathcal{T}_\ell$, $\mathcal{V}_K$ denotes the set of vertices of K.

The Galerkin finite element method constructs an approximation of the weak solution u of (2.1) by solving the problem: Find $u_\ell^{\text{ex}} \in V_\ell$ such that

$$(\nabla u_\ell^{\text{ex}}, \nabla v_\ell) = (f, v_\ell) \qquad \forall v_\ell \in V_\ell. \tag{2.5}$$

The problem (2.5) is equivalent to solving the system of linear algebraic equations

$$\mathbb{A}_\ell \mathrm{U}_\ell^{\text{ex}} = \mathrm{F}_\ell, \tag{2.6}$$

where we employed ψ_ℓ^n, $1 \leq n \leq N_\ell$, the basis of the ℓ-th level space V_ℓ such that $u_\ell^{\text{ex}} := \sum_{n=1}^{N_\ell} (\mathrm{U}_\ell^{\text{ex}})_n \psi_\ell^n$. Hence, $(\mathbb{A}_\ell)_{mn} := (\nabla\psi_\ell^n, \nabla\psi_\ell^m)$ is the symmetric positive-definite stiffness matrix and $(\mathrm{F}_\ell)_m := (f, \psi_\ell^m)$ is the corresponding right-hand side vector.

However, in this work we do not assume that the algebraic system (2.6) is solved exactly (for $\ell \geq 1$). Let us denote by $\mathrm{U}_\ell \in \mathbb{R}^{N_\ell}$ an *arbitrary approximation* to the exact solution $\mathrm{U}_\ell^{\text{ex}}$ of system (2.6), corresponding to a continuous piecewise polynomial $u_\ell = \sum_{n=1}^{N_\ell} (\mathrm{U}_\ell)_n \psi_\ell^n \in V_\ell$. The *algebraic residual vector*

R_ℓ associated with U_ℓ is given by

$$\mathrm{R}_\ell := \mathrm{F}_\ell - \mathbb{A}_\ell \mathrm{U}_\ell. \tag{2.7}$$

Moreover, we introduce its functional representation $\mathfrak{r}_\ell \in \mathbb{P}_{\mathbf{p}_\ell}(\mathcal{T}_\ell)$, $\mathfrak{r}_\ell|_{\partial\Omega} = 0$, i.e. a *discontinuous* polynomial of total degree at most $p_{\ell,K}$ on each $K \in \mathcal{T}_\ell$ vanishing on the boundary $\partial\Omega$ and satisfying

$$(\mathfrak{r}_\ell, \psi_\ell^n) = (\mathrm{R}_\ell)_n \qquad 1 \leq n \leq N_\ell. \tag{2.8}$$

Following (Papež et al., 2018, Section 5.1), we define $\mathfrak{r}_\ell$ in an elementwise manner by prescribing $\mathfrak{r}_\ell|_K \in \mathbb{P}_{p_{\ell,K}}(K)$, $\mathfrak{r}_\ell|_{\partial K \cap \partial\Omega} = 0$ for each simplex $K \in \mathcal{T}_\ell$ individually such that

$$(\mathfrak{r}_\ell, \psi_\ell^n)_K = \frac{(\mathrm{R}_\ell)_n}{N_\ell^n} \qquad \text{for each } \psi_\ell^n \text{ non-vanishing on } K, \tag{2.9}$$

where N_ℓ^n denotes the number of elements forming the support of the basis function ψ_ℓ^n. Note that the property (2.8) together with the definition of the algebraic system (2.6) yield the functional equivalent of algebraic relation (2.7)

$$(\mathfrak{r}_\ell, v_\ell) = (f, v_\ell) - (\nabla u_\ell, \nabla v_\ell) \qquad v_\ell \in V_\ell. \tag{2.10}$$

2.3 Guaranteed total and algebraic a posteriori error bounds

Let the iteration number $\ell \geq 0$ and an arbitrary approximate solution $u_\ell \in V_\ell$ be fixed. In this section we derive the a posteriori error bounds based on equilibrated flux reconstructions by local problems, see e.g. Destuynder and Métivet (1999), Braess et al. (2009), Ern and Vohralík (2015), Dolejší et al. (2016), Ern and Vohralík (2016), adapted to the present setting of conforming *hp*-finite elements. To be more precise, we will follow the concepts from the works of Jiránek et al. (2010), Ern and Vohralík (2013), Rey et al. (2014) and Papež et al. (2017) in order to distinguish in the guaranteed upper bound $\eta(u_\ell, \mathcal{T}_\ell)$ on the *total energy error* $\|\nabla(u - u_\ell)\|$ two different contributions: one serving as the guaranteed upper bound on the *algebraic error* $\|\nabla(u_\ell^{\mathrm{ex}} - u_\ell)\|$, and the rest which corresponds to the *discretization error* $\|\nabla(u - u_\ell^{\mathrm{ex}})\|$. Finally, for the total energy error; we also need to construct a guaranteed lower bound, so that a reliable confidence interval for the true value of $\|\nabla(u - u_\ell)\|$ is at our disposal. The two main ingredients for the error estimators bounding from above the total and the algebraic error in energy norm are an $\mathbf{H}(\mathrm{div}, \Omega)$-conforming *total flux reconstruction* and an $\mathbf{H}(\mathrm{div}, \Omega)$-conforming *algebraic error flux reconstruction*:

Definition 2.3.1 (Total flux reconstruction $\boldsymbol{\sigma}_{\ell,\mathrm{tot}}$)**.** *We call total flux recon-*

struction any function $\boldsymbol{\sigma}_{\ell,\mathrm{tot}}$ *constructed from the approximate solution* u_ℓ *satisfying*

$$\boldsymbol{\sigma}_{\ell,\mathrm{tot}} \in \mathbf{H}(\mathrm{div},\Omega), \tag{2.11a}$$
$$(\nabla\cdot\boldsymbol{\sigma}_{\ell,\mathrm{tot}}, q_\ell)_K = (f, q_\ell)_K \quad \forall K \in \mathcal{T}_\ell, \quad \forall q_\ell \in \mathbb{P}_{p_{\ell,K}}(K). \tag{2.11b}$$

Definition 2.3.2 (Algebraic error flux reconstruction $\boldsymbol{\sigma}_{\ell,\mathrm{alg}}$)**.** *We call algebraic error flux reconstruction any function* $\boldsymbol{\sigma}_{\ell,\mathrm{alg}}$ *constructed from* $\mathfrak{r}_\ell$ *defined in* (2.9)*, which satisfies*

$$\boldsymbol{\sigma}_{\ell,\mathrm{alg}} \in \mathbf{H}(\mathrm{div},\Omega), \tag{2.12a}$$
$$(\nabla\cdot\boldsymbol{\sigma}_{\ell,\mathrm{alg}}, q_\ell)_K = (\mathfrak{r}_\ell, q_\ell)_K \quad \forall K \in \mathcal{T}_\ell, \quad \forall q_\ell \in \mathbb{P}_{p_{\ell,K}}(K). \tag{2.12b}$$

Moreover, as we uncover in Theorem 2.3.3, there exists a natural decomposition of the total flux reconstruction $\boldsymbol{\sigma}_{\ell,\mathrm{tot}}$ from Definition 2.3.1 in the form

$$\boldsymbol{\sigma}_{\ell,\mathrm{tot}} := \boldsymbol{\sigma}_{\ell,\mathrm{alg}} + \boldsymbol{\sigma}_{\ell,\mathrm{dis}}, \tag{2.13}$$

with $\boldsymbol{\sigma}_{\ell,\mathrm{alg}}$ of Definition 2.3.2 and $\boldsymbol{\sigma}_{\ell,\mathrm{dis}} \in \mathbf{H}(\mathrm{div},\Omega)$, the *discretization flux reconstruction*, for which (2.12b) and (2.11b) yield

$$(\nabla\cdot\boldsymbol{\sigma}_{\ell,\mathrm{dis}}, q_\ell)_K = (f - \mathfrak{r}_\ell, q_\ell)_K \quad \forall K \in \mathcal{T}_\ell, \quad \forall q_\ell \in \mathbb{P}_{p_{\ell,K}(K)}. \tag{2.14}$$

Note that unlike in the work Papež et al. (2017), here the properties (2.11b), (2.12b), and (2.14) are imposed on the divergences of the flux reconstructions $\boldsymbol{\sigma}_{\ell,\mathrm{tot}}$, $\boldsymbol{\sigma}_{\ell,\mathrm{alg}}$, and $\boldsymbol{\sigma}_{\ell,\mathrm{dis}}$ only in a weak sense.

Theorem 2.3.3 (Guaranteed upper bound on total and algebraic errors)**.** *Let* $u \in H^1_0(\Omega)$ *be the weak solution of the problem* (2.1) *and* $u_\ell^{\mathrm{ex}} \in V_\ell$ *be its exact finite element approximation given by* (2.5)*. Let* $u_\ell \in V_\ell$ *be arbitrary. Furthermore, let* $\boldsymbol{\sigma}_{\ell,\mathrm{tot}}$, $\boldsymbol{\sigma}_{\ell,\mathrm{alg}}$ *be given by Definitions 2.3.1 and 2.3.2, respectively, and* $\boldsymbol{\sigma}_{\ell,\mathrm{dis}} \in \mathbf{H}(\mathrm{div},\Omega)$ *by* (2.13)*. Then the following upper bound on the energy norm of the total error holds true:*

$$\|\nabla(u - u_\ell)\| \le \eta(u_\ell,\mathcal{T}_\ell) := \left\{\sum_{K\in\mathcal{T}_\ell} \eta_K^2(u_\ell)\right\}^{\frac{1}{2}}, \tag{2.15a}$$
$$\eta_K(u_\ell) := \underbrace{\|\nabla u_\ell + \boldsymbol{\sigma}_{\ell,\mathrm{dis}}\|_K}_{\eta_{\mathrm{dis},K}(u_\ell)} + \underbrace{\|\boldsymbol{\sigma}_{\ell,\mathrm{alg}}\|_K}_{\eta_{\mathrm{alg},K}(u_\ell)} + \underbrace{\frac{h_K}{\pi}\|f - \nabla\cdot\boldsymbol{\sigma}_{\ell,\mathrm{tot}}\|_K}_{\eta_{\mathrm{osc},K}(u_\ell)}, \tag{2.15b}$$

and we have the upper bound on the energy norm of the algebraic error

$$\|\nabla(u_\ell^{\mathrm{ex}} - u_\ell)\| \le \eta_{\mathrm{alg}}(u_\ell,\mathcal{T}_\ell) := \left\{\sum_{K\in\mathcal{T}_\ell} \eta_{\mathrm{alg},K}^2(u_\ell)\right\}^{\frac{1}{2}}. \tag{2.16}$$

Proof. The proof follows the proofs of equivalent statements in Ern and Vohralík (2015), Dolejší et al. (2016), Papež et al. (2017) in a straightforward way: Since $(u - u_\ell) \in V_\ell$, the energy norm of the total error reads

$$\|\nabla(u - u_\ell)\| = \sup_{v \in H^1_0(\Omega), \|\nabla v\| = 1} (\nabla(u - u_\ell), \nabla v). \tag{2.17}$$

Fix $v \in H^1_0(\Omega)$ with $\|\nabla v\| = 1$. Employing the definition of the weak solution (2.1), adding and subtracting the total error flux reconstruction $\boldsymbol{\sigma}_{\ell,\mathrm{tot}} \in \mathbf{H}(\mathrm{div}, \Omega)$ in combination with the Green theorem yield

$$(\nabla(u - u_\ell), \nabla v) = (f, v) - (\nabla u_\ell, \nabla v) = (f - \nabla\cdot\boldsymbol{\sigma}_{\ell,\mathrm{tot}}, v) - (\nabla u_\ell + \boldsymbol{\sigma}_{\ell,\mathrm{tot}}, \nabla v). \tag{2.18}$$

The first term of the right-hand side of (2.18) is treated as in the proof of (Ern and Vohralík, 2015, Theorem 3.3), employing the equilibrium property (2.11b) per simplex $K \in \mathcal{T}_\ell$, followed by applying Cauchy-Schwarz and Poincaré inequality

$$(f - \nabla\cdot\boldsymbol{\sigma}_{\ell,\mathrm{tot}}, v) = \sum_{K \in \mathcal{T}_\ell} (f - \nabla\cdot\boldsymbol{\sigma}_{\ell,\mathrm{tot}}, v - \Pi_{\mathbb{P}_0(K)}(v))_K \leq \sum_{K \in \mathcal{T}_\ell} \|f - \nabla\cdot\boldsymbol{\sigma}_{\ell,\mathrm{tot}}\|_K \|\nabla v\|_K. \tag{2.19}$$

The second term is then bounded simply using the Cauchy Schwarz inequality on each simplex

$$(\nabla u_\ell + \boldsymbol{\sigma}_{\ell,\mathrm{tot}}, \nabla v) \leq \sum_{K \in \mathcal{T}_\ell} \|\nabla u_\ell + \boldsymbol{\sigma}_{\ell,\mathrm{tot}}\|_K \|\nabla v\|_K \tag{2.20}$$

Combining (2.19) and (2.20), using the Cauchy-Schwarz inequality once again, the fact that $\|\nabla v\| = 1$ and the triangle inequality together with the decomposition (2.13) give the upper bound (2.15).

For the upper bound of the algebraic error, recalling that $(u_\ell^{\mathrm{ex}} - u_\ell) \in V_\ell$, we have $\|\nabla(u_\ell^{\mathrm{ex}} - u_\ell)\| = \sup_{v_\ell \in V_\ell, \|\nabla v_\ell\| = 1} (\nabla(u_\ell^{\mathrm{ex}} - u_\ell), \nabla v_\ell)$. Fixing $v_\ell \in V_\ell$, employing the definition of the exact finite element approximation (2.5) and the relation (2.10) lead to applying the crucial equilibration property (2.12b) of the algebraic residual lifting $\boldsymbol{\sigma}_{\ell,\mathrm{alg}}$

$$(\nabla(u_\ell^{\mathrm{ex}} - u_\ell), \nabla v_\ell) = (f, v_\ell) - (\nabla u_\ell, \nabla v_\ell) = (\mathfrak{r}_\ell, v_\ell) = \sum_{K \in \mathcal{T}_\ell} (\nabla\cdot\boldsymbol{\sigma}_{\ell,\mathrm{alg}}, v_\ell)_K. \tag{2.21}$$

Let us remark that it is sufficient to enforce weakly the equilibration property (2.12b), as opposed to Papež et al. (2017) where it is enforced strongly, to prove the algebraic error upper bound (2.16). As $\boldsymbol{\sigma}_{\ell,\mathrm{alg}} \in \mathbf{H}(\mathrm{div}, \Omega)$ and $V_\ell \subset H^1_0(\Omega)$, we are allowed to use the Green theorem also on each term of the sum in (2.21) without any redundant boundary terms. Finally using the Cauchy-Schwarz inequality twice and the constraint $\|\nabla v_\ell\| = 1$ conclude the proof of (2.16). □

As discussed in, e.g. (Ern and Vohralík, 2015, Remark 3.6), the term $\eta_{\mathrm{osc},K}(u_\ell)$ represents, for all $K \in \mathcal{T}_\ell$, a local oscillation in the source datum f that, under suitable smoothness assumptions, converges to zero two orders faster than the error. The detailed description of the actual construction of the algebraic error flux reconstruction $\boldsymbol{\sigma}_{\ell,\mathrm{alg}}$ and the discretization flux reconstruction $\boldsymbol{\sigma}_{\ell,\mathrm{dis}}$, yielding the total flux reconstruction $\boldsymbol{\sigma}_{\ell,\mathrm{tot}}$, is given in Section 2.4.2.

Following (Papež et al., 2018, Theroem 2), the key ingredient for bounding the total energy error from below is:

Definition 2.3.4 (Total residual lifting $\rho_{\ell,\mathrm{tot}}$)**.** *For each vertex $\mathbf{a} \in \mathcal{V}_\ell$, let $V_\ell^{\mathbf{a}}$ be a finite-dimensional subspace of $H^1_*(\omega_\ell^{\mathbf{a}})$*

$$H^1_*(\omega_\ell^{\mathbf{a}}) := \{v \in H^1(\omega_\ell^{\mathbf{a}}), (v,1)_{\omega_\ell^{\mathbf{a}}} = 0\}, \qquad \mathbf{a} \in \mathcal{V}_\ell^{\mathrm{int}}, \tag{2.22a}$$

$$H^1_*(\omega_\ell^{\mathbf{a}}) := \{v \in H^1(\omega_\ell^{\mathbf{a}}), v = 0 \text{ on } \partial\omega_\ell^{\mathbf{a}} \cap \partial\Omega\}, \quad \mathbf{a} \in \mathcal{V}_\ell^{\mathrm{ext}}. \tag{2.22b}$$

The total residual lifting is constructed as $\rho_{\ell,\mathrm{tot}} := \sum_{\mathbf{a}\in\mathcal{V}_\ell} \psi_\ell^{\mathbf{a}} \rho_{\ell,\mathrm{tot}}^{\mathbf{a}} \in H^1_0(\Omega)$, where each vertex contribution solves the local primal finite element problem

$$\left(\nabla\rho_{\ell,\mathrm{tot}}^{\mathbf{a}}, \nabla v_\ell\right)_{\omega_\ell^{\mathbf{a}}} = (f, \psi_\ell^{\mathbf{a}} v_\ell)_{\omega_\ell^{\mathbf{a}}} - (\nabla u_\ell, \nabla(\psi_\ell^{\mathbf{a}} v_\ell))_{\omega_\ell^{\mathbf{a}}} \qquad \forall v_\ell \in V_\ell^{\mathbf{a}}. \tag{2.23}$$

Theorem 2.3.5 (Guaranteed lower bound on the total error)**.** *Let $u \in H^1_0(\Omega)$ be the weak solution of the problem (2.1). Let $\rho_{\ell,\mathrm{tot}}$ be associated with the approximate solution u_ℓ as in Definition 2.3.4. Then, the following holds true:*

$$\|\nabla(u - u_\ell)\| \geq \frac{\sum_{\mathbf{a}\in\mathcal{V}_\ell} \|\nabla\rho_{\ell,\mathrm{tot}}^{\mathbf{a}}\|^2_{\omega_\ell^{\mathbf{a}}}}{\|\nabla\rho_{\ell,\mathrm{tot}}\|} =: \mu(u_\ell). \tag{2.24}$$

2.4 The inexact *hp*-adaptive algorithm

In this section we present the modules `ONE_SOLVER_STEP`, `ESTIMATE`, `MARK`, and `REFINE` of the adaptive loop described in Scheme 2.2. We recall that $\ell \geq 0$ denotes the iteration number.

2.4.1 The module `ONE_SOLVER_STEP`

First, let the current iteration number be $\ell = 0$. Note that at this stage the nested sequence of spaces characterized by (2.3) and (2.4) contains only the initial H^1_0-conforming finite element space V_0. This represents a special case where the module `ONE_SOLVER_STEP` takes as input only the space V_0 and sets the output function $u_0 \in V_0$ directly to be the exact solution of (2.5); here the corresponding (still small) linear algebraic problem (2.6) is considered to be solved exactly.

Otherwise, for the iteration $\ell \geq 1$, the module `ONE_SOLVER_STEP` may and in most cases will be called several times due to the coupling with the

ESTIMATE module (cf. Scheme 2.2). Let $P_{\ell-1}^{\ell} : V_{\ell-1} \to V_\ell$ be a canonical prolongation operator between the consecutive nested finite element spaces. Before the initial call of ONE_SOLVER_STEP at iteration ℓ, we initialize the ℓ-th level approximation $u_\ell \in V_\ell$ of the exact finite element solution u_ℓ^{ex}, by setting $u_\ell := P_{\ell-1}^{\ell} u_{\ell-1}$. This corresponds to setting the initial guess for the algebraic solver. The module ONE_SOLVER_STEP for $\ell \geq 1$ takes as input not only the space V_ℓ, but also the current approximation u_ℓ which is in turn improved and returned as the output of the module. Here, by the improvement of u_ℓ, we mean applying one or a given small number of steps of the given iterative algebraic solver to the system (2.6) assembled within the initial call of ONE_SOLVER_STEP at the iteration ℓ.

The quality of the output u_ℓ is then assessed by the module ESTIMATE and if necessary, see section 2.4.3, u_ℓ is passed again as an input to the successive call of module ONE_SOLVER_STEP.

2.4.2 The module ESTIMATE

The module ESTIMATE crucially relies on the theoretical developments of Section 2.3. It takes as input the current approximation u_ℓ to the exact finite element solution u_ℓ^{ex}, computes the corresponding flux reconstructions $\boldsymbol{\sigma}_{\ell,\mathrm{alg}}$, $\boldsymbol{\sigma}_{\ell,\mathrm{dis}}$, $\boldsymbol{\sigma}_{\ell,\mathrm{tot}}$ and the total residual lifting $\rho_{\ell,\mathrm{tot}}$ defined in Section 2.3, and finally outputs a collection of local error indicators $\{\eta_{\mathrm{alg},K}(u_\ell), \eta_{\mathrm{dis},K}(u_\ell), \eta_{\mathrm{osc},K}(u_\ell)\}_{K\in\mathcal{T}_\ell}$ together with the lower bound $\mu(u_\ell)$ defined in Theorems 2.3.3 and 2.3.5, respectively. In what follows, we outline all the necessary details concerning the actual construction of the flux reconstructions $\boldsymbol{\sigma}_{\ell,\mathrm{alg}}$ and $\boldsymbol{\sigma}_{\ell,\mathrm{dis}}$, hence also their sum $\boldsymbol{\sigma}_{\ell,\mathrm{tot}}$, and the lifting $\rho_{\ell,\mathrm{tot}}$. Once they are all properly constructed, the local error indicators $\eta_{*,K}(u_\ell)$ of (2.15b) and $\mu(u_\ell)$ defined in (2.24) are evaluated.

2.4.2.1 Multilevel construction of algebraic error flux reconstruction $\boldsymbol{\sigma}_{\ell,\mathrm{alg}}$

In order to obtain the algebraic error flux reconstruction $\boldsymbol{\sigma}_{\ell,\mathrm{alg}}$ of Definition 2.3.2, we use the multilevel approach introduced by Papež et al. (2017). We extend it here to the present conforming *hp*-finite element setting. The multilevel approach seems like a natural choice, especially in the present adaptive framework, where for the current space V_ℓ, built up on the pair $(\mathcal{T}_\ell, \mathbf{p}_\ell)$, the hierarchy of its nested finite element subspaces $\{V_j\}_{0\leq j<\ell}$, together with the meshes and polynomial degree distributions $\{(\mathcal{T}_j, \mathbf{p}_j)\}_{0\leq j<\ell}$, are readily at hand from the previous iterations of the adaptive loop. We will refer to the mesh levels 0 and ℓ as the coarsest and the finest level, respectively.

Firstly, following Papež et al. (2017), for the algebraic residual $\mathfrak{r}_\ell \in \mathbb{P}_{\mathbf{p}_\ell}(\mathcal{T}_\ell)$ given by (2.9) we introduce the *coarsest-level Riesz representer* $\varphi_{0,\mathrm{alg}} \in V_0$

$$(\nabla\varphi_{0,\mathrm{alg}}, \nabla v_0) = (\mathfrak{r}_\ell, v_0) \quad \forall v_0 \in V_0. \tag{2.25}$$

For each $\mathbf{a} \in \mathcal{V}_j$, $0 \leq j \leq \ell$, recall the definition of a simplex patch $\mathcal{T}_j^{\mathbf{a}}$ with the corresponding subdomain $\omega_j^{\mathbf{a}}$. In addition, let us introduce for each coarse vertex $\mathbf{a} \in \mathcal{V}_{j-1}$, $1 \leq j \leq \ell$, a simplex patch $\mathcal{T}_{j,j-1}^{\mathbf{a}}$ of all the next finer level simplices $K \in \mathcal{T}_j$ such that $K \subset \omega_{j-1}^{\mathbf{a}}$, cf. Figure 2.1, and the local polynomial degree $p_{\mathbf{a}}^{\mathrm{alg}} := \max_{K \in \mathcal{T}_{j,j-1}^{\mathbf{a}}} p_{j,K}$ (any other choice so that $p_{\mathbf{a}}^{\mathrm{alg}} \geq \max_{K \in \mathcal{T}_{j,j-1}^{\mathbf{a}}} p_{j,K}$ can also be considered).

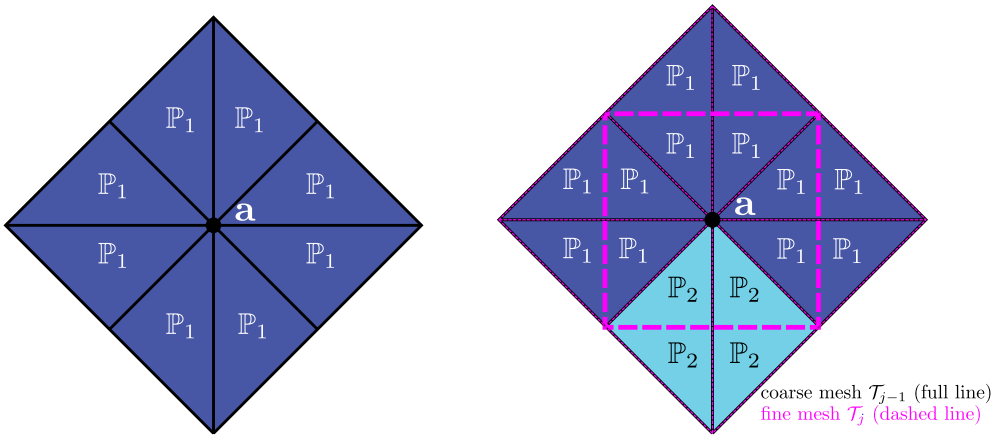

Figure 2.1: Patches of simplices $\mathcal{T}_{j-1}^{\mathbf{a}}$ (*left*) and $\mathcal{T}_{j,j-1}^{\mathbf{a}}$ (*right*) on the subdomain $\omega_{j-1}^{\mathbf{a}}$ around a coarse vertex $\mathbf{a} \in \mathcal{T}_{j-1}$ together with the corresponding polynomial degree distributions. Note that in this case, the local polynomial degree $p_{\mathbf{a}}^{\mathrm{alg}} = 2$.

Let the mesh level $1 \leq j \leq \ell$ be fixed together with the vertex from the next coarser mesh $\mathbf{a} \in \mathcal{V}_{j-1}$. We define the local p-th order Raviart–Thomas–Nédélec space on the subdomain $\omega_{j-1}^{\mathbf{a}}$ with the mesh induced by the next finer mesh $\mathcal{T}_j$ by

$$\mathbf{RTN}_p\left(\omega_{j-1}^{\mathbf{a}}\right) = \{\mathbf{v}_j \in \mathbf{H}(\mathrm{div}, \omega_{j-1}^{\mathbf{a}});\, \mathbf{v}_j|_K \in \mathbf{RTN}_p(K), \quad \forall K \in \mathcal{T}_{j,j-1}^{\mathbf{a}}\}, \tag{2.26}$$

where $\mathbf{RTN}_p(K) = [\mathbb{P}_p(K)]^d + \mathbb{P}_p(K)\mathbf{x}$ is the usual p-th order Raviart–Thomas–Nédélec space (cf. Brezzi and Fortin (1991), Roberts and Thomas (1991)) on a simplex $K \in \mathcal{T}_j$. Furthermore, we consider the pair of local mixed finite element spaces $(\mathbf{V}_{j,j-1}^{\mathbf{a}}, Q_{j,j-1}^{\mathbf{a}})$ which are defined by

$$\begin{aligned} \mathbf{V}_{j,j-1}^{\mathbf{a}} &:= \{\mathbf{v}_j \in \mathbf{RTN}_{p_{\mathbf{a}}^{\mathrm{alg}}}\left(\omega_{j-1}^{\mathbf{a}}\right);\, \mathbf{v}_j \cdot \mathbf{n}_{\omega_{j-1}^{\mathbf{a}}} = 0 \text{ on } \partial\omega_{j-1}^{\mathbf{a}}\}, \\ Q_{j,j-1}^{\mathbf{a}} &:= \{q_j \in \mathbb{P}_{p_{\mathbf{a}}^{\mathrm{alg}}}\left(\mathcal{T}_{j,j-1}^{\mathbf{a}}\right);\, (q_j, 1)_{\omega_{j-1}^{\mathbf{a}}} = 0\}, \end{aligned} \qquad \text{if } \mathbf{a} \in \mathcal{V}_{j-1}^{\mathrm{int}}, \tag{2.27a}$$

$$\begin{aligned} \mathbf{V}_{j,j-1}^{\mathbf{a}} &:= \{\mathbf{v}_j \in \mathbf{RTN}_{p_{\mathbf{a}}^{\mathrm{alg}}}\left(\omega_{j-1}^{\mathbf{a}}\right);\, \mathbf{v}_j \cdot \mathbf{n}_{\omega_{j-1}^{\mathbf{a}}} = 0 \text{ on } \partial\omega_{j-1}^{\mathbf{a}} \setminus \partial\Omega\}, \\ Q_{j,j-1}^{\mathbf{a}} &:= \mathbb{P}_{p_{\mathbf{a}}^{\mathrm{alg}}}\left(\mathcal{T}_{j,j-1}^{\mathbf{a}}\right), \end{aligned} \qquad \text{if } \mathbf{a} \in \mathcal{V}_{j-1}^{\mathrm{ext}}, \tag{2.27b}$$

where $\mathbf{n}_{\omega_{j-1}^{\mathbf{a}}}$ denotes the unit outward normal to $\omega_{j-1}^{\mathbf{a}}$. For an interior vertex $\mathbf{a} \in \mathcal{V}_{j-1}^{\mathrm{int}}$, the degrees of freedom of the spaces $\mathbf{V}_{j,j-1}^{\mathbf{a}}$ and $Q_{j,j-1}^{\mathbf{a}}$ with the local

polynomial degree $p_{\mathbf{a}}^{\mathrm{alg}}$ equal to two are illustrated in Figure 2.2.

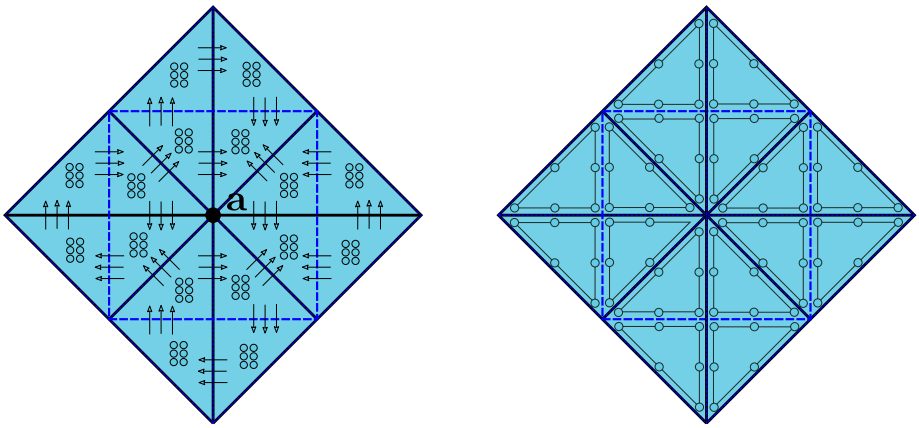

Figure 2.2: Degrees of freedom of the local mixed finite element spaces $\mathbf{V}_{j,j-1}^{\mathbf{a}}$ (*left*, arrows and bullets) and $Q_{j,j-1}^{\mathbf{a}}$ (*right*, bullets) with $p_{\mathbf{a}}^{\mathrm{alg}} = 2$; interior vertex $\mathbf{a} \in \mathcal{V}_{j-1}^{\mathrm{int}}$. On the right, leaving out one degree of freedom of the broken space $\mathbb{P}_{p_{\mathbf{a}}^{\mathrm{alg}}}\left(\mathcal{T}_{j,j-1}^{\mathbf{a}}\right)$ corresponds to the zero mean value constraint posed on the functions in $Q_{j,j-1}^{\mathbf{a}}$. The underlying mesh and the choice of $p_{\mathbf{a}}^{\mathrm{alg}}$ correspond to the simplex patch $\mathcal{T}_{j,j-1}^{\mathbf{a}}$ from Figure 2.1.

Once the coarsest-level Riesz representer $\varphi_{0,\mathrm{alg}}$ of (2.25) is computed, the algebraic error flux reconstruction $\boldsymbol{\sigma}_{\ell,\mathrm{alg}}$ is constructed via solving the local dual mixed finite element problems on simplex patches $\mathcal{T}_{j,j-1}^{\mathbf{a}}$ around the coarse vertices $\mathbf{a} \in \mathcal{V}_{j-1}$, starting from $j = 1$ and up to the current finest level $j = \ell$:

Definition 2.4.1 (Construction of $\boldsymbol{\sigma}_{\ell,\mathrm{alg}}$)**.** *Let $u_\ell \in V_\ell$ be arbitrary. The algebraic error flux reconstruction $\boldsymbol{\sigma}_{\ell,\mathrm{alg}}$ is constructed as*

$$\boldsymbol{\sigma}_{\ell,\mathrm{alg}} := \sum_{j=1}^{\ell} \sum_{\mathbf{a} \in \mathcal{V}_{j-1}} \boldsymbol{\sigma}_{j,\mathrm{alg}}^{\mathbf{a}}, \tag{2.28}$$

where:

- *On level $j = 1$, for each vertex $\mathbf{a} \in \mathcal{V}_0$, $(\boldsymbol{\sigma}_{1,\mathrm{alg}}^{\mathbf{a}}, \gamma_1^{\mathbf{a}}) \in \mathbf{V}_{1,0}^{\mathbf{a}} \times Q_{1,0}^{\mathbf{a}}$ solves*

$$\left(\boldsymbol{\sigma}_{1,\mathrm{alg}}^{\mathbf{a}}, \mathbf{v}_1\right)_{\omega_0^{\mathbf{a}}} - \left(\gamma_1^{\mathbf{a}}, \nabla\cdot\mathbf{v}_1\right)_{\omega_0^{\mathbf{a}}} = 0 \qquad \forall \mathbf{v}_1 \in \mathbf{V}_{1,0}^{\mathbf{a}}, \tag{2.29a}$$

$$\left(\nabla\cdot\boldsymbol{\sigma}_{1,\mathrm{alg}}^{\mathbf{a}}, q_1\right)_{\omega_0^{\mathbf{a}}} = \left(\mathfrak{r}_\ell \psi_0^{\mathbf{a}} - \nabla\varphi_{0,\mathrm{alg}}\cdot\nabla\psi_0^{\mathbf{a}}, q_1\right)_{\omega_0^{\mathbf{a}}} \qquad \forall q_1 \in Q_{1,0}^{\mathbf{a}}; \tag{2.29b}$$

  or, equivalently,

$$\boldsymbol{\sigma}_{1,\mathrm{alg}}^{\mathbf{a}} := \operatorname*{arg\,min}_{\mathbf{v}_1 \in \mathbf{V}_{1,0}^{\mathbf{a}}, \nabla\cdot\mathbf{v}_1 = \Pi_{Q_{1,0}^{\mathbf{a}}}\left(\mathfrak{r}_\ell \psi_0^{\mathbf{a}} - \nabla\varphi_{0,\mathrm{alg}}\cdot\nabla\psi_0^{\mathbf{a}}\right)} \|\mathbf{v}_1\|_{\omega_0^{\mathbf{a}}}. \tag{2.30}$$

- *On level* $2 \le j \le \ell$, *for each vertex* $\mathbf{a} \in \mathcal{V}_{j-1}$, $(\boldsymbol{\sigma}^{\mathbf{a}}_{j,\mathrm{alg}}, \gamma^{\mathbf{a}}_{j}) \in \mathbf{V}^{\mathbf{a}}_{j,j-1} \times Q^{\mathbf{a}}_{j,j-1}$ *solves*

$$\big(\boldsymbol{\sigma}^{\mathbf{a}}_{j,\mathrm{alg}}, \mathbf{v}_j\big)_{\omega^{\mathbf{a}}_{j-1}} - \big(\gamma^{\mathbf{a}}_{j}, \nabla{\cdot}\mathbf{v}_j\big)_{\omega^{\mathbf{a}}_{j-1}} = 0 \qquad \forall \mathbf{v}_j \in \mathbf{V}^{\mathbf{a}}_{j,j-1}, \tag{2.31a}$$

$$\big(\nabla{\cdot}\boldsymbol{\sigma}^{\mathbf{a}}_{j,\mathrm{alg}}, q_j\big)_{\omega^{\mathbf{a}}_{j-1}} = \left(\mathfrak{r}_\ell \psi^{\mathbf{a}}_{j-1} - \sum_{i=1}^{j-1} \psi^{\mathbf{a}}_{j-1} \nabla{\cdot}\boldsymbol{\sigma}_{i,\mathrm{alg}}, q_j\right)_{\omega^{\mathbf{a}}_{j-1}} \qquad \forall q_j \in Q^{\mathbf{a}}_{j,j-1}; \tag{2.31b}$$

where we set $\boldsymbol{\sigma}_{i,\mathrm{alg}} := \sum_{\mathbf{a}\in\mathcal{V}_{i-1}} \boldsymbol{\sigma}^{\mathbf{a}}_{i,\mathrm{alg}}$, *for* $1 \le i \le j-1$. *Equivalently, problem* (2.31) *can be restated as*

$$\boldsymbol{\sigma}^{\mathbf{a}}_{j,\mathrm{alg}} := \operatorname*{arg\,min}_{\mathbf{v}_j \in \mathbf{V}^{\mathbf{a}}_{j,j-1}, \nabla{\cdot}\mathbf{v}_j = \Pi_{Q^{\mathbf{a}}_{j,j-1}} \left(\mathfrak{r}_\ell \psi^{\mathbf{a}}_{j-1} - \sum_{i=1}^{j-1} \psi^{\mathbf{a}}_{j-1} \nabla{\cdot}\boldsymbol{\sigma}_{i,\mathrm{alg}}\right)} \|\mathbf{v}_j\|_{\omega^{\mathbf{a}}_{j-1}}. \tag{2.32}$$

Here, each vertex contribution $\boldsymbol{\sigma}^{\mathbf{a}}_{\cdot,\mathrm{alg}}$ *is extended by zero outside its initial domain of definition.*

Note that the Neumann compatibility condition for problem (2.29) is satified for all $\mathbf{a} \in \mathcal{V}_0^{\mathrm{int}}$ due to the definition of $\varphi_{0,\mathrm{alg}}$ (take $v_0 = \psi^{\mathbf{a}}_0$ as a test function in (2.25)). Thus (2.29b) is satisfied for all the test functions from $\mathbb{P}_{p^{\mathrm{alg}}_{\mathbf{a}}}(\mathcal{T}^{\mathbf{a}}_{1,0})$, not only those with zero mean value. Due to the discontinuous nature of this broken polynomial space and the fact that for each $K \in \mathcal{T}_1$, with the parent element $\widetilde{K} \in \mathcal{T}_0$, $p_{1,K} \le \min_{\mathbf{a}\in\mathcal{V}_{\widetilde{K}}} p^{\mathrm{alg}}_{\mathbf{a}}$, we have

$$\begin{aligned}(\nabla{\cdot}\boldsymbol{\sigma}_{1,\mathrm{alg}}, q_1)_K &= \sum_{\mathbf{a}\in\mathcal{V}_{\widetilde{K}}} \big(\nabla{\cdot}\boldsymbol{\sigma}^{\mathbf{a}}_{1,\mathrm{alg}}, q_1\big)_K = \sum_{\mathbf{a}\in\mathcal{V}_{\widetilde{K}}} (\mathfrak{r}_\ell \psi^{\mathbf{a}}_0 - \nabla\varphi_{0,\mathrm{alg}}{\cdot}\nabla\psi^{\mathbf{a}}_0, q_1)_K \\ &= (\mathfrak{r}_\ell, q_1)_K \quad \forall K \in \mathcal{T}_1 \quad \forall q_1 \in \mathbb{P}_{p_{1,K}}(K),\end{aligned} \tag{2.33}$$

where we have employed the partition of unity via $\sum_{\mathbf{a}\in\mathcal{V}_{\widetilde{K}}} \psi^{\mathbf{a}}_0|_K = 1|_K$. At level $j = 2$, for each interior vertex $\mathbf{a} \in \mathcal{V}_1^{\mathrm{int}}$, the Neumann compatibility condition for problem (2.31) $(\mathfrak{r}_\ell - \nabla{\cdot}\boldsymbol{\sigma}_{1,\mathrm{alg}}, \psi^{\mathbf{a}}_1)_{\omega^{\mathbf{a}}_1} = 0$ is a direct consequence of (2.33), since $\psi^{\mathbf{a}}_1|_K \in \mathbb{P}_{p_{1,K}}(K)$ for each $K \in \mathcal{T}^{\mathbf{a}}_1$. Thus, similarly to (2.29b) also (2.31b), so far only at level $j = 2$, is satisfied for all the test functions from $\mathbb{P}_{p^{\mathrm{alg}}_{\mathbf{a}}}(\mathcal{T}^{\mathbf{a}}_{2,1})$ without any zero-mean value restrictions. Then, similarly to (2.33), we use the discontinuous nature of the broken space $\mathbb{P}_{p^{\mathrm{alg}}_{\mathbf{a}}}(\mathcal{T}^{\mathbf{a}}_{2,1})$, our choice of local polynomial degrees $p^{\mathrm{alg}}_{\mathbf{a}}$ used in definition of the spaces (2.27), for each vertex $\mathbf{a} \in \mathcal{V}_1$, such that $p_{2,K} \le \min_{\mathbf{a}\in\mathcal{V}_{\widetilde{K}}} p^{\mathrm{alg}}_{\mathbf{a}}$, for each $K \in \mathcal{T}_2$ with the parent element $\widetilde{K} \in \mathcal{T}_1$, and the partition of unity via $\sum_{\mathbf{a}\in\mathcal{V}_{\widetilde{K}}} \psi^{\mathbf{a}}_1|_K = 1$ to

obtain

$$(\mathfrak{r}_\ell - \sum_{i=1}^{2} \nabla\cdot\boldsymbol{\sigma}_{i,\mathrm{alg}}, q_2)_K = 0 \quad \forall K \in \mathcal{T}_2 \quad \forall q_2 \in \mathbb{P}_{p_{2,K}}(K). \tag{2.34}$$

Property (2.34) in turn yields the Neumann compatibility condition on the third level. Progressing successively, at remaining levels $3 \leq j \leq \ell - 1$, we always have the property

$$\left(\mathfrak{r}_\ell - \sum_{i=1}^{j} \nabla\cdot\boldsymbol{\sigma}_{i,\mathrm{alg}}, q_j\right)_K = 0 \quad \forall K \in \mathcal{T}_j \quad \forall q_j \in \mathbb{P}_{p_{j,K}}(K), \tag{2.35}$$

yielding the Neumann compatibility condition on the next level $j+1$, thus (2.31b) is satisfied for all the test functions from the broken polynomial space $\mathbb{P}_{p_{\mathbf{a}}^{\mathrm{alg}}}(\mathcal{T}_{j,j-1}^{\mathbf{a}})$, for each $\mathbf{a} \in \mathcal{V}_{j-1}$, $2 \leq j \leq \ell$. Furthermore, as a result of the Neumann compatibility condition on the finest level, on each finest simplex $K \in \mathcal{T}_\ell$, the sum of local contributions $\sum_{\mathbf{a}\in\mathcal{V}_{\ell-1}} \boldsymbol{\sigma}_{\ell,\mathrm{alg}}^{\mathbf{a}}$ admits the following property:

$$\left(\sum_{\mathbf{a}\in\mathcal{V}_{\ell-1}} \nabla\cdot\boldsymbol{\sigma}_{\ell,\mathrm{alg}}^{\mathbf{a}}, q_\ell\right)_K = \sum_{\mathbf{a}\in\mathcal{V}_{\tilde{K}}} \left(\nabla\cdot\boldsymbol{\sigma}_{\ell,\mathrm{alg}}^{\mathbf{a}}, q_\ell\right)_K = \left(\mathfrak{r}_\ell - \sum_{i=1}^{\ell-1} \nabla\cdot\boldsymbol{\sigma}_{i,\mathrm{alg}}, q_\ell\right)_K \quad \forall q_\ell \in \mathbb{P}_{p_{\ell,K}}(K). \tag{2.36}$$

Lemma 2.4.2 (Properties of $\boldsymbol{\sigma}_{\ell,\mathrm{alg}}$)**.** *The algebraic error flux reconstruction $\boldsymbol{\sigma}_{\ell,\mathrm{alg}}$ constructed in Defintion 2.4.1 satisfies the properties of Definition 2.3.2.*

Proof. For $1 \leq j \leq \ell$, each local contribution $\boldsymbol{\sigma}_{j,\mathrm{alg}}^{\mathbf{a}} \in \mathbf{H}(\mathrm{div}, \omega_{j-1}^{\mathbf{a}})$, $\mathbf{a} \in \mathcal{V}_{j-1}$, by construction. Imposing the homogeneous Neumann boundary conditions in the definition of the local spaces (2.27) and extending by zero outside of $\omega_{j-1}^{\mathbf{a}}$ then give the overall $\mathbf{H}(\mathrm{div}, \Omega)$-conformity (2.12a) of $\boldsymbol{\sigma}_{\ell,\mathrm{alg}}$ as it is defined by (2.28). Then, splitting the sum in the definition (2.28) in combination with the property (2.36) yields for each $K \in \mathcal{T}_\ell$,

$$\begin{aligned}(\nabla\cdot\boldsymbol{\sigma}_{\ell,\mathrm{alg}}, q_\ell)_K &= \left(\sum_{\mathbf{a}\in\mathcal{V}_{\ell-1}} \nabla\cdot\boldsymbol{\sigma}_{\ell,\mathrm{alg}}^{\mathbf{a}} + \sum_{i=1}^{\ell-1} \nabla\cdot\boldsymbol{\sigma}_{i,\mathrm{alg}}, q_\ell\right)_K \\ &= (\mathfrak{r}_\ell, q_\ell)_K \quad \forall q_\ell \in \mathbb{P}_{p_{\ell,K}}(K).\end{aligned}$$

Hence, the algebraic error flux reconstruction $\boldsymbol{\sigma}_{\ell,\mathrm{alg}}$ indeed satisfies (2.12b). □

Remark 2.4.3 (Comparison with previous developments)**.** *The local problems in Definition 2.4.1 differ from those of* (Papež et al., 2017, Definition 6.3) *in two aspects:* (i) *the local spaces on each simplex patch are assigned a specific polynomial degree along the lines of* Daniel et al. (2018a), Dolejší et al.

(2016); (ii) *the right-hand sides of the local problems* (2.31), *namely the divergence constraints in* (2.31b), *differ from their counterparts in* (Papež et al., 2017, Definition 6.3). *In particular, the first level algebraic error flux reconstruction* $\boldsymbol{\sigma}_{1,\mathrm{alg}}$ *is now successively corrected on the finer levels without the need of introducing the* L^2*-orthogonal projections onto global coarser spaces, which is not suitable anymore because of the possibly varying polynomial degrees* $p_{\mathbf{a}}^{\mathrm{alg}}$ *across the neighboring patches.*

2.4.2.2 Construction of the discretization flux reconstruction $\boldsymbol{\sigma}_{\ell,\mathrm{dis}}$

Next, we present the details on the actual construction of the $\mathbf{H}(\mathrm{div},\Omega)$-conforming discretization flux reconstruction $\boldsymbol{\sigma}_{\ell,\mathrm{dis}}$. Similarly to the above construction of $\boldsymbol{\sigma}_{\ell,\mathrm{alg}}$, we construct $\boldsymbol{\sigma}_{\ell,\mathrm{dis}}$ locally via mixed finite element solves, but this time only on the finest simplex patches $\mathcal{T}_\ell^{\mathbf{a}}$ around the finest mesh vertices $\mathbf{a} \in \mathcal{V}_\ell$. Namely, we follow the approach of (Papež et al., 2017, Definition 7.1), (Papež et al., 2018, Sec. 4.4), and (Ern and Vohralík, 2013, Definition 6.9) adapted to the present setting with varying polynomial degree. For each $\mathbf{a} \in \mathcal{V}_\ell$, we consider the local polynomial degree $p_{\mathbf{a}}^{\mathrm{dis}} := \max_{K\in\mathcal{T}_\ell^{\mathbf{a}}} p_{\ell,K}$ (again any other choice so that $p_{\mathbf{a}}^{\mathrm{dis}} \geq \max_{K\in\mathcal{T}_\ell^{\mathbf{a}}} p_{\ell,K}$ can also be employed). For a fixed finest vertex $\mathbf{a} \in \mathcal{V}_\ell$, let

$$\mathbf{RTN}_p(\omega_\ell^{\mathbf{a}}) = \{\mathbf{v}_\ell \in \mathbf{H}(\mathrm{div},\omega_\ell^{\mathbf{a}});\ \mathbf{v}_\ell|_K \in \mathbf{RTN}_p(K), \quad \forall K \in \mathcal{T}_\ell^{\mathbf{a}}\}. \tag{2.37}$$

Then, we define the local spaces with homogeneous Neumann boundary condition

$$\begin{aligned} &\mathbf{V}_\ell^{\mathbf{a}} := \{\mathbf{v}_\ell \in \mathbf{RTN}_{p_{\mathbf{a}}^{\mathrm{dis}}}(\omega_\ell^{\mathbf{a}});\ \mathbf{v}_\ell{\cdot}\mathbf{n}_{\omega_\ell^{\mathbf{a}}} = 0 \text{ on } \partial\omega_\ell^{\mathbf{a}}\},\\ &Q_\ell^{\mathbf{a}} := \{q_\ell \in \mathbb{P}_{p_{\mathbf{a}}^{\mathrm{dis}}}(\mathcal{T}_\ell^{\mathbf{a}});\ (q_\ell,1)_{\omega_\ell^{\mathbf{a}}} = 0\}, \end{aligned} \quad \text{if } \mathbf{a} \in \mathcal{V}_\ell^{\mathrm{int}}, \tag{2.38a}$$

$$\begin{aligned} &\mathbf{V}_\ell^{\mathbf{a}} := \{\mathbf{v}_\ell \in \mathbf{RTN}_{p_{\mathbf{a}}^{\mathrm{dis}}}(\omega_\ell^{\mathbf{a}});\ \mathbf{v}_\ell{\cdot}\mathbf{n}_{\omega_\ell^{\mathbf{a}}} = 0 \text{ on } \partial\omega_\ell^{\mathbf{a}} \setminus \partial\Omega\},\\ &Q_\ell^{\mathbf{a}} := \mathbb{P}_{p_{\mathbf{a}}^{\mathrm{dis}}}(\mathcal{T}_\ell^{\mathbf{a}}), \end{aligned} \quad \text{if } \mathbf{a} \in \mathcal{V}_\ell^{\mathrm{ext}}, \tag{2.38b}$$

with $\mathbf{n}_{\omega_\ell^{\mathbf{a}}}$ denoting the unit outward normal to $\omega_\ell^{\mathbf{a}}$.

Definition 2.4.4 (Construction of $\boldsymbol{\sigma}_{\ell,\mathrm{dis}}$)**.** *Let* $u_\ell \in V_\ell$ *be the approximation used in Definition 2.4.1. We construct the discretization flux reconstruction* $\boldsymbol{\sigma}_{\ell,\mathrm{dis}}$ *as*

$$\boldsymbol{\sigma}_{\ell,\mathrm{dis}} := \sum_{\mathbf{a}\in\mathcal{V}_\ell} \boldsymbol{\sigma}_{\ell,\mathrm{dis}}^{\mathbf{a}}, \tag{2.39}$$

where, for each vertex $\mathbf{a} \in \mathcal{V}_\ell$, $(\boldsymbol{\sigma}_{\ell,\mathrm{dis}}^{\mathbf{a}}, \gamma_\ell^{\mathbf{a}}) \in \mathbf{V}_\ell^{\mathbf{a}} \times Q_\ell^{\mathbf{a}}$ *solves*

$$\big(\boldsymbol{\sigma}_{\ell,\mathrm{dis}}^{\mathbf{a}}, \mathbf{v}_\ell\big)_{\omega_\ell^{\mathbf{a}}} - (\gamma_\ell^{\mathbf{a}}, \nabla{\cdot}\mathbf{v}_\ell)_{\omega_\ell^{\mathbf{a}}} = -(\psi_\ell^{\mathbf{a}}\nabla u_\ell, \mathbf{v}_\ell)_{\omega_\ell^{\mathbf{a}}} \qquad \forall \mathbf{v}_\ell \in \mathbf{V}_\ell^{\mathbf{a}}, \tag{2.40a}$$

$$\big(\nabla{\cdot}\boldsymbol{\sigma}_{\ell,\mathrm{dis}}^{\mathbf{a}}, q_\ell\big)_{\omega_\ell^{\mathbf{a}}} = (f\psi_\ell^{\mathbf{a}} - \nabla u_\ell{\cdot}\nabla\psi_\ell^{\mathbf{a}} - \mathfrak{r}_\ell\psi_\ell^{\mathbf{a}}, q_\ell)_{\omega_\ell^{\mathbf{a}}} \quad \forall q_\ell \in Q_\ell^{\mathbf{a}}, \tag{2.40b}$$

and where $\boldsymbol{\sigma}^{\mathbf{a}}_{\ell,\mathrm{dis}}$ *is extended by zero outside* $\omega^{\mathbf{a}}_{\ell}$.

The Neumann compatibility condition for problem (2.40) is satisfied for all $\mathbf{a} \in \mathcal{V}^{\mathrm{int}}_{\ell}$ as a direct consequence of (2.10).

Lemma 2.4.5 (Properties of $\boldsymbol{\sigma}_{\ell,\mathrm{dis}}$)**.** *The discretization flux reconstruction* $\boldsymbol{\sigma}_{\ell,\mathrm{dis}}$ *from Definition 2.4.4 belongs to* $\mathbf{H}(\mathrm{div},\Omega)$ *and on each simplex* $K \in \mathcal{T}_{\ell}$*, it satisfies*

$$(\nabla\cdot\boldsymbol{\sigma}_{\ell,\mathrm{dis}}, q_{\ell})_K = (f - \mathfrak{r}_{\ell}, q_{\ell})_K \quad \forall K \in \mathcal{T}_{\ell}, \quad \forall q_{\ell} \in \mathbb{P}_{p_{\ell,K}(K)}. \tag{2.41}$$

Proof. Since each local contribution $\boldsymbol{\sigma}^{\mathbf{a}}_{\ell,\mathrm{dis}}$, $\mathbf{a} \in \mathcal{V}_{\ell}$, lies in $\mathbf{H}(\mathrm{div},\omega^{\mathbf{a}}_{\ell})$, the overall $\mathbf{H}(\mathrm{div},\Omega)$-conformity is a direct consequence of (2.39). Next, as a result of the Neumann compatibility condition, we are allowed to take any function $q_{\ell} \in \mathbb{P}_{p^{\mathrm{dis}}_{\mathbf{a}}}(\mathcal{T}^{\mathbf{a}}_{\ell})$ as a test function in (2.40b), without any zero mean value restriction. On each $K \in \mathcal{T}_{\ell}$, we have $p_{\ell,K} \le \min_{\mathbf{a}\in\mathcal{V}_K} p^{\mathrm{dis}}_{\mathbf{a}}$. Hence, combining (2.39) with (2.40b) and employing the partition of unity $\sum_{\mathbf{a}\in\mathcal{V}_K} \psi^{\mathbf{a}}_{\ell}|_K = 1|_K$, we see that

$$\begin{aligned}(\nabla\cdot\boldsymbol{\sigma}_{\ell,\mathrm{dis}}, q_{\ell})_K &= \sum_{\mathbf{a}\in\mathcal{V}_K} \big(\nabla\cdot\boldsymbol{\sigma}^{\mathbf{a}}_{\ell,\mathrm{dis}}, q_{\ell}\big)_K = \sum_{\mathbf{a}\in\mathcal{V}_K} (f\psi^{\mathbf{a}}_{\ell} - \nabla u_{\ell}\cdot\nabla\psi^{\mathbf{a}}_{\ell} - \mathfrak{r}_{\ell}\psi^{\mathbf{a}}_{\ell}, q_{\ell})_K \\ &= (f - \mathfrak{r}_{\ell}, q_{\ell})_K \quad \forall K \in \mathcal{T}_{\ell} \quad \forall q_{\ell} \in \mathbb{P}_{p_{\ell,K}}(K),\end{aligned} \tag{2.42}$$

which concludes the proof. □

2.4.2.3 Discrete spaces for the total residual lifting $\rho_{\ell,\mathrm{tot}}$

Finally, for each finest vertex $\mathbf{a} \in \mathcal{V}_{\ell}$, we specify our choice for the $H^1_*(\omega^{\mathbf{a}}_{\ell})$-conforming scalar-valued spaces $V^{\mathbf{a}}_{\ell}$, in which we seek the local contributions of the total residual lifting $\rho_{\ell,\mathrm{tot}}$ of Definition 2.3.4:

$$V^{\mathbf{a}}_{\ell} := \{v_{\ell} \in H^1(\omega^{\mathbf{a}}_{\ell}); v_{\ell} \in \mathbb{P}_{p^{\mathrm{dis}}_{\mathbf{a}}}(K),\ \forall K \in \mathcal{T}^{\mathbf{a}}_{\ell},\ (v_{\ell},1)_{\omega^{\mathbf{a}}_{\ell}} = 0\} \qquad \mathbf{a} \in \mathcal{V}^{\mathrm{int}}_{\ell}, \tag{2.43a}$$

$$V^{\mathbf{a}}_{\ell} := \{v_{\ell} \in H^1(\omega^{\mathbf{a}}_{\ell}); v_{\ell} \in \mathbb{P}_{p^{\mathrm{dis}}_{\mathbf{a}}}(K),\ \forall K \in \mathcal{T}^{\mathbf{a}}_{\ell},\ v_{\ell} = 0 \text{ on } \partial\omega^{\mathbf{a}}_{\ell} \setminus \partial\Omega\} \quad \mathbf{a} \in \mathcal{V}^{\mathrm{ext}}_{\ell}. \tag{2.43b}$$

Other choices of $V^{\mathbf{a}}_{\ell}$ could be also considered, in particular considering the actual polynomial degree $p_{\ell,K}$, on each simplex $K \in \mathcal{T}^{\mathbf{a}}_{\ell}$, instead of the local degree $p^{\mathrm{dis}}_{\mathbf{a}}$ would be, from a theoretical viewpoint, also sufficient.

2.4.3 Adaptive stopping criteria for the algebraic solver

The output of the `ESTIMATE` module enables us to assess the quality of the current approximation u_{ℓ} and thus make a reasonable decision if another call

of the module ONE_SOLVER_STEP is really needed. It is considered to be unnecessary, as discussed e.g. in Becker et al. (1995), Jiránek et al. (2010), Arioli et al. (2013a), Ern and Vohralík (2013), Papež et al. (2018) and the references therein, if the current algebraic error is smaller than the total error by a factor $0 < \gamma_\ell < 1$ (typically of order 0.1), i.e.

$$\|\nabla (u_\ell^{\mathrm{ex}} - u_\ell)\| \leq \gamma_\ell \|\nabla (u - u_\ell)\|. \tag{2.44}$$

In order to ensure (2.44), we require that our current approximation u_ℓ satisfies the following global (safe) stopping criterion

$$\eta_{\mathrm{alg}}(u_\ell, \mathcal{T}_\ell) \leq \gamma_\ell \, \mu(u_\ell). \tag{2.45}$$

This typically allows us to avoid possible unnecessary iterations of the algebraic solver within the ONE_SOLVER_STEP module in case of the use of the classical stopping criterion for the algebraic solver based on the Euclidean norm of the algebraic residual vector (2.7)

$$\frac{\|\mathrm{R}_\ell\|}{\|\mathrm{F}_\ell\|} \leq \varepsilon, \tag{2.46}$$

with ε prescribed at a very small value,thus without exploiting any knowledge of the error estimators.

2.4.4 The module MARK

The module MARK takes as input the local error estimators computed within the ESTIMATE module, corresponding to the current approximation u_ℓ satisfying the stopping criterion from Section 2.4.3. It outputs a set of marked vertices $\widetilde{\mathcal{V}}_\ell^\theta \subset \mathcal{V}_\ell$ using a bulk-chasing criterion inspired by the well-known Dörfler's marking criterion Dörfler (1996). The choice of marking vertices instead of marking simplices directly is motivated by the nature of our *hp*-decision criterion in the module REFINE (see Section 2.4.5).

For a fixed threshold parameter $\theta \in (0, 1]$, the set of marked vertices $\widetilde{\mathcal{V}}_\ell^\theta$ is selected in such a way that

$$\eta\left(u_\ell, \bigcup_{\mathbf{a} \in \widetilde{\mathcal{V}}_\ell^\theta} \mathcal{T}_\ell^{\mathbf{a}}\right) \geq \theta \, \eta(u_\ell, \mathcal{T}_\ell), \tag{2.47}$$

where, for a subset $\mathcal{S} \subset \mathcal{T}_\ell$, we employ the notation $\eta(u_\ell, \mathcal{S}) := \left\{\sum_{K \in \mathcal{S}} \eta_K(u_\ell)^2\right\}^{1/2}$. Then, letting

$$\mathcal{M}_\ell^\theta := \bigcup_{\mathbf{a} \in \widetilde{\mathcal{V}}_\ell^\theta} \mathcal{T}_\ell^{\mathbf{a}} \subset \mathcal{T}_\ell \tag{2.48}$$

be the collection of all the simplices that belong to a patch associated with

a marked vertex, we observe that (2.47) means that $\eta(u_\ell, \mathcal{M}_\ell^\theta) \geq \theta\, \eta(u_\ell, \mathcal{T}_\ell)$. To select a set $\widetilde{\mathcal{V}}_\ell^\theta$ of minimal cardinality, the mesh vertices in $\mathcal{V}_\ell$ are sorted by comparing the vertex-based error estimators $\eta(u_\ell, \mathcal{T}_\ell^{\mathbf{a}})$ for all $\mathbf{a} \in \mathcal{V}_\ell$, and a greedy algorithm is employed to build the set $\widetilde{\mathcal{V}}_\ell^\theta$. A possibly slightly larger set $\widetilde{\mathcal{V}}_\ell^\theta$ can be constructed with linear cost in terms of the number of mesh vertices by using the algorithm proposed in (Dörfler, 1996, Section 5.2).

2.4.5 The module REFINE

The module REFINE, as in the previous paper by Daniel et al. (2018a), takes as input the set of marked vertices $\widetilde{\mathcal{V}}_\ell^\theta$ and outputs the mesh $\mathcal{T}_{\ell+1}$ and the polynomial-degree distribution $\mathbf{p}_{\ell+1}$ to be used at the next iteration of the adaptive loop from Scheme 2.2. This module proceeds in three steps. First, an *hp*-decision is made on all the marked vertices, so that each marked vertex $\mathbf{a} \in \widetilde{\mathcal{V}}_\ell^\theta$ is flagged either for *h*-refinement or for *p*-refinement. This means that the set $\widetilde{\mathcal{V}}_\ell^\theta$ is split into two disjoint subsets $\widetilde{\mathcal{V}}_\ell^\theta = \widetilde{\mathcal{V}}_\ell^h \cup \widetilde{\mathcal{V}}_\ell^p$ with obvious notation. Then, in the second step, the subsets $\widetilde{\mathcal{V}}_\ell^h$ and $\widetilde{\mathcal{V}}_\ell^p$ are used to define subsets $\mathcal{M}_\ell^h$ and $\mathcal{M}_\ell^p$ of the set of marked simplices $\mathcal{M}_\ell^\theta$ (see (2.48)). The subsets $\mathcal{M}_\ell^h$ and $\mathcal{M}_\ell^p$ are not necessarily disjoint which means that some simplices can be flagged for *hp*-refinement. Finally, the two subsets $\mathcal{M}_\ell^h$ and $\mathcal{M}_\ell^p$ are used to construct $\mathcal{T}_{\ell+1}$ and $\mathbf{p}_{\ell+1}$.

2.4.5.1 *hp*-decision on vertices

Our *hp*-decision on marked vertices is made on the basis of two local primal solves on the patch $\mathcal{T}_\ell^{\mathbf{a}}$ attached to each marked vertex $\mathbf{a} \in \widetilde{\mathcal{V}}_\ell^\theta$. The idea is to construct two distinct local patch-based spaces in order to emulate separately the effects of *h*- and *p*-refinement. We first consider the case where the two local primal solves use Dirichlet conditions. Let us denote the polynomial-degree distribution in the patch $\mathcal{T}_\ell^{\mathbf{a}}$ by the vector $\mathbf{p}_\ell^{\mathbf{a}} := (p_{\ell,K})_{K \in \mathcal{T}_\ell^{\mathbf{a}}}$.

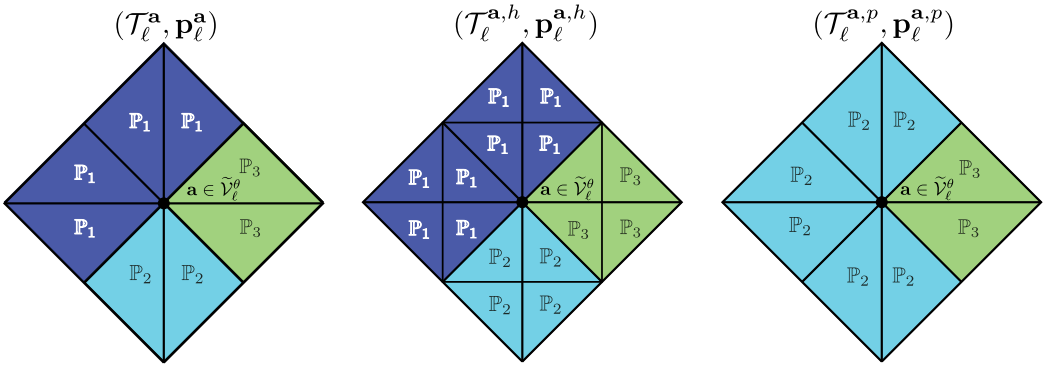

Figure 2.3: An example of patch $\mathcal{T}_\ell^{\mathbf{a}}$ together with its polynomial-degree distribution $\mathbf{p}_\ell^{\mathbf{a}}$ (*left*), its *h*-refined version (*center*), and its *p*-refined version (*right*) from Definitions 2.4.6 and 2.4.7, respectively.

Definition 2.4.6 (*h*-refinement residual – Dirichlet conditions)**.** *Let* $\mathbf{a} \in \widetilde{\mathcal{V}}_\ell^\theta$ *be a marked vertex with associated patch* $\mathcal{T}_\ell^{\mathbf{a}}$ *and polynomial-degree distribution* $\mathbf{p}_\ell^{\mathbf{a}}$*. We set*

$$V_\ell^{\mathbf{a},h} := \mathbb{P}_{\mathbf{p}_\ell^{\mathbf{a},h}}(\mathcal{T}_\ell^{\mathbf{a},h}) \cap H_0^1(\omega_\ell^{\mathbf{a}}), \tag{2.49}$$

where $\mathcal{T}_\ell^{\mathbf{a},h}$ *is obtained as a matching simplicial refinement of* $\mathcal{T}_\ell^{\mathbf{a}}$ *by dividing each simplex* $K \in \mathcal{T}_\ell^{\mathbf{a}}$ *into at least two children simplices, and the polynomial-degree distribution* $\mathbf{p}_\ell^{\mathbf{a},h}$ *is obtained from* $\mathbf{p}_\ell^{\mathbf{a}}$ *by assigning to each newly-created simplex the same polynomial degree as its parent. Then, we let* $r^{\mathbf{a},h} \in V_\ell^{\mathbf{a},h}$ *solve*

$$(\nabla r^{\mathbf{a},h}, \nabla v^{\mathbf{a},h})_{\omega_\ell^{\mathbf{a}}} = (f, v^{\mathbf{a},h})_{\omega_\ell^{\mathbf{a}}} - (\nabla u_\ell, \nabla v^{\mathbf{a},h})_{\omega_\ell^{\mathbf{a}}} \qquad \forall\, v^{\mathbf{a},h} \in V_\ell^{\mathbf{a},h}.$$

Definition 2.4.7 (*p*-refinement residual – Dirichlet conditions)**.** *Let* $\mathbf{a} \in \widetilde{\mathcal{V}}_\ell^\theta$ *be a marked vertex with associated patch* $\mathcal{T}_\ell^{\mathbf{a}}$ *and polynomial-degree distribution* $\mathbf{p}_\ell^{\mathbf{a}}$*. We set*

$$V_\ell^{\mathbf{a},p} := \mathbb{P}_{\mathbf{p}_\ell^{\mathbf{a},p}}(\mathcal{T}_\ell^{\mathbf{a},p}) \cap H_0^1(\omega_\ell^{\mathbf{a}}), \tag{2.50}$$

where $\mathcal{T}_\ell^{\mathbf{a},p} := \mathcal{T}_\ell^{\mathbf{a}}$*, and the polynomial-degree distribution* $\mathbf{p}_\ell^{\mathbf{a},p}$ *is obtained from* $\mathbf{p}_\ell^{\mathbf{a}}$ *by assigning to each simplex* $K \in \mathcal{T}_\ell^{\mathbf{a},p} = \mathcal{T}_\ell^{\mathbf{a}}$ *the polynomial degree* $p_{\ell,K} + \delta_K^{\mathbf{a}}$ *where*

$$\delta_K^{\mathbf{a}} := \begin{cases} 1 & \text{if } p_{\ell,K} = \min_{K' \in \mathcal{T}_\ell^{\mathbf{a}}} p_{\ell,K'}, \\ 0 & \text{otherwise.} \end{cases} \tag{2.51}$$

Then, we let $r^{\mathbf{a},p} \in V_\ell^{\mathbf{a},p}$ *solve*

$$(\nabla r^{\mathbf{a},p}, \nabla v^{\mathbf{a},p})_{\omega_\ell^{\mathbf{a}}} = (f, v^{\mathbf{a},p})_{\omega_\ell^{\mathbf{a}}} - (\nabla u_\ell, \nabla v^{\mathbf{a},p})_{\omega_\ell^{\mathbf{a}}} \qquad \forall\, v^{\mathbf{a},p} \in V_\ell^{\mathbf{a},p}.$$

The local residual liftings $r^{\mathbf{a},h}$ and $r^{\mathbf{a},p}$ from Definitions 2.4.6 and 2.4.7, respectively, are used to define the following two disjoint subsets of the set of marked vertices $\widetilde{\mathcal{V}}_\ell^\theta$:

$$\widetilde{\mathcal{V}}_\ell^h := \{\mathbf{a} \in \widetilde{\mathcal{V}}_\ell^\theta \mid \|\nabla r^{\mathbf{a},h}\|_{\omega_\ell^{\mathbf{a}}} \geq \|\nabla r^{\mathbf{a},p}\|_{\omega_\ell^{\mathbf{a}}}\}, \tag{2.52a}$$

$$\widetilde{\mathcal{V}}_\ell^p := \{\mathbf{a} \in \widetilde{\mathcal{V}}_\ell^\theta \mid \|\nabla r^{\mathbf{a},h}\|_{\omega_\ell^{\mathbf{a}}} < \|\nabla r^{\mathbf{a},p}\|_{\omega_\ell^{\mathbf{a}}}\}, \tag{2.52b}$$

in such a way that

$$\widetilde{\mathcal{V}}_\ell^\theta = \widetilde{\mathcal{V}}_\ell^h \cup \widetilde{\mathcal{V}}_\ell^p, \qquad \widetilde{\mathcal{V}}_\ell^h \cap \widetilde{\mathcal{V}}_\ell^p = \emptyset.$$

The above *hp*-decision criterion on vertices means that a marked vertex is flagged for *h*-refinement if $\|\nabla r^{\mathbf{a},h}\|_{\omega_\ell^{\mathbf{a}}}$ is larger than $\|\nabla r^{\mathbf{a},p}\|_{\omega_\ell^{\mathbf{a}}}$; otherwise, this vertex is flagged for *p*-refinement.

For the construction of the residuals $r^{\mathbf{a},h}$ and $r^{\mathbf{a},p}$ in Definitions 2.4.6 and 2.4.7, respectively, we considered homogeneous Dirichlet boundary conditions as in Daniel et al. (2018a). Alternatively, while keeping the local criterion (2.52) unchanged, it is possible to define the *h*- and *p*-refinement residuals by solving the local problems with homogeneous Neumann boundary condi-

tions. We will also consider these alternative definitions in our numerical experiments.

Definition 2.4.8 (*h*-refinement residual – Neumann conditions)**.** *Let* $\mathbf{a} \in \widetilde{\mathcal{V}}_\ell^\theta$ *be a marked vertex. Let the simplicial submesh* $\mathcal{T}_\ell^{\mathbf{a},h}$ *and the corresponding polynomial degree distribution* $\mathbf{p}_\ell^{\mathbf{a},h}$ *be as in Definition 2.4.6. We recall the definition of space* $H^1_*(\omega_\ell^{\mathbf{a}})$ *in* (2.22) *and we set*

$$V_\ell^{\mathbf{a},h} := \mathbb{P}_{\mathbf{p}_\ell^{\mathbf{a},h}}(\mathcal{T}_\ell^{\mathbf{a},h}) \cap H^1_*(\omega_\ell^{\mathbf{a}}). \tag{2.53}$$

Then, we let $r^{\mathbf{a},h} \in V_\ell^{\mathbf{a},h}$ *solve*

$$(\nabla r^{\mathbf{a},h}, \nabla v^{\mathbf{a},h})_{\omega_\ell^{\mathbf{a}}} = (f, w_{\psi_\ell^{\mathbf{a}}}(v^{\mathbf{a},h}))_{\omega_\ell^{\mathbf{a}}} - (\nabla u_\ell, \nabla w_{\psi_\ell^{\mathbf{a}}}(v^{\mathbf{a},h}))_{\omega_\ell^{\mathbf{a}}} \qquad \forall\, v^{\mathbf{a},h} \in V_\ell^{\mathbf{a},h}, \tag{2.54}$$

where $w_{\psi_\ell^{\mathbf{a}}}(v^{\mathbf{a},h})$ *stands for weighting a function* $v^{\mathbf{a},h} \in V_\ell^{\mathbf{a},h}$ *by the hat function* $\psi_\ell^{\mathbf{a}}$ *such that*

$$w_{\psi_\ell^{\mathbf{a}}}(v^{\mathbf{a},h}) \in \mathbb{P}_{\mathbf{p}_\ell^{\mathbf{a},h}}(\mathcal{T}_\ell^{\mathbf{a},h}) \cap H^1(\omega_\ell^{\mathbf{a}}) \qquad \text{and} \qquad w_{\psi_\ell^{\mathbf{a}}}(v^{\mathbf{a},h})(\mathbf{x}) = \psi_\ell^{\mathbf{a}}(\mathbf{x}) \cdot v^{\mathbf{a},h}(\mathbf{x}) \tag{2.55}$$

with the nodes $\mathbf{x}$ *uniquely determining a function in* $\mathbb{P}_{\mathbf{p}_\ell^{\mathbf{a},h}}(\mathcal{T}_\ell^{\mathbf{a},h}) \cap H^1(\omega_\ell^{\mathbf{a}})$.

Definition 2.4.9 (*p*-refinement residual – Neumann conditions)**.** *Let* $\mathbf{a} \in \widetilde{\mathcal{V}}_\ell^\theta$ *be a marked vertex associated with the simplicial mesh* $\mathcal{T}_\ell^{\mathbf{a},p}$ *and corresponding polynomial degree distribution* $\mathbf{p}_\ell^{\mathbf{a},p}$ *as in Definition 2.4.7. We set*

$$V_\ell^{\mathbf{a},p} := \mathbb{P}_{\mathbf{p}_\ell^{\mathbf{a},p}}(\mathcal{T}_\ell^{\mathbf{a},p}) \cap H^1_*(\omega_\ell^{\mathbf{a}}). \tag{2.56}$$

Then, we let $r^{\mathbf{a},p} \in V_\ell^{\mathbf{a},p}$ *solve*

$$(\nabla r^{\mathbf{a},p}, \nabla v^{\mathbf{a},p})_{\omega_\ell^{\mathbf{a}}} = (f, w_{\psi_\ell^{\mathbf{a}}}(v^{\mathbf{a},p}))_{\omega_\ell^{\mathbf{a}}} - (\nabla u_\ell, \nabla w_{\psi_\ell^{\mathbf{a}}}(v^{\mathbf{a},p}))_{\omega_\ell^{\mathbf{a}}} \qquad \forall\, v^{\mathbf{a},p} \in V_\ell^{\mathbf{a},p}, \tag{2.57}$$

where $w_{\psi_\ell^{\mathbf{a}}}(v^{\mathbf{a},h})$*, similarly to* (2.55)*, stands for weighting a function* $v^{\mathbf{a},p} \in V_\ell^{\mathbf{a},p}$ *by a hat function* $\psi_\ell^{\mathbf{a}}$ *such that*

$$w_{\psi_\ell^{\mathbf{a}}}(v^{\mathbf{a},p}) \in \mathbb{P}_{\mathbf{p}_\ell^{\mathbf{a},p}}(\mathcal{T}_\ell^{\mathbf{a},p}) \cap H^1(\omega_\ell^{\mathbf{a}}) \qquad \text{and} \qquad w_{\psi_\ell^{\mathbf{a}}}(v^{\mathbf{a},p})(\mathbf{x}) = \psi_\ell^{\mathbf{a}}(\mathbf{x}) \cdot v^{\mathbf{a},p}(\mathbf{x})$$

with the nodes $\mathbf{x}$ *uniquely determining a function in* $\mathbb{P}_{\mathbf{p}_\ell^{\mathbf{a},p}}(\mathcal{T}_\ell^{\mathbf{a},p}) \cap H^1(\omega_\ell^{\mathbf{a}})$.

2.4.5.2 *hp*-decision on simplices

The second step in the module `REFINE` is to use the subsets $\widetilde{\mathcal{V}}_\ell^h$ and $\widetilde{\mathcal{V}}_\ell^p$ to decide whether *h*-, *p*- , or *hp*-refinement should be performed on each simplex having at least one flagged vertex. To this purpose, we define the following subsets:

$$\mathcal{M}_\ell^h := \{K \in \mathcal{T}_\ell \mid \mathcal{V}_K \cap \widetilde{\mathcal{V}}_\ell^h \neq \emptyset\} \subset \mathcal{M}_\ell^\theta, \tag{2.58a}$$

$$\mathcal{M}_\ell^p := \{K \in \mathcal{T}_\ell \mid \mathcal{V}_K \cap \widetilde{\mathcal{V}}_\ell^p \neq \emptyset\} \subset \mathcal{M}_\ell^\theta. \tag{2.58b}$$

In other words, a simplex $K \in \mathcal{T}_\ell$ is flagged for h-refinement (resp., p-refinement) if it has at least one vertex flagged for h-refinement (resp., p-refinement). Note that the subsets $\mathcal{M}_\ell^h$ and $\mathcal{M}_\ell^p$ are not necessarily disjoint since a simplex can have some vertices flagged for h-refinement and others flagged for p-refinement; such simplices are then flagged for hp-refinement. Note also that $\mathcal{M}_\ell^h \cup \mathcal{M}_\ell^p = \cup_{\mathbf{a}\in\widetilde{\mathcal{V}}_\ell^\theta} \mathcal{T}_\ell^{\mathbf{a}} = \mathcal{M}_\ell^\theta$ is indeed the set of marked simplices considered in the module `MARK`.

2.4.5.3 hp-refinement

In this last and final step, the subsets $\mathcal{M}_\ell^h$ and $\mathcal{M}_\ell^p$ are used to produce first the next mesh $\mathcal{T}_{\ell+1}$ and then the next polynomial-degree distribution $\mathbf{p}_{\ell+1}$ on the mesh $\mathcal{T}_{\ell+1}$.

The next mesh $\mathcal{T}_{\ell+1}$ is a matching simplicial refinement of $\mathcal{T}_\ell$ obtained by dividing each flagged simplex $K \in \mathcal{M}_\ell^h$ into at least two simplices in a way that is consistent with the matching simplicial refinement of $\mathcal{T}_\ell^{\mathbf{a}}$ considered in Definition 2.4.6 to build $\mathcal{T}_\ell^{\mathbf{a},h}$, i.e., such that $\mathcal{T}_\ell^{\mathbf{a},h} \subset \mathcal{T}_{\ell+1}$ for all $\mathbf{a} \in \widetilde{\mathcal{V}}_\ell^h$. Note that to preserve the conformity of the mesh, additional refinements beyond the set of flagged simplices $\mathcal{M}_\ell^h$ may be carried out when building $\mathcal{T}_{\ell+1}$. Several algorithms can be considered to refine the mesh. In our numerical experiments, we used the newest vertex bisection algorithm, cf. Sewell (1972), Mitchell (1989).

After having constructed the next mesh $\mathcal{T}_{\ell+1}$, we assign the next polynomial-degree distribution $\mathbf{p}_{\ell+1}$ as follows. For all $K \in \mathcal{T}_{\ell+1}$, let $\widetilde{K}$ denote its parent simplex in $\mathcal{T}_\ell$. We then set

$$p_{\ell+1,K} := p_{\ell,\widetilde{K}} \qquad \text{if } \widetilde{K} \notin \mathcal{M}_\ell^p, \tag{2.59}$$

that is, we assign the same polynomial degree to the children of a simplex that is not flagged for p-refinement, whereas we set

$$p_{\ell+1,K} := \max_{\mathbf{a}\in\mathcal{V}_{\widetilde{K}}\cap\widetilde{\mathcal{V}}_\ell^p} \left(p_{\ell,\widetilde{K}} + \delta_{\widetilde{K}}^{\mathbf{a}}\right) \qquad \text{if } \widetilde{K} \in \mathcal{M}_\ell^p, \tag{2.60}$$

that is, we assign to the children of a simplex $\widetilde{K} \in \mathcal{M}_\ell^p$ flagged for p-refinement the largest of the polynomial degrees considered in Definition 2.4.7 to build the local residual liftings associated with the vertices of $\widetilde{K}$ flagged for p-refinement.

2.5 Guaranteed bound on the error reduction

In this section we extend the results of our previous work (Daniel et al., 2018a, Section 5), where a computable guaranteed bound on the error reduction factor between two consecutive steps of an adaptive procedure with an exact solver

has been derived. We recall that the adaptive strategy of Daniel et al. (2018a) generates a sequence of exact finite element solutions $\{u_\ell^{\mathrm{ex}}\}_{\ell\geq 0}$. For a fixed $\ell \geq 0$, let us denote by $C_{\mathrm{red}}^{\mathrm{ex}}$ the bound on the energy error reduction factor between $u_\ell^{\mathrm{ex}} \in V_\ell$ and $u_{\ell+1}^{\mathrm{ex}} \in V_{\ell+1}$ derived in (Daniel et al., 2018a, Theorem 5.2) such that

$$\|\nabla(u - u_{\ell+1}^{\mathrm{ex}})\| \leq C_{\mathrm{red}}^{\mathrm{ex}} \|\nabla(u - u_\ell^{\mathrm{ex}})\| \quad \text{with} \quad 0 \leq C_{\mathrm{red}}^{\mathrm{ex}} \leq 1. \tag{2.61}$$

Using the current notation, and letting $\omega_\ell := \cup_{\mathbf{a}\in\widetilde{\mathcal{V}}_\ell^\theta} \omega_\ell^{\mathbf{a}}$, the definition of $C_{\mathrm{red}}^{\mathrm{ex}}$ reads

$$C_{\mathrm{red}}^{\mathrm{ex}} := \sqrt{1 - \left(\theta \frac{\underline{\eta}_{\mathcal{M}_\ell^\theta}^{\mathrm{ex}}}{\eta(u_\ell^{\mathrm{ex}}, \mathcal{M}_\ell)}\right)^2}, \tag{2.62}$$

with the total error estimator $\eta(u_\ell^{\mathrm{ex}}, \mathcal{M}_\ell)$ of Theorem 2.3.3 (the local algebraic error estimator $\eta_{\mathrm{alg},K}(u_\ell^{\mathrm{ex}}) := 0$ for each $K \in \mathcal{T}_\ell$), and the discrete lower bound $\underline{\eta}_{\mathcal{M}_\ell^\theta}^{\mathrm{ex}} \leq \|\nabla(u_{\ell+1}^{\mathrm{ex}} - u_\ell^{\mathrm{ex}})\|_{\omega_\ell}$ defined in (Daniel et al., 2018a, Lemma 5.1).

The aim of this section is to derive an equivalent of the bound (2.61) between the two *inexact* solutions $u_\ell \in V_\ell$ and $u_{\ell+1} \in V_{\ell+1}$ obtained by the iterative procedure of Scheme 2.2 in the form

$$\|\nabla(u - u_{\ell+1})\| \leq C_{\mathrm{red}} \|\nabla(u - u_\ell)\|.$$

It turns out essential to first estimate a guaranteed bound on the error reduction between the current inexact solution $u_\ell \in V_\ell$ and the (unavailable) exact solution on the next level $u_\ell^{\mathrm{ex}} \in V_{\ell+1}$. For this we start by extending the discrete lower bound of (Daniel et al., 2018a, Lemma 5.1) to the present setting:

Lemma 2.5.1 (Guaranteed lower bound on the incremental error on marked simplices)**.** *Let the mesh $\mathcal{T}_{\ell+1}$ and the polynomial-degree distribution $\mathbf{p}_{\ell+1}$ result from the* `REFINE` *module of Section 2.4.5, and recall that $V_{\ell+1} = \mathbb{P}_{\mathbf{p}_{\ell+1}}(\mathcal{T}_{\ell+1}) \cap H_0^1(\Omega)$ is the finite element space to be used on iteration $(\ell+1)$ of the adaptive loop of Scheme 2.2. For all the marked vertices $\mathbf{a} \in \widetilde{\mathcal{V}}_\ell^\theta$, let us set, in extension of (2.49), (2.50),*

$$V_\ell^{\mathbf{a},hp} := V_{\ell+1}|_{\omega_\ell^{\mathbf{a}}} \cap H_0^1(\omega_\ell^{\mathbf{a}}), \tag{2.63}$$

and construct the residual lifting $r^{\mathbf{a},hp} \in V_\ell^{\mathbf{a},hp}$ by solving

$$(\nabla r^{\mathbf{a},hp}, \nabla v^{\mathbf{a},hp})_{\omega_\ell^{\mathbf{a}}} = (f, v^{\mathbf{a},hp})_{\omega_\ell^{\mathbf{a}}} - (\nabla u_\ell, \nabla v^{\mathbf{a},hp})_{\omega_\ell^{\mathbf{a}}} \qquad \forall\, v^{\mathbf{a},hp} \in V_\ell^{\mathbf{a},hp}. \tag{2.64}$$

Then, after extending $r^{\mathbf{a},hp}$ by zero outside $\omega_\ell^{\mathbf{a}}$, for the current inexact approximation $u_\ell \in V_\ell$ and the exact approximation $u_{\ell+1}^{\mathrm{ex}} \in V_{\ell+1}$ on the next level,

the following holds true:

$$\|\nabla(u_{\ell+1}^{\mathrm{ex}} - u_\ell)\|_{\omega_\ell} \geq \underline{\eta}_{\mathcal{M}_\ell^\theta}, \quad \underline{\eta}_{\mathcal{M}_\ell^\theta} := \begin{cases} \dfrac{\sum_{\mathbf{a}\in\widetilde{\mathcal{V}}_\ell^\theta} \left\|\nabla r^{\mathbf{a},hp}\right\|_{\omega_\ell^{\mathbf{a}}}^2}{\left\|\nabla\left(\sum_{\mathbf{a}\in\widetilde{\mathcal{V}}_\ell^\theta} r^{\mathbf{a},hp}\right)\right\|_{\omega_\ell}} & \text{if } \sum_{\mathbf{a}\in\widetilde{\mathcal{V}}_\ell^\theta} r^{\mathbf{a},hp} \neq 0, \\ 0 & \text{otherwise.} \end{cases} \tag{2.65}$$

Proof. We remark that the definition of the residual liftings $r^{\mathbf{a},hp}$ (2.64) employs directly the inexact approximation u_ℓ unlike in (Daniel et al., 2018a, Lemma 5.1) where u_ℓ^{ex} (in the present notation) was considered. Nevertheless, the arguments to prove the lower bound $\underline{\eta}_{\mathcal{M}_\ell^\theta}^{\mathrm{ex}}$ of (Daniel et al., 2018a, Lemma 5.1) stay valid and can be used to show (2.65). □

In case of the use of residuals $r^{\mathbf{a},h}$ and $r^{\mathbf{a},p}$ from Definitions 2.4.8 and 2.4.9, respectively, in the local criterion (2.52) within the `REFINE` module, the above lower bound can be adjusted as well.

Lemma 2.5.2 (Guaranteed lower bound on the incremental error on marked simplices – alternative definition)**.** *Let the assumptions of Lemma 2.5.1 be satisfied. Moreover, let us set for all the marked vertices* $\mathbf{a} \in \widetilde{\mathcal{V}}_\ell^\theta$*, in extension of* (2.53) *and* (2.56)*,*

$$V_\ell^{\mathbf{a},hp} := V_{\ell+1}|_{\omega_\ell^{\mathbf{a}}} \cap H_*^1(\omega_\ell^{\mathbf{a}}). \tag{2.66}$$

Then, for each marked vertex $\mathbf{a} \in \widetilde{\mathcal{V}}_\ell^\theta$*, construct the residual lifting* $r^{\mathbf{a},hp} \in V_\ell^{\mathbf{a},hp}$ *by solving*

$$(\nabla r^{\mathbf{a},hp}, \nabla v^{\mathbf{a},hp})_{\omega_\ell^{\mathbf{a}}} = (f, w_{\psi_\ell^{\mathbf{a}}}(v^{\mathbf{a},hp}))_{\omega_\ell^{\mathbf{a}}} - (\nabla u_\ell, \nabla w_{\psi_\ell^{\mathbf{a}}}(v^{\mathbf{a},hp}))_{\omega_\ell^{\mathbf{a}}} \quad \forall\, v^{\mathbf{a},hp} \in V_\ell^{\mathbf{a},hp}, \tag{2.67}$$

where $w_{\psi_\ell^{\mathbf{a}}}(v^{\mathbf{a},hp})$ *stands for weighting a function* $v^{\mathbf{a},hp} \in V_\ell^{\mathbf{a},hp}$ *by hat function* $\psi_\ell^{\mathbf{a}}$ *such that*

$$w_{\psi_\ell^{\mathbf{a}}}(v^{\mathbf{a},p}) \in V_{\ell+1}|_{\omega_\ell^{\mathbf{a}}} \qquad \text{and} \qquad w_{\psi_\ell^{\mathbf{a}}}(v^{\mathbf{a},p})(\mathbf{x}) = \psi_\ell^{\mathbf{a}}(\mathbf{x}) \cdot v^{\mathbf{a},p}(\mathbf{x})$$

with the nodes $\mathbf{x}$ *uniquely determining a function in* $V_{\ell+1}|_{\omega_\ell^{\mathbf{a}}}$*. After extending each* $r^{\mathbf{a},hp}$ *by zero outside* $\omega_\ell^{\mathbf{a}}$*, the following lower bound holds true:*

$$\|\nabla(u_{\ell+1}^{\mathrm{ex}} - u_\ell)\|_{\omega_\ell} \geq \underline{\eta}_{\mathcal{M}_\ell^\theta}, \ \underline{\eta}_{\mathcal{M}_\ell^\theta} := \begin{cases} \dfrac{\sum_{\mathbf{a}\in\widetilde{\mathcal{V}}_\ell^\theta} \left\|\nabla r^{\mathbf{a},hp}\right\|_{\omega_\ell^{\mathbf{a}}}^2}{\left\|\nabla\left(\sum_{\mathbf{a}\in\widetilde{\mathcal{V}}_\ell^\theta} w_{\psi_\ell^{\mathbf{a}}}(r^{\mathbf{a},hp})\right)\right\|_{\omega_\ell}} & \text{if } \sum_{\mathbf{a}\in\widetilde{\mathcal{V}}_\ell^\theta} r^{\mathbf{a},hp} \neq 0, \\ 0 & \text{otherwise.} \end{cases} \tag{2.68}$$

Proof. Let us note that $(u_{\ell+1}^{\mathrm{ex}} - u_\ell)|_{\omega_\ell}$ belongs to the space $V_{\ell+1}(\omega_\ell)$, a restriction of the finite element space $V_{\ell+1}$ to ω_ℓ. However, note that it does not

necessarily belong to the homogeneous Dirichlet subspace $V^0_{\ell+1}(\omega_\ell)$. The definition of the energy norm $\|\nabla(u^{\rm ex}_{\ell+1}-u_\ell)\|_{\omega_\ell}$ and the fact that $v_{\ell+1}\in V^0_{\ell+1}(\omega_\ell)$ extended by zero outside ω_ℓ is a member of the space $V_{\ell+1}$ so that it can be used as a test function in the definition (2.5) of $u^{\rm ex}_{\ell+1}$ on the mesh $\mathcal{T}_{\ell+1}$ yield

$$\begin{aligned}\|\nabla(u^{\rm ex}_{\ell+1}-u_\ell)\|_{\omega_\ell} &= \sup_{v_{\ell+1}\in V_{\ell+1}(\omega_\ell)} \frac{(\nabla(u^{\rm ex}_{\ell+1}-u_\ell),\nabla v_{\ell+1})_{\omega_\ell}}{\|\nabla v_{\ell+1}\|_{\omega_\ell}}\\ &\geq \sup_{v_{\ell+1}\in V^0_{\ell+1}(\omega_\ell)} \frac{(\nabla(u^{\rm ex}_{\ell+1}-u_\ell),\nabla v_{\ell+1})_{\omega_\ell}}{\|\nabla v_{\ell+1}\|_{\omega_\ell}}\\ &= \sup_{v_{\ell+1}\in V^0_{\ell+1}(\omega_\ell)} \frac{(f,v_{\ell+1})_{\omega_\ell}-(\nabla u_\ell,\nabla v_{\ell+1})_{\omega_\ell}}{\|\nabla v_{\ell+1}\|_{\omega_\ell}}.\end{aligned}$$

Now, choose the test function $v_{\ell+1}:=\sum_{\mathbf{a}\in\widetilde{\mathcal{V}}^\theta_\ell} w_{\psi^{\mathbf{a}}_\ell}(r^{\mathbf{a},hp})$; note that, due to the weighting $w_{\psi^{\mathbf{a}}_\ell}(\cdot)$, such choice of $v_{\ell+1}$ indeed belongs to $V^0_{\ell+1}(\omega_\ell)$. Then, we infer that

$$\begin{aligned}\Big(f,\sum_{\mathbf{a}\in\widetilde{\mathcal{V}}^\theta_\ell} w_{\psi^{\mathbf{a}}_\ell}(r^{\mathbf{a},hp})\Big)_{\omega_\ell} &- \Big(\nabla u_\ell,\sum_{\mathbf{a}\in\widetilde{\mathcal{V}}^\theta_\ell} w_{\psi^{\mathbf{a}}_\ell}(r^{\mathbf{a},hp})\Big)_{\omega_\ell}\\ &= \sum_{\mathbf{a}\in\widetilde{\mathcal{V}}^\theta_\ell}\{(f,w_{\psi^{\mathbf{a}}_\ell}(r^{\mathbf{a},hp}))_{\omega_\ell}-(\nabla u_\ell,\nabla w_{\psi^{\mathbf{a}}_\ell}(r^{\mathbf{a},hp}))_{\omega_\ell}\}\\ &= \sum_{\mathbf{a}\in\widetilde{\mathcal{V}}^\theta_\ell}\|\nabla r^{\mathbf{a},hp}\|^2_{\omega^{\mathbf{a}}_\ell},\end{aligned}$$

where we have employed (2.67) with $r^{\mathbf{a},hp}$ as a test function. This implies the assertion (2.68). □

We now proceed with an intermediate result giving a guaranteed bound on the error reduction factor between the current inexact approximation u_ℓ and the (unavailable) next level exact solution $u^{\rm ex}_{\ell+1}$.

Lemma 2.5.3 (Auxiliary guaranteed bound on the energy error reduction factor)**.** *Let θ be the threshold parameter used within the module* `MARK` *of Section 2.4.4 and let the mesh $\mathcal{T}_{\ell+1}$ and the polynomial degree distribution $\mathbf{p}_{\ell+1}$ be given by the* `REFINE` *module of Section 2.4.5. Next, let $V_{\ell+1}:=\mathbb{P}_{\mathbf{p}_{\ell+1}}(\mathcal{T}_{\ell+1})\cap H^1_0(\Omega)$ be the space to be used on iteration $(\ell+1)$ of the algorithm prescribed by Scheme 2.2. Let $\underline{\eta}_{\mathcal{M}^\theta_\ell}$ be the lower bound defined by (2.65) or (2.68), depending on the choice of the construction of residuals $r^{\mathbf{a},h}$, $r^{\mathbf{a},p}$ used within the* `REFINE` *module. Then, unless $\eta(u_\ell,\mathcal{T}_\ell)=0$, in which case $u_\ell=u$, and the adaptive loop terminates, the exact finite element solution*

$u_{\ell+1}^{\mathrm{ex}} \in V_{\ell+1}$ satisfies

$$\|\nabla(u - u_{\ell+1}^{\mathrm{ex}})\| \leq C_{\mathrm{red}}^{*} \|\nabla(u - u_\ell)\| \quad \text{with} \quad 0 \leq C_{\mathrm{red}}^{*} := \sqrt{1 - \frac{\underline{\eta}_{\mathcal{M}_\ell^\theta}^2}{\eta^2(u_\ell, \mathcal{T}_\ell)}} \leq 1. \tag{2.69}$$

Proof. Since the Galerkin orthogonality property between the current approximation $u_\ell \in V_\ell$ and the exact finite element solution $u_{\ell+1}^{\mathrm{ex}} \in V_{\ell+1}$ holds true, we have

$$\|\nabla(u - u_{\ell+1}^{\mathrm{ex}})\|^2 = \|\nabla(u - u_\ell)\|^2 - \|\nabla(u_{\ell+1}^{\mathrm{ex}} - u_\ell)\|^2. \tag{2.70}$$

Afterwards, employing the lower bound $\underline{\eta}_{\mathcal{M}_\ell^\theta}$ and the total error upper bound $\eta(u_\ell, \mathcal{T}_\ell)$ from (2.15) in (2.70) yields

$$\begin{aligned} \|\nabla(u - u_{\ell+1}^{\mathrm{ex}})\|^2 &\leq \|\nabla(u - u_\ell)\|^2 - \underline{\eta}_{\mathcal{M}_\ell^\theta}^2 \frac{\|\nabla(u - u_\ell)\|^2}{\|\nabla(u - u_\ell)\|^2} \\ &\leq \|\nabla(u - u_\ell)\|^2 \left(1 - \frac{\underline{\eta}_{\mathcal{M}_\ell^\theta}^2}{\eta^2(u_\ell, \mathcal{T}_\ell)}\right). \end{aligned}$$

The assertion (2.69) then follows by taking the square root. □

Finally, we are ready to present the result on a computable guaranteed bound on the reduction factor in the inexact setting:

Theorem 2.5.4 (Guaranteed bound on the energy error reduction factor between two inexact solutions)**.** *Let the assumptions of Lemma 2.5.3 be satisfied and let C_{red}^{*} be given by (2.69). Moreover, let $u_{\ell+1} \in V_{\ell+1}$ be the inexact finite element approximation on iteration $(\ell+1)$ of the procedure prescribed by Scheme 2.2, satisfying the global stopping criterion*

$$\eta_{\mathrm{alg}}(u_{\ell+1}, \mathcal{T}_{\ell+1}) \leq \gamma_{\ell+1}\, \mu(u_{\ell+1}), \tag{2.71}$$

with the parameter

$$0 \leq \gamma_{\ell+1} \leq (1 - C_{\mathrm{red}}^{*}). \tag{2.72}$$

Then, the resulting error reduction between the inexact solution $u_\ell \in V_\ell$ from the current iteration ℓ and the next approximation $u_{\ell+1}$ to be computed on the next iteration verifies

$$\|\nabla(u - u_{\ell+1})\| \leq C_{\mathrm{red}} \|\nabla(u - u_\ell)\| \quad \text{with} \quad 0 \leq C_{\mathrm{red}} := \frac{C_{\mathrm{red}}^{*}}{(1 - \gamma_{\ell+1})} \leq 1. \tag{2.73}$$

Proof. We start by adding and subtracting $\nabla u_{\ell+1}^{\mathrm{ex}}$ inside the norm on the left hand side of (2.73). The triangle inequality then yields

$$\|\nabla(u - u_{\ell+1})\| \leq \|\nabla(u - u_{\ell+1}^{\mathrm{ex}})\| + \|\nabla(u_{\ell+1}^{\mathrm{ex}} - u_{\ell+1})\|. \tag{2.74}$$

For bounding the first term, we employ the auxiliary bound (2.69). The second term of (2.74), the algebraic error on iteration $(\ell+1)$, is first bounded from above by the algebraic error estimate (2.16). Then, the stopping criterion (2.71) with the parameter $\gamma_{\ell+1}$ in combination with the total energy error lower bound (2.24) give

$$\|\nabla(u_{\ell+1}^{\mathrm{ex}} - u_{\ell+1})\| \leq \eta_{\mathrm{alg}}(u_{\ell+1}, \mathcal{T}_{\ell+1}) \leq \gamma_{\ell+1}\, \mu(u_{\ell+1}) \leq \gamma_{\ell+1}\, \|\nabla(u - u_{\ell+1})\|,$$

whence we infer (2.73). The condition (2.72) on parameter $\gamma_{\ell+1}$ then ensures the upper bound $C_{\mathrm{red}} \leq 1$. □

Remark 2.5.5 (Extreme case equivalent to the use of an exact solver)**.** *In Theorem 2.5.4 we do not exclude the extreme case when the auxiliary upper bound $C_{\mathrm{red}}^{*} = 1$. This in turn leads to the stopping criterion (2.71) with the parameter $\gamma_{\ell+1} = 0$, which is equivalent to computing the exact finite element solution $u_{\ell+1}^{\mathrm{ex}}$. However, we note that in our numerical experiments, reported in Section 2.6, we never encountered such a situation when the exact solver would be necessary.*

Remark 2.5.6 (Motivation)**.** *We believe that, under some additional assumptions on the refinements, such as the the interior node property* Morin et al. (2002)*, one could actually show $C_{\mathrm{red}}^{*} < 1$. The convergence of the proposed method would then easily follow. We do not address this topic here, however, it represents a subject of our active research.*

2.6 Numerical experiments

We now illustrate the capabilities and robustness of the proposed adaptive solver using two types of test cases in two space dimensions. We consider two problems with a (relatively) smooth weak solution and one with a singular weak solution.

We focus on the influence of the inexact algebraic solver on the performance of the proposed *hp*-refinement strategy described in Section 2.4.5. While employing the adaptive stopping criterion (2.45) with the parameter γ_ℓ satisfying (2.72), we assess the quality of the guaranteed bound on the reduction factor C_{red} from Theorem 2.5.4 throughout the adaptive process in terms of the effectivity index defined as

$$I_{\mathrm{red}}^{\mathrm{eff}} := \frac{C_{\mathrm{red}}}{\frac{\|\nabla(u-u_{\ell+1})\|}{\|\nabla(u-u_\ell)\|}}. \tag{2.75}$$

We also verify the sharpness of the underlying discrete lower bound $\underline{\eta}_{\mathcal{M}_\ell^\theta}$ given by (2.65) or (2.68) in terms of the effectivity index defined as

$$I_{\mathrm{LB}}^{\mathrm{eff}} := \frac{\|\nabla(u_{\ell+1}^{\mathrm{ex}} - u_\ell)\|_{\omega_\ell}}{\underline{\eta}_{\mathcal{M}_\ell^\theta}}. \tag{2.76}$$

Besides that, we are interested in the comparison of the different stopping criteria for the algebraic solver with regard to the number of necessary iterations per step of the adaptive loop, the time spent on algebraic computations and their influence on the overall adaptive process. In all the example problems, we use the *hp*-multigrid method with 5 pre-smoothing Gauss-Seidel steps and no post-smoothing as the algebraic solver. We always take into account at most 10 last levels available from the current hierarchy of adaptively refined meshes at our disposal for the *hp*-multigrid solver, as well as for the algebraic error flux reconstruction $\boldsymbol{\sigma}_{\ell,\mathrm{alg}}$ from Definition 2.4.1. In other words, if the adaptive loop iteration counter $\ell \geq 10$, we adjust the range of the sum (2.28) in the following way

$$\boldsymbol{\sigma}_{\ell,\mathrm{alg}} := \sum_{j=\ell-8}^{\ell} \sum_{\mathbf{a}\in\mathcal{V}_{j-1}} \boldsymbol{\sigma}^{\mathbf{a}}_{j,\mathrm{alg}},$$

thus we solve problem (2.29) on level $j = \ell - 8$ and problem (2.31) on levels $\ell-7 \leq j \leq \ell$. Similarly, the multigrid solver uses the hierarchy $\{\mathcal{T}_j, \mathbf{p}_j\}_{\ell-9\leq j\leq \ell}$, for $\ell \geq 10$, instead of the complete available hierarchy $\{\mathcal{T}_j, \mathbf{p}_j\}_{0\leq j\leq \ell}$, which is used in case of the iteration counter ℓ being lower than 10. The (well-established) choice $\theta = 0.5$ for the marking parameter in (2.47) is considered. We examine the proposed *hp*-refinement strategy employing the local residuals $r^{\mathbf{a},h}$ and $r^{\mathbf{a},p}$ defined via solving the local problems with either homogeneous Dirichlet (Definitions 2.4.6 and 2.4.7) or homogeneous Neumann boundary conditions (Definitions 2.4.8 and 2.4.9). As mentioned above, we employ the newest vertex bisection algorithm Sewell (1972) to perform *h*-refinement and we use the polynomial-degree increment (2.51) to perform *p*-refinement.

2.6.1 Smooth solution (sharp Gaussian)

As the first test case, we consider the model problem (2.1) posed on a square domain $\Omega := (-1,1)\times(-1,1)$ with a weak solution containing a rather sharp peak

$$u(x,y) = (x^2-1)(y^2-1)\exp\left(-100(x^2+y^2)\right).$$

We start the computation with a coarse criss-cross mesh $\mathcal{T}_0$ with $\max_{K\in\mathcal{T}_0} h_K = 0.25$ and a uniform polynomial-degree distribution equal to 1 on all triangles. In the following, we present the results obtained using the proposed *hp*-refinement strategy employing the local residuals $r^{\mathbf{a},h}$ and $r^{\mathbf{a},p}$ defined by either the local Dirichlet or local Neumann problems.

2.6.1.1 Strategy driven by the local Dirichlet problems

Firstly, in Figure 2.4 we investigate the accuracy of the predicted reduction factor C_{red} (left panel) and the lower bound $\underline{\eta}_{\mathcal{M}_\ell^\theta}$ (center panel) by means of their effectivity indices (2.75) and (2.76) throughout the whole adaptive

procedure described in Scheme 2.2 with the module `REFINE` driven by solving the local Dirichlet problems from Definitions 2.4.6 and 2.4.7. We find the effectivity indices in both cases close to the optimal value of one. The corresponding values of the parameter $\gamma_{\ell+1}$ used within the employed stopping criterion (2.71) are given in the right panel of Figure 2.4. A quantitative

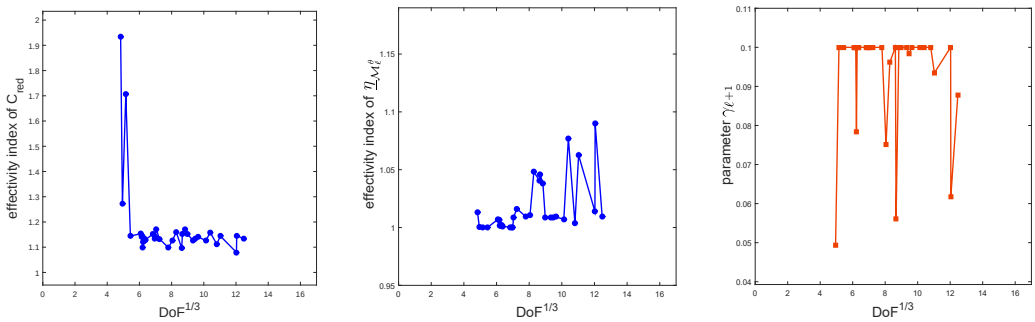

Figure 2.4: [Sharp-Gaussian of Section 2.6.1] The effectivity index for the error reduction factor estimate C_{red} of Theorem 2.5.4 given by (2.75) (*left*); the effectivity index of the discrete lower bound $\underline{\eta}_{\mathcal{M}_\ell^\theta}$ of Lemma 2.5.1 given by (2.76) (*center*); corresponding values of the parameter $\gamma_{\ell+1}$ used in (2.73) (*right*).

assessment of the proposed adaptive strategy with the inexact solver and various stopping criteria is presented in Figure 2.5 (left panel) where we plot the relative error $\|\nabla(u-u_\ell)\|/\|\nabla u\|$ as a function of the cumulative time spent on the algebraic computations in linear-logarithmic scale. We observe that the strategy with inexact solver piloted by the adaptive stopping criterion leads to the steepest error decrease with respect to the computational effort. This is mostly due to cutting off unnecessary algebraic iterations as reported in the right panel of Figure 2.5. Figure 2.6 (left panel) displays the mesh and polynomial-degree distribution obtained after 17 steps of the adaptive procedure. On the right panel of Figure 2.6, we plot the corresponding inexact numerical solution obtained with the adaptive stopping criterion (2.45) for the algebraic solver, i.e. after the second V-cycle of the *hp*-multigrid solver. The detailed evolution of the total error lower bound (2.24) and algebraic error upper bound (2.16), the two main ingredients for the stopping criterion (2.45), throughout the iterations of the algebraic solver at the 17th level of refinement is plotted on the left panel of Figure 2.7. The annotations illustrate when the classical stopping criterion (2.46) with various levels for the tolerance ε are reached. The corresponding values of the true algebraic error in comparison with the algebraic error upper bound, and the norm of the algebraic residual vector $\|\mathrm{R}_\ell\|$ are given on the right panel of Figure 2.7. We observe that the algebraic error upper bound, as well as the norm $\|\mathrm{R}_\ell\|$, closely follow the actual value of the algebraic error, with our error estimate giving a slightly tighter bound during the first three multigrid iterations. In Figure 2.8, left panel, we depict the total energy error along with its upper and lower bounds

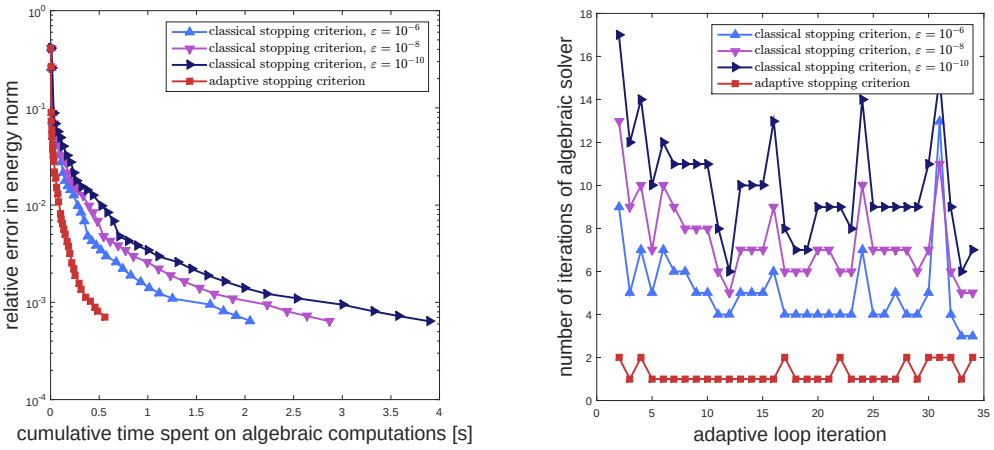

Figure 2.5: [Sharp-Gaussian of Section 2.6.1] The relative energy error $\|\nabla(u - u_\ell)\|/\|\nabla u\|$ as a function of cumulative time spent on algebraic computations with the stopping criteria (2.45) and (2.46) (*left*) and the respective numbers of algebraic solver iterations per step of the adaptive procedure of Scheme 2.2 (*right*).

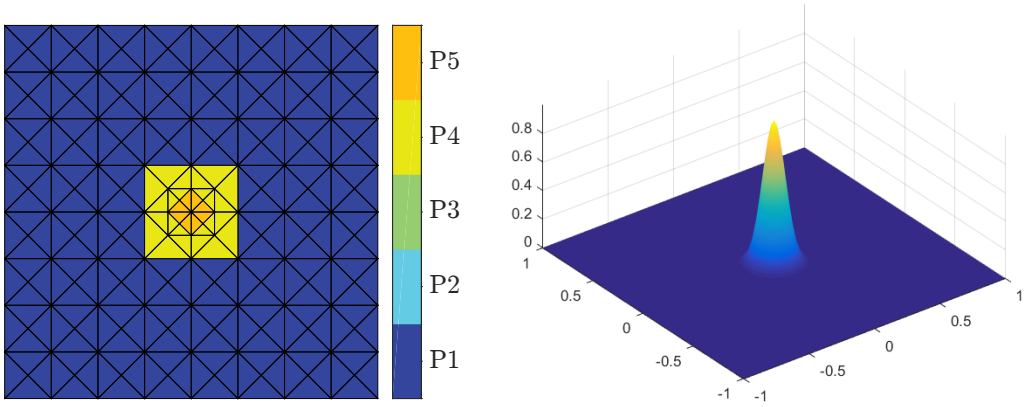

Figure 2.6: [Sharp-Gaussian of Section 2.6.1] The mesh and polynomial-degree distribution $(\mathcal{T}_{17}, \mathbf{p}_{17})$ (*left*) along with the corresponding numerical solution u_{17} obtained after 17 iterations of the *hp*-adaptive procedure (*right*).

during the multigrid iterations. The quantitative evaluation of all the estimators computed within the module `ESTIMATE` in terms of their effectivity indices, i.e. the ratio of the estimates over the error for the upper bounds and the reciprocal for the lower bound, is given on the right panel of Figure 2.8. We note that also these effectivity indices take values close to the optimal value of one. The spatial distributions of the actual total and algebraic errors with the total upper error indicators and algebraic upper error indicators at the moment when the algebraic iterations are stopped on step $\ell = 17$ of the *hp*-adaptive loop, as dictated by the adaptive stopping criterion (2.45), are displayed in Figures 2.9 and 2.10. We see that the actual and predicted error distributions match very nicely.

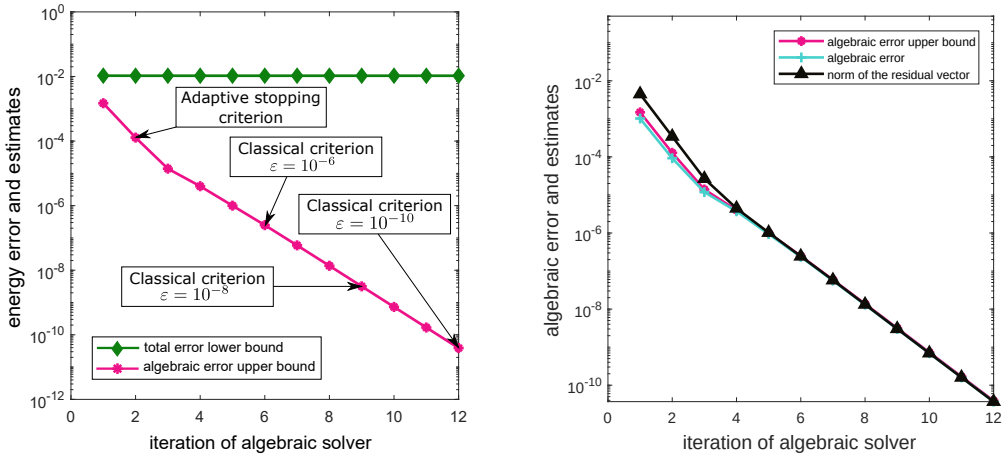

Figure 2.7: [Sharp-Gaussian of Section 2.6.1] Algebraic error upper bound $\eta_{\text{alg}}(u_{17}, \mathcal{T}_{17})$ in comparison with total error lower bound $\mu(u_{17})$ (*left*) and with true algebraic error $\|\nabla(u_{17}^{\text{ex}} - u_{17})\|$ and norm of algebraic residual vector $\|R_{17}\|$ (*right*) as a function of algebraic solver iterations.

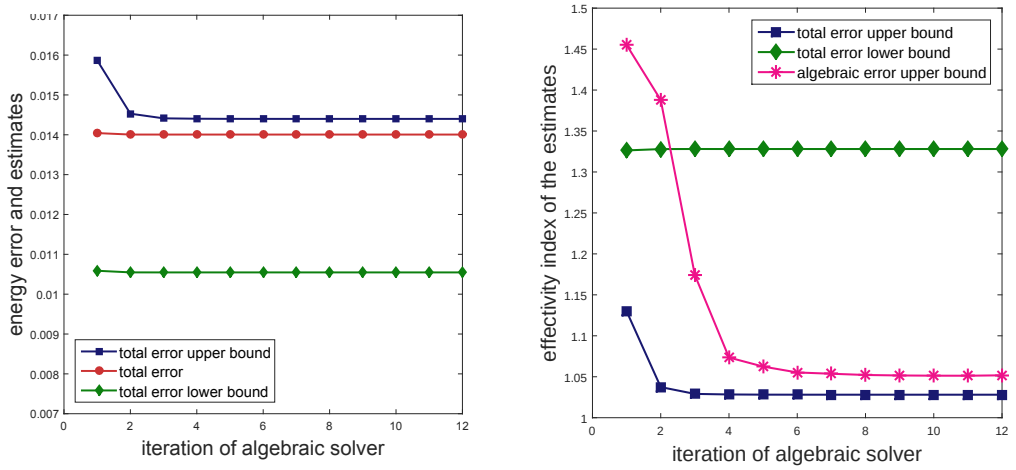

Figure 2.8: [Sharp-Gaussian of Section 2.6.1] Total energy error with its upper and lower bound (*left*) and effectivity indices of total error upper bound (2.15), total error lower bound (2.24), and algebraic error upper bound (2.16) (*right*), throughout the iterations of the multigrid solver.

2.6.1.2 Strategy driven by the local Neumann problems

We also present the results obtained while employing in the adaptive procedure the local residuals $r^{\mathbf{a},h}$ and $r^{\mathbf{a},p}$ defined via solving the local Neumann problems as proposed in Definitions 2.4.8 and 2.4.9. The use of these residuals leads to slightly different meshes and polynomial-degree distributions during the adaptive process (not presented here). In particular, we plot the effectivity indices of the estimated reduction factor C_{red} and of the underlying lower bound $\underline{\eta}_{\mathcal{M}_\ell^\theta}$ in Figure 2.11. We find these estimates a little less precise compared to the ones presented in Figure 2.4, yet the effectivity indices are still quite close to one. The savings when using the adaptive stopping

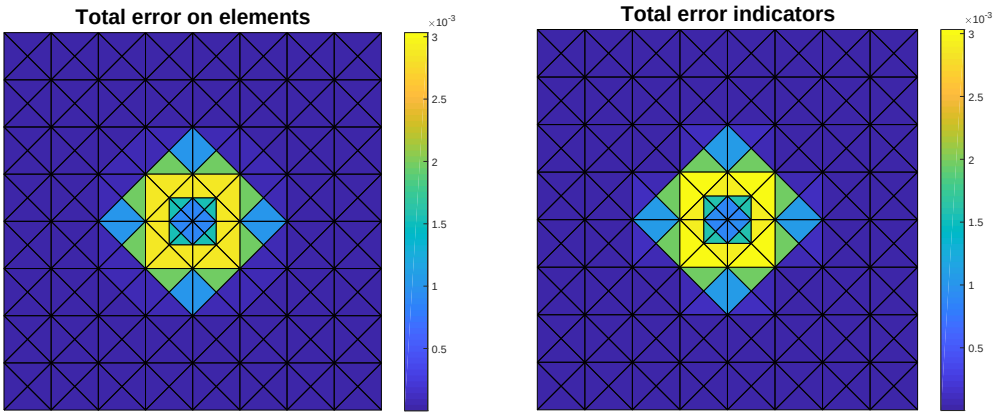

Figure 2.9: [Sharp-Gaussian of Section 2.6.1] Elementwise distribution of the total energy error $\|\nabla(u - u_{17})\|$ (*left*) and total upper error indicators $\eta_K(u_{17})$ (*right*).

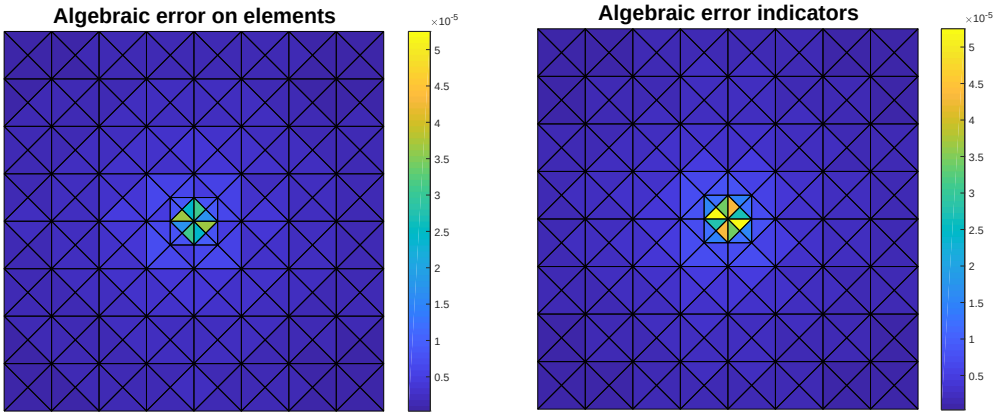

Figure 2.10: [Sharp-Gaussian of Section 2.6.1] Elementwise distribution of the algebraic energy error $\|\nabla(u_{17}^{\mathrm{ex}} - u_{17})\|$ (*left*) and algebraic upper error indicators (*right*) with the adaptive stopping criterion (2.45) satisfied, $\gamma_{17} = 0.1$.

criterion (2.45) compared to the classical stopping criterion (2.46) are then demonstrated in Figure 2.12 in terms of the time spent on algebraic computations and in terms of the number of necessary iterations of the algebraic solver.

2.6.2 Exponential convergence

In Figure 2.13 we show that the proposed *hp*-refinement strategy (driven by solving either local Dirichlet problems or local Neumann problems) still leads, even in the presence of inexact solver, to meshes and polynomial degree distributions for which the relative error decreases exponentially fast. We plot the relative error $\|\nabla(u - u_\ell)\|/\|\nabla u\|$ as a function of $\mathrm{DoF}_\ell^{\frac{1}{3}}$ in logarithmic-linear scale for our strategy with inexact solver, the pure *h*-version of the adaptive loop with exact solver as given in Scheme 2.1, and while using the

uniform h-refinement. For further comparison with different adaptive hp-refinement strategies (with exact algebraic solver) for this model problem we refer to (Daniel et al., 2018a, Section 6.1).

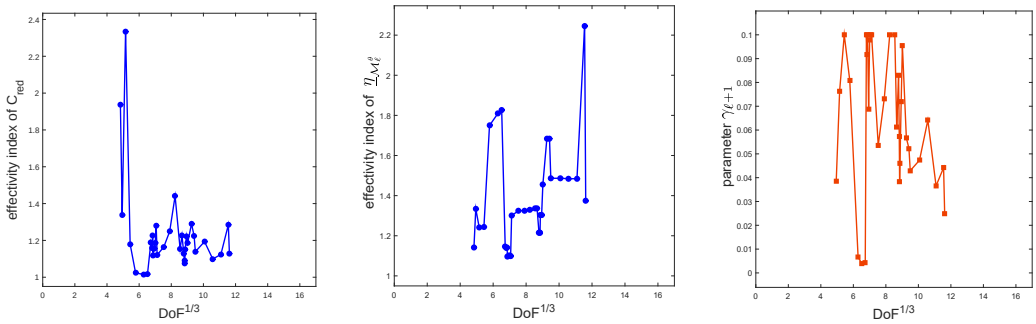

Figure 2.11: [Sharp-Gaussian of Section 2.6.1, strategy with local Neumann problems] The effectivity index for the error reduction factor estimate C_{red} of Theorem 2.5.4 (*left*); the effectivity index of the discrete lower bound $\underline{\eta}_{\mathcal{M}_\ell^\theta}$ of Lemma 2.5.2 given by (2.76) (*center*); corresponding values of parameter $\gamma_{\ell+1}$ used in (2.73) (*right*).

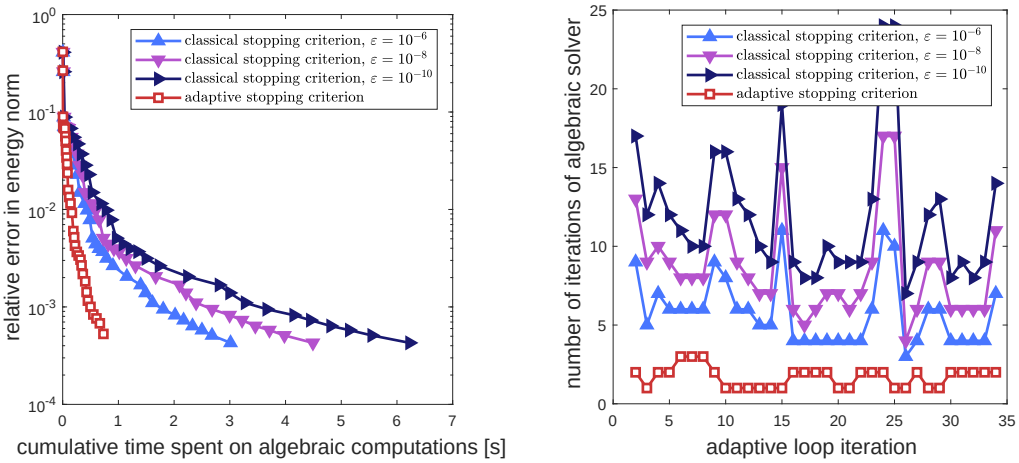

Figure 2.12: [Sharp-Gaussian of Section 2.6.1, strategy with local Neumann problems] The relative energy error $\|\nabla(u - u_\ell)\|/\|\nabla u\|$ as a function of cumulative time spent on algebraic computations of the stopping criteria (2.45) and (2.46) (*left*) and the respective numbers of algebraic solver iterations per step of the adaptive procedure of Scheme 2.2 (*right*).

2.6.3 Smooth solution (asymmetric wave front)

Looking at the results of Section 2.6.1, namely Figures 2.5 and 2.12, one could be tempted to employ at each iteration of the adaptive procedure only a single iteration of the algebraic solver with the hope to eventually converge to the correct solution, while saving a substantial amount of computational effort.

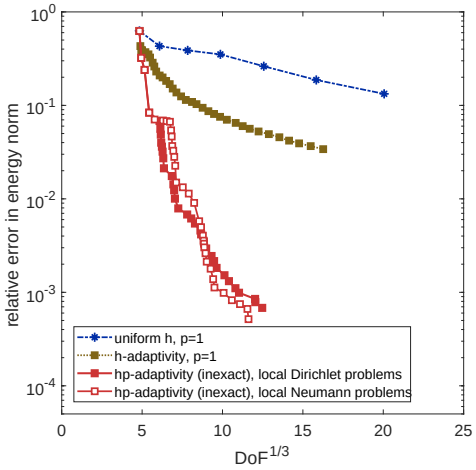

Figure 2.13: [Sharp-Gaussian of Section 2.6.1] Relative energy error $\|\nabla(u-u_\ell)\|/\|\nabla u\|$ as a function of $\mathrm{DoF}_\ell^{\frac{1}{3}}$, obtained with our *hp*-refinement strategy (driven by solving local Dirichlet problems and also local Neumann problems) with inexact algebraic solver, purely *h*-adaptive version with exact solver and using uniform *h*-refinement.

This kind of heuristic approach may actually be beneficial in cases when we launch the adaptive process with a good enough initial guess. However, as we demonstrate here in a fabricated setting, in case of an inaccurate initial guess, it is our adaptive strategy that represents a safe choice, while outperforming both the heuristic approach and the adaptive strategies with algebraic solver piloted by the classical stopping criteria.

To illustrate our point, we consider as the second test case a problem posed on the square domain $\Omega := (0,1)\times(0,1)$ with the exact solution (in polar coordinates)

$$u(r) = \arctan\left(\alpha(r-r_0)\right), \quad r = \sqrt{(x-x_\mathrm{c})^2+(y-y_\mathrm{c})^2}$$

containing a wave front asymmetric within the domain. The parameter $\alpha := 100$ prescribes the steepness of the circular wave front with radius $r_0 := 0.92$ centred at the point $(x_\mathrm{c}, y_\mathrm{c}) := (1.5, 0.25)$, see Figure 2.14 (left panel) (for other variants of the wave front problem, we refer to (Mitchell and McClain, 2011, Sections 5.16–5.19)). For this test case and also the test case of Section 2.6.4, the total error upper bound $\eta(u_\ell, \mathcal{T}_\ell)$ employed within the adaptive procedure takes into account the error from the approximation of the inhomogeneous Dirichlet boundary condition prescribed by the exact solution on $\partial\Omega$; to this purpose, we proceed as described in (Dolejší et al., 2016, Theorem 3.3) and the references therein.

We start the computation with a criss-cross grid $\mathcal{T}_0$ with $\max_{K\in\mathcal{T}_0} h_K = 0.125$. In contrast to the other test cases and the description of the module `ONE_SOLVER_STEP` in Section 2.4.1, this time we solve the algebraic system inexactly even at the initial level $\ell = 0$ using a geometric V-cycle multigrid

solver with hierarchy of 4 additional meshes obtained by uniform coarsening of the mesh $\mathcal{T}_0$. As the initial guess for the algebraic solver, we consider a vector corresponding to a function which does not approximate the wave front well and contains a peak in the region where the exact solution is more or less flat. We display the contour plot of the initial guess function in the right panel of Figure 2.14. In the left panel of Figure 2.15, we plot the obtained mesh and polynomial degree distribution $(\mathcal{T}_{20}, \mathbf{p}_{20})$ after 20 iterations of the adaptive procedure driven by solving local Neumann problems (Definitions 2.4.8 and 2.4.9) and when employing the so-called heuristic approach, i.e. performing only a single iteration of the algebraic solver at each level of refinement. Note the extra refinements present in the region of the peak of the initial guess function: these are not at all present when employing the adaptive stopping criterion (2.45) for the algebraic solver, see the right panel of Figure 2.15. Figure 2.16 shows the spatial distribution of the actual total error and the total upper error indicators corresponding to $(\mathcal{T}_{20}, \mathbf{p}_{20})$ from Figure 2.15 (right panel) at the moment when the algebraic solver is stopped using (2.45) with $\gamma_{20} = 0.1$. Moreover, Figure 2.17 presents the comparison of our adaptive strategy with different stopping criteria for the algebraic solver in terms of the number of necessary algebraic iterations per iteration of the adaptive loop, and in terms of the amount of time spent on the algebraic computations in order to reach a relative estimated error lower than 0.01. We observe that while using the heuristic approach, compared to the use of the adaptive stopping criterion, nine additional iterations of the adaptive loop were necessary (due to incorrect refinements at the beginning of the adaptive process). Even though only one single iteration is performed per each adaptive loop iteration, we altogether spend approximately 4 times more time on algebraic computations than in the case of using adaptive stopping criterion. The heuristic approach surprisingly turns out to be comparable with the use of the classical criterion with $\varepsilon = 10^{-6}$ in this overall cost assessment. Then, Figure 2.18 presents the effectivity indices for the reduction factor C_{red} and the lower bound $\underline{\eta}_{\mathcal{M}_\ell^\theta}$ which are quite promising even for this test case. The value of parameter γ_ℓ was throughout the whole adaptive procedure equal to 0.1. Lastly, Figure 2.19 shows the error decay with respect to $\mathrm{DoF}_\ell^{\frac{1}{3}}$ when using the proposed strategy with inexact algebraic solver and, for comparison, also while using a pure h-adaptive version of the loop given by Scheme 2.1, and using simply uniform h-refinement. We observe that also for this model problem, the proposed strategy leads to an exponential convergence rate.

2.6.4 Singular solution (L-shape domain)

As a model problem with singular exact solution, we consider the classic reentrant corner problem, cf. Mitchell and McClain (2011), Dolejší et al. (2016), Daniel et al. (2018a), posed on the L-shape domain $\Omega = (-1, 1) \times (-1, 1) \setminus$

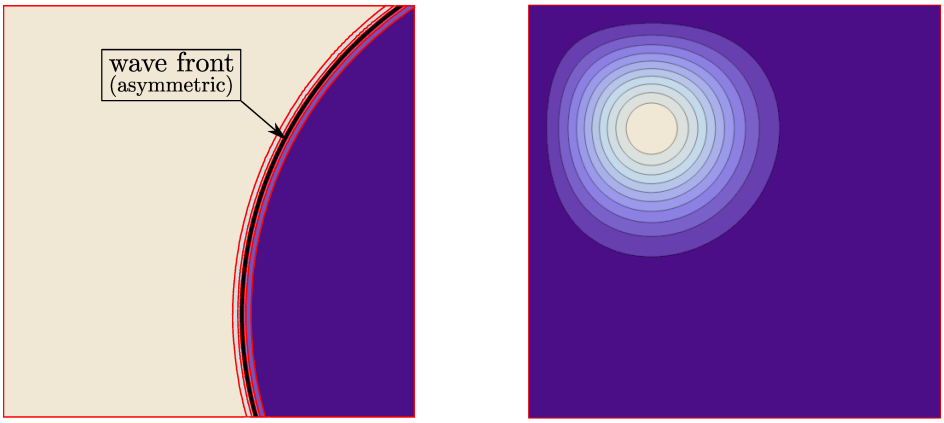

Figure 2.14: [Asymmetric wave front of Section 2.6.3] Contour plots of the exact solution (*left*) and the function inducing the initial guess for the algebraic solver (*right*).

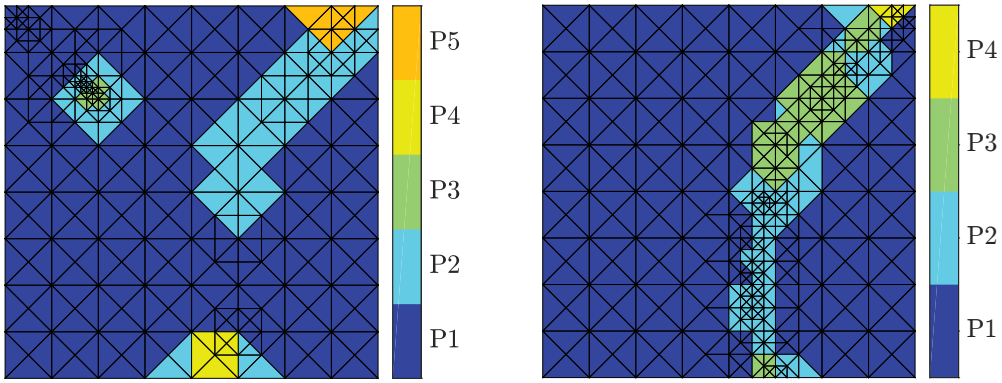

Figure 2.15: [Asymmetric wave front of Section 2.6.3] The mesh and polynomial degree distribution $(\mathcal{T}_{20}, \mathbf{p}_{20})$ obtained while using the so-called heuristic approach (one multigrid iteration on each *hp*-adaptive step) (*left*) and while employing the adaptive stopping criterion (2.45) (*right*).

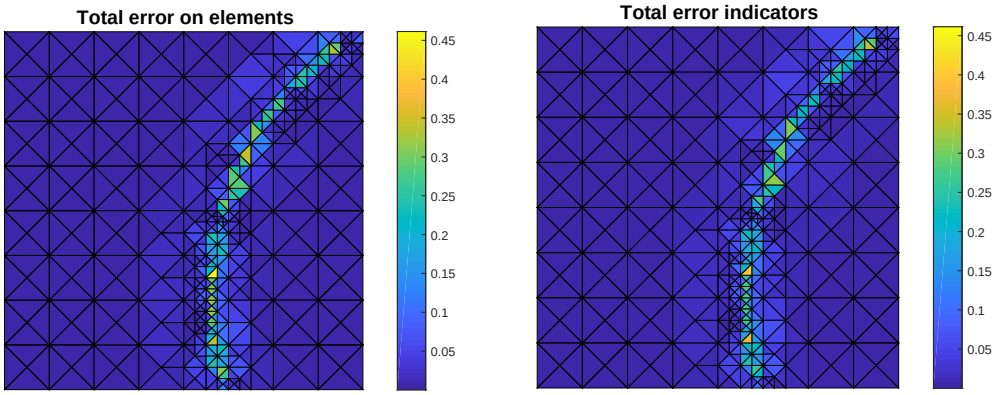

Figure 2.16: [Asymmetric wave front of Section 2.6.3] Elementwise distribution of the total energy error $\|\nabla(u - u_{20})\|$ (*left*) and total upper error indicators $\eta_K(u_{20})$ (*right*). The effectivity index of the estimate is 1.1106.

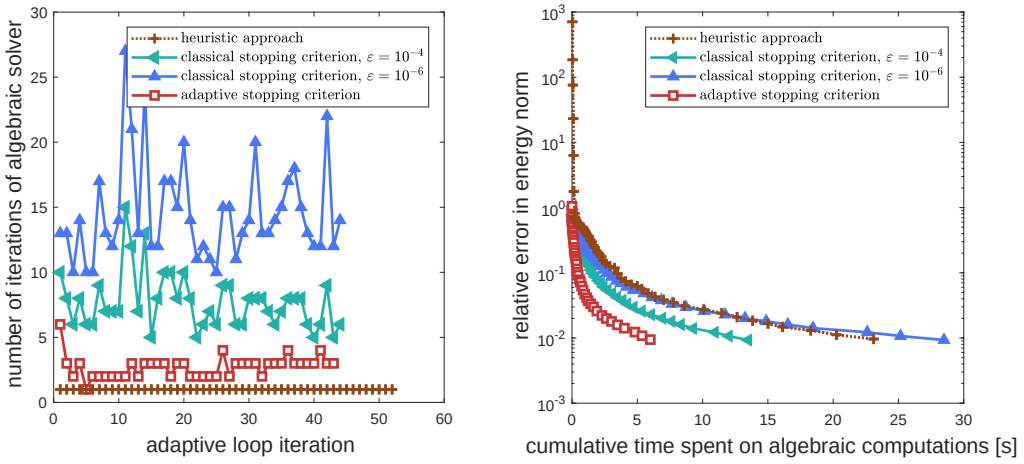

Figure 2.17: [Asymmetric wave front of Section 2.6.3] The relative energy error $\|\nabla(u-u_\ell)\|/\|\nabla u\|$ as a function of cumulative time spent on algebraic computations for various stopping criteria of Section 2.4.3 (*left*) and the respective numbers of algebraic solver iterations per step of the adaptive procedure of Scheme 2.2 (*right*).

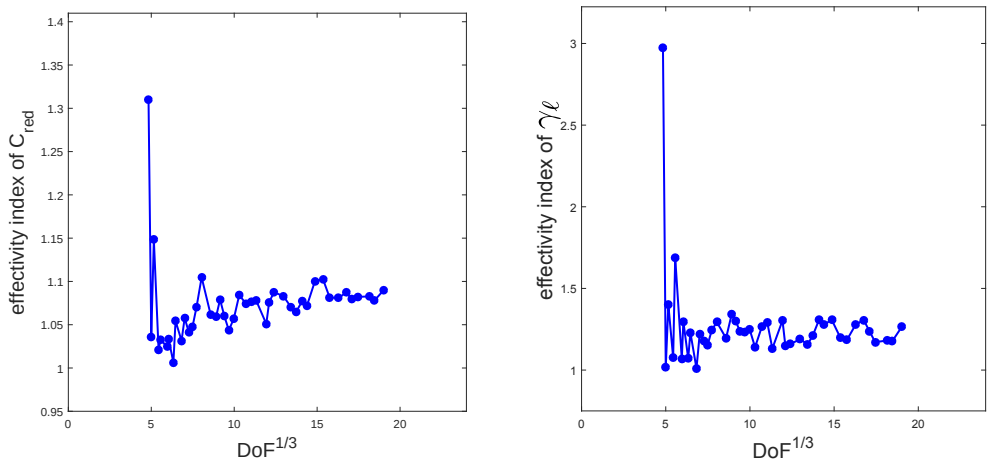

Figure 2.18: [Asymmetric wave front of Section 2.6.3] The effectivity indices for the error reduction factor estimate C_{red} of Theorem 2.5.4 given by (2.75) (*left*) and the discrete lower bound $\underline{\eta}_{\mathcal{M}_\ell^\theta}$ of Lemma 2.5.2 given by (2.76) (*right*).

$[0,1]\times[-1,0]$ with $f=0$ and the weak solution (in polar coordinates)

$$u(r,\varphi) = r^{\frac{2}{3}}\sin\left(\frac{2\varphi}{3}\right).$$

We start the computation on a coarse criss-cross grid $\mathcal{T}_0$ with $\max_{K\in\mathcal{T}_0} h_K = 0.25$ and all the polynomial degrees set uniformly to 1. We present here the results obtained with our strategy driven by solving the local Dirichlet problems only. We note that the results obtained with the strategy employing the local residuals $r^{\mathbf{a},h}$ and $r^{\mathbf{a},p}$ from Definitions 2.4.8 and 2.4.9 are very similar.

First, in Figure 2.20, we assess the quality of the estimated reduction fac-

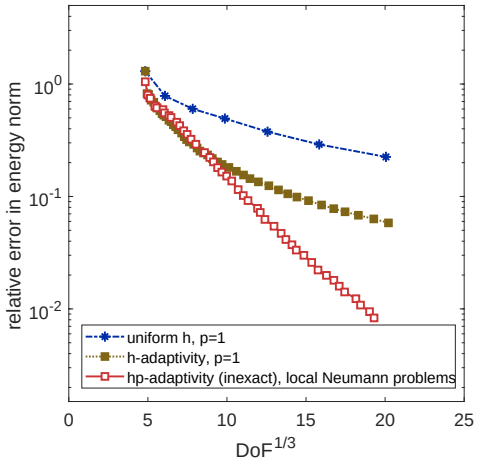

Figure 2.19: [Asymmetric wave front of Section 2.6.3] Relative energy error $\|\nabla(u-u_\ell)\|/\|\nabla u\|$ as a function of $\mathrm{DoF}_\ell^{\frac{1}{3}}$, obtained with our *hp*-refinement strategy (driven by solving local Neumann problems) with inexact algebraic solver, purely *h*-adaptive version with exact solver and using uniform *h*-refinement.

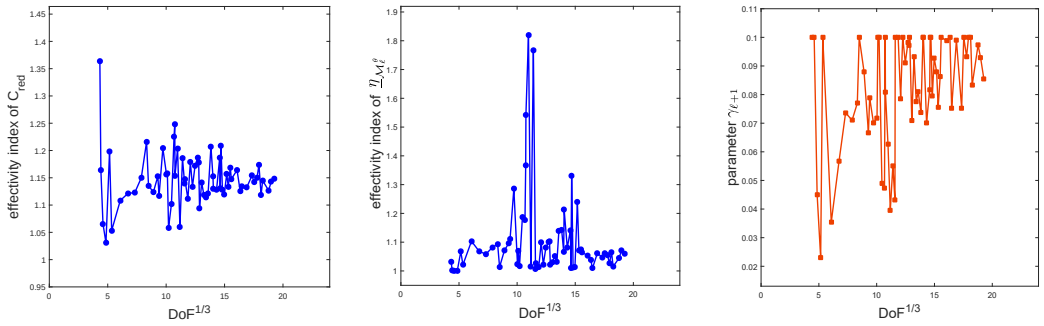

Figure 2.20: [L-shape domain of Section 2.6.4] The effectivity index for the error reduction factor estimate C_{red} of Theorem 2.5.4 given by (2.75) (*left*); the effectivity index of the discrete lower bound $\underline{\eta}_{\mathcal{M}_\ell^\theta}$ of Lemma 2.5.1 given by (2.76) (*center*); corresponding values of the parameter $\gamma_{\ell+1}$ used in (2.73) (*right*).

tor C_{red} and the lower bound $\underline{\eta}_{\mathcal{M}_\ell^\theta}$. We observe that the effectivity indices remain close to the optimal value of one also for this test case. In the right panel of Figure 2.20, we plot the corresponding values of the parameter $\gamma_{\ell+1}$ used within the stopping criterion (2.71). Next, Figure 2.21 demonstrates how the use of the stopping criterion (2.71) allows one to cut off the unnecessary iterations of the multigrid solver and save a substantial portion of the computational time spent on algebraic computations. Using the multigrid solver controlled by (2.71), to reach the relative error lower than 10^{-5}, one saves about 50%, or even 75%, of the computational time dedicated to the algebraic solver in case of the use of the classical stopping criterion (2.46) with $\varepsilon = 10^{-8}$ or $\varepsilon = 10^{-10}$, respectively. In the left panel of Figure 2.22, we in-

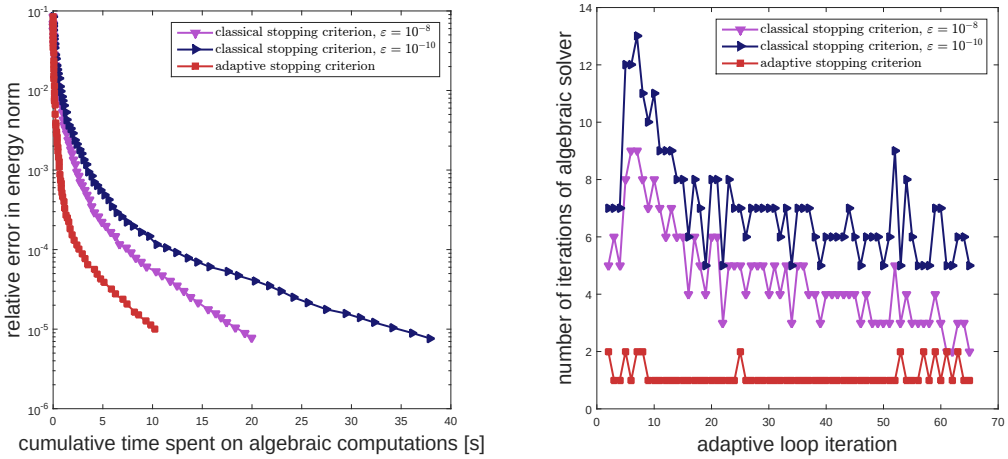

Figure 2.21: [L-shape domain of Section 2.6.4] The relative energy error $\|\nabla(u-u_\ell)\|/\|\nabla u\|$ as a function of cumulative time spent on algebraic computations for various stopping criteria of Section 2.4.3 (*left*) and the respective numbers of algebraic solver iterations per step of the adaptive procedure of Scheme 2.2 (*right*).

vestigate the evolution of the total error lower bound (2.24) and the algebraic error upper bound (2.16) throughout the iterations of the multigrid solver at the 7th level of refinement. The annotations therein indicate at which iteration of the algebraic solver our adaptive and the classical stopping criteria are satisfied. The quality of all the error bounds computed within the `ESTIMATE` module, at the same level of refinement, can be appreciated in the right panel of Figure 2.22. The corresponding mesh and polynomial degree distribution $(\mathcal{T}_7, \mathbf{p}_7)$ is displayed in the left panel of Figure 2.23. In Figure 2.23 (central and right panels) and Figure 2.24, we show the spatial distribution of the actual total and algebraic errors along with the total upper error indicators and algebraic upper error indicators after the 2nd iteration of multigrid solver on the 7th step of the *hp*-adaptive loop, i.e. at the moment when we stopped the multigrid solver as dictated by the adaptive stopping criterion (2.45). To conclude, we display in Figure 2.25 the overall decay of the relative error as a function of $\mathrm{DoF}_\ell^{\frac{1}{3}}$ in logarithmic-linear scale, to illustrate that also for this problem with singular exact solution, the present *hp*-adaptive strategy with inexact algebraic solver leads to an asymptotic exponential convergence rate. We display also the results obtained with uniform *h*-refinement, with pure *h*-version of the adaptive loop from Scheme 2.1, and its *hp*-version based on a priori knowledge of the weak solution leading to the best possible convergence rate. For further comparison with some other *hp*-refinement strategies (with exact algebraic solver), we refer to (Daniel et al., 2018a, Section 6.2), (Mitchell and McClain, 2011, Section 5.4).

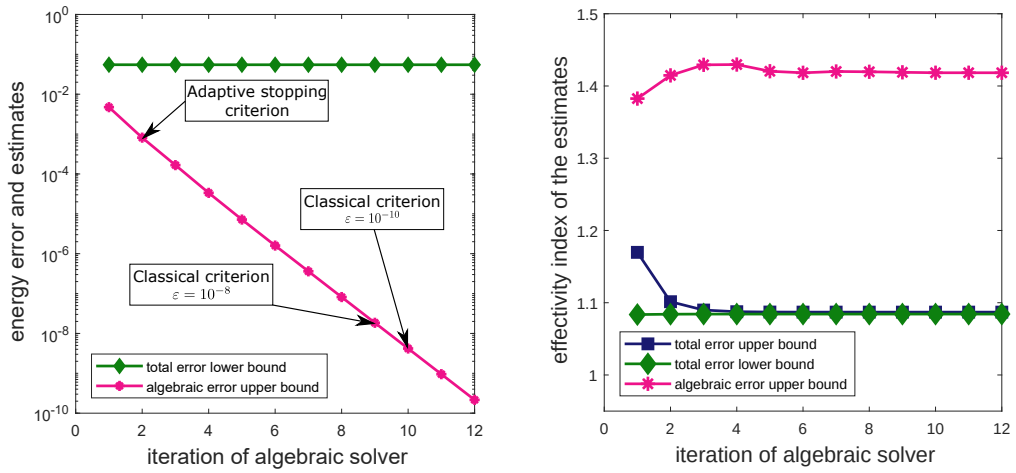

Figure 2.22: [L-shape domain of Section 2.6.4] Algebraic error upper bound $\eta_{\text{alg}}(u_7, \mathcal{T}_7)$ in comparison with total error lower bound $\mu(u_7)$ (*left*); effectivity indices of total error upper bound (2.15), total error lower bound (2.24), and algebraic error upper bound (2.16) (*right*), throughout the iterations of the multigrid solver.

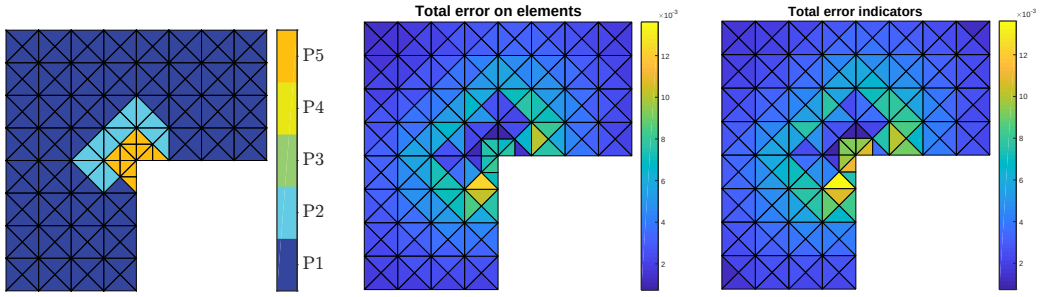

Figure 2.23: [L-shape domain of Section 2.6.4] The mesh and polynomial degree distrbution $(\mathcal{T}_7, \mathbf{p}_7)$; the corresponding elementwise distribution of the total energy error $\|\nabla(u - u_7)\|$ (*left*) and the total error indicators $\eta_K(u_7)$ (*right*).

2.7 Conclusions

In this work, we extended our adaptive *hp*-refinement strategy for solving elliptic problems by taking into account an inexact algebraic solver within the adaptive loop. We constructed flux reconstructions and a total residual lifting by solving small local problems on patches of elements, yielding guaranteed a posteriori error bounds on algebraic and total errors. Then we proposed an adaptive stopping criterion for the iterative algebraic solver ensuring the desired balance between the algebraic and the total error. The total error indicators are employed to mark mesh vertices; the actual *hp*-refinement decision is driven by solving additional local problems on the patches of elements associated with the marked vertices. Once the next mesh and polynomial degree distribution have been determined, solving one additional local problem per marked vertex leads to a fully computable guaranteed bound on the

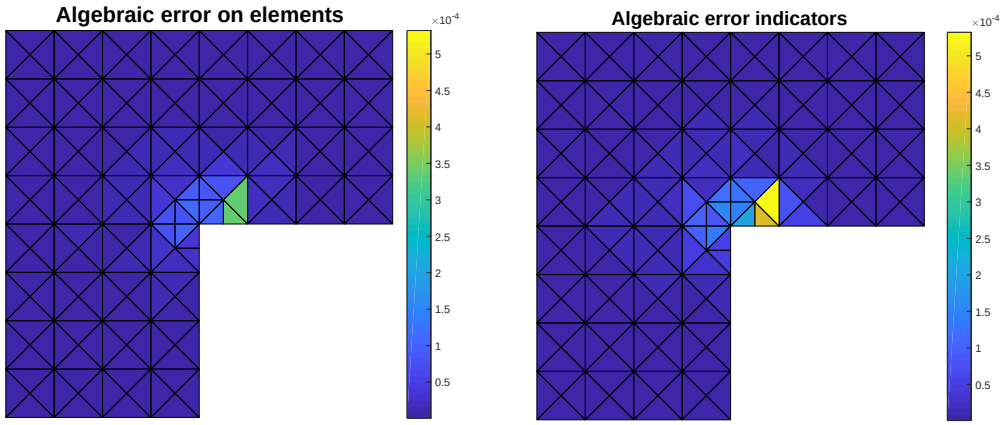

Figure 2.24: [L-shape domain of Section 2.6.4] Elementwise distribution of the algebraic energy error $\|\nabla(u_7^{\mathrm{ex}} - u_7)\|$ (*left*) and the algebraic error indicators $\eta_{\mathrm{alg},K}(u_7)$ (*right*) obtained with the adaptive stopping criterion (2.45) satisfied, $\gamma_\ell = 0.04$.

error reduction factor between two successive inexact approximations. We considered here two options for the local problems on patches around marked vertices, with homogeneous Dirichlet and homogeneous Neumann boundary conditions. The numerical experiments demonstrated the accuracy of the estimated quantities while highlighting the applicability of the presented strategy. For all the test cases the obtained meshes and polynomial degree distributions lead to asymptotic exponential convergence rates. The further analysis of the reduction factor C_{red}, as indicated in Remark 2.5.6, is on the agenda.

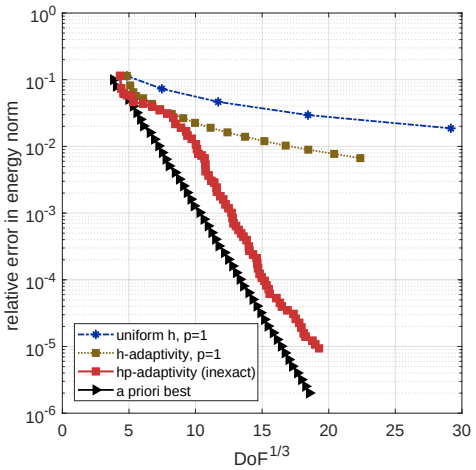

Figure 2.25: [L-shape domain of Section 2.6.4] Relative energy error $\|\nabla(u-u_\ell)\|/\|\nabla u\|$ as a function of $\mathrm{DoF}_\ell^{\frac{1}{3}}$, obtained with our *hp*-refinement strategy (driven by solving local Dirichlet problems) with inexact algebraic solver, using uniform *h*-refinement, purely *h*-adaptive version of adaptive loop from Scheme 2.1, and its *hp*-version exploiting the a priori knowledge of the weak solution.

Chapter 3

Convergence of adaptive hp-refinement strategies with computable guaranteed bound on the error reduction factor

We expose in this chapter the results of the article Daniel and Vohralík (2018), currently in preparation. This work was done in collaboration with Martin Vohralík.

Contents

Abstract

We analyze the adaptive refinement strategies for conforming *hp*-finite element approximations of elliptic problems proposed in Daniel et al. (2018a) for exact solvers and in Daniel et al. (2018b) for inexact algebraic solvers. Both of these strategies are driven by guaranteed equilibrated flux a posteriori error estimators. The employed *hp*-refinement criterion stems from solving two separate local residual problems posed only on the patches of elements around marked vertices selected by a bulk-chasing criterion. In particular, these references derived a fully computable real number serving as a guaranteed bound on the ratio of the error on two successive steps of the *hp*-adaptive loop. Here, our focus is on theoretical analysis of such error reduction factors. Upon introducing some additional assumptions on the *h*- and *p*-refinements which ensure discrete stability of the equilibrated fluxes, we prove that the computable reduction factors are strictly lower than one, in both exact and inexact algebraic solver setting. Hence, a linear convergence of the two adaptive strategies is granted.

3.1 Introduction

The adaptive finite element method (AFEM) is used in practice and theoretically studied for more than three decades. The analysis of the (optimal) convergence of AFEM is surely catalysed by the extensive research dedicated to efficient and reliable *a posteriori error estimates*, see e.g. the survey books by Ainsworth and Oden (2000) and Verfürth (2013). Roughly a decade after the pioneering works by Gui and Babuška (1986b,a), Babuška and Guo (1986a,b), the *h*-adaptive strategy for elliptic problems of Dörfler (1996) laid the ground for Morin et al. (2000), to prove a plain convergence result. Binev et al. (2004) followed with a modification of the method from Morin et al. (2000) which they proved to have not only optimal convergence rate but also optimal complexity in terms of the number of degrees of freedom. Other important results are to be found in Morin et al. (2003, 2008), Cascón et al. (2008), and Carstensen et al. (2014). Most of the convergence results were stated for methods driven by residual-type a posteriori error estimates; the works addressing other types of estimators include those

by Kreuzer and Siebert (2011) and Cascón and Nochetto (2012). In contrast, convergence of *hp*-AFEM approximations has been addressed only recently in Dörfler and Heuveline (2007), Bürg and Dörfler (2011), and Bank et al. (2013). The most recent state of the art optimality result is to our knowledge by Canuto et al. (2017a) hinging on an coarsening module due to Binev (2013, 2018) and the result of Canuto et al. (2017b) hinging on a saturation condition assumption.

In this work, we aim to complete our recently proposed *hp*-adaptive refinement strategy with *computable guaranteed bound* on the *error reduction factor* (Daniel et al. (2018a)) and its counterpart in an *inexact algebraic solver setting* (Daniel et al. (2018b)) by rigorous convergence proofs. As in Daniel et al. (2018a,b), we examine the Poisson equation with homogeneous Dirichlet boundary conditions. Let $\Omega \subset \mathbb{R}^d$, $d = 2, 3$, be a polygonal/polyhedral domain (open, bounded, and connected set) with a Lipschitz boundary $\partial\Omega$, and let $H^1_0(\Omega)$ denote the Sobolev space of all functions in $L^2(\Omega)$ which have all their first-order weak derivatives in $L^2(\Omega)$ and a vanishing trace on $\partial\Omega$. Assuming that $f \in L^2(\Omega)$, the model problem in its weak form reads: find $u \in H^1_0(\Omega)$ such that

$$(\nabla u, \nabla v) = (f, v) \qquad \forall v \in H^1_0(\Omega), \tag{3.1}$$

where $(\cdot, \cdot)$ stands for the $L^2(\Omega)$ or $[L^2(\Omega)]^d$ inner product. The conforming *hp*-finite element method is used to discretize the model problem (3.1). Therein, we consider only matching simplicial meshes without hanging nodes.

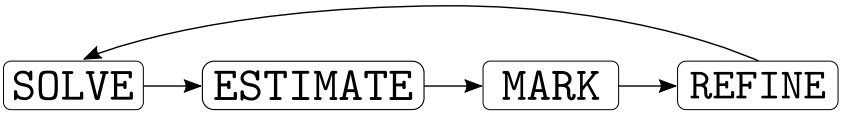

Scheme 3.1: Paradigm of an *hp*-adaptive algorithm employing an exact algebraic solver.

The first part of this chapter (Sections 3.2–3.5) is dedicated to the study of the *hp*-adaptive algorithm in the *exact setting*, i.e. we assume exact (up to machine precision) solution of all the resulting linear algebraic problems. Typically, such algorithms follow the well-established paradigm presented in Scheme 3.1. Particularly, in Daniel et al. (2018a), we showed that between two consecutive steps of the adaptive loop from Scheme 3.1, it is possible to compute explicitly a real number $C_{\ell,\mathrm{red}} \in [0, 1]$ such that

$$\|\nabla(u - u^{\mathrm{ex}}_{\ell+1})\| \leq C_{\ell,\mathrm{red}} \|\nabla(u - u^{\mathrm{ex}}_{\ell})\|, \tag{3.2}$$

where u^{ex}_{ℓ} and $u^{\mathrm{ex}}_{\ell+1}$ denote the exact finite element solutions from the respective iterations ℓ and $\ell + 1$ of the adaptive loop. Even though we provided numerical evidence in (Daniel et al., 2018a, Section 6), we did not prove that the reduction factor $C_{\ell,\mathrm{red}}$ of (Daniel et al., 2018a, Section 5) is bounded by

a generic constant strictly smaller than one; this is the subject of our study here. In order to achieve it, in contrast to Daniel et al. (2018a), in Section 3.3 we introduce slightly modified versions of the modules `MARK` and `REFINE` of Scheme 3.1 with some additional assumptions on the employed h- and p-refinement methods. The key ingredients of the proof are the extension of marked region in module `MARK` by one layer of elements, see Section 3.3.2, some interior node properties requested for h-refinement, a stronger p-refinement used within module `REFINE`, see Section 3.3.3, and the discrete stability of the local equilibrated fluxes computed within the module `ESTIMATE`, proved in Section 3.4. The only assumption is that we need to limit the maximal polynomial degree since the present analysis is not p-robust. This is restrictive from the theoretical viewpoint but completely reasonable in practice.

Scheme 3.2: Paradigm of an adaptive loop employing an inexact algebraic solver.

However, as discussed in Daniel et al. (2018b), see also the references therein, the use of exact algebraic solvers within the hp-adaptive algorithm is not desirable, and not even feasible in most cases. Hence, in the second part of this chapter (starting with Section 3.6), we extend our results concerning the convergence of the hp-adaptive algorithm in the exact setting to the *inexact setting*. Following Daniel et al. (2018b), we incorporate the use of an arbitrary inexact algebraic solver within the framework of adaptive algorithm of Scheme 3.1 by replacing the module `SOLVE` by an adaptive sub-loop consisting of modules `ONE_SOLVER_STEP` and `ESTIMATE`, see Scheme 3.2. We note that incorporating the inexact solver is essential also for bounding the computational complexity of AFEM algorithms, cf. the seminal works of Binev et al. (2004) and Stevenson (2005b, 2007). In these seminal works, however, the authors present their h-adaptive AFEM algorithms in an abstract setting and the inexact approximations are assumed to be sufficiently/arbitrarily close to the exact ones. We treat carefully our choice of a practical *adaptive stopping criterion* for the algebraic solver in order to ensure the convergence of the adaptive algorithm. The idea is to balance adaptively the algebraic error and the discretization error at each step of the adaptive procedure, cf. Becker et al. (1995), Becker and Mao (2009), Becker et al. (2010), Jiránek et al. (2010), Arioli et al. (2013a), Ern and Vohralík (2013), Becker et al. (2015), Rey et al. (2014), Papež et al. (2017) and the references therein. In particular, the algebraic error estimates proposed by Becker and Mao (2009), Becker et al. (2010) depend on a constant $\rho_{\mathrm{it}} < 1$ from an a priori argument which requires that the employed iterative solver contracts the algebraic error at least by a factor ρ_{it}

on each iteration, see (Becker and Mao, 2009, (6.2)–(6.3)). Arioli et al. (2013a) proposed a practical stopping criterion leading to convergence of the inexact adaptive algorithm employing the conjugate gradient method as the algebraic solver, where the results are conditioned by a good estimate on the smallest eigenvalue of the finite element system matrix. In contrast to these results, the advantage of the present work is that no request on the algebraic solver is made and our bounds on algebraic, discretization, and total error do not contain any generic constant and remain fully computable, see Section 3.6.1. Consequently, the values of the stopping parameter $\widetilde{\gamma}_\ell$, which expresses the percentage of the algebraic error with respect to the total error, do not need to theoretically take excessively small (and unknown) values but can stay around the reasonable-in-practice value 0.1. The proper choice of stopping criterion together with the modifications of modules `MARK` and `REFINE`, introduced in the exact setting, then allow us to show, in extension of (3.2), the error reduction property between two consecutive inexact approximations u_ℓ and $u_{\ell+1}$ produced by the adaptive loop of Scheme 3.2

$$\|\nabla(u - u_{\ell+1})\| \leq C_{\ell,\mathrm{red}} \|\nabla(u - u_\ell)\|, \tag{3.3}$$

with the fully computable factor $0 \leq C_{\ell,\mathrm{red}} \leq C < 1$. This theoretical result improves the developments of (Daniel et al., 2018b, Theorem 5.4), where the reduction factor, derived therein in a slightly different form in comparison to the present $C_{\ell,\mathrm{red}}$, was not showed to be bounded by a generic constant strictly smaller than one. In particular, the reduction property (3.3), showed in Section 3.8 here, implies the convergence of the adaptive algorithm prescribed by Scheme 3.2.

3.2 Framework and notation

Within the adaptive loops of Schemes 3.1 and 3.2, a sequence $\{(\mathcal{T}_\ell, \mathbf{p}_\ell)\}_{\ell \geq 0}$, with $\ell \geq 0$ the iteration counter, is generated. Each pair $(\mathcal{T}_\ell, \mathbf{p}_\ell)$ consists of a matching simplicial mesh $\mathcal{T}_\ell$ of the computational domain Ω, i.e. a finite collection of (closed) simplices $K \in \mathcal{T}_\ell$ covering $\overline{\Omega}$ and such that the intersection of two different simplices is either empty or their d'-dimensional common face, $0 \leq d' \leq d-1$, and of a polynomial-degree distribution vector $\mathbf{p}_\ell := \{p_{\ell,K}\}_{K \in \mathcal{T}_\ell}$ which assigns a degree $p_{\ell,K} \in \mathbb{N}_{\geq 1}$ to each simplex $K \in \mathcal{T}_\ell$. Moreover, each pair $(\mathcal{T}_\ell, \mathbf{p}_\ell)$ prescribes a discrete finite-dimensional space V_ℓ, defined as

$$V_\ell := \mathbb{P}_{\mathbf{p}_\ell}(\mathcal{T}_\ell) \cap H^1_0(\Omega), \qquad \forall \ell \geq 0,$$

where $\mathbb{P}_{\mathbf{p}_\ell}(\mathcal{T}_\ell)$ denotes the space of piecewise polynomials of total degree at most $p_{\ell,K}$ on each simplex $K \in \mathcal{T}_\ell$. Let us denote by N_ℓ the dimension of the ℓ-th level space V_ℓ. Note that we enforce the $H^1_0(\Omega)$-conformity of the spaces

V_ℓ for all $\ell \geq 0$. In addition, we make the following nestedness assumption:

$$V_\ell \subset V_{\ell+1}, \qquad \forall \ell \geq 0. \tag{3.4}$$

The initial pair $(\mathcal{T}_0, \mathbf{p}_0)$ is assumed to be given. Then, the purpose of each step $\ell \geq 0$ of the adaptive loops of Schemes 3.1 and 3.2 is to determine the next pair $(\mathcal{T}_{\ell+1}, \mathbf{p}_{\ell+1})$. The nestedness property (3.4) gives us two crucial restrictions on the meshes and polynomial-degree distributions defining the spaces V_ℓ: (i) the sequence of meshes $\{\mathcal{T}_\ell\}_{\ell\geq 0}$ needs to be *hierarchically nested*, i.e., for all $\ell \geq 1$ the mesh $\mathcal{T}_\ell$ is a refinement of $\mathcal{T}_{\ell-1}$ such that for all $K \in \mathcal{T}_\ell$, there is a unique simplex $\widetilde{K} \in \mathcal{T}_{\ell-1}$, called the parent of K, satisfying $K \subseteq \widetilde{K}$; (ii) The local polynomial degree is *locally increasing*, i.e., for all $\ell \geq 1$ and all $K \in \mathcal{T}_\ell$, $p_{\ell,K} \geq p_{\ell-1,\widetilde{K}}$, where $\widetilde{K} \in \mathcal{T}_{\ell-1}$ is the parent of K. Moreover, we assume the following standard shape-regularity property: There exists a constant $\kappa_\mathcal{T} > 0$ such that $\max_{K\in\mathcal{T}_\ell} h_K/\rho_K \leq \kappa_\mathcal{T}$ for all $\ell \geq 0$, where h_K is the diameter of K and ρ_K is the diameter of the largest ball inscribed in K.

We denote by $\mathcal{V}_\ell$ ($\mathcal{F}_\ell$) the set of vertices ($(d-1)$-dimensional faces) of $\mathcal{T}_\ell$ decomposed into interior vertices ($(d-1)$-dimensional faces) $\mathcal{V}_\ell^{\text{int}}$ ($\mathcal{F}_\ell^{\text{int}}$) and boundary vertices ($(d-1)$-dimensional faces) $\mathcal{V}_\ell^{\text{ext}}$ ($\mathcal{F}_\ell^{\text{ext}}$). For each vertex $\mathbf{a} \in \mathcal{V}_\ell$, $\ell \geq 0$, the so-called hat function $\psi_\ell^{\mathbf{a}}$ is the continuous, piecewise affine function that takes the value 1 at the vertex $\mathbf{a}$ and the value 0 at all the other vertices of $\mathcal{V}_\ell$; the function $\psi_\ell^{\mathbf{a}}$ is in V_ℓ for all $\mathbf{a} \in \mathcal{V}_\ell^{\text{int}}$ and all polynomial degrees $\mathbf{p}_\ell$. Furthermore, we consider the simplex patch $\mathcal{T}_\ell^{\mathbf{a}} \subset \mathcal{T}_\ell$ which is the collection of the simplices sharing the vertex $\mathbf{a} \in \mathcal{V}_\ell$, with $\omega_\ell^{\mathbf{a}}$ the corresponding open subdomain of Ω, coinciding with the support of $\psi_\ell^{\mathbf{a}}$. Let $\mathcal{F}_\ell^{\mathbf{a}} \subset \mathcal{F}_\ell$ denote the set of all the $(d-1)$-dimensional faces in the patch $\mathcal{T}_\ell^{\mathbf{a}}$. This set can be further decomposed into $\mathcal{F}_\ell^{\mathbf{a},\text{int}}$, the subset of faces from $\mathcal{F}_\ell^{\mathbf{a}}$ that share the vertex $\mathbf{a}$ and are shared by two distinct simplices in $\mathcal{T}_\ell^{\mathbf{a}}$, and $\mathcal{F}_\ell^{\mathbf{a},\text{ext}}$, the faces from $\mathcal{F}_\ell^{\mathbf{a}}$ lying in $\partial\omega_\ell^{\mathbf{a}}$, so that $\mathcal{F}_\ell^{\mathbf{a}} = \mathcal{F}_\ell^{\mathbf{a},\text{int}} \cup \mathcal{F}_\ell^{\mathbf{a},\text{ext}}$. For any $F \in \mathcal{F}_\ell$, $\mathbf{n}_F$ stands for a unit vector normal to F with an arbitrary but fixed orientation. The operator $[\![\cdot]\!]$ yields the jump, in the direction of $\mathbf{n}_F$, of the traces of the argument from the two simplices that share $F \in \mathcal{F}_\ell^{\text{int}}$, and the actual trace for $F \in \mathcal{F}_\ell^{\text{ext}}$. Finally, for each simplex $K \in \mathcal{T}_\ell$, $\mathcal{V}_{\ell,K}$ denotes the set of vertices of K and $\mathcal{F}_{\ell,K}$ denotes the set of $(d-1)$-dimensional faces of element $K \in \mathcal{T}_\ell$.

3.3 The *hp*-adaptive algorithm – exact setting

In this section, we first recall the modules `SOLVE` and `ESTIMATE` as defined in Daniel et al. (2018a). Afterwards, we introduce the slightly modified versions of the remaining modules `MARK` and `REFINE` from the adaptive loop of Scheme 3.1, allowing us to prove the convergence of such an adaptive algorithm. In order to avoid technicalities with data oscillation, we suppose:

Assumption 3.3.1 (Source term f)**.** *In the following analysis, the datum f is assumed to be piecewise polynomial of variable degree at most $\mathbf{p}_f$ with respect*

to the coarsest partition $\mathcal{T}_0$, $f \in \mathbb{P}_{\mathbf{p}_f}(\mathcal{T}_0)$, *such that* $\mathbf{p}_f \leq \mathbf{p}_0 - 1$. *In the special case* $f|_K$, $K \in \mathcal{T}_0$, *we set* $p_{f,K} := 0$.

3.3.1 The modules SOLVE and ESTIMATE

Let $\ell \geq 0$ denote the current iteration counter. The module SOLVE takes as input the current finite element space $V_\ell \subset H^1_0(\Omega)$ and outputs the Galerkin approximation $u_\ell^{\mathrm{ex}} \in V_\ell$ of the weak solution u of (3.1) defined as the unique solution of

$$(\nabla u_\ell^{\mathrm{ex}}, \nabla v_\ell) = (f, v_\ell) \qquad \forall v_\ell \in V_\ell. \tag{3.5}$$

Note that obtaining u_ℓ^{ex} is equivalent to computing the exact solution of the system of linear algebraic equations

$$\mathbb{A}_\ell \mathrm{U}_\ell^{\mathrm{ex}} = \mathrm{F}_\ell, \tag{3.6}$$

where $\{\psi_\ell^n\}_{1\leq n\leq N_\ell}$ is the basis of the ℓ-th level space V_ℓ such that $u_\ell^{\mathrm{ex}} := \sum_{n=1}^{N_\ell} (\mathrm{U}_\ell^{\mathrm{ex}})_n \, \psi_\ell^n$.

Following Destuynder and Métivet (1999), Braess and Schöberl (2008), Ern and Vohralík (2015), Dolejší et al. (2016), Ern and Vohralík (2016), see also the references therein, the module ESTIMATE relies on an equilibrated flux a posteriori error estimate on the energy error $\|\nabla(u - u_\ell^{\mathrm{ex}})\|$. The module ESTIMATE takes as input the finite element solution u_ℓ^{ex} and outputs a collection of local error indicators $\{\eta_K\}_{K\in\mathcal{T}_\ell}$.

The equilibrated flux is constructed locally on the simplex patches $\mathcal{T}_\ell^{\mathbf{a}}$ attached to each vertex $\mathbf{a} \in \mathcal{V}_\ell$. For this construction, we consider as in Dolejší et al. (2016), Daniel et al. (2018a) the local polynomial degree $p_{\mathbf{a}}^{\mathrm{est}} := \max_{K\in\mathcal{T}_\ell^{\mathbf{a}}} p_{\ell,K}$ (any other choice so that $p_{\mathbf{a}}^{\mathrm{est}} \geq \max_{K\in\mathcal{T}_\ell^{\mathbf{a}}} p_{\ell,K}$ can also be employed). For a fixed vertex $\mathbf{a} \in V_\ell$, let the broken space

$$\mathbf{RTN}_p(\mathcal{T}_\ell^{\mathbf{a}}) := \{\mathbf{v}_\ell \in [L^2(\omega_\ell^{\mathbf{a}})]^d;\ \mathbf{v}_\ell|_K \in \mathbf{RTN}_p(K), \quad \forall K \in \mathcal{T}_\ell^{\mathbf{a}}\},$$

where $\mathbf{RTN}_p(K) := [\mathbb{P}_p(K)]^d + \mathbb{P}_p(K)\mathbf{x}$ is the usual p-th order Raviart–Thomas–Nédélec space (cf. Brezzi and Fortin (1991), Roberts and Thomas (1991)) on a simplex $K \in \mathcal{T}_\ell$. Then, the patchwise normal-trace-continuous spaces $\mathbf{V}_\ell^{\mathbf{a}}$ with homogeneous Neumann boundary conditions in which the local equilibration will be performed are defined by

$$\mathbf{V}_\ell^{\mathbf{a}} := \begin{cases} \{\mathbf{v}_\ell \in \mathbf{RTN}_{p_{\mathbf{a}}^{\mathrm{est}}}(\mathcal{T}_\ell^{\mathbf{a}}) \cap \mathbf{H}(\mathrm{div}, \omega_\ell^{\mathbf{a}});\ \mathbf{v}_\ell\cdot\mathbf{n}_{\omega_\ell^{\mathbf{a}}} = 0 \text{ on } \partial\omega_\ell^{\mathbf{a}}\} & \text{if } \mathbf{a} \in \mathcal{V}_\ell^{\mathrm{int}} \\ \{\mathbf{v}_\ell \in \mathbf{RTN}_{p_{\mathbf{a}}^{\mathrm{est}}}(\mathcal{T}_\ell^{\mathbf{a}}) \cap \mathbf{H}(\mathrm{div}, \omega_\ell^{\mathbf{a}});\ \mathbf{v}_\ell\cdot\mathbf{n}_{\omega_\ell^{\mathbf{a}}} = 0 \text{ on } \partial\omega_\ell^{\mathbf{a}} \setminus \partial\Omega\} & \text{if } \mathbf{a} \in \mathcal{V}_\ell^{\mathrm{ext}}. \end{cases} \tag{3.7}$$

Definition 3.3.2 (Equilibrated flux $\boldsymbol{\sigma}_\ell$ by local minimizations)**.** *Let* u_ℓ^{ex} *be the solution of* (3.5). *For each vertex* $\mathbf{a} \in \mathcal{V}_\ell$, *let the local equilibrated flux* $\boldsymbol{\sigma}_\ell^{\mathbf{a}} \in \mathbf{V}_\ell^{\mathbf{a}}$

be defined by the local minimization problem

$$\boldsymbol{\sigma}_\ell^{\mathbf{a}} := \underset{\substack{\mathbf{v}_\ell \in \mathbf{V}_\ell^{\mathbf{a}},\\ \nabla\cdot\mathbf{v}_\ell = \psi_\ell^{\mathbf{a}} f - \nabla\psi_\ell^{\mathbf{a}}\cdot\nabla u_\ell}}{\arg\min} \|\psi_\ell^{\mathbf{a}}\nabla u_\ell^{\mathrm{ex}} + \mathbf{v}_\ell\|_{\omega_\ell^{\mathbf{a}}}. \tag{3.8}$$

Then, extending each local contribution $\boldsymbol{\sigma}_\ell^{\mathbf{a}}$ *by zero outside* $\omega_\ell^{\mathbf{a}}$*, the global* $\mathbf{H}(\mathrm{div},\Omega)$*-conforming equilibrated flux* $\boldsymbol{\sigma}_\ell$ *is constructed as*

$$\boldsymbol{\sigma}_\ell := \sum_{\mathbf{a}\in\mathcal{V}_\ell} \boldsymbol{\sigma}_\ell^{\mathbf{a}}.$$

Note that the Neumann compatibility condition $\int_{\omega_\ell^{\mathbf{a}}} \psi_\ell^{\mathbf{a}} f - \nabla\psi_\ell^{\mathbf{a}}\cdot\nabla u_\ell = 0$ for the problem (3.8) is satisfied for all $\mathbf{a} \in \mathcal{V}_\ell^{\mathrm{int}}$ as a direct consequence of (3.5) (consider $\psi_\ell^{\mathbf{a}}$ as a test function in (3.5)). The global $\mathbf{H}(\mathrm{div},\Omega)$-conformity of $\boldsymbol{\sigma}_\ell$ follows from imposing the zero normal trace of functions in the local spaces $\mathbf{V}_\ell^{\mathbf{a}}$, cf. the definition (3.7). Then, as stated in Destuynder and Métivet (1999), Braess and Schöberl (2008), see also (Dolejší et al., 2016, Theorem 3.3), the following guaranteed upper bound on the energy error holds true

$$\|\nabla(u-u_\ell^{\mathrm{ex}})\| \le \eta(u_\ell^{\mathrm{ex}},\mathcal{T}_\ell) := \left\{\sum_{K\in\mathcal{T}_\ell} \eta_K^2(u_\ell^{\mathrm{ex}})\right\}^{\frac{1}{2}}, \quad \eta_K := \|\nabla u_\ell^{\mathrm{ex}} + \boldsymbol{\sigma}_\ell\|_K. \tag{3.9}$$

Note that due to Assumption 3.3.1 the local estimator η_K does not include the so-called data oscillation term, as opposed to (Dolejší et al., 2016, Theorem 3.3).

3.3.2 The module MARK

The module MARK takes as input the local error estimators from (3.9) and proceeds in two phases.

The first phase corresponds to the module MARK used in Daniel et al. (2018a). We select the smallest subset of marked vertices $\widetilde{\mathcal{V}}_\ell^\theta \subset \mathcal{V}_\ell$ using a bulk-chasing criterion inspired by the well-known Dörfler's criterion (cf. Dörfler (1996))

$$\eta\left(u_\ell^{\mathrm{ex}}, \bigcup_{\mathbf{a}\in\widetilde{\mathcal{V}}_\ell^\theta} \mathcal{T}_\ell^{\mathbf{a}}\right) \ge \theta\,\eta(u_\ell^{\mathrm{ex}},\mathcal{T}_\ell), \tag{3.10}$$

where $\theta \in (0,1]$ is a fixed threshold parameter, and for a subset $\mathcal{S} \subset \mathcal{T}_\ell$, we adopt the notation $\eta(u_\ell^{\mathrm{ex}},\mathcal{S}) := \{\sum_{K\in\mathcal{S}} \eta_K(u_\ell^{\mathrm{ex}})^2\}^{1/2}$. Then, letting

$$\mathcal{M}_\ell^\theta := \bigcup_{\mathbf{a}\in\widetilde{\mathcal{V}}_\ell^\theta} \mathcal{T}_\ell^{\mathbf{a}} \subset \mathcal{T}_\ell$$

be the collection of all the simplices that belong to a patch associated with a

marked vertex, we observe that (3.10) means that $\eta(u_\ell^{\mathrm{ex}}, \mathcal{M}_\ell^\theta) \geq \theta\, \eta(u_\ell^{\mathrm{ex}}, \mathcal{T}_\ell)$. Let us denote by $\omega_\ell := \bigcup_{\mathbf{a}\in\widetilde{\mathcal{V}}_\ell^\theta} \omega_\ell^{\mathbf{a}}$ the open subdomain corresponding to the set of elements $\mathcal{M}_\ell^\theta$. A possible reduction of computational cost of such algorithm is proposed in (Dörfler, 1996, Section 5.2).

In a second phase, we define an extension of the set of marked vertices $\widetilde{\mathcal{V}}_\ell^\sharp$ with the corresponding set of elements $\mathcal{M}_\ell^\sharp$ in the following way

$$\widetilde{\mathcal{V}}_\ell^\sharp := \bigcup_{K\in\mathcal{M}_\ell^\theta} \mathcal{V}_{\ell,K} \quad \text{and} \quad \mathcal{M}_\ell^\sharp := \bigcup_{\mathbf{a}\in\widetilde{\mathcal{V}}_\ell^\sharp} \mathcal{T}_\ell^{\mathbf{a}},$$

In other words, we extend the set $\mathcal{M}_\ell^\theta$ by one more layer of neighbouring elements in contact with the boundary $\partial\omega_\ell$, see Figure 3.1 for an illustration. In addition, let us define by $\omega_\ell^\sharp := \bigcup_{\mathbf{a}\in\widetilde{\mathcal{V}}_\ell^\sharp} \omega_\ell^{\mathbf{a}}$ the corresponding open

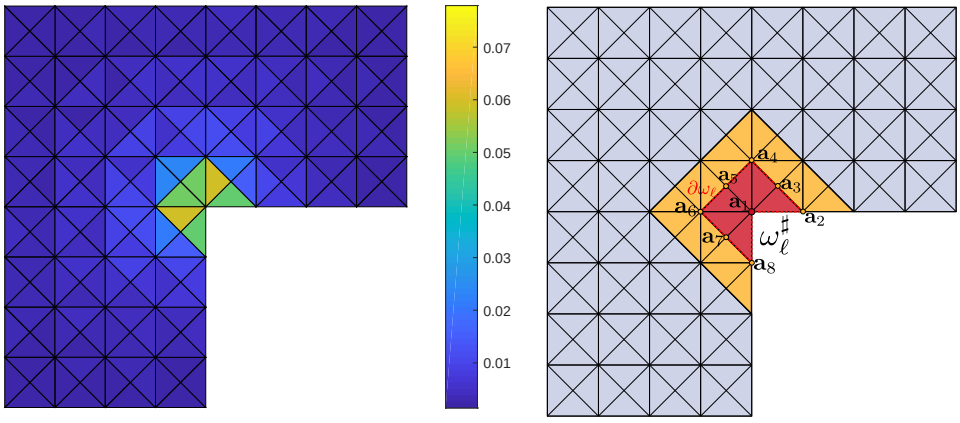

Figure 3.1: An example of local error estimators $\eta_K(u_\ell^{\mathrm{ex}})$ from (3.9) (*left*) and illustration of the corresponding set of marked vertices $\widetilde{\mathcal{V}}_\ell^\theta = \{\mathbf{a}_1\}$ and its extension $\widetilde{\mathcal{V}}_\ell^\sharp = \{\mathbf{a}_1, \mathbf{a}_2, \ldots, \mathbf{a}_8\}$, $\theta = 0.5$ (*right*). The region highlighted in red color corresponds to the subdomain ω_ℓ, and its union with the yellow region region amounts to the subdomain $\omega_\ell^\sharp$.

subdomain of $\mathcal{M}_\ell^\sharp$. This extension is motivated by the structure of the error estimate (3.9), stemming from equilibrated flux $\boldsymbol{\sigma}_\ell$ composed of local patchwise contributions $\boldsymbol{\sigma}_\ell^{\mathbf{a}}$. It plays a particular role later in our convergence proof, when we decompose the error estimate $\eta(u_\ell^{\mathrm{ex}}, \mathcal{M}_\ell^\theta)$ into a sum of local patchwise contributions in (3.55) with their corresponding domains of definitions possibly exceeding ω_ℓ, but always included in the extended domain $\omega_\ell^\sharp$. The present theoretical analysis requires the extension of the marked region. This is the price we pay to estimate the error reduction factor $C_{\ell,\mathrm{red}}$ of (3.2) more precisely compared to the following:

Remark 3.3.3 (Marking without the additional layer)**.** *One could employ the following patchwise form of the error estimate, cf.* (Ern and Vohralík, 2015,

Lemma 3.22) *and* (Canuto et al., 2017b, Proposition 3.1),

$$\|\nabla(u-u_\ell^{\mathrm{ex}})\| \leq \sqrt{d+1}\left\{\sum_{\mathbf{a}\in\mathcal{V}_\ell}\eta_{\mathbf{a}}(u_\ell^{\mathrm{ex}})^2\right\}^{\frac{1}{2}}, \quad \eta_{\mathbf{a}}(u_\ell^{\mathrm{ex}}) := \|\psi_\ell^{\mathbf{a}}\nabla u_\ell^{\mathrm{ex}} + \boldsymbol{\sigma}_\ell^{\mathbf{a}}\|_{\omega_\ell^{\mathbf{a}}}, \tag{3.11}$$

instead of the essentially elementwise form (3.9)*. This would result in no need to extend the obtained set of marked vertices* $\widetilde{\mathcal{V}}_\ell^\theta$ *by the additional layer and overall a simpler hp-adaptive algorithm. However, the presence of the constant* $\sqrt{d+1}$ *already in the error estimate* (3.11) *would lead to deterioration of the bound on the error reduction factor* $C_{\ell,\mathrm{red}}$*.*

3.3.3 The module REFINE

The module REFINE takes as input the extended set of marked vertices $\widetilde{\mathcal{V}}_\ell^\sharp$ and outputs the mesh $\mathcal{T}_{\ell+1}$ and the polynomial-degree distribution $\mathbf{p}_{\ell+1}$ to be used at the next iteration of the adaptive loop from Scheme 3.1. In the following we only highlight the changes with respect to the module REFINE proposed in Daniel et al. (2018a,b) and provide a summary of the present slightly modified version in Algorithm 3.

We denote the polynomial-degree distribution in the patch $\mathcal{T}_\ell^{\mathbf{a}}$ by the vector $\mathbf{p}_\ell^{\mathbf{a}} := \{p_{\ell,K}\}_{K\in\mathcal{T}_\ell^{\mathbf{a}}}$. The idea employed in Daniel et al. (2018a,b) is to emulate separately the effects of h- and p-refinement on a patch assigned to a marked vertex using two distinct local patch-based spaces. For this purpose, let us introduce a matching simplicial refinement $\mathcal{T}_\ell^{\mathbf{a},h}$ (see the center panel of Figure 3.2), obtained from $\mathcal{T}_\ell^{\mathbf{a}}$ by dividing each simplex $K\in\mathcal{T}_\ell^{\mathbf{a}}$ into at least six children simplices such that a node interior to all the elements $K\in\mathcal{T}_\ell^{\mathbf{a}}$ as well as all the faces $F\in\mathcal{F}_\ell^{\mathbf{a},\mathrm{int}}$ is created, cf. the requirement of having an interior node and its implementation in two and three dimensions in Morin et al. (2002). The corresponding polynomial-degree distribution $\mathbf{p}_\ell^{\mathbf{a},h}$ is simply obtained from $\mathbf{p}_\ell^{\mathbf{a}}$ by assigning to each newly-created simplex the same polynomial degree as its parent. Next, let the polynomial-degree distribution vector $\mathbf{p}_\ell^{\mathbf{a},p}$ be set by assigning to each simplex $K\in\mathcal{T}_\ell^{\mathbf{a},p} := \mathcal{T}_\ell^{\mathbf{a}}$ the polynomial degree $\max\{p_{\ell,K}+d-1, p_{f,K}+d+1\}$, with $p_{f,K}$ the local polynomial degree of f on K (see the right panel of Figure 3.2). We note that the employed refinement methods differ from those suggested in Daniel et al. (2018a,b). In particular, the stricter requirements on h- and p-refinements are motivated by the theory developed in Section 3.4.

Following Daniel et al. (2018a,b), the *hp*-decision is made on the basis of the two local primal solves on the patches $\mathcal{T}_\ell^{\mathbf{a}}$, but this time, for each vertex $\mathbf{a}$ from the extended set of marked vertices $\widetilde{\mathcal{V}}_\ell^\sharp$, not only for the vertices from the set $\widetilde{\mathcal{V}}_\ell^\theta$ as in Daniel et al. (2018a,b). Hence, for each vertex $\mathbf{a}\in\widetilde{\mathcal{V}}_\ell^\sharp$, we consider the local patch-based spaces $V_\ell^{\mathbf{a},h}$ and $V_\ell^{\mathbf{a},p}$ given by

$$V_\ell^{\mathbf{a},h} := \mathbb{P}_{\mathbf{p}_\ell^{\mathbf{a},h}}(\mathcal{T}_\ell^{\mathbf{a},h})\cap H_0^1(\omega_\ell^{\mathbf{a}}), \quad V_\ell^{\mathbf{a},p} := \mathbb{P}_{\mathbf{p}_\ell^{\mathbf{a},p}}(\mathcal{T}_\ell^{\mathbf{a},p})\cap H_0^1(\omega_\ell^{\mathbf{a}}), \tag{3.12}$$

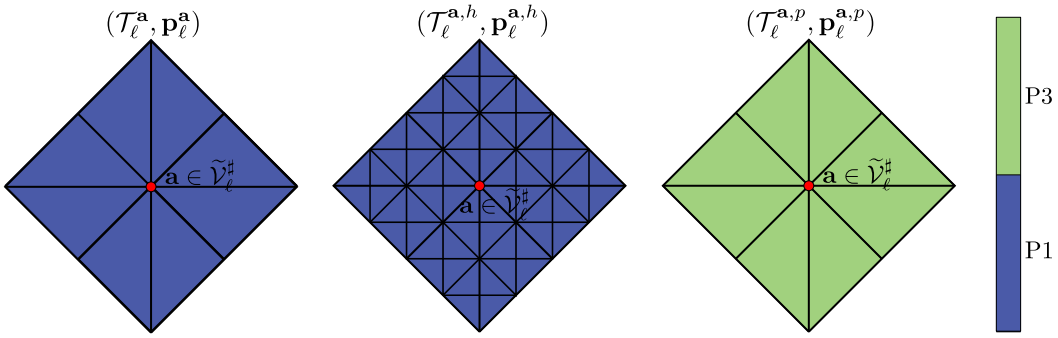

Figure 3.2: An example of patch $\mathcal{T}_\ell^{\mathbf{a}}$ together with its polynomial-degree distribution $\mathbf{p}_\ell^{\mathbf{a}}$ (*left*), its h-refined version (*center*), and its p-refined version (*right*).

and we let $r^{\mathbf{a},h} \in V_\ell^{\mathbf{a},h}$ and $r^{\mathbf{a},p} \in V_\ell^{\mathbf{a},p}$, the h- and p-refinement residual liftings respectively, solve

$$(\nabla r^{\mathbf{a},h}, \nabla v^{\mathbf{a},h})_{\omega_\ell^{\mathbf{a}}} = (f, v^{\mathbf{a},h})_{\omega_\ell^{\mathbf{a}}} - (\nabla u_\ell^{\mathrm{ex}}, \nabla v^{\mathbf{a},h})_{\omega_\ell^{\mathbf{a}}} \qquad \forall\, v^{\mathbf{a},h} \in V_\ell^{\mathbf{a},h}, \quad (3.13a)$$

$$(\nabla r^{\mathbf{a},p}, \nabla v^{\mathbf{a},p})_{\omega_\ell^{\mathbf{a}}} = (f, v^{\mathbf{a},p})_{\omega_\ell^{\mathbf{a}}} - (\nabla u_\ell^{\mathrm{ex}}, \nabla v^{\mathbf{a},p})_{\omega_\ell^{\mathbf{a}}} \qquad \forall\, v^{\mathbf{a},p} \in V_\ell^{\mathbf{a},p}. \quad (3.13b)$$

We consider here the case where the two local primal solves use Dirichlet boundary conditions; for the possible use of Neumann boundary conditions, we refer to Daniel et al. (2018b). The rest of the module `REFINE` including the hp-decision criterion and an actual refinement leading to the new pair $(\mathcal{T}_{\ell+1}, \mathbf{p}_{\ell+1})$ is outlined in Algorithm 3. We note that in order to prove convergence, we need to limit the maximal polynomial degree by a user-defined value $p_{\max}$. In order to not exceed this threshold, h-refinement may be employed also for elements for which p-refinement is suggested by our refinement criterion, cf. lines 7–8 in Algorithm 3. However, such restrictions on maximal polynomial degree are typically present in practical implementations of hp-methods.

3.3.4 Discrete lower bound on the incremental error on marked simplices

Once the new pair $(\mathcal{T}_{\ell+1}, \mathbf{p}_{\ell+1})$ is determined within the `REFINE` module of Section 3.3.3 (recall that $V_{\ell+1} := \mathbb{P}_{\mathbf{p}_{\ell+1}}(\mathcal{T}_{\ell+1}) \cap H_0^1(\Omega)$), the finite element space to be used on iteration $(\ell+1)$ of the adaptive loop of Scheme 3.1 is at our disposal. We now proceed by extending the discrete lower bound of (Daniel et al., 2018a, Lemma 5.1) to the present setting. For all the vertices $\mathbf{a}$ from the extended set of marked vertices $\widetilde{\mathcal{V}}_\ell^\sharp$, let us set, in extension of (3.12),

$$V_\ell^{\mathbf{a},hp} := V_{\ell+1}|_{\omega_\ell^{\mathbf{a}}} \cap H_0^1(\omega_\ell^{\mathbf{a}}) \quad (3.14)$$

and construct the residual lifting $r^{\mathbf{a},hp} \in V_\ell^{\mathbf{a},hp}$ by solving

$$(\nabla r^{\mathbf{a},hp}, \nabla v^{\mathbf{a},hp})_{\omega_\ell^{\mathbf{a}}} = (f, v^{\mathbf{a},hp})_{\omega_\ell^{\mathbf{a}}} - (\nabla u_\ell^{\mathrm{ex}}, \nabla v^{\mathbf{a},hp})_{\omega_\ell^{\mathbf{a}}} \qquad \forall\, v^{\mathbf{a},hp} \in V_\ell^{\mathbf{a},hp}. \quad (3.15)$$

Algorithm 3 (**module** `REFINE`)

module `REFINE` $(\widetilde{\mathcal{V}}_\ell^\sharp)$
  ▷ **Input:** extended set of marked vertices $\widetilde{\mathcal{V}}_\ell^\sharp$
  ▷ **Output:** new pair $(\mathcal{T}_{\ell+1}, \mathbf{p}_{\ell+1})$
  for all $\mathbf{a} \in \widetilde{\mathcal{V}}_\ell^\sharp$ **do**
    Compute the residual liftings $r^{\mathbf{a},h}$, $r^{\mathbf{a},p}$ given by (3.13a) and (3.13b)
  end for
  ▷ hp-decision on vertices:
  Set $\widetilde{\mathcal{V}}_\ell^p := \{\mathbf{a} \in \widetilde{\mathcal{V}}_\ell^\sharp \mid \|\nabla r^{\mathbf{a},h}\|_{\omega_\ell^\mathbf{a}} < \|\nabla r^{\mathbf{a},p}\|_{\omega_\ell^\mathbf{a}} \text{ and } p_\mathbf{a}^{\mathrm{est}} \leq (p_{\max} - d)\}$
  Set $\widetilde{\mathcal{V}}_\ell^h := \widetilde{\mathcal{V}}_\ell^\sharp \setminus \widetilde{\mathcal{V}}_\ell^p$
  ▷ hp-decision on simplices:
  Select $\mathcal{M}_\ell^h := \{K \in \mathcal{T}_\ell \mid \mathcal{V}_{\ell,K} \cap \widetilde{\mathcal{V}}_\ell^h \neq \emptyset\} \subset \mathcal{M}_\ell^\sharp$
  Select $\mathcal{M}_\ell^p := \{K \in \mathcal{T}_\ell \mid \mathcal{V}_{\ell,K} \cap \widetilde{\mathcal{V}}_\ell^p \neq \emptyset\} \subset \mathcal{M}_\ell^\sharp$
  ▷ hp-refinement:
  Build $\mathcal{T}_{\ell+1}$ from $\mathcal{T}_\ell$ and $\mathcal{M}_\ell^h$, such that $\mathcal{T}_\ell^{\mathbf{a},h} \subset \mathcal{T}_{\ell+1}$, $\forall \mathbf{a} \in \widetilde{\mathcal{V}}_\ell^h$
  for all $K \in \mathcal{T}_{\ell+1}$ with its parent element $\widetilde{K} \in \mathcal{T}_\ell$ **do**
    $$p_{\ell+1,K} := \begin{cases} p_{\ell,\widetilde{K}} & \text{if } \widetilde{K} \notin \mathcal{M}_\ell^p \\ p_{\ell,\widetilde{K}} + \max\{d-1, p_{f,\widetilde{K}} + d + 1 - p_{\ell,\widetilde{K}}\} & \text{if } \widetilde{K} \in \mathcal{M}_\ell^p \end{cases}$$
  end for
end module

Then, after extending $r^{\mathbf{a},hp}$ by zero outside $\omega_\ell^\mathbf{a}$, we have for the current approximation $u_\ell^{\mathrm{ex}} \in V_\ell$ and the next level's approximation $u_{\ell+1}^{\mathrm{ex}} \in V_{\ell+1}$, by (Daniel et al., 2018a, Lemma 5.1) used with the extended set $\widetilde{\mathcal{V}}_\ell^\sharp$ in place of $\widetilde{\mathcal{V}}_\ell^\theta$:

$$\|\nabla(u_{\ell+1}^{\mathrm{ex}} - u_\ell^{\mathrm{ex}})\|_{\omega_\ell^\sharp} \geq \underline{\eta}_{\mathcal{M}_\ell^\sharp}, \quad \underline{\eta}_{\mathcal{M}_\ell^\sharp} := \begin{cases} \dfrac{\sum_{\mathbf{a}\in\widetilde{\mathcal{V}}_\ell^\sharp} \left\|\nabla r^{\mathbf{a},hp}\right\|_{\omega_\ell^\mathbf{a}}^2}{\left\|\nabla\left(\sum_{\mathbf{a}\in\widetilde{\mathcal{V}}_\ell^\sharp} r^{\mathbf{a},hp}\right)\right\|_{\omega_\ell^\sharp}} & \text{if } \sum_{\mathbf{a}\in\widetilde{\mathcal{V}}_\ell^\sharp} r^{\mathbf{a},hp} \neq 0, \\ 0 & \text{otherwise.} \end{cases} \tag{3.16}$$

Moreover, the above lower bound can be further localized using the fact that each simplex has $(d+1)$ vertices as

$$\underline{\eta}_{\mathcal{M}_\ell^\sharp} \geq \frac{\left\{\sum_{\mathbf{a}\in\widetilde{\mathcal{V}}_\ell^\sharp} \|\nabla r^{\mathbf{a},hp}\|_{\omega_\ell^\mathbf{a}}^2\right\}^{1/2}}{\sqrt{d+1}}; \tag{3.17}$$

this can be seen from

$$\left\|\nabla\left(\sum_{\mathbf{a}\in\widetilde{\mathcal{V}}_\ell^\sharp} r^{\mathbf{a},hp}\right)\right\|_{\omega_\ell^\sharp}^2 = \sum_{K\in\mathcal{M}_\ell^\sharp} \left\|\sum_{\mathbf{a}\in\widetilde{\mathcal{V}}_\ell^\sharp\cap\mathcal{V}_K} \nabla r^{\mathbf{a},hp}\right\|_K^2$$

$$\leq \sum_{K\in\mathcal{M}_\ell^\sharp}(d+1)\sum_{\mathbf{a}\in\widetilde{\mathcal{V}}_\ell^\sharp\cap\mathcal{V}_K}\|\nabla r^{\mathbf{a},hp}\|_K^2$$
$$=(d+1)\sum_{\mathbf{a}\in\widetilde{\mathcal{V}}_\ell^\sharp}\|\nabla r^{\mathbf{a},hp}\|_{\omega_\ell^\mathbf{a}}^2.$$

3.4 Discrete stability of equilibrated fluxes in an exact setting

From now on, we use the shorthand notation $x_1 \lesssim x_2$ when there exists a generic positive constant C that only depends on the space dimension d, the shape-regularity $\kappa_\mathcal{T}$ of the underlying hierarchy of meshes, and the polynomial degree of approximation employed locally such that $x_1 \leq Cx_2$. Our main tool will be the following:

Proposition 3.4.1 (Discrete stability of the local flux equilibration)**.** *Let $u_\ell^{\mathrm{ex}} \in V_\ell$ satisfy the hat function orthogonality*

$$(f,\psi_\ell^\mathbf{a})_{\omega_\ell^\mathbf{a}} - (\nabla u_\ell^{\mathrm{ex}},\nabla\psi_\ell^\mathbf{a})_{\omega_\ell^\mathbf{a}} = 0 \qquad \forall\mathbf{a}\in\mathcal{V}_\ell^{\mathrm{int}},$$

let the local equilibrated flux $\boldsymbol{\sigma}_\ell^\mathbf{a}$ be constructed by (3.8), and let $r^{\mathbf{a},hp}$ be given by (3.15). Then there holds

$$\|\psi_\ell^\mathbf{a}\nabla u_\ell^{\mathrm{ex}} + \boldsymbol{\sigma}_\ell^\mathbf{a}\|_{\omega_\ell^\mathbf{a}} \lesssim \|\nabla r^{\mathbf{a},hp}\|_{\omega_\ell^\mathbf{a}} \quad \forall\mathbf{a}\in\widetilde{\mathcal{V}}_\ell^\sharp. \tag{3.18}$$

To prove Proposition 3.4.1 we will rely on the two following auxiliary results employing the bubble function technique, cf. Verfürth (2013):

Lemma 3.4.2 (Discrete stability of the element residuals)**.** *Let $r^{\mathbf{a},hp}$ be given by (3.15). Then*

$$h_K\|f+\Delta u_\ell^{\mathrm{ex}}\|_K \lesssim \|\nabla r^{\mathbf{a},hp}\|_K \quad \forall K\in\mathcal{T}_\ell^\mathbf{a} \quad \forall\mathbf{a}\in\widetilde{\mathcal{V}}_\ell^\sharp. \tag{3.19}$$

Proof. Fix the element $K\in\mathcal{T}_\ell^\mathbf{a}$ and set

$$v_K := (f+\Delta u_\ell^{\mathrm{ex}})|_K. \tag{3.20}$$

We note that $v_K \in \mathbb{P}_{\max\{p_{\ell,K}-2,p_{f,K}\}}(K)$, due to Assumption 3.3.1. Let us define ψ_K, the bubble function on element K, depending on which refinement has been applied within the `REFINE` module of Section 3.3.3 for the vertex $\mathbf{a}$, to be a function

$$\psi_K \in \begin{cases}\mathbb{P}_1\left(\mathcal{T}_{\ell+1}|_K\right)\cap H_0^1(K) & \text{if } \mathbf{a}\in\widetilde{\mathcal{V}}_\ell^h\\ \mathbb{P}_{d+1}\left(K\right)\cap H_0^1(K) & \text{if } \mathbf{a}\in\widetilde{\mathcal{V}}_\ell^p,\end{cases} \quad \text{with} \quad \|\psi_K\|_{\infty,K}=1. \tag{3.21}$$

The equivalence of norms on finite-dimensional spaces gives

$$(v_K, v_K)_K \lesssim (v_K, \psi_K v_K)_K. \tag{3.22}$$

This in combination with (3.20) yields

$$\|v_K\|_K^2 \lesssim (v_K, \psi_K v_K)_K = (f, \psi_K v_K)_K + (\Delta u_\ell^{\mathrm{ex}}, \psi_K v_K)_K.$$

Then, noting that $\nabla u_\ell^{\mathrm{ex}} \in \mathbf{H}(\mathrm{div}, K)$ and $\psi_K v_K \in H_0^1(K)$, employing the Green theorem and using (3.15) and the Cauchy–Schwarz inequality, we obtain

$$\begin{aligned} \|v_K\|_K^2 &\lesssim (f, \psi_K v_K)_K - (\nabla u_\ell^{\mathrm{ex}}, \nabla(\psi_K v_K))_K = (\nabla r^{\mathbf{a},hp}, \nabla(\psi_K v_K))_K, \\ &\leq \|\nabla r^{\mathbf{a},hp}\|_K \|\nabla(\psi_K v_K)\|_K, \end{aligned} \tag{3.23}$$

where we have also crucially employed that $\psi_K v_K$ extended by zero is contained in the space $V_\ell^{\mathbf{a},hp}$ due to (3.14) and (3.21). In particular, we use the fact that either h-refinement has been employed and then $\mathcal{T}_{\ell+1}$ contains an interior node, or p-refinement has been applied and then the polynomial degree has been increased to at least $\mathbf{p}_{\ell,K} + d$. Then, using the inverse inequality (cf., e.g. (Quarteroni and Valli, 1994, Proposition 6.3.2)), we have

$$\|\nabla(\psi_K v_K)\|_K \lesssim h_K^{-1} \|\psi_K v_K\|_K. \tag{3.24}$$

Moreover, from the definition of the bubble function ψ_K, there holds

$$\|\psi_K v_K\|_K \leq \|\psi_K\|_{\infty,K} \|v_K\|_K = \|v_K\|_K. \tag{3.25}$$

Finally, (3.23) with (3.24) and (3.25) lead to the assertion of the lemma. □

Lemma 3.4.3 (Discrete stability of the face residuals)**.** *Let $r^{\mathbf{a},hp}$ be given by (3.15), let $\mathcal{T}_F$ denote the set of elements containing the two elements $K \in \mathcal{T}_\ell^{\mathbf{a}}$ that share a face $F \in \mathcal{F}_\ell^{\mathbf{a},\mathrm{int}}$, and let ω_F be the corresponding open subdomain. Then*

$$h_F^{\frac{1}{2}} \|[\![\nabla u_\ell^{\mathrm{ex}} \cdot \mathbf{n}_F]\!]\|_F \lesssim \|\nabla r^{\mathbf{a},hp}\|_{\omega_F} \quad \forall F \in \mathcal{F}_\ell^{\mathbf{a},\mathrm{int}} \quad \forall \mathbf{a} \in \widetilde{\mathcal{V}}_\ell^\sharp.$$

Proof. Fix an edge $F \in \mathcal{F}_\ell^{\mathbf{a},\mathrm{int}}$. This time, set

$$v_F := [\![\nabla u_\ell^{\mathrm{ex}} \cdot \mathbf{n}_F]\!]|_F \tag{3.26}$$

and note that $v_F \in \mathbb{P}_{\max\{p_{\ell,K}-1, p_{0,K'}-1\}}$, where $K, K' \in \mathcal{T}_\ell^{\mathbf{a}}$ share the face F. Let ψ_F be the bubble function on $\mathcal{T}_F$, depending on the refinement method applied within the `REFINE` module of Section 3.3.3, namely for the vertex $\mathbf{a}$

$$\psi_F \in \begin{cases} \mathbb{P}_1(\mathcal{T}_{\ell+1}|_{\mathcal{T}_F}) \cap H_0^1(\omega_F) & \text{if } \mathbf{a} \in \widetilde{\mathcal{V}}_\ell^h \\ \mathbb{P}_d(\mathcal{T}_F) \cap H_0^1(\omega_F) & \text{if } \mathbf{a} \in \widetilde{\mathcal{V}}_\ell^p. \end{cases} \quad \text{with} \quad \|\psi_F\|_{\infty,\omega_F} = 1.$$

Then, by equivalence of norms on finite-dimensional spaces, similarly to (3.22), there holds

$$(v_F, v_F)_F \lesssim (v_F, \psi_F v_F)_F. \tag{3.27}$$

Let us keep the same notation for the extension of the function v_F, with its original domain of definition being only the face F, to a function defined on the simplices of $\mathcal{T}_F$. The extension is done by constant values in the direction of the barycenter of the face towards the vertex opposite to F. Then, the following estimate holds true

$$\|v_F\|_{\omega_F} \lesssim h_F^{\frac{1}{2}} \|v_F\|_F. \tag{3.28}$$

Employing (3.27), (3.26), and expanding the jump term with $\mathcal{T}_F := \{K, K'\}$ and the convention that $\mathbf{n}_F$ points from K to K', we have

$$\begin{aligned} \|v_F\|_F^2 \lesssim (v_F, \psi_F v_F)_F &= \left((\nabla u_\ell^{\mathrm{ex}}|_K)\,|_F \cdot \mathbf{n}_F, \psi_F v_F\right)_F - \left((\nabla u_\ell^{\mathrm{ex}}|_{K'})\,|_F \cdot \mathbf{n}_F, \psi_F v_F\right)_F \\ &= \left((\nabla u_\ell^{\mathrm{ex}}|_K)\,|_{\partial K} \cdot \mathbf{n}_{\partial K}, \psi_F v_F\right)_{\partial K} + \left((\nabla u_\ell^{\mathrm{ex}}|_{K'})\,|_{\partial K'} \cdot \mathbf{n}_{\partial K'}, \psi_F v_F\right)_{\partial K'}. \end{aligned} \tag{3.29}$$

We have also used the fact that $(\psi_F v_F)\,|_{\partial\omega_F} = 0$ due to the definition of the bubble function ψ_F. Moreover, $(\psi_F v_F)\,|_K \in H^1(K)$ and $\nabla u_\ell^{\mathrm{ex}} \in \mathbf{H}(\mathrm{div}, K)$, for each simplex $K \in \mathcal{T}_F$, so we are able to apply the Green theorem for both of the terms on the right-hand side of (3.29). Adding and subtracting $(f, \psi_F v_F)_{\omega_F}$, as $\psi_F v_F$ extended by zero is in $V_\ell^{\mathbf{a},hp}$, and recalling the discrete problem (3.15), we finally obtain

$$\begin{aligned} \|v_F\|_F^2 \lesssim (\nabla u_\ell^{\mathrm{ex}}, \nabla(\psi_F v_F))_{\omega_F} - (f, \psi_F v_F)_{\omega_F} + (f + \Delta u_\ell^{\mathrm{ex}}, \psi_F v_F)_{\omega_F} \\ = -(\nabla r^{\mathbf{a},hp}, \nabla(\psi_F v_F))_{\omega_F} + (f + \Delta u_\ell^{\mathrm{ex}}, \psi_F v_F)_{\omega_F}. \end{aligned} \tag{3.30}$$

Again, the face interior node property/appropriate polynomial degree increase were important. From the definition of the bubble function ψ_F, there holds

$$\|\psi_F v_F\|_{\omega_F} \leq \|\psi_F\|_{\infty,\omega_F} \|v_F\|_{\omega_F} = \|v_F\|_{\omega_F}, \tag{3.31}$$

while the inverse inequality and the shape-regularity of the mesh $\mathcal{T}_\ell$ give

$$\|\nabla(\psi_F v_F)\|_{\omega_F} \lesssim h_F^{-1} \|\psi_F v_F\|_{\omega_F}. \tag{3.32}$$

Then, the following chain of inequalities holds true due to the Cauchy–Schwarz inequality, (3.31), (3.32), and (3.28):

$$\begin{aligned} \|v_F\|_F^2 &\lesssim \|\nabla r^{\mathbf{a},hp}\|_{\omega_F} \|\nabla(\psi_F v_F)\|_{\omega_F} + \|f + \Delta u_\ell^{\mathrm{ex}}\|_{\omega_F} \|\psi_F v_F\|_{\omega_F} \\ &\lesssim \|\nabla r^{\mathbf{a},hp}\|_{\omega_F} h_F^{-1} \|v_F\|_{\omega_F} + \|f + \Delta u_\ell^{\mathrm{ex}}\|_{\omega_F} \|v_F\|_{\omega_F} \\ &\lesssim \left(\|\nabla r^{\mathbf{a},hp}\|_{\omega_F} + h_F \|f + \Delta u_\ell^{\mathrm{ex}}\|_{\omega_F}\right) h_F^{-\frac{1}{2}} \|v_F\|_F. \end{aligned}$$

The assertion of the lemma then follows from the above result combined

with (3.19) and the shape-regularity of the mesh $\mathcal{T}_\ell$. □

Proof of Proposition 3.4.1. Following (Diening et al., 2019, Appendix B), we will crucially employ two reformulations of the local minimization problem (3.8). The Euler–Lagrange conditions for (3.8), imposing the divergence constraint via a Lagrange multiplier, amount to solving the local Neumann mixed finite element problem: seek the pair $(\boldsymbol{\sigma}_\ell^{\mathbf{a}}, \gamma_\ell^{\mathbf{a}}) \in \mathbf{V}_\ell^{\mathbf{a}} \times Q_\ell^{\mathbf{a}}$ such that

$$(\boldsymbol{\sigma}_\ell^{\mathbf{a}}, \mathbf{v}_\ell)_{\omega_\ell^{\mathbf{a}}} - (\gamma_\ell^{\mathbf{a}}, \nabla\cdot\mathbf{v}_\ell)_{\omega_\ell^{\mathbf{a}}} = -(\psi_\ell^{\mathbf{a}}\nabla u_\ell^{\mathrm{ex}}, \mathbf{v}_\ell)_{\omega_\ell^{\mathbf{a}}} \qquad \forall \mathbf{v}_\ell \in \mathbf{V}_\ell^{\mathbf{a}}, \tag{3.33a}$$

$$(\nabla\cdot\boldsymbol{\sigma}_\ell^{\mathbf{a}}, q_\ell)_{\omega_\ell^{\mathbf{a}}} = (\psi_\ell^{\mathbf{a}} f - \nabla u_\ell^{\mathrm{ex}}\cdot\nabla\psi_\ell^{\mathbf{a}}, q_\ell)_{\omega_\ell^{\mathbf{a}}} \qquad \forall q_\ell \in Q_\ell^{\mathbf{a}}, \tag{3.33b}$$

with the patchwise discontinuous piecewise polynomial spaces $Q_\ell^{\mathbf{a}}$ defined by

$$Q_\ell^{\mathbf{a}} := \begin{cases} \{q_\ell \in \mathbb{P}_{p_{\mathbf{a}}^{\mathrm{est}}}(\mathcal{T}_\ell^{\mathbf{a}}) \,;\, (q_\ell, 1)_{\omega_\ell^{\mathbf{a}}} = 0\} & \text{if } \mathbf{a} \in \mathcal{V}_\ell^{\mathrm{int}}, \\ \mathbb{P}_{p_{\mathbf{a}}^{\mathrm{est}}}(\mathcal{T}_\ell^{\mathbf{a}}) & \text{if } \mathbf{a} \in \mathcal{V}_\ell^{\mathrm{ext}}. \end{cases} \tag{3.34}$$

Next, imposing the normal trace continuity constraint on faces from $\mathcal{F}_\ell^{\mathbf{a},\mathrm{int}}$ and the no-flux condition on all faces from $\mathcal{F}_\ell^{\mathbf{a},\mathrm{ext}}$ for $\mathbf{a} \in \mathcal{V}_\ell^{\mathrm{int}}$ and only faces from $\mathcal{F}_\ell^{\mathbf{a},\mathrm{ext}}$ not lying on $\partial\Omega$ for $\mathbf{a} \in \mathcal{V}_\ell^{\mathrm{ext}}$ via a Lagrange multiplier leads to the hybridized formulation: Seek $\boldsymbol{\sigma}_\ell^{\mathbf{a}}$ in the broken space $\mathbf{RTN}_{p_{\mathbf{a}}^{\mathrm{est}}}(\mathcal{T}_\ell^{\mathbf{a}})$, $\gamma_\ell^{\mathbf{a}} \in Q_\ell^{\mathbf{a}}$, and $\lambda_\ell^F \in \mathbb{P}_{p_{\mathbf{a}}^{\mathrm{est}}}(F)$ for all $F \in \mathcal{F}_\ell^{\mathbf{a}} \setminus \mathcal{F}_\ell^{\mathbf{a},\partial\Omega}$ such that

$$\sum_{K\in\mathcal{T}_\ell^{\mathbf{a}}} (\psi_\ell^{\mathbf{a}}\nabla u_\ell^{\mathrm{ex}} + \boldsymbol{\sigma}_\ell^{\mathbf{a}},\, \mathbf{v}_\ell)_K - \sum_{K\in\mathcal{T}_\ell^{\mathbf{a}}} (\nabla\cdot\mathbf{v}_\ell,\, \gamma_\ell^{\mathbf{a}})_K + \sum_{K\in\mathcal{T}_\ell^{\mathbf{a}}} \sum_{F\in\mathcal{F}_{\ell,K}\setminus\mathcal{F}_\ell^{\mathbf{a},\partial\Omega}} \big(\mathbf{v}_\ell\cdot\mathbf{n}_K,\, \lambda_\ell^F\big)_F = 0 \qquad \forall \mathbf{v}_\ell \in \mathbf{RTN}_{p_{\mathbf{a}}^{\mathrm{est}}}(\mathcal{T}_\ell^{\mathbf{a}}), \tag{3.35a}$$

$$\sum_{K\in\mathcal{T}_\ell^{\mathbf{a}}} (\nabla\cdot\boldsymbol{\sigma}_\ell^{\mathbf{a}},\, q_\ell)_K = \sum_{K\in\mathcal{T}_\ell^{\mathbf{a}}} (\psi_\ell^{\mathbf{a}} f - \nabla\psi_\ell^{\mathbf{a}}\cdot\nabla u_\ell^{\mathrm{ex}},\, q_\ell)_K \quad \forall q_\ell \in Q_\ell^{\mathbf{a}}, \tag{3.35b}$$

$$-\sum_{K\in\omega_F} (\boldsymbol{\sigma}_\ell^{\mathbf{a}}\cdot\mathbf{n}_K,\, \xi_\ell)_F = 0 \qquad \forall \xi_\ell \in \mathbb{P}_{p_{\mathbf{a}}^{\mathrm{est}}}(F), \forall F \in \mathcal{F}_\ell^{\mathbf{a}} \setminus \mathcal{F}_\ell^{\mathbf{a},\partial\Omega}, \tag{3.35c}$$

where we used the notation

$$\mathcal{F}_\ell^{\mathbf{a},\partial\Omega} := \begin{cases} \emptyset & \text{if } \mathbf{a} \in \mathcal{V}_\ell^{\mathrm{int}}, \\ \mathcal{F}_\ell^{\mathbf{a},\mathrm{ext}} \cap \mathcal{F}_\ell^{\mathrm{ext}} & \text{if } \mathbf{a} \in \mathcal{V}_\ell^{\mathrm{ext}}. \end{cases} \tag{3.36}$$

We note that $\psi_\ell^{\mathbf{a}}\nabla u_\ell^{\mathrm{ex}} + \boldsymbol{\sigma}_\ell^{\mathbf{a}} \in \mathbf{RTN}_{p_{\mathbf{a}}^{\mathrm{est}}}(\mathcal{T}_\ell^{\mathbf{a}})$, thus we can use it as a test function $\mathbf{v}_\ell$ in (3.35a). Afterwards, employing $\gamma_\ell^{\mathbf{a}}$ as a test function q_ℓ in (3.35b) and λ_ℓ^F as ξ_ℓ in (3.35c), summing (3.35c) over all $F \in F \in \mathcal{F}_\ell^{\mathbf{a}} \setminus \mathcal{F}_\ell^{\mathbf{a},\partial\Omega}$, finally summing (3.35a)–(3.35c), we obtain

$$\|\psi_\ell^{\mathbf{a}}\nabla u_\ell^{\mathrm{ex}} + \boldsymbol{\sigma}_\ell^{\mathbf{a}}\|_{\omega_\ell^{\mathbf{a}}}^2 = \sum_{K\in\mathcal{T}_\ell^{\mathbf{a}}} (\psi_\ell^{\mathbf{a}} f - \nabla\psi_\ell^{\mathbf{a}}\cdot\nabla u_\ell^{\mathrm{ex}} + \nabla\cdot(\psi_\ell^{\mathbf{a}}\nabla u_\ell^{\mathrm{ex}}), \gamma_\ell^{\mathbf{a}})_K$$

$$
\begin{aligned}
&\quad - \sum_{F\in\mathcal{F}_\ell^{\mathbf{a}}\setminus\mathcal{F}_\ell^{\mathbf{a},\partial\Omega}} (\llbracket \psi_\ell^{\mathbf{a}} \nabla u_\ell^{\mathrm{ex}}\cdot\mathbf{n}_F\rrbracket, \lambda_\ell^F)_F \\
&= \sum_{K\in\mathcal{T}_\ell^{\mathbf{a}}} (\psi_\ell^{\mathbf{a}}(f+\Delta u_\ell^{\mathrm{ex}}), \gamma_\ell^{\mathbf{a}})_K - \sum_{F\in\mathcal{F}_\ell^{\mathbf{a}}\setminus\mathcal{F}_\ell^{\mathbf{a},\partial\Omega}} (\psi_\ell^{\mathbf{a}} \llbracket \nabla u_\ell^{\mathrm{ex}}\cdot\mathbf{n}_F\rrbracket, \lambda_\ell^F)_F \qquad (3.37)\\
&\le \sum_{K\in\mathcal{T}_\ell^{\mathbf{a}}} \|\psi_\ell^{\mathbf{a}}(f+\Delta u_\ell^{\mathrm{ex}})\|_K \|\gamma_\ell^{\mathbf{a}}\|_K + \sum_{F\in\mathcal{F}_\ell^{\mathbf{a},\mathrm{int}}} \|\psi_\ell^{\mathbf{a}} \llbracket \nabla u_\ell^{\mathrm{ex}}\cdot\mathbf{n}_F\rrbracket\|_F \|\lambda_\ell^F\|_F,
\end{aligned}
$$

where for the estimate on the right-hand side of (3.37) we have also used the fact that the hat function $\psi_\ell^{\mathbf{a}}|_F = 0\ \forall F \in \mathcal{F}_\ell^{\mathbf{a},\mathrm{ext}}$ for vertices $\mathbf{a}\in\mathcal{V}_\ell^{\mathrm{int}}$, and the boundary faces are excluded from the sum and $\psi_\ell^{\mathbf{a}}|_F = 0\ \forall F \in \mathcal{F}_\ell^{\mathbf{a},\mathrm{ext}}\setminus\mathcal{F}_\ell^{\mathbf{a},\partial\Omega}$ for $\mathbf{a}\in\mathcal{V}_\ell^{\mathrm{ext}}$.

We now proceed by bounding the terms in the estimate of (3.37). Firstly, by the inf-sup stability of the mixed discretization (3.33), see e.g. Brezzi and Fortin (1991) or (Vohralík, 2010, Theorem 5.9), we have

$$
\|\gamma_\ell^{\mathbf{a}}\|_{\omega_\ell^{\mathbf{a}}} \lesssim h_{\omega_\ell^{\mathbf{a}}} \|\psi_\ell^{\mathbf{a}}\nabla u_\ell^{\mathrm{ex}} + \boldsymbol{\sigma}_\ell^{\mathbf{a}}\|_{\omega_\ell^{\mathbf{a}}}. \qquad (3.38)
$$

Secondly, the $\|\psi_\ell^{\mathbf{a}}\|_{\infty,K}\le 1$ together with Lemma 3.4.2 yield the estimate

$$
\|\psi_\ell^{\mathbf{a}}(f+\Delta u_\ell^{\mathrm{ex}})\|_K \le \|f+\Delta u_\ell^{\mathrm{ex}}\|_K \lesssim h_K^{-1}\|\nabla r^{\mathbf{a},hp}\|_K \quad \forall K\in\mathcal{T}_\ell^{\mathbf{a}}. \qquad (3.39)
$$

Combining (3.37) with (3.39), the Cauchy–Schwarz inequality, the shape-regularity yielding $h_K \approx h_{\omega_\ell^{\mathbf{a}}}$, and (3.38), we obtain the estimate on the first term

$$
\begin{aligned}
\sum_{K\in\mathcal{T}_\ell^{\mathbf{a}}} \|\psi_\ell^{\mathbf{a}}(f+\Delta u_\ell^{\mathrm{ex}})\|_K \|\gamma_\ell^{\mathbf{a}}\|_K &\lesssim \sum_{K\in\mathcal{T}_\ell^{\mathbf{a}}} h_K^{-1}\|\nabla r^{\mathbf{a},hp}\|_K \|\gamma_\ell^{\mathbf{a}}\|_K \\
&\lesssim h_{\omega_\ell^{\mathbf{a}}}^{-1}\|\nabla r^{\mathbf{a},hp}\|_{\omega_\ell^{\mathbf{a}}} \|\gamma_\ell^{\mathbf{a}}\|_{\omega_\ell^{\mathbf{a}}} \\
&\lesssim \|\nabla r^{\mathbf{a},hp}\|_{\omega_\ell^{\mathbf{a}}} \|\psi_\ell^{\mathbf{a}}\nabla u_\ell^{\mathrm{ex}} + \boldsymbol{\sigma}_\ell^{\mathbf{a}}\|_{\omega_\ell^{\mathbf{a}}}. \qquad (3.40)
\end{aligned}
$$

We continue by bounding the second term in the estimate of (3.37). By the characterization of the degrees of freedom in the Raviart–Thomas–Nédélec spaces, if $F\in\mathcal{F}_\ell^{\mathbf{a},\mathrm{int}}$ is a face of an element $K\in\mathcal{T}_\ell^{\mathbf{a}}$, we have

$$
\|\lambda_\ell^F\|_F = \sup_{\substack{\mathbf{v}_\ell\in\mathbf{RTN}_{p_{\mathbf{a}}^{\mathrm{est}}}(K)\\ \mathbf{v}_\ell\cdot\mathbf{n}_K|_F\neq 0\\ \mathbf{v}_\ell\cdot\mathbf{n}_K|_{F'}=0\,\forall F'\in\mathcal{F}_{\ell,K},F'\neq F\\ (\mathbf{v}_\ell,\mathbf{r}_\ell)_K=0\,\forall\mathbf{r}_\ell\in\left[\mathbb{P}_{p_{\mathbf{a}}^{\mathrm{est}}-1}(K)\right]^d}} \frac{(\mathbf{v}_\ell\cdot\mathbf{n}_K, \lambda_\ell^F)_F}{\|\mathbf{v}_\ell\cdot\mathbf{n}_K\|_F}. \qquad (3.41)
$$

Fix $\mathbf{v}_\ell\in\mathbf{RTN}_{p_{\mathbf{a}}^{\mathrm{est}}}(K)$ with the constraints as in (3.41). Using this $\mathbf{v}_\ell$ as a test function in (3.35a) and the Cauchy–Schwarz inequality, we obtain

$$
(\mathbf{v}_\ell\cdot\mathbf{n}_K, \lambda_\ell^F)_F = (\nabla\cdot\mathbf{v}_\ell, \gamma_\ell^{\mathbf{a}})_K - (\psi_\ell^{\mathbf{a}}\nabla u_\ell^{\mathrm{ex}} + \boldsymbol{\sigma}_\ell^{\mathbf{a}}, \mathbf{v}_\ell)_K
$$

$$\leq \|\nabla\cdot\mathbf{v}_\ell\|_K\|\gamma_\ell^{\mathbf{a}}\|_K + \|\psi_\ell^{\mathbf{a}}\nabla u_\ell^{\mathrm{ex}} + \boldsymbol{\sigma}_\ell^{\mathbf{a}}\|_K\|\mathbf{v}_\ell\|_K. \tag{3.42}$$

We now treat the two terms of (3.42) separately. For the first term, we start by employing the following inverse inequality

$$\|\nabla\cdot\mathbf{v}_\ell\|_K \lesssim h_K^{-1}\|\mathbf{v}_\ell\|_K.$$

Furthermore, by scaling arguments, under the constraints of (3.41), we have

$$\|\mathbf{v}_\ell\|_K \lesssim h_F^{\frac{1}{2}}\|\mathbf{v}_\ell\cdot\mathbf{n}_K\|_F. \tag{3.43}$$

The first term of (3.42) can then be bounded as follows:

$$\begin{aligned}\|\nabla\cdot\mathbf{v}_\ell\|_K\|\gamma_\ell^{\mathbf{a}}\|_K &\lesssim h_K^{-1}\|\mathbf{v}_\ell\|_K\|\gamma_\ell^{\mathbf{a}}\|_K \lesssim h_F^{-\frac{1}{2}}\|\mathbf{v}_\ell\cdot\mathbf{n}_K\|_F\|\gamma_\ell^{\mathbf{a}}\|_K \\ &\lesssim h_F^{\frac{1}{2}}\|\mathbf{v}_\ell\cdot\mathbf{n}_K\|_F\|\psi_\ell^{\mathbf{a}}\nabla u_\ell^{\mathrm{ex}} + \boldsymbol{\sigma}_\ell^{\mathbf{a}}\|_{\omega_\ell^{\mathbf{a}}},\end{aligned} \tag{3.44}$$

where we have also used the bound (3.38) and the mesh shape-regularity yielding $h_{\omega_\ell^{\mathbf{a}}} \approx h_K \approx h_F$. On the other hand, (3.43) leads to the following bound on the second term of (3.42)

$$\|\psi_\ell^{\mathbf{a}}\nabla u_\ell^{\mathrm{ex}} + \boldsymbol{\sigma}_\ell^{\mathbf{a}}\|_K\|\mathbf{v}_\ell\|_K \lesssim h_F^{\frac{1}{2}}\|\psi_\ell^{\mathbf{a}}\nabla u_\ell^{\mathrm{ex}} + \boldsymbol{\sigma}_\ell^{\mathbf{a}}\|_K\|\mathbf{v}_\ell\cdot\mathbf{n}_K\|_F. \tag{3.45}$$

In order to bound the supremum in (3.41), we combine (3.44), (3.45), and (3.42), to get

$$\|\lambda_\ell^F\|_F \lesssim h_F^{\frac{1}{2}}\|\psi_\ell^{\mathbf{a}}\nabla u_\ell^{\mathrm{ex}} + \boldsymbol{\sigma}_\ell^{\mathbf{a}}\|_{\omega_\ell^{\mathbf{a}}}. \tag{3.46}$$

Afterwards, $\|\psi_\ell^{\mathbf{a}}\|_F \leq 1$ and Lemma 3.4.3 yield

$$\|\psi_\ell^{\mathbf{a}}[\![\nabla u_\ell^{\mathrm{ex}}\cdot\mathbf{n}_F]\!]\|_F \leq \|[\![\nabla u_\ell^{\mathrm{ex}}]\!]\cdot\mathbf{n}_F\|_F \lesssim h_F^{-\frac{1}{2}}\|\nabla r^{\mathbf{a},hp}\|_{\omega_F}. \tag{3.47}$$

Using (3.46), (3.47), the shape-regularity yielding $h_F \approx h_{F'}$, $\forall F, F' \in \mathcal{F}_\ell^{\mathbf{a},\mathrm{int}}$, and the Cauchy–Schwarz inequality, we get

$$\begin{aligned}\sum_{F\in\mathcal{F}_\ell^{\mathbf{a},\mathrm{int}}}\|\psi_\ell^{\mathbf{a}}[\![\nabla u_\ell^{\mathrm{ex}}\cdot\mathbf{n}_F]\!]\|_F\|\lambda_\ell^F\|_F &\lesssim \sum_{F\in\mathcal{F}_\ell^{\mathbf{a},\mathrm{int}}}\|\psi_\ell^{\mathbf{a}}[\![\nabla u_\ell^{\mathrm{ex}}\cdot\mathbf{n}_F]\!]\|_F\, h_F^{\frac{1}{2}}\|\psi_\ell^{\mathbf{a}}\nabla u_\ell^{\mathrm{ex}} + \boldsymbol{\sigma}_\ell^{\mathbf{a}}\|_{\omega_\ell^{\mathbf{a}}} \\ &\lesssim \|\nabla r^{\mathbf{a},hp}\|_{\omega_\ell^{\mathbf{a}}}\|\psi_\ell^{\mathbf{a}}\nabla u_\ell^{\mathrm{ex}} + \boldsymbol{\sigma}_\ell^{\mathbf{a}}\|_{\omega_\ell^{\mathbf{a}}}.\end{aligned} \tag{3.48}$$

Finally, combining the bounds (3.40) and (3.48) with (3.37) proves the estimate (3.18). □

3.5 The proof of convergence with an exact solver

Our first main result is:

Theorem 3.5.1 (Guaranteed contractive bound on the energy error reduction factor)**.** *Let the pair* $(\mathcal{T}_{\ell+1}, \mathbf{p}_{\ell+1})$ *be obtained by the module* `REFINE` *of Section 3.3.3, and let* $V_{\ell+1} = \mathbb{P}_{\mathbf{p}_{\ell+1}}(\mathcal{T}_{\ell+1}) \cap H^1_0(\Omega)$ *be the finite element space to be used on iteration* $(\ell+1)$ *of the adaptive algorithm prescribed by Scheme 3.1. Let also* $\underline{\eta}_{\mathcal{M}^\sharp_\ell}$ *be the computable discrete lower bound defined by (3.16). Then, two options arise. Either* $\eta(u^{\mathrm{ex}}_\ell, \mathcal{M}^\theta_\ell) = 0$*, in which case* $u_\ell = u$*, and the adaptive loop terminates. Or the new numerical solution* $u^{\mathrm{ex}}_{\ell+1} \in V_{\ell+1}$ *satisfies*

$$\|\nabla(u - u^{\mathrm{ex}}_{\ell+1})\| \leq C_{\ell,\mathrm{red}} \|\nabla(u - u^{\mathrm{ex}}_\ell)\| \tag{3.49}$$

with

$$0 \leq C_{\ell,\mathrm{red}} := \sqrt{1 - \theta^2 \frac{\underline{\eta}^2_{\mathcal{M}^\sharp_\ell}}{\eta^2(u^{\mathrm{ex}}_\ell, \mathcal{M}^\theta_\ell)}} \leq C_{\theta,d,\kappa_{\mathcal{T}},p_{\max}} < 1, \tag{3.50}$$

where $C_{\ell,\mathrm{red}}$ *is a fully computable bound on the error reduction factor and* $C_{\theta,d,\kappa_{\mathcal{T}},p_{\max}}$ *is a generic constant only depending on the marking parameter* θ*, the space dimension* d*, the mesh shape-regularity* $\kappa_{\mathcal{T}}$*, and the maximal polynomial degree* $p_{\max}$*.*

Proof. Let us assume that $\eta(u^{\mathrm{ex}}_\ell, \mathcal{M}^\theta_\ell) \neq 0$, the other case being trivial. The proof proceeds in two steps. In the first step, we follow the proof of (Daniel et al., 2018a, Theorem 5.2), see also proofs of (Morin et al., 2002, Theorem 3.1), (Stevenson, 2007, Theorem 5.3), hinging on the Pythagorean relation

$$\|\nabla(u - u^{\mathrm{ex}}_{\ell+1})\|^2 = \|\nabla(u - u^{\mathrm{ex}}_\ell)\|^2 - \|\nabla(u^{\mathrm{ex}}_{\ell+1} - u^{\mathrm{ex}}_\ell)\|^2. \tag{3.51}$$

By the computable lower bound on the incremental error (3.16) and the marking criterion (3.10), we have

$$\begin{aligned}\|\nabla(u^{\mathrm{ex}}_{\ell+1} - u^{\mathrm{ex}}_\ell)\| &\geq \|\nabla(u^{\mathrm{ex}}_{\ell+1} - u^{\mathrm{ex}}_\ell)\|_{\omega^\sharp_\ell} \geq \underline{\eta}_{\mathcal{M}^\sharp_\ell} \\ &= \frac{\underline{\eta}_{\mathcal{M}^\sharp_\ell}}{\eta(u^{\mathrm{ex}}_\ell, \mathcal{M}^\theta_\ell)} \eta(u^{\mathrm{ex}}_\ell, \mathcal{M}^\theta_\ell) \geq \theta \frac{\underline{\eta}_{\mathcal{M}^\sharp_\ell}}{\eta(u^{\mathrm{ex}}_\ell, \mathcal{M}^\theta_\ell)} \eta(u^{\mathrm{ex}}_\ell, \mathcal{T}_\ell).\end{aligned} \tag{3.52}$$

Hence, combining (3.51) with (3.52) and using the error estimate (3.9), we infer

$$\|\nabla(u - u^{\mathrm{ex}}_{\ell+1})\|^2 \leq \underbrace{\left(1 - \theta^2 \frac{\underline{\eta}^2_{\mathcal{M}^\sharp_\ell}}{\eta^2(u^{\mathrm{ex}}_\ell, \mathcal{M}^\theta_\ell)}\right)}_{=C^2_{\ell,\mathrm{red}}} \|\nabla(u - u^{\mathrm{ex}}_\ell)\|^2. \tag{3.53}$$

In the second step, we show that the reduction factor $C_{\ell,\mathrm{red}}$ defined in (3.50) is indeed bounded by a strictly positive constant $C_{\theta,d,\kappa_{\mathcal{T}},p_{\max}} < 1$. First, we

verify that $C^2_{\ell,\mathrm{red}}$ from (3.50) is strictly lower than one, i.e.

$$1 - \theta^2 \frac{\underline{\eta}^2_{\mathcal{M}^\sharp_\ell}}{\eta^2(u^{\mathrm{ex}}_\ell, \mathcal{M}^\theta_\ell)} < 1. \tag{3.54}$$

As $\theta \in (0,1]$, (3.54) is equivalent to showing that $\frac{\underline{\eta}^2_{\mathcal{M}^\sharp_\ell}}{\eta^2(u^{\mathrm{ex}}_\ell, \mathcal{M}^\theta_\ell)} > 0$. In order to verify this, we show that $\frac{\underline{\eta}^2_{\mathcal{M}^\sharp_\ell}}{\eta^2(u^{\mathrm{ex}}_\ell, \mathcal{M}^\theta_\ell)} \geq \frac{1}{C^2}$, with a constant C strictly greater than 1, i.e. $\eta^2(u^{\mathrm{ex}}_\ell, \mathcal{M}^\theta_\ell) \leq C^2 \underline{\eta}^2_{\mathcal{M}^\sharp_\ell}$. For this, we decompose the error estimate $\eta^2(u^{\mathrm{ex}}_\ell, \mathcal{M}^\theta_\ell)$, using the partition of unity $\sum_{\mathbf{a}\in\mathcal{V}_K} \psi^{\mathbf{a}}_\ell|_K = 1$, the Cauchy–Schwarz inequality, and the fact that each simplex has $(d+1)$ vertices

$$\begin{aligned}
\eta^2(u^{\mathrm{ex}}_\ell, \mathcal{M}^\theta_\ell) &= \sum_{K\in\mathcal{M}^\theta_\ell} \|\nabla u^{\mathrm{ex}}_\ell + \boldsymbol{\sigma}_\ell\|^2_K \\
&= \sum_{K\in\mathcal{M}^\theta_\ell} \Big\| \sum_{\mathbf{a}\in\mathcal{V}_{\ell,K}} (\psi^{\mathbf{a}}_\ell \nabla u^{\mathrm{ex}}_\ell + \boldsymbol{\sigma}^{\mathbf{a}}_\ell) \Big\|^2_K \\
&\leq \sum_{K\in\mathcal{M}^\theta_\ell} (d+1) \sum_{\mathbf{a}\in\mathcal{V}_{\ell,K}} \|\psi^{\mathbf{a}}_\ell \nabla u^{\mathrm{ex}}_\ell + \boldsymbol{\sigma}^{\mathbf{a}}_\ell\|^2_K \\
&= (d+1) \sum_{\mathbf{a}\in\widetilde{\mathcal{V}}^\sharp_\ell} \|\psi^{\mathbf{a}}_\ell \nabla u^{\mathrm{ex}}_\ell + \boldsymbol{\sigma}^{\mathbf{a}}_\ell\|^2_{\omega^{\mathbf{a}}_\ell \cap \omega_\ell} \\
&\leq (d+1) \sum_{\mathbf{a}\in\widetilde{\mathcal{V}}^\sharp_\ell} \|\psi^{\mathbf{a}}_\ell \nabla u^{\mathrm{ex}}_\ell + \boldsymbol{\sigma}^{\mathbf{a}}_\ell\|^2_{\omega^{\mathbf{a}}_\ell}.
\end{aligned} \tag{3.55}$$

We note that in (3.55), we have crucially employed the extended set of marked vertices $\widetilde{\mathcal{V}}^\sharp_\ell$ of Section 3.3.2. Next, Proposition 3.4.1 applied on each patchwise contribution $\|\psi^{\mathbf{a}}_\ell \nabla u^{\mathrm{ex}}_\ell + \boldsymbol{\sigma}^{\mathbf{a}}_\ell\|_{\omega^{\mathbf{a}}_\ell}$ of the sum in (3.55) and the localization (3.17) of $\underline{\eta}_{\mathcal{M}^\sharp_\ell}$ given by (3.16) yield

$$\eta^2(u^{\mathrm{ex}}_\ell, \mathcal{M}^\theta_\ell) \leq C^2_{d,\kappa_{\mathcal{T}},p_{\max}} \underline{\eta}^2_{\mathcal{M}^\sharp_\ell} \tag{3.56}$$

with a constant $C_{d,\kappa_{\mathcal{T}},p_{\max}} > 1$, depending only on the space dimension d, the mesh shape-regularity $\kappa_{\mathcal{T}}$, and the maximal polynomial degree $p_{\max}$. Finally, employing (3.56) to bound $C_{\ell,\mathrm{red}}$ in (3.53) from above and defining the constant $C_{\theta,d,\kappa_{\mathcal{T}},p_{\max}}$ as

$$C_{\theta,d,\kappa_{\mathcal{T}},p_{\max}} := \sqrt{1 - \frac{\theta^2}{C^2_{d,\kappa_{\mathcal{T}},p_{\max}}}} < 1$$

finishes the proof. □

Assuming all the algebraic computations being performed in exact arithmetics, Theorem 3.5.1 in particular implies:

Corollary 3.5.2 (Convergence of the adaptive algorithm)**.** *Let the Assumptions of Theorem 3.5.1 be satisfied. Then*

$$\lim_{\ell\to\infty} \|\nabla(u - u_\ell^{\mathrm{ex}})\| = 0.$$

Remark 3.5.3 (Comparison with previous works)**.** *In contrast to the other results, see e.g. the reduction properties in* Morin et al. (2002), Stevenson (2007), Cascón and Nochetto (2012), Carstensen et al. (2014), Canuto et al. (2017a,b)*, the reduction factor* $C_{\ell,\mathrm{red}}$ *of* (3.49) *remains fully computable as in* Daniel et al. (2018a)*. Notably, in* Canuto et al. (2017b)*, the authors have showed a reduction property which is actually p-robust, i.e. with a constant independent of the polynomial degrees* $\mathbf{p}_\ell$*, under additional assumption of a local saturation property on each marked patch. This property has been, so far, only observed numerically. It requests p-refinement of form* $p_{\ell+1,K} = p_{\ell,K} + \lceil \lambda p_{\ell,K} \rceil$*, and not the increment of the local polynomial degree by a constant factor which we employ in this work. We note that the present reduction factor* $C_{\ell,\mathrm{red}}$ *of Theorem 3.5.1 has the same structure as the one of* (Daniel et al., 2018a, Theorem 5.2)*.*

3.6 The inexact *hp*-adaptive algorithm

We now briefly review the building blocks of an inexact *hp*-adaptive algorithm of Scheme 3.2 by summing up the necessary ingredients and notation of modules `ONE_SOLVER_STEP` and `ESTIMATE` from (Daniel et al., 2018b, Sections 4.1 and 4.2). A new version of the adaptive stopping criterion controlling the adaptive sub-loop in Scheme 3.2 is defined in Section 3.6.2. In the present inexact setting, we crucially employ slightly modified modules `MARK` and `REFINE`, described in Section 3.6.3, and formulate in Section 3.6.5 the necessary conditions on the parameter of the adaptive stopping criterion ensuring convergence of the adaptive algorithm also in this case.

3.6.1 Adaptive sub-loop of `ONE_SOLVER_STEP` and `ESTIMATE`

Let $\ell \geq 1$ be the current iteration number; we do not consider here the initial state with $\ell = 0$ (cf. (Daniel et al., 2018b, Section 4.1)) when simply the exact algebraic solver and *hp*-refinement criteria from Section 3.3 are used. We employ the module `ONE_SOLVER_STEP` exactly as in Daniel et al. (2018b) with its output being an inexact approximation $u_\ell := \sum_{n=1}^{N_\ell} (\mathrm{U}_\ell)_n \psi_\ell^n \in V_\ell$ of the Galerkin approximation u_ℓ^{ex} given by (3.5). The vector $\mathrm{U}_\ell \in \mathbb{R}^{N_\ell}$ denotes the current approximation to the exact solution $\mathrm{U}_\ell^{\mathrm{ex}}$ of the system (3.6). We recall that the algebraic residual vector R_ℓ associated with U_ℓ is given by

$$\mathrm{R}_\ell := \mathrm{F}_\ell - \mathbb{A}_\ell \mathrm{U}_\ell. \tag{3.57}$$

Moreover, we employ its functional representation $\mathfrak{r}_\ell \in \mathbb{P}_{\mathbf{p}_\ell}(\mathcal{T}_\ell)$, $\mathfrak{r}_\ell|_{\partial\Omega} = 0$, satisfying

$$(\mathfrak{r}_\ell, \psi_\ell^n) = (\mathrm{R}_\ell)_n \qquad 1 \leq n \leq N_\ell. \tag{3.58}$$

For details regarding the construction of such $\mathfrak{r}_\ell$, we refer to (Papež et al., 2018, Section 5.1). Note that the property (3.58) together with the algebraic system (3.6) yield the functional equivalent of the algebraic relation (3.57)

$$(\mathfrak{r}_\ell, v_\ell) = (f, v_\ell) - (\nabla u_\ell, \nabla v_\ell) \qquad v_\ell \in V_\ell. \tag{3.59}$$

The quality of the current approximate solution u_ℓ obtained by `ONE_SOLVER_STEP` is subsequently assessed within the `ESTIMATE` module identical to the one from (Daniel et al., 2018b, Section 4.2) based on equilibrated flux reconstructions by local problems on patches. The module `ESTIMATE` in the inexact setting outputs a collection of local error indicators $\{\eta_{\mathrm{alg},K}(u_\ell), \eta_{\mathrm{dis},K}(u_\ell)\}_{K\in\mathcal{T}_\ell}$ together with the total error lower bound $\mu(u_\ell)$. Let us recall the definition of the discretization flux reconstruction:

Definition 3.6.1 (Discretization flux reconstruction $\boldsymbol{\sigma}_{\ell,\mathrm{dis}}$ by local minimization)**.** *Let u_ℓ be the current inexact approximation obtained by the module* `ONE_SOLVER_STEP`*. For each $\mathbf{a} \in \mathcal{V}_\ell$, let the local discretization flux reconstruction $\boldsymbol{\sigma}^{\mathbf{a}}_{\ell,\mathrm{dis}} \in \mathbf{V}^{\mathbf{a}}_\ell$ be given by the following local minimization problem*

$$\boldsymbol{\sigma}^{\mathbf{a}}_{\ell,\mathrm{dis}} := \operatorname*{arg\,min}_{\substack{\mathbf{v}_\ell \in \mathbf{V}^{\mathbf{a}}_\ell,\\ \nabla\cdot\mathbf{v}_\ell = \psi^{\mathbf{a}}_\ell f - \nabla\psi^{\mathbf{a}}_\ell\cdot\nabla u_\ell - \psi^{\mathbf{a}}_\ell \mathfrak{r}_\ell}} \|\psi^{\mathbf{a}}_\ell \nabla u_\ell + \mathbf{v}_\ell\|_{\omega^{\mathbf{a}}_\ell}. \tag{3.60}$$

Then, the discretization flux reconstruction is defined as $\boldsymbol{\sigma}_{\ell,\mathrm{dis}} := \sum_{\mathbf{a}\in\mathcal{V}_\ell} \boldsymbol{\sigma}^{\mathbf{a}}_{\ell,\mathrm{dis}}$, with each local contribution $\boldsymbol{\sigma}^{\mathbf{a}}_{\ell,\mathrm{dis}}$ being extended by zero outside of $\omega^{\mathbf{a}}_\ell$.

Note that the Neumann compatibility condition for the problem (3.60) is a direct consequence of (3.59). Moreover, using the multilevel construction described in (Papež et al., 2017, Section 6) and (Daniel et al., 2018b, Section 4.2), we build the algebraic error flux reconstruction $\boldsymbol{\sigma}_{\ell,\mathrm{alg}} \in \mathbf{H}(\mathrm{div}, \Omega)$ such that

$$(\nabla\cdot\boldsymbol{\sigma}_{\ell,\mathrm{alg}}, q_\ell)_K = (\mathfrak{r}_\ell, q_\ell)_K \quad \forall K \in \mathcal{T}_\ell, \quad \forall q_\ell \in \mathbb{P}_{p_{\ell,K}}(K). \tag{3.61}$$

Then, as established in Daniel et al. (2018b), cf. also Jiránek et al. (2010), Ern and Vohralík (2013), Papež et al. (2017), the following upper bounds on the energy norm of the total and algebraic error hold true:

$$\underbrace{\|\nabla(u - u_\ell)\|}_{\text{total error}} \leq \eta(u_\ell, \mathcal{T}_\ell) := \left\{ \sum_{K\in\mathcal{T}_\ell} \eta_K^2(u_\ell) \right\}^{\frac{1}{2}},$$
$$\text{with } \eta_K(u_\ell) := \underbrace{\|\nabla u_\ell + \boldsymbol{\sigma}_{\ell,\mathrm{dis}}\|_K}_{\eta_{\mathrm{dis},K}(u_\ell)} + \underbrace{\|\boldsymbol{\sigma}_{\ell,\mathrm{alg}}\|_K}_{\eta_{\mathrm{alg},K}(u_\ell)}, \tag{3.62a}$$

$$\underbrace{\|\nabla\,(u_\ell^{\mathrm{ex}}-u_\ell)\|}_{\text{algebraic error}} \le \eta_{\mathrm{alg}}(u_\ell,\mathcal{T}_\ell) := \left\{\sum_{K\in\mathcal{T}_\ell}\eta_{\mathrm{alg},K}^2(u_\ell)\right\}^{\frac{1}{2}}. \tag{3.62b}$$

Next, for each vertex $\mathbf{a}\in\mathcal{V}_\ell$, let $V_\ell^{\mathbf{a}}$ be a suitable finite-dimensional subspace of $H^1_*(\omega_\ell^{\mathbf{a}})$

$$H^1_*(\omega_\ell^{\mathbf{a}}) := \begin{cases} \{v\in H^1(\omega_\ell^{\mathbf{a}}),(v,1)_{\omega_\ell^{\mathbf{a}}}=0\} & \text{if } \mathbf{a}\in\mathcal{V}_\ell^{\mathrm{int}},\\ \{v\in H^1(\omega_\ell^{\mathbf{a}}),v=0 \text{ on } \partial\omega_\ell^{\mathbf{a}}\cap\partial\Omega\} & \text{if } \mathbf{a}\in\mathcal{V}_\ell^{\mathrm{ext}}.\end{cases}$$

Following (Papež et al., 2018, Theorem 2), cf. also Daniel et al. (2018b), we construct the total residual lifting $\rho_{\ell,\mathrm{tot}} := \sum_{\mathbf{a}\in\mathcal{V}_\ell}\psi_\ell^{\mathbf{a}}\rho_{\ell,\mathrm{tot}}^{\mathbf{a}} \in H^1_0(\Omega)$, where each vertex contribution solves the local primal finite element problem

$$\left(\nabla\rho_{\ell,\mathrm{tot}}^{\mathbf{a}},\nabla v_\ell\right)_{\omega_\ell^{\mathbf{a}}} = (f,\psi_\ell^{\mathbf{a}}v_\ell)_{\omega_\ell^{\mathbf{a}}} - (\nabla u_\ell,\nabla(\psi_\ell^{\mathbf{a}}v_\ell))_{\omega_\ell^{\mathbf{a}}} \qquad \forall v_\ell\in V_\ell^{\mathbf{a}}.$$

Then, besides the upper bounds (3.62a) and (3.62b), the following lower bound on the total error is at our disposal, supposing $\rho_{\ell,\mathrm{tot}}\neq 0$,

$$\|\nabla\,(u-u_\ell)\| \ge \frac{\sum_{\mathbf{a}\in\mathcal{V}_\ell}\|\nabla\rho_{\ell,\mathrm{tot}}^{\mathbf{a}}\|_{\omega_\ell^{\mathbf{a}}}^2}{\|\nabla\rho_{\ell,\mathrm{tot}}\|} =: \mu(u_\ell). \tag{3.63}$$

3.6.2 Adaptive stopping criterion for the algebraic solver

The above error estimators computed within module `ESTIMATE` enable us to objectively stop the adaptive sub-loop between the modules `ONE_SOLVER_STEP` and `ESTIMATE` once the current approximation u_ℓ is such that

$$\|\nabla(u_\ell^{\mathrm{ex}}-u_\ell)\| \le \gamma_\ell\|\nabla(u-u_\ell^{\mathrm{ex}})\|, \tag{3.64}$$

i.e. when the algebraic error is lower than a fraction (typically $\gamma_\ell>0$ is of order 0.1) of the discretization error. Relying on the output of the module `ESTIMATE`, the requirement (3.64) is ensured due to Galerkin orthogonality of u_ℓ^{ex}

$$\|\nabla(u-u_\ell)\|^2 = \|\nabla(u-u_\ell^{\mathrm{ex}})\|^2 + \|\nabla(u_\ell^{\mathrm{ex}}-u_\ell)\|^2$$

and (3.62b), (3.63) by the following criterion

$$\eta_{\mathrm{alg}}(u_\ell,\mathcal{T}_\ell) \le \gamma_\ell \underbrace{\sqrt{\mu^2(u_\ell)-\eta_{\mathrm{alg}}^2(u_\ell,\mathcal{T}_\ell)}}_{\text{discretization error lower bound}},$$

which is equivalent to criterion

$$\eta_{\mathrm{alg}}(u_\ell,\mathcal{T}_\ell) \le \widetilde{\gamma}_\ell\,\mu(u_\ell), \tag{3.65}$$

with

$$\widetilde{\gamma}_\ell = \frac{\gamma_\ell}{(1+\gamma_\ell^2)^{\frac{1}{2}}} < 1,$$

already used in Papež et al. (2017), Daniel et al. (2018b). The choice of the parameter $\widetilde{\gamma}_\ell$ in (3.65) will follow from the theoretical analysis to be carried out in Section 3.8 below.

3.6.3 Modules MARK and REFINE

For the seek of brevity, we keep the notation introduced in Section 3.3.2 unchanged. The module MARK in the inexact setting takes as input an inexact approximation u_ℓ and the corresponding error indicators computed within module ESTIMATE. It proceeds again in two phases. However, in the marking criterion (3.10) we employ in place of the total error estimator $\eta(u_\ell, \cdot)$ only its component corresponding to the discretization error, so the modified bulk chasing criterion to select a subset of marked vertices $\widetilde{\mathcal{V}}_\ell^\theta \subset \mathcal{V}_\ell$ reads

$$\eta_{\mathrm{dis}}\Big(u_\ell, \bigcup_{\mathbf{a}\in\widetilde{\mathcal{V}}_\ell^\theta} \mathcal{T}_\ell^{\mathbf{a}}\Big) \geq \theta\, \eta_{\mathrm{dis}}(u_\ell, \mathcal{T}_\ell), \tag{3.66}$$

where $\eta_{\mathrm{dis}}(u_\ell, \mathcal{S}) := \{\sum_{K\in\mathcal{S}} \eta_{\mathrm{dis},K}(u_\ell)^2\}^{\frac{1}{2}}$, for any subset $\mathcal{S} \subset \mathcal{T}_\ell$, and $\theta \in (0,1]$ a fixed threshold parameter. The rest of the module follows straightforwardly the steps described in Section 3.3.2 leading to the extended set of marked vertices $\widetilde{\mathcal{V}}_\ell^\sharp$. In the module REFINE , the new pair $(\mathcal{T}_{\ell+1}, \mathbf{p}_{\ell+1})$ is determined on the basis of the two local problems (3.13), but with an approximate solution u_ℓ in place of the exact Galerkin approximation u_ℓ^{ex} that is not at our disposal here.

3.6.4 Discrete lower bound on the incremental error on marked simplices

Proceeding as in the exact setting, for each vertex from the extended set of marked vertices $\widetilde{\mathcal{V}}_\ell^\sharp$, let the residual lifting $r^{\mathbf{a},hp} \in V_\ell^{\mathbf{a},hp}$ be defined as the solution of the local problem (3.15), but with u_ℓ^{ex} replaced by the inexact approximation u_ℓ:

$$(\nabla r^{\mathbf{a},hp}, \nabla v^{\mathbf{a},hp})_{\omega_\ell^{\mathbf{a}}} = (f, v^{\mathbf{a},hp})_{\omega_\ell^{\mathbf{a}}} - (\nabla u_\ell, \nabla v^{\mathbf{a},hp})_{\omega_\ell^{\mathbf{a}}} \qquad \forall\, v^{\mathbf{a},hp} \in V_\ell^{\mathbf{a},hp}, \tag{3.67}$$

with the local space $V_\ell^{\mathbf{a},hp}$ given by (3.14). Extending the residual liftings $r^{\mathbf{a},hp}$ by zero outside $\omega_\ell^{\mathbf{a}}$, let $u_{\ell+1}^{\mathrm{ex}} \in V_{\ell+1}$ be the (unavailable) exact Galerkin approximation on the next level. By (Daniel et al., 2018b, Lemma 5.1) used

with the extended set $\widetilde{\mathcal{V}}_\ell^\sharp$ in place of $\widetilde{\mathcal{V}}_\ell^\theta$, the following lower bound holds true

$$\|\nabla(u_{\ell+1}^{\mathrm{ex}} - u_\ell)\|_{\omega_\ell^\sharp} \geq \underline{\eta}^*_{\mathcal{M}_\ell^\sharp}, \quad \underline{\eta}^*_{\mathcal{M}_\ell^\sharp} := \begin{cases} \dfrac{\sum_{\mathbf{a}\in\widetilde{\mathcal{V}}_\ell^\sharp} \left\|\nabla r^{\mathbf{a},hp}\right\|^2_{\omega_\ell^{\mathbf{a}}}}{\left\|\nabla\left(\sum_{\mathbf{a}\in\widetilde{\mathcal{V}}_\ell^\sharp} r^{\mathbf{a},hp}\right)\right\|_{\omega_\ell^\sharp}} & \text{if } \sum_{\mathbf{a}\in\widetilde{\mathcal{V}}_\ell^\sharp} r^{\mathbf{a},hp} \neq 0, \\ 0 & \text{otherwise.} \end{cases} \tag{3.68}$$

We note that the localization in the spirit of (3.17) is again possible here.

3.6.5 Conditions on the adaptive stopping criterion parameter $\widetilde{\gamma}_\ell$

We now specify the required conditions on the parameter $\widetilde{\gamma}_\ell$ in the adaptive stopping criterion (3.65) that will ensure error reduction on each adaptive loop step and convergence of the inexact hp-adaptive algorithm of Scheme 3.2.

Let the iteration counter $\ell \geq 1$ be given. First, it turns out to be necessary to emulate the hp-refinement decision for the current inexact approximation u_ℓ. More precisely, after computing the error estimators associated with the current approximation u_ℓ within the `ESTIMATE` module, we actually perform a supplementary call of the modules `MARK` and `REFINE`, defined in Section 3.6.3, in order to obtain the auxiliary set of marked vertices and the auxiliary refinement suggestions. Thus, the corresponding auxiliary local patchwise spaces $V_\ell^{\mathbf{a},hp}$ given by (3.14) can be constructed. Furthermore, for each vertex $\mathbf{a}$ from the auxiliary set of marked vertices, we construct the residual lifting $r^{\mathbf{a},hp} \in V_\ell^{\mathbf{a},hp}$ by solving the local problem (3.67) and we define the following fully computable constants

$$C_{\mathrm{st}}^{\mathbf{a}} := \frac{\|\psi_\ell^{\mathbf{a}}\nabla u_\ell + \boldsymbol{\sigma}^{\mathbf{a}}_{\ell,\mathrm{dis}}\|_{\omega_\ell^{\mathbf{a}}}}{\|\nabla r^{\mathbf{a},hp}\|_{\omega_\ell^{\mathbf{a}}} + \|\boldsymbol{\sigma}_{\ell,\mathrm{alg}}\|_{\omega_\ell^{\mathbf{a}}}} \quad \forall \mathbf{a} \in \widetilde{\mathcal{V}}_\ell^\sharp, \quad \text{and} \quad C_{\mathrm{st}} := \max_{\mathbf{a}\in\widetilde{\mathcal{V}}_\ell^\sharp} C_{\mathrm{st}}^{\mathbf{a}}. \tag{3.69}$$

We will prove below in Section 3.7 that these constants are uniformly bounded. We note that computationally, their value is typically in the range 1–10. We require that the parameter $\widetilde{\gamma}_\ell$ in the adaptive stopping criterion (3.65), used to evaluate the current approximation u_ℓ, is such that

$$0 < \widetilde{\gamma}_\ell < \frac{\theta}{\sqrt{2}(d+1)C_{\mathrm{st}} + \theta} \qquad \text{for } \ell = 1 \tag{3.70a}$$

$$0 < \widetilde{\gamma}_\ell < \min\left(\frac{\theta}{\sqrt{2}(d+1)C_{\mathrm{st}} + \theta}, (1 - C^*_{\ell-1,\mathrm{red}})\right) \qquad \text{for } \ell \geq 2, \tag{3.70b}$$

where C_{st} is given by (3.69) and $C^*_{\ell-1,\mathrm{red}}$ is the bound on the auxiliary error reduction between the inexact approximation $u_{\ell-1}$ and the exact (unavailable) approximation u_ℓ^{ex}, defined by (3.81) in Lemma 3.8.1 below. We note that the number $C^*_{\ell-1,\mathrm{red}}$ is computable and at our disposal at the end of the $(\ell-1)$-th iteration of the adaptive loop. We remark also that conditions (3.70) allow us

to use the reasonable choice of $\widetilde{\gamma}_\ell \approx 0.1$ in most cases, in contrast to (to our knowledge) all results available in the literature so far. Moreover,

$$\widetilde{\gamma}_\ell < 1. \tag{3.71}$$

3.7 Discrete stability of equilibrated fluxes in an inexact setting

In this section, we extend the result of Section 3.4 to the inexact setting. Recall that $x_1 \lesssim x_2$ means that there exists a generic positive constant C that only depends on the space dimension d, the shape-regularity $\kappa_{\mathcal{T}}$ of the underlying mesh, and the polynomial degree of approximation employed locally such that $x_1 \leq C x_2$. In particular, we show the following counterpart of Proposition 3.4.1:

Proposition 3.7.1 (Discrete stability of the local flux equilibration in the inexact setting)**.** *Let the approximate solution u_ℓ satisfy*

$$(f, \psi_\ell^{\mathbf{a}})_{\omega_\ell^{\mathbf{a}}} - (\nabla u_\ell, \nabla \psi_\ell^{\mathbf{a}})_{\omega_\ell^{\mathbf{a}}} - (\mathfrak{r}_\ell, \psi_\ell^{\mathbf{a}})_{\omega_\ell^{\mathbf{a}}} = 0 \qquad \forall \mathbf{a} \in \mathcal{V}_\ell^{\mathrm{int}}.$$

Let the local discretization flux reconstruction $\boldsymbol{\sigma}_{\ell,\mathrm{dis}}^{\mathbf{a}}$ be constructed by (3.60), let the algebraic error flux reconstruction $\boldsymbol{\sigma}_{\ell,\mathrm{alg}} \in \mathbf{H}(\mathrm{div}, \Omega)$ satisfy (3.61), and let $r^{\mathbf{a},hp}$ be given by (3.67). Then there holds

$$\|\psi_\ell^{\mathbf{a}} \nabla u_\ell + \boldsymbol{\sigma}_{\ell,\mathrm{dis}}^{\mathbf{a}}\|_{\omega_\ell^{\mathbf{a}}} \lesssim \|\nabla r^{\mathbf{a},hp}\|_{\omega_\ell^{\mathbf{a}}} + \|\boldsymbol{\sigma}_{\ell,\mathrm{alg}}\|_{\omega_\ell^{\mathbf{a}}} \quad \forall \mathbf{a} \in \widetilde{\mathcal{V}}_\ell^\sharp.$$

Thus, the constants $C_{\mathrm{st}}^{\mathbf{a}}$ and C_{st} from (3.69) are uniformly bounded.

Proof. We follow the proof of Proposition 3.4.1 and the proof of (Papež et al., 2017, Theorem 5.6). For a fixed vertex $\mathbf{a} \in \widetilde{\mathcal{V}}_\ell^\sharp$, let us recall from the proof of Proposition 3.4.1 the two reformulations of the local minimization problem (3.60). First, it reads reads: find the pair $(\boldsymbol{\sigma}_{\ell,\mathrm{dis}}^{\mathbf{a}}, \gamma_\ell^{\mathbf{a}}) \in \mathbf{V}_\ell^{\mathbf{a}} \times Q_\ell^{\mathbf{a}}$ such that

$$\left(\boldsymbol{\sigma}_{\ell,\mathrm{dis}}^{\mathbf{a}}, \mathbf{v}_\ell\right)_{\omega_\ell^{\mathbf{a}}} - (\gamma_\ell^{\mathbf{a}}, \nabla \cdot \mathbf{v}_\ell)_{\omega_\ell^{\mathbf{a}}} = -(\psi_\ell^{\mathbf{a}} \nabla u_\ell, \mathbf{v}_\ell)_{\omega_\ell^{\mathbf{a}}} \qquad \forall \mathbf{v}_\ell \in \mathbf{V}_\ell^{\mathbf{a}}, \tag{3.72a}$$

$$\left(\nabla \cdot \boldsymbol{\sigma}_{\ell,\mathrm{dis}}^{\mathbf{a}}, q_\ell\right)_{\omega_\ell^{\mathbf{a}}} = (\psi_\ell^{\mathbf{a}} f - \nabla u_\ell \cdot \nabla \psi_\ell^{\mathbf{a}} - \psi_\ell^{\mathbf{a}} \mathfrak{r}_\ell, q_\ell)_{\omega_\ell^{\mathbf{a}}} \quad \forall q_\ell \in Q_\ell^{\mathbf{a}}, \tag{3.72b}$$

with the test and trial spaces $\mathbf{V}_\ell^{\mathbf{a}}$, $Q_\ell^{\mathbf{a}}$ defined by (3.7) and (3.34), respectively. On the other hand, the hybridized formulation reads: find $\boldsymbol{\sigma}_{\ell,\mathrm{dis}}^{\mathbf{a}}$ in the broken space $\mathbf{RTN}_{p_{\mathbf{a}}^{\mathrm{est}}}(\mathcal{T}_\ell^{\mathbf{a}})$, $\gamma_\ell^{\mathbf{a}} \in Q_\ell^{\mathbf{a}}$, and $\lambda_\ell^F \in \mathbb{P}_{p_{\mathbf{a}}^{\mathrm{est}}}(F)$, for all $F \in \mathcal{F}_\ell^{\mathbf{a}} \setminus \mathcal{F}_\ell^{\mathbf{a},\partial\Omega}$, such that

$$\sum_{K\in\mathcal{T}_\ell^{\mathbf{a}}}\left(\psi_\ell^{\mathbf{a}}\nabla u_\ell+\boldsymbol{\sigma}_{\ell,\mathrm{dis}}^{\mathbf{a}},\,\mathbf{v}_\ell\right)_K-\sum_{K\in\mathcal{T}_\ell^{\mathbf{a}}}(\nabla\cdot\mathbf{v}_\ell,\,\gamma_\ell^{\mathbf{a}})_K+\sum_{K\in\mathcal{T}_\ell^{\mathbf{a}}}\sum_{F\in\mathcal{F}_{\ell,K}\setminus\mathcal{F}_\ell^{\mathbf{a},\partial\Omega}}\left(\mathbf{v}_\ell\cdot\mathbf{n}_K,\,\lambda_\ell^F\right)_F=0\qquad\forall\mathbf{v}_\ell\in\mathbf{RTN}_{p_{\mathbf{a}}^{\mathrm{est}}}(\mathcal{T}_\ell^{\mathbf{a}}),\tag{3.73a}$$

$$\sum_{K\in\mathcal{T}_\ell^{\mathbf{a}}}\left(\nabla\cdot\boldsymbol{\sigma}_{\ell,\mathrm{dis}}^{\mathbf{a}},\,q_\ell\right)_K=\sum_{K\in\mathcal{T}_\ell^{\mathbf{a}}}(\psi_\ell^{\mathbf{a}}f-\nabla\psi_\ell^{\mathbf{a}}\cdot\nabla u_\ell-\psi_\ell^{\mathbf{a}}\mathfrak{r}_\ell,\,q_\ell)_K\quad\forall q_\ell\in Q_\ell^{\mathbf{a}},\tag{3.73b}$$

$$-\sum_{K\in\mathcal{T}_F}\left(\boldsymbol{\sigma}_{\ell,\mathrm{dis}}^{\mathbf{a}}\cdot\mathbf{n}_K,\,\xi_\ell\right)_F=0\qquad\forall\xi_\ell\in\mathbb{P}_{p_{\mathbf{a}}^{\mathrm{est}}}(F),\forall F\in\mathcal{F}_\ell^{\mathbf{a}}\setminus\mathcal{F}_\ell^{\mathbf{a},\partial\Omega},\tag{3.73c}$$

with $\mathcal{F}_\ell^{\mathbf{a},\partial\Omega}$ given by (3.36). In this hybridized formulation, we are allowed to employ $\psi_\ell^{\mathbf{a}}\nabla u_\ell+\boldsymbol{\sigma}_{\ell,\mathrm{dis}}^{\mathbf{a}}\in\mathbf{RTN}_{p_{\mathbf{a}}^{\mathrm{est}}}(\mathcal{T}_\ell^{\mathbf{a}})$ as a test function $\mathbf{v}_\ell$ in (3.73a). Furthermore, employing $\gamma_\ell^{\mathbf{a}}$ as q_ℓ in (3.73b), λ_ℓ^F as ξ_ℓ in (3.73c), followed by summing (3.73a)–(3.73c), analogously to (3.37), we obtain

$$\|\psi_\ell^{\mathbf{a}}\nabla u_\ell+\boldsymbol{\sigma}_{\ell,\mathrm{dis}}^{\mathbf{a}}\|_{\omega_\ell^{\mathbf{a}}}^2\le\sum_{K\in\mathcal{T}_\ell^{\mathbf{a}}}\|\psi_\ell^{\mathbf{a}}(f+\Delta u_\ell+\mathfrak{r}_\ell)\|_K\|\gamma_\ell^{\mathbf{a}}\|_K+\sum_{F\in\mathcal{F}_\ell^{\mathbf{a},\mathrm{int}}}\|\psi_\ell^{\mathbf{a}}[\![\nabla u_\ell\cdot\mathbf{n}_F]\!]\|_F\|\lambda_\ell^F\|_F.\tag{3.74}$$

We have also used the fact that the hat function $\psi_\ell^{\mathbf{a}}|_F=0\ \forall F\in\mathcal{F}_\ell^{\mathbf{a},\mathrm{ext}}$ for vertices $\mathbf{a}\in\mathcal{V}_\ell^{\mathrm{int}}$, whereas the boundary faces are excluded from the sum and $\psi_\ell^{\mathbf{a}}|_F=0\ \forall F\in\mathcal{F}_\ell^{\mathbf{a},\mathrm{ext}}\setminus\mathcal{F}_\ell^{\mathbf{a},\partial\Omega}$ for $\mathbf{a}\in\mathcal{V}_\ell^{\mathrm{ext}}$.

We proceed by treating the first term of (3.74). First, to bound $\|\psi_\ell^{\mathbf{a}}(f+\Delta u_\ell+\mathfrak{r}_\ell)\|_K$ from above, we employ the triangle inequality

$$\|\psi_\ell^{\mathbf{a}}(f+\Delta u_\ell+\mathfrak{r}_\ell)\|_K\le\|\psi_\ell^{\mathbf{a}}\|_{\infty,K}\,\|f+\Delta u_\ell-\mathfrak{r}_\ell\|_K\le\|f+\Delta u_\ell\|_K+\|\mathfrak{r}_\ell\|_K\quad\forall K\in\mathcal{T}_\ell^{\mathbf{a},h}.\tag{3.75}$$

We note that the arguments used in proof of Lemma 3.4.2 stay valid also in the inexact setting with only approximate solution u_ℓ and $r^{\mathbf{a},hp}$ now solving (3.67) instead of (3.15). Hence, the element residual $\|f+\Delta u_\ell\|_K$ in (3.75) satisfies the property analogous to (3.19) from Lemma 3.4.2,

$$h_K\|f+\Delta u_\ell\|_K\lesssim\|\nabla r^{\mathbf{a},hp}\|_K.\tag{3.76}$$

To treat $\|\mathfrak{r}_\ell\|_K$, we use the property (3.61) of the algebraic error flux reconstruction $\boldsymbol{\sigma}_{\ell,\mathrm{alg}}$ and an inverse inequality. We thus obtain

$$\|\mathfrak{r}_\ell\|_K=\|\nabla\cdot\boldsymbol{\sigma}_{\ell,\mathrm{alg}}\|_K\lesssim h_K^{-1}\|\boldsymbol{\sigma}_{\ell,\mathrm{alg}}\|_K.\tag{3.77}$$

The inf-sup stability of discretization (3.72), similarly to (3.38), yields

$$\|\gamma_\ell^{\mathbf{a}}\|_{\omega_\ell^{\mathbf{a}}}\lesssim h_{\omega_\ell^{\mathbf{a}}}\|\psi_\ell^{\mathbf{a}}\nabla u_\ell+\boldsymbol{\sigma}_{\ell,\mathrm{dis}}^{\mathbf{a}}\|_{\omega_\ell^{\mathbf{a}}}.\tag{3.78}$$

Combining (3.75) with (3.76) and (3.77), using the Cauchy–Schwarz inequality, the shape-regularity yielding $h_K \approx h_{\omega_\ell^{\mathbf{a}}}$, and estimate (3.78), we arrive at

$$\begin{aligned}\sum_{K\in\mathcal{T}_\ell^{\mathbf{a}}} \|\psi_\ell^{\mathbf{a}}(f+\Delta u_\ell+\mathfrak{r}_\ell)\|_K\|\gamma_\ell^{\mathbf{a}}\|_K &\lesssim \sum_{K\in\mathcal{T}_\ell^{\mathbf{a}}} h_K^{-1}(\|\nabla r^{\mathbf{a},hp}\|_K+\|\boldsymbol{\sigma}_{\ell,\mathrm{alg}}\|_K)\|\gamma_\ell^{\mathbf{a}}\|_K\\ &\lesssim h_{\omega_\ell^{\mathbf{a}}}^{-1}(\|\nabla r^{\mathbf{a},hp}\|_{\omega_\ell^{\mathbf{a}}}+\|\boldsymbol{\sigma}_{\ell,\mathrm{alg}}\|_{\omega_\ell^{\mathbf{a}}})\|\gamma_\ell^{\mathbf{a}}\|_{\omega_\ell^{\mathbf{a}}}\\ &\lesssim (\|\nabla r^{\mathbf{a},hp}\|_{\omega_\ell^{\mathbf{a}}}+\|\boldsymbol{\sigma}_{\ell,\mathrm{alg}}\|_{\omega_\ell^{\mathbf{a}}})\|\psi_\ell^{\mathbf{a}}\nabla u_\ell^{\mathrm{ex}}+\boldsymbol{\sigma}_\ell^{\mathbf{a}}\|.\end{aligned} \tag{3.79}$$

On the other hand, for bounding the second term of (3.74), the arguments used to obtain (3.48) in the proof of Proposition 3.4.1 remain valid also in the inexact setting, so that

$$\sum_{F\in\mathcal{F}_\ell^{\mathbf{a},\mathrm{int}}} \|\psi_\ell^{\mathbf{a}}[\![\nabla u_\ell\cdot\mathbf{n}_F]\!]\|_F\|\lambda_\ell^F\|_F \lesssim \|\nabla r^{\mathbf{a},hp}\|_{\omega_\ell^{\mathbf{a}}}\|\psi_\ell^{\mathbf{a}}\nabla u_\ell+\boldsymbol{\sigma}_{\ell,\mathrm{dis}}^{\mathbf{a}}\|_{\omega_\ell^{\mathbf{a}}}. \tag{3.80}$$

Finally, employing the bounds (3.79) and (3.80) in (3.74) finishes the proof. □

3.8 The proof of convergence with an inexact solver

We start with an intermediate result giving a guaranteed bound on the error reduction factor between the current inexact approximation u_ℓ and the (unavailable) next level exact solution $u_{\ell+1}^{\mathrm{ex}}$. Namely, the following lemma improves the result of (Daniel et al., 2018b, Lemma 5.3) in showing that the reduction factor is strictly smaller than one:

Lemma 3.8.1 (Guaranteed contractive bound on the auxiliary energy error reduction factor)**.** *Let the current inexact approximation u_ℓ be obtained by the adaptive sub-loop of Section 3.6.1 employing the stopping criterion (3.65) with the parameter $\widetilde{\gamma}_\ell$ satisfying (3.70). Let also the pair $(\mathcal{T}_{\ell+1},\mathbf{p}_{\ell+1})$ be obtained by the module* `REFINE` *of Section 3.6.3 and let $\underline{\eta}^*_{\mathcal{M}_\ell^\sharp}$ be the computable discrete lower bound defined by (3.68). Then, unless $\eta(u_\ell,\mathcal{T}_\ell)=0$, in which case $u_\ell=u$ and the adaptive loop terminates, the next (unavailable) exact finite element solution $u_{\ell+1}^{\mathrm{ex}}\in V_{\ell+1}$ satisfies*

$$\|\nabla(u-u_{\ell+1}^{\mathrm{ex}})\| \le C^*_{\ell,\mathrm{red}}\|\nabla(u-u_\ell)\| \tag{3.81}$$

with

$$0\le C^*_{\ell,\mathrm{red}} := \sqrt{1-\frac{\left(\underline{\eta}^*_{\mathcal{M}_\ell^\sharp}\right)^2+\|\boldsymbol{\sigma}_{\ell,\mathrm{alg}}\|^2}{\eta^2(u_\ell,\mathcal{T}_\ell)}+\widetilde{\gamma}_\ell^2} \le C^*_{\theta,\widetilde{\gamma}_\ell,d,\kappa_{\mathcal{T}},p_{\max}}<1, \tag{3.82}$$

where $C^*_{\ell,\mathrm{red}}$ *is a fully computable bound on the auxiliary error reduction factor and* $C^*_{\theta,\widetilde{\gamma}_\ell,d,\kappa_{\mathcal{T}},p_{\max}}$ *is a generic constant only depending on the marking parameter* θ*, the stopping criterion coefficient* $\widetilde{\gamma}_\ell$*, the space dimension* d*, the mesh shape-regularity* $\kappa_{\mathcal{T}}$*, and the maximal polynomial degree* $p_{\max}$*.*

Proof. Let us consider only the non trivial case when $\eta(u_\ell,\mathcal{T}_\ell)\neq 0$. We follow the proofs of Theorem 3.5.1 and Lemma 5.3 of Daniel et al. (2018b) and proceed in two steps. In the first step, we note that the Pythagorean relation between the current (available) inexact approximation u_ℓ and the (unavailable) next level exact finite element solution $u^{\mathrm{ex}}_{\ell+1}\in V_{\ell+1}$ holds true, we thus have

$$\|\nabla(u-u^{\mathrm{ex}}_{\ell+1})\|^2=\|\nabla(u-u_\ell)\|^2-\|\nabla(u^{\mathrm{ex}}_{\ell+1}-u_\ell)\|^2. \tag{3.83}$$

Employing the discrete lower bound (3.68) to bound the second term of on the right-hand side of (3.83), adding and subtracting $\|\boldsymbol{\sigma}_{\ell,\mathrm{alg}}\|^2$, using the adaptive stopping criterion (3.65) with parameter $\widetilde{\gamma}_\ell$ satisfying (3.70), and the total error bounds (3.63) and (3.62a), we obtain the following chain of inequalities leading to the computable bound on the auxiliary reduction factor $C^*_{\ell,\mathrm{red}}$ of (3.82):

$$\begin{aligned}
\|\nabla(u-u^{\mathrm{ex}}_{\ell+1})\|^2 &\leq \|\nabla(u-u_\ell)\|^2-\left(\underline{\eta}^*_{\mathcal{M}^\sharp_\ell}\right)^2-\|\boldsymbol{\sigma}_{\ell,\mathrm{alg}}\|^2+\|\boldsymbol{\sigma}_{\ell,\mathrm{alg}}\|^2\\
&=\|\nabla(u-u_\ell)\|^2-\frac{\left(\underline{\eta}^*_{\mathcal{M}^\sharp_\ell}\right)^2+\|\boldsymbol{\sigma}_{\ell,\mathrm{alg}}\|^2}{\eta^2(u_\ell,\mathcal{T}_\ell)}\eta^2(u_\ell,\mathcal{T}_\ell)+\|\boldsymbol{\sigma}_{\ell,\mathrm{alg}}\|^2\\
&\leq\|\nabla(u-u_\ell)\|^2-\frac{\left(\underline{\eta}^*_{\mathcal{M}^\sharp_\ell}\right)^2+\|\boldsymbol{\sigma}_{\ell,\mathrm{alg}}\|^2}{\eta^2(u_\ell,\mathcal{T}_\ell)}\eta^2(u_\ell,\mathcal{T}_\ell)+\widetilde{\gamma}^2_\ell\,\mu^2(u_\ell)\\
&\leq\underbrace{\left(1-\frac{\left(\underline{\eta}^*_{\mathcal{M}^\sharp_\ell}\right)^2+\|\boldsymbol{\sigma}_{\ell,\mathrm{alg}}\|^2}{\eta^2(u_\ell,\mathcal{T}_\ell)}+\widetilde{\gamma}^2_\ell\right)}_{=(C^*_{\ell,\mathrm{red}})^2}\|\nabla(u-u_\ell)\|^2.
\end{aligned}\tag{3.84}$$

In the second step, we show that the reduction factor $C^*_{\ell,\mathrm{red}}$ defined in (3.82) is indeed bounded by a strictly positive constant $C^*_{\theta,\widetilde{\gamma}_\ell,d,\kappa_{\mathcal{T}},p_{\max}}<1$. The bound on the total error estimate $\eta(u_\ell,\mathcal{T}_\ell)\leq\eta_{\mathrm{alg}}(u_\ell,\mathcal{T}_\ell)+\eta_{\mathrm{dis}}(u_\ell,\mathcal{T}_\ell)$, with the estimators $\eta_\bullet(u_\ell,\mathcal{S}):=\{\sum_{K\in\mathcal{S}}\eta_{\bullet,K}(u_\ell)^2\}^{\frac{1}{2}}$ defined for any subset $\mathcal{S}\subseteq\mathcal{T}_\ell$, together with the stopping criterion (3.65) and the total error lower bound (3.63) and upper bound (3.62a), yield

$$\begin{aligned}
\eta(u_\ell,\mathcal{T}_\ell)&\leq\eta_{\mathrm{alg}}(u_\ell,\mathcal{T}_\ell)+\eta_{\mathrm{dis}}(u_\ell,\mathcal{T}_\ell)\\
&\leq\widetilde{\gamma}_\ell\,\mu(u_\ell)+\eta_{\mathrm{dis}}(u_\ell,\mathcal{T}_\ell)\leq\widetilde{\gamma}_\ell\,\eta(u_\ell,\mathcal{T}_\ell)+\eta_{\mathrm{dis}}(u_\ell,\mathcal{T}_\ell).
\end{aligned}$$

Thus, since $\widetilde{\gamma}_\ell<1$ from (3.71), we can bound the total error estimate $\eta(u_\ell,\mathcal{T}_\ell)$

only by means of its component corresponding to the discretization error

$$\eta(u_\ell, \mathcal{T}_\ell) \leq \frac{\eta_{\mathrm{dis}}(u_\ell, \mathcal{T}_\ell)}{(1-\widetilde{\gamma}_\ell)}. \tag{3.85}$$

Employing (3.85) and the marking criterion (3.66) to bound $(C^*_{\ell,\mathrm{red}})^2$ leads to

$$\begin{aligned}(C^*_{\ell,\mathrm{red}})^2 &= 1 - \frac{\left(\underline{\eta}^*_{\mathcal{M}_\ell^\sharp}\right)^2 + \|\boldsymbol{\sigma}_{\ell,\mathrm{alg}}\|^2}{\eta^2(u_\ell,\mathcal{T}_\ell)} + \widetilde{\gamma}_\ell^2 \leq 1-(1-\widetilde{\gamma}_\ell)^2 \frac{\left(\underline{\eta}^*_{\mathcal{M}_\ell^\sharp}\right)^2 + \|\boldsymbol{\sigma}_{\ell,\mathrm{alg}}\|^2}{\eta^2_{\mathrm{dis}}(u_\ell,\mathcal{T}_\ell)} + \widetilde{\gamma}_\ell^2 \\ &\leq 1- (1-\widetilde{\gamma}_\ell)^2\,\theta^2\,\frac{\left(\underline{\eta}^*_{\mathcal{M}_\ell^\sharp}\right)^2 + \|\boldsymbol{\sigma}_{\ell,\mathrm{alg}}\|^2}{\eta^2_{\mathrm{dis}}(u_\ell,\mathcal{M}_\ell^\theta)} + \widetilde{\gamma}_\ell^2. \end{aligned} \tag{3.86}$$

We continue by showing that $\frac{\left(\underline{\eta}^*_{\mathcal{M}_\ell^\sharp}\right)^2 + \|\boldsymbol{\sigma}_{\ell,\mathrm{alg}}\|^2}{\eta^2_{\mathrm{dis}}(u_\ell,\mathcal{M}_\ell^\theta)} \geq \frac{1}{C^2}$, with a constant C strictly greater than 1. For this, we proceed similarly as in the exact setting while relying on Proposition 3.7.1. By decomposition of the error estimate $\eta_{\mathrm{dis}}(u_\ell,\mathcal{T}_\ell)$, using the partition of unity $\sum_{\mathbf{a}\in\mathcal{V}_K}\psi_\ell^{\mathbf{a}}|_K = 1$, the Cauchy–Schwarz inequality, the fact that each simplex has $(d+1)$ vertices, and the extended set of marked vertices $\widetilde{\mathcal{V}}_\ell^\sharp$, we can derive

$$\begin{aligned}\eta^2_{\mathrm{dis}}(u_\ell,\mathcal{M}_\ell^\theta) &= \sum_{K\in\mathcal{M}_\ell^\theta} \|\nabla u_\ell + \boldsymbol{\sigma}_{\ell,\mathrm{dis}}\|_K^2 = \sum_{K\in\mathcal{M}_\ell^\theta} \Big\| \sum_{\mathbf{a}\in\mathcal{V}_{\ell,K}} (\psi_\ell^{\mathbf{a}}\nabla u_\ell + \boldsymbol{\sigma}^{\mathbf{a}}_{\ell,\mathrm{dis}})\Big\|_K^2 \\ &\leq \sum_{K\in\mathcal{M}_\ell^\theta} (d+1) \sum_{\mathbf{a}\in\mathcal{V}_{\ell,K}} \|\psi_\ell^{\mathbf{a}}\nabla u_\ell + \boldsymbol{\sigma}^{\mathbf{a}}_{\ell,\mathrm{dis}}\|_K^2 \\ &= (d+1)\sum_{\mathbf{a}\in\widetilde{\mathcal{V}}_\ell^\sharp} \|\psi_\ell^{\mathbf{a}}\nabla u_\ell + \boldsymbol{\sigma}^{\mathbf{a}}_{\ell,\mathrm{dis}}\|^2_{\omega_\ell^{\mathbf{a}}\cap\omega_\ell} \\ &\leq (d+1)\sum_{\mathbf{a}\in\widetilde{\mathcal{V}}_\ell^\sharp} \|\psi_\ell^{\mathbf{a}}\nabla u_\ell + \boldsymbol{\sigma}^{\mathbf{a}}_{\ell,\mathrm{dis}}\|^2_{\omega_\ell^{\mathbf{a}}}. \end{aligned} \tag{3.87}$$

Furthermore, Proposition 3.7.1 with the constant C_{st}, introduced in Section 3.6.5, applied on each patchwise contribution $\|\psi_\ell^{\mathbf{a}}\nabla u_\ell + \boldsymbol{\sigma}^{\mathbf{a}}_{\ell,\mathrm{dis}}\|^2_{\omega_\ell^{\mathbf{a}}}$ in (3.87), the inequality $a^2+b^2 \leq 2a^2+2b^2$ for $a,b\geq 0$, and the localization of the lower bound $\underline{\eta}^*_{\mathcal{M}_\ell^\sharp}$ in the spirit of (3.17) lead to

$$\begin{aligned}\eta^2_{\mathrm{dis}}(u_\ell,\mathcal{M}_\ell^\theta) &\leq (d+1)C_{\mathrm{st}}^2 \sum_{\mathbf{a}\in\widetilde{\mathcal{V}}_\ell^\sharp} (\|\nabla r^{\mathbf{a},hp}\|_{\omega_\ell^{\mathbf{a}}} + \|\boldsymbol{\sigma}_{\ell,\mathrm{alg}}\|_{\omega_\ell^{\mathbf{a}}})^2 \\ &\leq 2(d+1)C_{\mathrm{st}}^2 \left(\sum_{\mathbf{a}\in\widetilde{\mathcal{V}}_\ell^\sharp} \|\nabla r^{\mathbf{a},hp}\|^2_{\omega_\ell^{\mathbf{a}}} + \sum_{\mathbf{a}\in\widetilde{\mathcal{V}}_\ell^\sharp} \|\boldsymbol{\sigma}_{\ell,\mathrm{alg}}\|^2_{\omega_\ell^{\mathbf{a}}} \right) \\ &\leq 2(d+1)^2 C_{\mathrm{st}}^2 \left(\frac{\sum_{\mathbf{a}\in\widetilde{\mathcal{V}}_\ell^\sharp} \|\nabla r^{\mathbf{a},hp}\|^2_{\omega_\ell^{\mathbf{a}}}}{d+1} + \|\boldsymbol{\sigma}_{\ell,\mathrm{alg}}\|^2_{\omega_\ell^\sharp} \right) \end{aligned}$$

$$\leq 2(d+1)^2 C_{\mathrm{st}}^2 \left(\left(\underline{\eta}^*_{\mathcal{M}_\ell^\sharp} \right)^2 + \|\boldsymbol{\sigma}_{\ell,\mathrm{alg}}\|^2 \right). \tag{3.88}$$

Thus, using (3.88) to bound the ratio $\frac{\left(\underline{\eta}^*_{\mathcal{M}_\ell^\sharp} \right)^2 + \|\boldsymbol{\sigma}_{\ell,\mathrm{alg}}\|^2}{\eta^2_{\mathrm{dis}}(u_\ell, \mathcal{M}_\ell^\theta)}$ in (3.86), we obtain

$$(C^*_{\ell,\mathrm{red}})^2 \leq 1 - \frac{(1-\widetilde{\gamma}_\ell)^2\,\theta^2}{2(d+1)^2 C_{\mathrm{st}}^2} + \widetilde{\gamma}_\ell^2. \tag{3.89}$$

Then, in order to show that $(C^*_{\ell,\mathrm{red}})^2 < 1$, we need to verify $1 - \frac{(1-\widetilde{\gamma}_\ell)^2\ \theta^2}{2(d+1)^2\ (C_{\mathrm{st}})^2} + \widetilde{\gamma}_\ell^2 < 1$, or equivalently

$$\widetilde{\gamma}_\ell^2 < \frac{(1-\widetilde{\gamma}_\ell)^2\,\theta^2}{2(d+1)^2 C_{\mathrm{st}}^2}. \tag{3.90}$$

Taking the square root and rearranging the terms of (3.90) yields (recall that $\widetilde{\gamma}_\ell < 1$)

$$-\frac{(1-\widetilde{\gamma}_\ell)-1}{(1-\widetilde{\gamma}_\ell)} < \frac{\theta}{\sqrt{2}(d+1)C_{\mathrm{st}}}.$$

This can be simplified to

$$\frac{1}{1-\widetilde{\gamma}_\ell} < 1 + \frac{\theta}{\sqrt{2}(d+1)C_{\mathrm{st}}} = \frac{\sqrt{2}(d+1)C_{\mathrm{st}} + \theta}{\sqrt{2}(d+1)C_{\mathrm{st}}},$$

which can be further reorganized in order to obtain the condition (3.70a) on $\widetilde{\gamma}_\ell$

$$\widetilde{\gamma}_\ell < 1 - \frac{\sqrt{2}(d+1)C_{\mathrm{st}}}{\sqrt{2}(d+1)C_{\mathrm{st}} + \theta} = \frac{\theta}{\sqrt{2}(d+1)C_{\mathrm{st}} + \theta} < 1.$$

Therefore, as the parameter $\widetilde{\gamma}_\ell$ is taken such that the condition (3.70a) is satisfied, the right-hand side of (3.89) is indeed strictly lower than 1. Thus, defining the constant $C^*_{\theta,\widetilde{\gamma}_\ell,d,\kappa_{\mathcal{T}},p_{\max}}$ as

$$C^*_{\theta,\widetilde{\gamma}_\ell,d,\kappa_{\mathcal{T}},p_{\max}} := \sqrt{1 - \frac{(1-\widetilde{\gamma}_\ell)^2\,\theta^2}{2(d+1)^2 C_{\mathrm{st}}^2} + \widetilde{\gamma}_\ell^2} < 1$$

finishes the proof. □

The second main result of this chapter, completing Theorem 3.5.1 in the inexact setting, is summarized in the following:

Theorem 3.8.2 (Guaranteed bound on the energy error reduction factor between two inexact solutions)**.** *Let the current inexact approximation u_ℓ be obtained by the adaptive sub-loop of Section 3.6.1 employing the stopping criterion (3.65) with the parameter $\widetilde{\gamma}_\ell$ satisfying (3.70). Let the pair $(\mathcal{T}_{\ell+1}, \mathbf{p}_{\ell+1})$ be obtained by the module* `REFINE` *of Section 3.6.3 and let $\underline{\eta}^*_{\mathcal{M}_\ell^\sharp}$ be the computable*

discrete lower bound defined by (3.68). *Let also* $C^*_{\ell,\mathrm{red}} < 1$ *be given by* (3.82). *Moreover, let* $u_{\ell+1} \in V_{\ell+1}$ *be the inexact finite element approximation on iteration* $(\ell+1)$ *of the adaptive loop prescribed by Scheme 3.2 satisfying the stopping criterion*

$$\eta_{\mathrm{alg}}(u_{\ell+1}, \mathcal{T}_{\ell+1}) \leq \widetilde{\gamma}_{\ell+1}\, \mu(u_{\ell+1}) \tag{3.91}$$

with the parameter $\widetilde{\gamma}_{\ell+1}$ *satisfying the conditions* (3.70) *(with the iteration counter* ℓ *set to* $\ell+1$*). Then the resulting error reduction between the current inexact approximation* u_ℓ *and the next inexact approximation* $u_{\ell+1}$ *verifies*

$$\|\nabla(u_{\ell+1} - u)\| \leq C_{\ell,\mathrm{red}} \|\nabla(u_\ell - u)\| \quad \text{with} \quad 0 \leq C_{\ell,\mathrm{red}} := \frac{C^*_{\ell,\mathrm{red}}}{(1 - \widetilde{\gamma}_{\ell+1})} < 1. \tag{3.92}$$

Proof. Following the proof of (Daniel et al., 2018b, Theorem 5.4), we add and subtract $\nabla u^{\mathrm{ex}}_{\ell+1}$ inside the norm on the left hand side of (3.92). By triangle inequality, we have

$$\|\nabla(u - u_{\ell+1})\| \leq \|\nabla(u - u^{\mathrm{ex}}_{\ell+1})\| + \|\nabla(u^{\mathrm{ex}}_{\ell+1} - u_{\ell+1})\|. \tag{3.93}$$

For bounding the first term, we employ the auxiliary estimate (3.81). We bound the second term of (3.93), i.e. the algebraic error on the iteration $(\ell+1)$, by the algebraic error estimate $\eta_{\mathrm{alg}}(u_{\ell+1}, \mathcal{T}_{\ell+1})$ defined in (3.62b). Afterwards, the stopping criterion (3.91) with the parameter $\widetilde{\gamma}_{\ell+1}$ and the total error lower bound (3.63) lead to

$$\|\nabla(u^{\mathrm{ex}}_{\ell+1} - u_{\ell+1})\| \leq \eta_{\mathrm{alg}}(u_{\ell+1}, \mathcal{T}_{\ell+1}) \leq \widetilde{\gamma}_{\ell+1}\, \mu(u_{\ell+1}) \leq \widetilde{\gamma}_{\ell+1} \|\nabla(u - u_{\ell+1})\|.$$

The error reduction property of (3.92) then follows from

$$\|\nabla(u - u_{\ell+1})\| \leq C^*_{\ell,\mathrm{red}} \|\nabla(u - u_\ell)\| + \widetilde{\gamma}_{\ell+1} \|\nabla(u - u_{\ell+1})\|.$$

In contrast to the proof of (Daniel et al., 2018b, Theorem 5.4), the auxiliary reduction factor $C^*_{\ell,\mathrm{red}}$ is strictly smaller than one and the conditions (3.70) ensure that the reduction factor $C_{\ell,\mathrm{red}}$ is also strictly smaller than one. □

In extension to Corollary 3.5.2, Theorem 3.8.2 implies:

Corollary 3.8.3 (Convergence of the adaptive algorithm with inexact solvers)**.** *Let the assumptions of Theorem 3.8.2 be satisfied. Then*

$$\lim_{\ell \to \infty} \|\nabla(u - u_\ell)\| = 0.$$

3.9 Conclusions and outlook

The contribution of this work is the theoretical study of the adaptive refinement strategies for conforming *hp*-AFEM proposed in Daniel et al. (2018a) for

exact solvers and in Daniel et al. (2018b) for inexact solvers. We described in detail all the necessary modifications of these two methods in order to guarantee strict error reduction on each step of the adaptive loop, and consequent convergence of the resulting adaptive algorithms. The present theoretical results need to be further verified by appropriate numerical experiments. In particular, numerical tests are expected to confirm that the obtained meshes and polynomial degree distributions still lead to asymptotic exponential convergence and that the values of stopping coefficient $\widetilde{\gamma}_\ell$ from (3.65), which needs to satisfy the conditions (3.70), remain reasonable. The further theoretical analysis concerning the computational (quasi-)optimality of the proposed adaptive algorithms will be a subject of some forthcoming work.

Appendix A

Implementation details of *hp*-AFEM

All the numerical experiments in this thesis are performed in MATLAB (2017). Furthermore, for generating the initial meshes only, Matlab's Partial Differential Equation Toolbox™ is used. We use our own implementation of *conforming hp*-AFEM and also arbitrary degree Raviart–Thomas–Nédélec spaces.

The main goal of this Appendix is to enlighten the implementation of the *hp*-finite element method employing test spaces with possibly varying polynomial degree among the mesh elements. In particular, we follow the implementation recommendations proposed by Bangerth and Kayser-Herold (2009). While implementing the *hp*-version of the finite element method one needs to deal with the redundant degrees of freedom in order to maintain the conformity/continuity of the numerical solution. Even though we consider only conforming meshes here, we still cannot avoid the presence of "hanging nodes" in form of the redundant degrees of freedom (we will refer to them as "hanging DOFs") on the interior edges between elements with different polynomial degrees of local basis functions associated with them. There are two widely used approaches how to handle this situation and remain the C^0-continuity of the final approximation:

- adding/removing the redundant degrees of freedom from one of the elements; thus extending/reducing the local approximation spaces
- introducing *constraints* for the "hanging DOFs".

As suggested by Bangerth and Kayser-Herold (2009), we choose the second approach. In our implementation, it is always the element with lower polynomial degree that dominates the one with higher polynomial degree, i.e. the values of the redundant degrees of freedom on the element with higher polynomial degree are constrained using the values of the degrees of freedom on the adjacent lower degree element. In the following, let us take a closer look at a particular case in order to clarify the definition of such constraints.

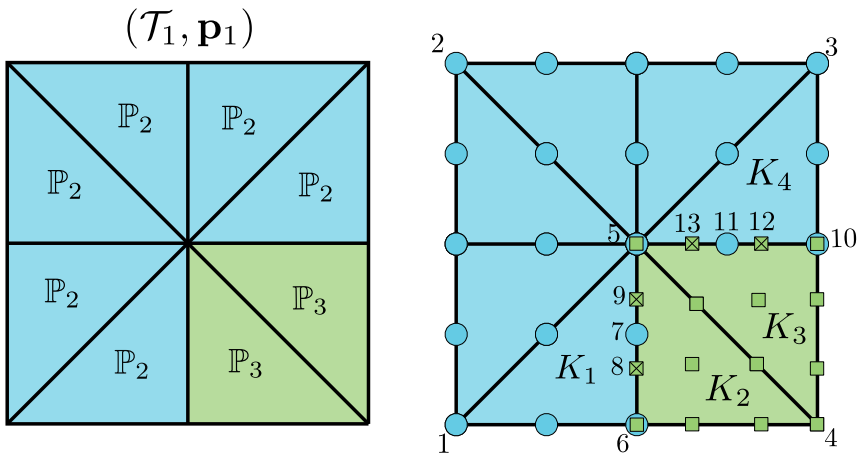

Figure A1: An example mesh $\mathcal{T}_1$ consisting of 8 elements together with the polynomial degree distribution $\mathbf{p}_1$ (*left*) and the distribution of the degrees of freedom with a snippet of their global numbering (*right*), $N_1 = 34$.

The goal is to find a discrete function $u_1 \in V_1$ solving

$$(\nabla u_1, \nabla v_1) = (f, v_1) \qquad \forall v_1 \in V_1, \tag{A.1}$$

with the $H_0^1(\Omega)$-conforming test space V_1 built up on the mesh $\mathcal{T}_1$ and the polynomial degree distribution $\mathbf{p}_1 = \{p_{K_1}, \dots, p_{K_8}\}$, cf. Daniel et al. (2018a), illustrated in Figure A1 (left). Note that the matrix form of problem (A.1) with

$$V_1 := \mathbb{P}_{\mathbf{p}_1}(\mathcal{T}_1) \cap H_0^1(\Omega), \tag{A.2}$$

is not directly accessible due to the complexity of such space.

For the mesh $\mathcal{T}_1$ and polynomial degree distribution $\mathbf{p}_1$ from Figure A1, let N_1 be the total number of global degrees of freedom, see Figure A1 (right) for the particular distribution of the Lagrangian nodes associated with them. The "hanging DOFs", redundant degrees of freedom, are in this case the degrees of freedom 8, 9 (⊠ on K_2) and 12, 13 (⊠ on K_3), lying on the interior edges between elements K_1, K_2 and K_3, K_4. The values of these "hanging DOFs" will be constrained by the degrees of freedom 5, 6, 7 and 5, 10 11 of the adjacent lower degree elements, respectively. In general, for a mesh $\mathcal{T}_\ell$, we consider a degree of freedom to be a "hanging DOF" if its corresponding Lagrangian node lies on an interior edge between elements with different polynomial degrees and it belongs only to the element with the higher polynomial degree.

We consider a set of global (possibly discontinuous) basis functions

$$\widehat{\psi}_1^i \in \mathbb{P}_{\mathbf{p}_1}(\mathcal{T}_1), \qquad i = 1, \dots, N_1, \tag{A.3}$$

constructed by gluing together all the local basis functions from the local spaces $\mathbb{P}_{p_K}(K)$, $K \in \mathcal{T}_1$, corresponding to the same global Lagrangian node. For illustration, in Figure A2 we plot such basis function corresponding to the

interior vertex of the mesh from Figure A1. Note that the space V_1 from (A.2)

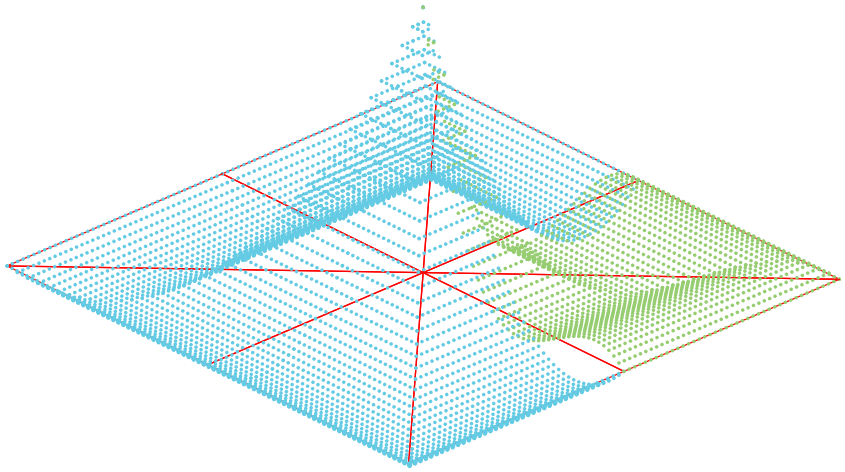

Figure A2: The global basis function $\widehat{\psi}_1^5$ constructed by gluing the local basis functions corresponding to the interior vertex of the mesh from Figure A1; note the discontinuity on the edges between elements with different polynomial degrees.

forms a subspace of the space $\widehat{V}_1 := \mathrm{span}\{\widehat{\psi}_1^1, \ldots, \widehat{\psi}_1^{N_1}\}$. This in turn yields the existence of a vector $\mathrm{U}_1 \in \mathbb{R}^{N_1}$ such that

$$u_1 = \sum_{i=1}^{N_1} (\mathrm{U}_1)_i \, \widehat{\psi}_1^i. \tag{A.4}$$

Let K_1 and K_2 be the elements from Figure A1 (right), note that the corresponding polynomial degrees are $p_{K_1} = 2$ and $p_{K_2} = 3$. The sought function u_1 is by its definition a C^0-continuous function, thus in particular on the edge $e_{K_1K_2} = K_1 \cap K_2$ we require

$$u_1(x)|_{K_1} = u_1(x)|_{K_2} \quad \forall x \in e_{K_1K_2}. \tag{A.5}$$

This gives us the constraints on the values of the coefficient vector U_1 from (A.4) corresponding to the "hanging DOFs". Formulated in the matrix form they read

$$\begin{pmatrix} (\mathrm{U}_1)_8 \\ (\mathrm{U}_1)_9 \end{pmatrix} = \underbrace{\begin{pmatrix} \widehat{\psi}_1^5|_{K_1}(x_8) & \widehat{\psi}_1^6|_{K_1}(x_8) & \widehat{\psi}_1^7|_{K_1}(x_8) \\ \widehat{\psi}_1^5|_{K_1}(x_9) & \widehat{\psi}_1^6|_{K_1}(x_9) & \widehat{\psi}_1^7|_{K_1}(x_9) \end{pmatrix}}_{\mathbb{C}_{K_1 \to K_2}} \begin{pmatrix} (\mathrm{U}_1)_5 \\ (\mathrm{U}_1)_6 \\ (\mathrm{U}_1)_7 \end{pmatrix}, \tag{A.6}$$

where the elements of the local constraint matrix $\mathbb{C}_{K_1 \to K_2}$ are computed by evaluating the restricted global basis functions $\widehat{\psi}_1^5|_{K_1}$, $\widehat{\psi}_1^6|_{K_1}$ and $\widehat{\psi}_1^7|_{K_1}$ in the points x_8, x_9 associated with the "hanging DOFs". Equivalently, the values of

$(\mathrm{U}_1)_{12}$, $(\mathrm{U}_1)_{13}$ are constrained by

$$\begin{pmatrix}(\mathrm{U}_1)_{12}\\(\mathrm{U}_1)_{13}\end{pmatrix} = \underbrace{\begin{pmatrix}\widehat{\psi}_1^5|_{K_4}(x_{12}) & \widehat{\psi}_1^{10}|_{K_4}(x_{12}) & \widehat{\psi}_1^{11}|_{K_4}(x_{12})\\ \widehat{\psi}_1^5|_{K_4}(x_{13}) & \widehat{\psi}_1^{10}|_{K_4}(x_{13}) & \widehat{\psi}_1^{11}|_{K_4}(x_{13})\end{pmatrix}}_{\mathbb{C}_{K_4\to K_3}} \begin{pmatrix}(\mathrm{U}_1)_5\\(\mathrm{U}_1)_{10}\\(\mathrm{U}_1)_{11}\end{pmatrix}. \tag{A.7}$$

Hence, there is exactly one constraint equation per each "hanging DOF".

The above local constraints (A.6)-(A.7) are homogeneous and each can be expressed using the whole vector U_1 as

$$c_i^T \mathrm{U}_1 = 0,$$

where $c_i \in \mathbb{R}^{N_1}$, $i = 1, \dots, N_\mathrm{c}$, is a vector of weights for the i-th constraint corresponding to the respective equation of local system such (A.6) and N_c is a total number of the constrained degrees of freedom (in this particular case $N_\mathrm{c} = 4$). The set of all constraints can be written in a compact form

$$\mathbb{C}_1 \mathrm{U}_1 = 0, \tag{A.8}$$

where the global constrained matrix $\mathbb{C}_1$ is simply defined as

$$\mathbb{C}_1 := \begin{pmatrix}(c_1)^T\\ \vdots \\ (c_{N_\mathrm{c}})^T\end{pmatrix}.$$

Once the constraint matrix $\mathbb{C}_1$ is computed, our original problem (A.1) posed in the space V_1 is equivalent to solving it with the test space $\widehat{V}_1$ defined above and in addition enforcing the constraint (A.8). This can be formulated as an overdetermined system

$$\begin{pmatrix}\widehat{\mathbb{A}}_1\\ \mathbb{C}_1\end{pmatrix} \mathrm{U}_1 = \begin{pmatrix}\widehat{\mathrm{F}}_1\\ 0\end{pmatrix}, \tag{A.9}$$

where $\widehat{\mathbb{A}}_1$ is the stiffness matrix with entries $(\widehat{\mathbb{A}}_1)_{mn} := (\nabla\widehat{\psi}_1^n, \nabla\widehat{\psi}_1^m)$ obtained from (A.1) by employing the basis of space $\widehat{V}_1$ and $\widehat{\mathrm{F}}_1$ is the corresponding right-hand side vector. In general, for more complicated problems, e.g. problems with indefinite operators, this constrained form is not practically suitable; even the existence of the solution is in general unclear. The proper way how to deal with this situation is to apply a *condensation procedure* on the system $\widehat{\mathbb{A}}_1 \mathrm{U}_1 = \widehat{\mathrm{F}}_1$.

Let us define the index set of all degrees of freedom as $\mathcal{I} := \{1, \dots, N_1\}$. Furthermore let $\mathcal{I}_\mathrm{c}$, $\mathcal{I}_\mathrm{u}$ be two disjoint index sets corresponding to constrained (⊠) and unconstrained (●, ■) degrees of freedom respectively, such that $\mathcal{I} = \mathcal{I}_\mathrm{c} \cup \mathcal{I}_\mathrm{u}$. We define the so-called *condensed* shape function for each

unconstrained degree of freedom as

$$\psi_1^i := \widehat{\psi}_1^i + \sum_{j \in \mathcal{I}_c} (c_j)_i \widehat{\psi}_1^j \quad \forall i \in \mathcal{I}_u. \tag{A.10}$$

Note that these new shape functions satisfy the $H_0^1(\Omega)$-conformity requirement, e.g. they are continuous, and they, in fact, form the basis of the space V_1. An illustration of the condensed shape function ψ_1^5 is given in Figure A3.

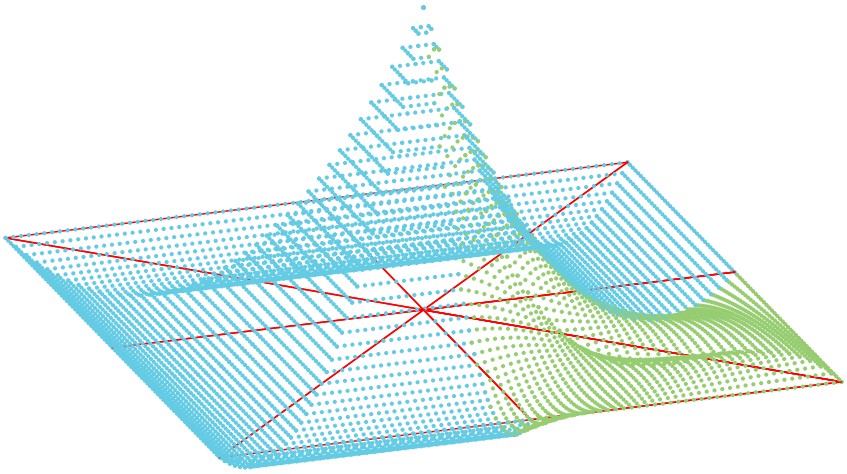

Figure A3: The condensed basis function ψ_1^5 constructed by (A.10).

Using the condensed shape functions from (A.10) we obtain the condensed linear system

$$\mathbb{A}_1 \mathrm{U}_1 = \mathrm{F}_1, \tag{A.11}$$

where

$$(\mathbb{A}_1)_{i,j} := \begin{cases} (\psi_1^j, \psi_1^i), & \text{if } i,j \in \mathcal{I}_u \\ 1, & \text{if } i = j \text{ and } i \in \mathcal{I}_c \\ 0, & \text{otherwise} \end{cases} \tag{A.12a}$$

$$(\mathrm{F}_1)_i := \begin{cases} (f, \psi_1^i), & \text{if } i \in \mathcal{I}_u \\ 0, & \text{if } i \in \mathcal{I}_c. \end{cases} \tag{A.12b}$$

We note that the dimensions of the matrix $\mathbb{A}_1$ and the right-hand side vector F_1 of the condensed system (A.11) remain the same as the dimensions of their counterparts $\widehat{\mathbb{A}}_1$ and $\widehat{\mathrm{F}}_1$ from (A.9). Not reducing the dimension indeed simplifies the algorithm remarkably from an implementation point of view. An example of the structure of the matrices $\mathbb{A}_1$ and $\widehat{\mathbb{A}}_1$ is provided in Figure A4.

The solution of the condensed system (A.11) uniquely determines only the unknowns corresponding to unconstrained degrees of freedom, as the condensation (A.12) implies $(\mathrm{U}_1)_i = 0$, for $i \in \mathcal{I}_c$. Subsequently, the already determined unknowns $(\mathrm{U}_1)_j$, $j \in \mathcal{I}_u$ can be employed in the system (A.8) to obtain the missing values $(\mathrm{U}_1)_i$, $i \in \mathcal{I}_c$, namely we set $(\mathrm{U}_1)_i := -(\mathbb{C}_1 \mathrm{U}_1)_i$,

$i \in \mathcal{I}_c$. Let us also remark that, the condensed forms $\mathbb{A}_1$, F_1 are in practice obtained without an explicit construction of the condensed basis functions defined by (A.10). All what is needed are the entries of their unconstrained equivalents $\widehat{\mathbb{A}}_1$, $\widehat{\mathrm{F}}_1$ which are subsequently combined using the entries of the global constraint matrix $\mathbb{C}_1$.

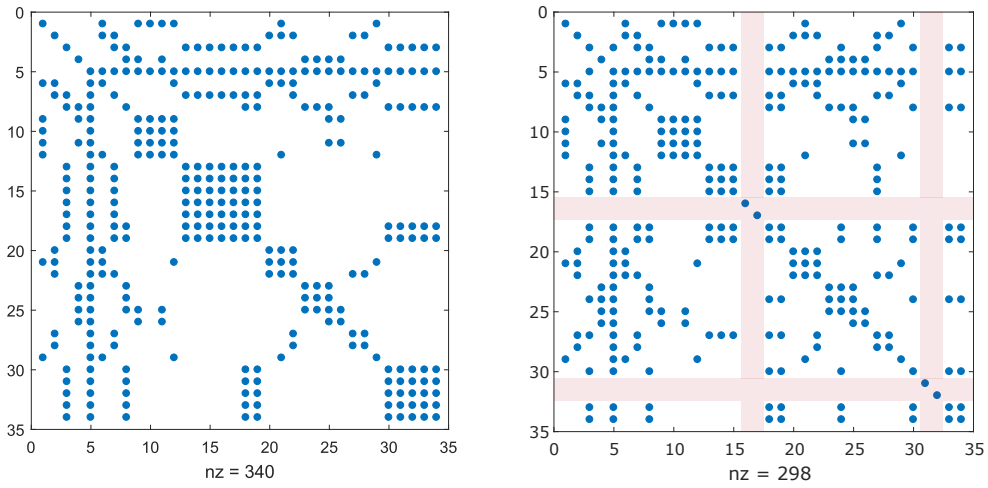

Figure A4: Illustration of the sparsity patterns of the stiffness matrix $\widehat{\mathbb{A}}_1$ (*left*) and the matrix $\mathbb{A}_1$ (*right*) obtained by its condensation via (A.12). Both matrices are computed in the setting prescribed by $(\mathcal{T}_1, \mathbf{p}_1)$ as displayed in the left panel of Figure A1, however, the indexing of degrees of freedom differs from that used in the right panel of Figure A1. Here, the global indices of four "hanging DOFs" are 16,17, 31 and 32 (corresponding lines and columns are highlighted in red).

Finally, the general workflow that we follow while solving the problems of form (A.1) with a mesh $\mathcal{T}_\ell$ and polynomial degree distribution $\mathbf{p}_\ell$ can be summed up in the following steps:

1. Identification of the hanging nodes (setting up the index sets $\mathcal{I}_c$, $\mathcal{I}_u$) on each interior edge between elements assigned with different polynomial degree.

2. Construction of the local constraints of type (A.6)-(A.7) yielding the overall global constraint matrix $\mathbb{C}_\ell$.

3. Assembling of the stiffness matrix $\widehat{\mathbb{A}}_\ell$ and right hand side vector $\widehat{\mathrm{F}}_\ell$ using all basis functions such (A.3).

4. Condensation of the assembled system via (A.12) followed by its resolution with a possibly inexact algebraic solver yielding the values of the unconstrained degrees of freedom only.

5. Computing the values of the constrained degrees of freedom from the constraint equation $\mathbb{C}_\ell \mathrm{U}_\ell = 0$.

Bibliography

S. Adjerid, M. Aiffa, and J. E. Flaherty. Computational methods for singularly perturbed systems. In *Analyzing multiscale phenomena using singular perturbation methods (Baltimore, MD, 1998)*, volume 56 of *Proc. Sympos. Appl. Math.*, pages 47–83. Amer. Math. Soc., Providence, RI, 1999. doi: 10.1090/psapm/056/1718897. URL https://doi.org/10.1090/psapm/056/1718897.

M. Ainsworth. A posteriori error estimation for discontinuous Galerkin finite element approximation. *SIAM J. Numer. Anal.*, 45(4):1777–1798, 2007. doi: 10.1137/060665993. URL http://dx.doi.org/10.1137/060665993.

M. Ainsworth and I. Babuška. Reliable and robust a posteriori error estimation for singularly perturbed reaction-diffusion problems. *SIAM J. Numer. Anal.*, 36(2):331–353, 1999.

M. Ainsworth and J. T. Oden. *A posteriori error estimation in finite element analysis*. Pure and Applied Mathematics (New York). Wiley-Interscience [John Wiley & Sons], New York, 2000.

M. Amrein, J. M. Melenk, and T. P. Wihler. An *hp*-adaptive Newton-Galerkin finite element procedure for semilinear boundary value problems. *Math. Methods Appl. Sci.*, 40(6):1973–1985, 2017.

M. Arioli, E. H. Georgoulis, and D. Loghin. Stopping criteria for adaptive finite element solvers. *SIAM J. Sci. Comput.*, 35(3):A1537–A1559, 2013a. doi: 10.1137/120867421. URL http://dx.doi.org/10.1137/120867421.

M. Arioli, J. Liesen, A. Międlar, and Z. Strakoš. Interplay between discretization and algebraic computation in adaptive numerical solution of elliptic PDE problems. *GAMM-Mitt.*, 36(1):102–129, 2013b. doi: 10.1002/gamm.201310006. URL https://doi.org/10.1002/gamm.201310006.

M. Aurada, M. Feischl, J. Kemetmüller, M. Page, and D. Praetorius. Each $H^{1/2}$-stable projection yields convergence and quasi-optimality of adaptive FEM with inhomogeneous Dirichlet data in $\mathbb{R}^d$. *ESAIM Math. Model. Numer. Anal.*, 47(4):1207–1235, 2013. doi: 10.1051/m2an/2013069. URL https://doi.org/10.1051/m2an/2013069.

I. Babuška and W. C. Rheinboldt. Error estimates for adaptive finite element computations. *SIAM J. Numer. Anal.*, 15(4):736–754, 1978.

I. Babuška and M. Suri. The *h-p* version of the finite element method with quasi-uniform meshes. *RAIRO Modél. Math. Anal. Numér.*, 21(2):199–238, 1987. doi: 10.1051/m2an/1987210201991. URL https://doi.org/10.1051/m2an/1987210201991.

I. Babuška and B. Guo. The *h-p* version of finite element method, part 1: The basic approximation results. *Comp. Mech.*, (1):21–41, 1986a.

I. Babuška and B. Guo. The *h-p* version of finite element method, part 2: General results and application. *Comp. Mech.*, (1):203–220, 1986b.

I. Babuška, B. A. Szabo, and I. N. Katz. The *p*-version of the finite element method. *SIAM J. Numer. Anal.*, 18(3):515–545, 1981. doi: 10.1137/0718033. URL https://doi.org/10.1137/0718033.

W. Bangerth and O. Kayser-Herold. Data structures and requirements for *hp* finite element software. *ACM Trans. Math. Software*, 36(1):Art. 4, 31, 2009. doi: 10.1145/1486525.1486529. URL http://dx.doi.org/10.1145/1486525.1486529.

R. Bank and H. Nguyen. *hp* adaptive finite elements based on derivative recovery and superconvergence. *Computing and Visualization in Science*, 14, 08 2012. doi: 10.1007/s00791-012-0179-7.

R. E. Bank and R. K. Smith. A posteriori error estimates based on hierarchical bases. *SIAM J. Numer. Anal.*, 30(4):921–935, 1993. doi: 10.1137/0730048. URL http://dx.doi.org/10.1137/0730048.

R. E. Bank and A. Weiser. Some a posteriori error estimators for elliptic partial differential equations. *Math. Comp.*, 44(170):283–301, 1985.

R. E. Bank, A. Parsania, and S. Sauter. Saturation estimates for *hp*-finite element methods. *Comput. Vis. Sci.*, 16(5):195–217, 2013. doi: 10.1007/s00791-015-0234-2. URL http://dx.doi.org/10.1007/s00791-015-0234-2.

S. Bartels and C. Carstensen. Each averaging technique yields reliable a posteriori error control in FEM on unstructured grids. II. Higher order FEM. *Math. Comp.*, 71(239):971–994, 2002.

R. Becker. An adaptive finite element method for the Stokes equations including control of the iteration error. In *ENUMATH 97 (Heidelberg)*, pages 609–620. World Sci. Publ., River Edge, NJ, 1998.

R. Becker and S. Mao. Convergence and quasi-optimal complexity of a simple adaptive finite element method. *M2AN Math. Model. Numer. Anal.*, 43(6): 1203–1219, 2009. doi: 10.1051/m2an/2009036. URL https://doi.org/10.1051/m2an/2009036.

R. Becker and R. Rannacher. An optimal control approach to a posteriori error estimation in finite element methods. *Acta Numer.*, 10:1–102, 2001.

R. Becker, C. Johnson, and R. Rannacher. Adaptive error control for multigrid finite element methods. *Computing*, 55(4):271–288, 1995. doi: 10.1007/BF02238483. URL http://dx.doi.org/10.1007/BF02238483.

R. Becker, S. Mao, and Z. Shi. A convergent nonconforming adaptive finite element method with quasi-optimal complexity. *SIAM J. Numer. Anal.*, 47 (6):4639–4659, 2010. doi: 10.1137/070701479. URL https://doi.org/10.1137/070701479.

R. Becker, D. Capatina, and J. Joie. Connections between discontinuous Galerkin and nonconforming finite element methods for the Stokes equations. *Numer. Methods Partial Differential Equations*, 28(3):1013–1041, 2012. doi: 10.1002/num.20671. URL http://dx.doi.org/10.1002/num.20671.

R. Becker, D. Capatina, and R. Luce. Stopping criteria based on locally reconstructed fluxes. In *Numerical mathematics and advanced applications—ENUMATH 2013*, volume 103 of *Lect. Notes Comput. Sci. Eng.*, pages 243–251. Springer, Cham, 2015.

R. Becker, D. Capatina, and R. Luce. Local flux reconstructions for standard finite element methods on triangular meshes. *SIAM J. Numer. Anal.*, 54 (4):2684–2706, 2016. doi: 10.1137/16M1064817. URL https://doi.org/10.1137/16M1064817.

K. S. Bey. *An hp-adaptive discontinuous Galerkin method for hyperbolic conservation laws*. ProQuest LLC, Ann Arbor, MI, 1994. URL http://gateway.proquest.com/openurl?url_ver=Z39.88-2004&rft_val_fmt=info:ofi/fmt:kev:mtx:dissertation&res_dat=xri:pqdiss&rft_dat=xri:pqdiss:9428458. Thesis (Ph.D.)–The University of Texas at Austin.

K. S. Bey, A. Patra, and J. T. Oden. *hp*-version discontinuous Galerkin methods for hyperbolic conservation laws: a parallel adaptive strategy. *Internat. J. Numer. Methods Engrg.*, 38(22):3889–3908, 1995. doi: 10.1002/nme.1620382209. URL https://doi.org/10.1002/nme.1620382209.

P. Binev. Instance optimality for *hp*-type approximation. *Oberwolfach Reports*, 39:14–16, 2013.

P. Binev. Tree approximation for hp-adaptivity. *SIAM J. Numer. Anal.*, 56 (6):3346–3357, 2018. ISSN 0036-1429. doi: 10.1137/18M1175070. URL https://doi.org/10.1137/18M1175070.

P. Binev, W. Dahmen, and R. DeVore. Adaptive finite element methods with convergence rates. *Numer. Math.*, 97(2):219–268, 2004. doi: 10.1007/s00211-003-0492-7. URL http://dx.doi.org/10.1007/s00211-003-0492-7.

D. Braess and J. Schöberl. Equilibrated residual error estimator for edge elements. *Math. Comp.*, 77(262):651–672, 2008. doi: 10.1090/S0025-5718-07-02080-7. URL http://dx.doi.org/10.1090/S0025-5718-07-02080-7.

D. Braess, V. Pillwein, and J. Schöberl. Equilibrated residual error estimates are p-robust. *Comput. Methods Appl. Mech. Engrg.*, 198(13-14):1189–1197, 2009.

J. H. Bramble and J. E. Pasciak. New estimates for multilevel algorithms including the V-cycle. *Math. Comp.*, 60(202):447–471, 1993. doi: 10.2307/2153097. URL https://doi.org/10.2307/2153097.

S. C. Brenner and L. R. Scott. *The mathematical theory of finite element methods*, volume 15 of *Texts in Applied Mathematics*. Springer, New York, third edition, 2008. doi: 10.1007/978-0-387-75934-0. URL http://dx.doi.org/10.1007/978-0-387-75934-0.

F. Brezzi and M. Fortin. *Mixed and hybrid finite element methods*, volume 15 of *Springer Series in Computational Mathematics*. Springer-Verlag, New York, 1991. doi: 10.1007/978-1-4612-3172-1. URL http://dx.doi.org/10.1007/978-1-4612-3172-1.

M. Bürg and W. Dörfler. Convergence of an adaptive hp finite element strategy in higher space-dimensions. *Appl. Numer. Math.*, 61(11):1132–1146, 2011. doi: 10.1016/j.apnum.2011.07.008. URL http://dx.doi.org/10.1016/j.apnum.2011.07.008.

C. Canuto, R. H. Nochetto, R. Stevenson, and M. Verani. Convergence and optimality of **hp-AFEM**. *Numer. Math.*, 135(4):1073–1119, 2017a. doi: 10.1007/s00211-016-0826-x. URL https://doi.org/10.1007/s00211-016-0826-x.

C. Canuto, R. H. Nochetto, R. Stevenson, and M. Verani. On p-robust saturation for hp-AFEM. *Comput. Math. Appl.*, 73(9):2004–2022, 2017b. URL https://doi.org/10.1016/j.camwa.2017.02.035.

C. Carstensen and S. Bartels. Each averaging technique yields reliable a posteriori error control in FEM on unstructured grids. I. Low order conforming, nonconforming, and mixed FEM. *Math. Comp.*, 71(239):945–969, 2002.

C. Carstensen and J. Gedicke. An adaptive finite element eigenvalue solver of asymptotic quasi-optimal computational complexity. *SIAM J. Numer. Anal.*, 50(3):1029–1057, 2012. doi: 10.1137/090769430. URL https://doi.org/10.1137/090769430.

C. Carstensen, M. Feischl, M. Page, and D. Praetorius. Axioms of adaptivity. *Comput. Math. Appl.*, 67(6):1195–1253, 2014. doi: 10.1016/j.camwa.2013.12.003. URL http://dx.doi.org/10.1016/j.camwa.2013.12.003.

J. M. Cascón and R. H. Nochetto. Quasioptimal cardinality of AFEM driven by nonresidual estimators. *IMA J. Numer. Anal.*, 32(1):1–29, 2012. doi: 10.1093/imanum/drr014. URL http://dx.doi.org/10.1093/imanum/drr014.

J. M. Cascón, C. Kreuzer, R. H. Nochetto, and K. G. Siebert. Quasi-optimal convergence rate for an adaptive finite element method. *SIAM J. Numer. Anal.*, 46(5):2524–2550, 2008. doi: 10.1137/07069047X. URL http://dx.doi.org/10.1137/07069047X.

P. G. Ciarlet. *The Finite Element Method for Elliptic Problems*, volume 4 of *Studies in Mathematics and its Applications*. North-Holland, Amsterdam, 1978.

S. Cochez-Dhondt and S. Nicaise. Equilibrated error estimators for discontinuous Galerkin methods. *Numer. Methods Partial Differential Equations*, 24 (5):1236–1252, 2008.

A. Cohen, R. DeVore, and R. H. Nochetto. Convergence rates for AFEM with H^{-1} data. *Found. Comput. Math.*, 12(5):671–718, 2012. doi: 10.1007/s10208-012-9120-1. URL https://doi.org/10.1007/s10208-012-9120-1.

R. Courant. Variational methods for the solution of problems of equilibrium and vibrations. *Bull. Amer. Math. Soc.*, 49:1–23, 1943. doi: 10.1090/S0002-9904-1943-07818-4. URL https://doi.org/10.1090/S0002-9904-1943-07818-4.

E. Creusé and S. Nicaise. A posteriori error estimations of a coupled mixed and standard Galerkin method for second order operators. *J. Comput. Appl. Math.*, 213(1):35–55, 2008. doi: 10.1016/j.cam.2006.12.027. URL http://dx.doi.org/10.1016/j.cam.2006.12.027.

E. Creusé and S. Nicaise. A posteriori error estimator based on gradient recovery by averaging for discontinuous Galerkin methods. *J. Comput. Appl. Math.*, 234(10):2903–2915, 2010. doi: 10.1016/j.cam.2010.03.027. URL https://doi.org/10.1016/j.cam.2010.03.027.

E. Creusé and S. Nicaise. *A posteriori* error estimator based on gradient recovery by averaging for convection-diffusion-reaction problems approximated by discontinuous Galerkin methods. *IMA J. Numer. Anal.*, 33(1): 212–241, 2013. doi: 10.1093/imanum/drr052. URL https://doi.org/10.1093/imanum/drr052.

E. Creusé, S. Nicaise, and E. Verhille. Robust equilibrated a posteriori error estimators for the Reissner-Mindlin system. *Calcolo*, 48(4):307–335, 2011. doi: 10.1007/s10092-011-0042-0. URL https://doi.org/10.1007/s10092-011-0042-0.

E. Creusé, S. Nicaise, and R. Tittarelli. A guaranteed equilibrated error estimator for the $\mathbf{A} - \varphi$ and $\mathbf{T} - \Omega$ magnetodynamic harmonic formulations of the Maxwell system. *IMA J. Numer. Anal.*, 37(2):750–773, 2017. doi: 10.1093/imanum/drw026. URL https://doi.org/10.1093/imanum/drw026.

P. Daniel and M. Vohralík. Convergence of adaptive *hp*-refinement strategies with computable guaranteed bound on the error reduction factor. In preparation, 2018.

P. Daniel, A. Ern, I. Smears, and M. Vohralík. An adaptive *hp*-refinement strategy with computable guaranteed bound on the error reduction factor. *Computers and Mathematics with Applications*, 76(5):967–983, 2018a. doi: https://doi.org/10.1016/j.camwa.2018.05.034. URL http://www.sciencedirect.com/science/article/pii/S0898122118303109.

P. Daniel, A. Ern, and M. Vohralík. An adaptive *hp*-refinement strategy with inexact solvers and computable guaranteed bound on the error reduction factor. HAL preprint 01931448, 2018b. URL https://hal.inria.fr/hal-01931448.

E. Dari, R. Durán, C. Padra, and V. Vampa. A posteriori error estimators for nonconforming finite element methods. *RAIRO Modél. Math. Anal. Numér.*, 30(4):385–400, 1996.

L. Demkowicz. *Computing with hp-adaptive finite elements. Vol. 1.* Chapman & Hall/CRC Applied Mathematics and Nonlinear Science Series. Chapman & Hall/CRC, Boca Raton, FL, 2007. doi: 10.1201/9781420011692. URL https://doi.org/10.1201/9781420011692. One and two dimensional elliptic and Maxwell problems, With 1 CD-ROM (UNIX).

L. Demkowicz, W. Rachowicz, and P. Devloo. A fully automatic *hp*-adaptivity. In *Proceedings of the Fifth International Conference on Spectral and High Order Methods (ICOSAHOM-01) (Uppsala)*, volume 17, pages 117–142, 2002. doi: 10.1023/A:1015192312705. URL http://dx.doi.org/10.1023/A:1015192312705.

P. Destuynder and B. Métivet. Explicit error bounds in a conforming finite element method. *Math. Comp.*, 68(228):1379–1396, 1999. doi: 10.1090/S0025-5718-99-01093-5. URL http://dx.doi.org/10.1090/S0025-5718-99-01093-5.

P. Deuflhard, P. Leinen, and H. Yserentant. Concepts of an adaptive hierarchical finite element code. *IMPACT of Computing in Science and Engineering*, 1(1):3 – 35, 1989. doi: https://doi.org/10.1016/0899-8248(89)90018-9. URL http://www.sciencedirect.com/science/article/pii/0899824889900189.

A. R. Díaz, N. Kikuchi, and J. E. Taylor. A method of grid optimization for finite element methods. *Comput. Methods Appl. Mech. Engrg.*, 41(1):29–45, 1983. doi: 10.1016/0045-7825(83)90051-8. URL https://doi.org/10.1016/0045-7825(83)90051-8.

L. Diening, C. Kreuzer, and R. Stevenson. Instance optimality of the adaptive maximum strategy. *Found. Comput. Math.*, 16(1):33–68, 2016. doi: 10.1007/s10208-014-9236-6. URL https://doi.org/10.1007/s10208-014-9236-6.

L. Diening, C. Kreuzer, I. Smears, and M. Vohralík. Equilibrated flux a posteriori estimates for the p-Laplace problem. In preparation, 2019.

V. Dolejší, A. Ern, and M. Vohralík. *hp*-adaptation driven by polynomial-degree-robust a posteriori error estimates for elliptic problems. *SIAM J. Sci. Comput.*, 38(5):A3220–A3246, 2016. doi: 10.1137/15M1026687. URL http://dx.doi.org/10.1137/15M1026687.

W. Dörfler. A convergent adaptive algorithm for Poisson's equation. *SIAM J. Numer. Anal.*, 33(3):1106–1124, 1996. doi: 10.1137/0733054. URL http://dx.doi.org/10.1137/0733054.

W. Dörfler and V. Heuveline. Convergence of an adaptive *hp* finite element strategy in one space dimension. *Appl. Numer. Math.*, 57(10):1108–1124, 2007. doi: 10.1016/j.apnum.2006.10.003. URL http://dx.doi.org/10.1016/j.apnum.2006.10.003.

R. Durán and R. Rodríguez. On the asymptotic exactness of Bank-Weiser's estimator. *Numer. Math.*, 62(3):297–303, 1992. doi: 10.1007/BF01396231. URL https://doi.org/10.1007/BF01396231.

T. Eibner and J. M. Melenk. An adaptive strategy for *hp*-FEM based on testing for analyticity. *Comput. Mech.*, 39(5):575–595, 2007. doi: 10.1007/s00466-006-0107-0. URL http://dx.doi.org/10.1007/s00466-006-0107-0.

A. Ern and J.-L. Guermond. *Theory and practice of finite elements*, volume 159 of *Applied Mathematical Sciences*. Springer-Verlag, New York, 2004. doi: 10.1007/978-1-4757-4355-5. URL http://dx.doi.org/10.1007/978-1-4757-4355-5.

A. Ern and M. Vohralík. Adaptive inexact Newton methods with a posteriori stopping criteria for nonlinear diffusion PDEs. *SIAM J. Sci. Comput.*, 35 (4):A1761–A1791, 2013. doi: 10.1137/120896918. URL http://dx.doi.org/10.1137/120896918.

A. Ern and M. Vohralík. Polynomial-degree-robust a posteriori estimates in a unified setting for conforming, nonconforming, discontinuous Galerkin, and mixed discretizations. *SIAM J. Numer. Anal.*, 53(2):1058–1081, 2015. doi: 10.1137/130950100. URL http://dx.doi.org/10.1137/130950100.

A. Ern and M. Vohralík. Stable broken H^1 and $\mathbf{H}(\mathrm{div})$ polynomial extensions for polynomial-degree-robust potential and flux reconstruction in three space dimensions. HAL Preprint 01422204, 2016.

T. Fankhauser, T. P. Wihler, and M. Wirz. The *hp*-adaptive FEM based on continuous Sobolev embeddings: isotropic refinements. *Comput. Math. Appl.*, 67(4):854–868, 2014. doi: 10.1016/j.camwa.2013.05.024. URL https://doi.org/10.1016/j.camwa.2013.05.024.

M. Feischl, M. Page, and D. Praetorius. Convergence and quasi-optimality of adaptive FEM with inhomogeneous Dirichlet data. *J. Comput. Appl. Math.*, 255:481–501, 2014. doi: 10.1016/j.cam.2013.06.009. URL https://doi.org/10.1016/j.cam.2013.06.009.

T. Führer, A. Haberl, D. Praetorius, and S. Schimanko. Adaptive BEM with inexact PCG solver yields almost optimal computational costs. *Numerische Mathematik*, Nov 2018. doi: 10.1007/s00211-018-1011-1. URL https://doi.org/10.1007/s00211-018-1011-1.

G. Gantner, A. Haberl, D. Praetorius, and B. Stiftner. Rate optimal adaptive FEM with inexact solver for nonlinear operators. *IMA J. Numer. Anal.*, 2017. doi: 10.1093/imanum/drx050. DOI 10.1093/imanum/drx050.

W. Gui and I. Babuška. The h, p and h-p versions of the finite element method in 1 dimension. III. The adaptive h-p version. *Numer. Math.*, 49 (6):659–683, 1986a. doi: 10.1007/BF01389735. URL http://dx.doi.org/10.1007/BF01389735.

W. Gui and I. Babuška. The h, p and h-p versions of the finite element method in 1 dimension. II. The error analysis of the h- and h-p versions. *Numer. Math.*, 49(6):613–657, 1986b. doi: 10.1007/BF01389734. URL http://dx.doi.org/10.1007/BF01389734.

W. Hackbusch. *Multigrid methods and applications*, volume 4 of *Springer Series in Computational Mathematics*. Springer-Verlag, Berlin, 1985.

M. Holst, R. Szypowski, and Y. Zhu. Adaptive finite element methods with inexact solvers for the nonlinear Poisson-Boltzmann equation. In *Domain decomposition methods in science and engineering XX*, volume 91 of *Lect. Notes Comput. Sci. Eng.*, pages 167–174. Springer, Heidelberg, 2013. doi: 10.1007/978-3-642-35275-1. URL https://doi.org/10.1007/978-3-642-35275-1.

P. Houston and E. Süli. A note on the design of *hp*-adaptive finite element methods for elliptic partial differential equations. *Comput. Methods Appl. Mech. Engrg.*, 194(2-5):229–243, 2005. doi: 10.1016/j.cma.2004.04.009. URL http://dx.doi.org/10.1016/j.cma.2004.04.009.

P. Houston and T. P. Wihler. An *hp*-adaptive Newton-discontinuous-Galerkin finite element approach for semilinear elliptic boundary value problems. *Math. Comp.*, 87(314):2641–2674, 2018. doi: 10.1090/mcom/3308. URL https://doi.org/10.1090/mcom/3308.

P. Houston, B. Senior, and E. Süli. Sobolev regularity estimation for *hp*-adaptive finite element methods. In *Numerical mathematics and advanced applications*, pages 631–656. Springer Italia, Milan, 2003.

P. Jiránek, Z. Strakoš, and M. Vohralík. A posteriori error estimates including algebraic error and stopping criteria for iterative solvers. *SIAM J. Sci. Comput.*, 32(3):1567–1590, 2010. doi: 10.1137/08073706X. URL http://dx.doi.org/10.1137/08073706X.

D. W. Kelly. The self-equilibration of residuals and complementary a posteriori error estimates in the finite element method. *Internat. J. Numer. Methods Engrg.*, 20(8):1491–1506, 1984. doi: 10.1002/nme.1620200811. URL http://dx.doi.org/10.1002/nme.1620200811.

K.-Y. Kim. A posteriori error analysis for locally conservative mixed methods. *Math. Comp.*, 76(257):43–66, 2007a.

K.-Y. Kim. A posteriori error estimators for locally conservative methods of nonlinear elliptic problems. *Appl. Numer. Math.*, 57(9):1065–1080, 2007b. doi: 10.1016/j.apnum.2006.09.010. URL http://dx.doi.org/10.1016/j.apnum.2006.09.010.

C. Kreuzer and K. G. Siebert. Decay rates of adaptive finite elements with Dörfler marking. *Numer. Math.*, 117(4):679–716, 2011. doi: 10.1007/s00211-010-0324-5. URL http://dx.doi.org/10.1007/s00211-010-0324-5.

P. Ladevèze. *Comparaison de modèles de milieux continus*. Ph.D. thesis, Université Pierre et Marie Curie (Paris 6), 1975.

R. Luce and B. I. Wohlmuth. A local a posteriori error estimator based on equilibrated fluxes. *SIAM J. Numer. Anal.*, 42(4):1394–1414, 2004. doi: 10.1137/S0036142903433790. URL http://dx.doi.org/10.1137/S0036142903433790.

J. A. Mackenzie and M. L. Robertson. A moving mesh method for the solution of the one-dimensional phase-field equations. *J. Comput. Phys.*, 181(2):526–544, 2002. doi: 10.1006/jcph.2002.7140. URL https://doi.org/10.1006/jcph.2002.7140.

MATLAB. *Version 9.2.0.556344 (R2017a)*. The MathWorks Inc., Natick, Massachusetts, United States, 2017.

C. Mavriplis. Adaptive mesh strategies for the spectral element method. *Comput. Methods Appl. Mech. Engrg.*, 116(1-4):77–86, 1994. doi: 10.1016/S0045-7825(94)80010-3. URL https://doi.org/10.1016/S0045-7825(94)80010-3. ICOSAHOM'92 (Montpellier, 1992).

D. Meidner, R. Rannacher, and J. Vihharev. Goal-oriented error control of the iterative solution of finite element equations. *J. Numer. Math.*, 17(2):143–172, 2009. doi: 10.1515/JNUM.2009.009. URL http://dx.doi.org/10.1515/JNUM.2009.009.

K. Mekchay and R. Nochetto. Convergence of adaptive finite element methods for general second order linear elliptic PDEs. *SIAM Journal on Numerical Analysis*, 43(5):1803–1827, 2005. doi: 10.1137/04060929X. URL https://doi.org/10.1137/04060929X.

J. M. Melenk and B. I. Wohlmuth. On residual-based a posteriori error estimation in *hp*-FEM. *Adv. Comput. Math.*, 15(1-4):311–331 (2002), 2001. A posteriori error estimation and adaptive computational methods.

W. F. Mitchell. A comparison of adaptive refinement techniques for elliptic problems. *ACM Trans. Math. Software*, 15(4):326–347 (1990), 1989. doi: 10.1145/76909.76912. URL http://dx.doi.org/10.1145/76909.76912.

W. F. Mitchell and M. A. McClain. A comparison of *hp*-adaptive strategies for elliptic partial differential equations (long version). *NISTIR 7824, National Institute of Standards and Technology*, 2011. URL https://math.nist.gov/~WMitchell/papers/nistir7824.pdf.

W. F. Mitchell and M. A. McClain. A comparison of *hp*-adaptive strategies for elliptic partial differential equations. *ACM Trans. Math. Software*, 41(1):Art. 2, 39, 2014. doi: 10.1145/2629459. URL http://dx.doi.org/10.1145/2629459.

P. Morin, R. H. Nochetto, and K. G. Siebert. Data oscillation and convergence of adaptive FEM. *SIAM J. Numer. Anal.*, 38(2):466–488, 2000. doi: 10.1137/S0036142999360044. URL http://dx.doi.org/10.1137/S0036142999360044.

P. Morin, R. H. Nochetto, and K. G. Siebert. Convergence of adaptive finite element methods. *SIAM Rev.*, 44(4):631–658 (2003), 2002. doi: 10.1137/S0036144502409093. URL http://dx.doi.org/10.1137/S0036144502409093. Revised reprint of "Data oscillation and convergence of adaptive FEM" [SIAM J. Numer. Anal. 38 (2000), no. 2, 466–488; MR1770058 (2001g:65157)].

P. Morin, R. H. Nochetto, and K. G. Siebert. Local problems on stars: a posteriori error estimators, convergence, and performance. *Math. Comp.*, 72(243):1067–1097, 2003. doi: 10.1090/S0025-5718-02-01463-1. URL http://dx.doi.org/10.1090/S0025-5718-02-01463-1.

P. Morin, K. G. Siebert, and A. Veeser. A basic convergence result for conforming adaptive finite elements. *Math. Models Methods Appl. Sci.*, 18(5):707–737, 2008. doi: 10.1142/S0218202508002838. URL https://doi.org/10.1142/S0218202508002838.

P. Neittaanmäki and S. Repin. *Reliable methods for computer simulation*, volume 33 of *Studies in Mathematics and its Applications*. Elsevier Science B.V., Amsterdam, 2004. Error control and a posteriori estimates.

R. H. Nochetto, K. G. Siebert, and A. Veeser. Theory of adaptive finite element methods: an introduction. In *Multiscale, nonlinear and adaptive approximation*, pages 409–542. Springer, Berlin, 2009. doi: 10.1007/978-3-642-03413-8_12. URL http://dx.doi.org/10.1007/978-3-642-03413-8_12.

A. Novotný, J. T. Pereira, E. Fancello, and C. de Barcellos. A fast *hp* adaptive finite element mesh design. *Computer Methods in Applied Mechanics and Engineering*, 190(1):133 – 148, 2000. doi: https://doi.org/10.1016/S0045-7825(99)00418-1. URL http://www.sciencedirect.com/science/article/pii/S0045782599004181.

J. Oden, A. Patra, and Y. Feng. An *hp* adaptive strategy. In *Adaptive, Multilevel, and Hierarchical Computational Strategies*, volume 157, pages 23–46. Publ by ASME, 12 1992.

J. Papež, U. Rüde, M. Vohralík, and B. Wohlmuth. Sharp algebraic and total a posteriori error bounds for h and p finite elements via a multilevel approach. HAL preprint 01662944, 2017. URL https://hal.inria.fr/hal-01662944.

J. Papež, Z. Strakoš, and M. Vohralík. Estimating and localizing the algebraic and total numerical errors using flux reconstructions. *Numer. Math.*, 138 (3):681–721, 2018. doi: 10.1007/s00211-017-0915-5. URL https://doi.org/10.1007/s00211-017-0915-5.

A. T. Patera and E. M. Rønquist. A general output bound result: application to discretization and iteration error estimation and control. *Math. Models Methods Appl. Sci.*, 11(4):685–712, 2001. doi: 10.1142/S0218202501001057. URL http://dx.doi.org/10.1142/S0218202501001057.

A. Patra and A. Gupta. A systematic strategy for simultaneous adaptive *hp* finite element mesh modification using nonlinear programming. *Computer Methods in Applied Mechanics and Engineering*, 190(29):3797 – 3818, 2001. doi: https://doi.org/10.1016/S0045-7825(00)00298-X. URL http://www.sciencedirect.com/science/article/pii/S004578250000298X.

W. Prager and J. L. Synge. Approximations in elasticity based on the concept of function space. *Quart. Appl. Math.*, 5:241–269, 1947.

A. Quarteroni and A. Valli. *Numerical approximation of partial differential equations*, volume 23 of *Springer Series in Computational Mathematics*. Springer-Verlag, Berlin, 1994. ISBN 3-540-57111-6.

W. Rachowicz, J. T. Oden, and L. Demkowicz. Toward a universal *h-p* adaptive finite element strategy. III. Design of *h-p* meshes. *Comput. Methods Appl. Mech. Engrg.*, 77(1-2):181–212, 1989. doi: 10.1016/0045-7825(89)90131-X. URL https://doi.org/10.1016/0045-7825(89)90131-X.

S. I. Repin. Two-sided estimates of deviation from exact solutions of uniformly elliptic equations. In *Proceedings of the St. Petersburg Mathematical Society, Vol. IX*, volume 209 of *Amer. Math. Soc. Transl. Ser. 2*, pages 143–171. Amer. Math. Soc., Providence, RI, 2003. doi: 10.1090/trans2/209/06. URL https://doi.org/10.1090/trans2/209/06.

S. I. Repin. *A posteriori estimates for partial differential equations*, volume 4 of *Radon Series on Computational and Applied Mathematics*. Walter de Gruyter GmbH & Co. KG, Berlin, 2008.

V. Rey, C. Rey, and P. Gosselet. A strict error bound with separated contributions of the discretization and of the iterative solver in non-overlapping domain decomposition methods. *Comput. Methods Appl. Mech. Engrg.*, 270: 293–303, 2014. doi: 10.1016/j.cma.2013.12.001. URL http://dx.doi.org/10.1016/j.cma.2013.12.001.

J. E. Roberts and J.-M. Thomas. Mixed and hybrid methods. In *Handbook of Numerical Analysis, Vol. II*, pages 523–639. North-Holland, Amsterdam, 1991.

A. Schmidt and K. G. Siebert. A posteriori estimators for the *h-p* version of the finite element method in 1D. *Appl. Numer. Math.*, 35(1):43–66, 2000. doi: 10.1016/S0168-9274(99)00046-X. URL https://doi.org/10.1016/S0168-9274(99)00046-X.

C. Schwab. *p- and hp-finite element methods*. Numerical Mathematics and Scientific Computation. The Clarendon Press, Oxford University Press, New York, 1998. Theory and applications in solid and fluid mechanics.

E. G. Sewell. *Automatic generation of triangulations for piecewise polynomial approximation*. ProQuest LLC, Ann Arbor, MI, 1972. Thesis (Ph.D.)–Purdue University.

P. Šolín and L. Demkowicz. Goal-oriented *hp*-adaptivity for elliptic problems. *Comput. Methods Appl. Mech. Engrg.*, 193(6-8):449–468, 2004. doi: 10.1016/j.cma.2003.09.015. URL http://dx.doi.org/10.1016/j.cma.2003.09.015.

R. Stevenson. An optimal adaptive finite element method. *SIAM J. Numer. Anal.*, 42(5):2188–2217, 2005a. doi: 10.1137/S0036142903425082. URL http://dx.doi.org/10.1137/S0036142903425082.

R. Stevenson. Optimality of a standard adaptive finite element method. *Found. Comput. Math.*, 7(2):245–269, 2007. doi: 10.1007/s10208-005-0183-0. URL http://dx.doi.org/10.1007/s10208-005-0183-0.

R. P. Stevenson. The uniform saturation property for a singularly perturbed reaction-diffusion equation. *Numer. Math.*, 101(2):355–379, 2005b. doi: 10.1007/s00211-005-0606-5. URL https://doi.org/10.1007/s00211-005-0606-5.

E. Süli, P. Houston, and C. Schwab. *hp*-finite element methods for hyperbolic problems. In *The mathematics of finite elements and applications, X, MAFELAP 1999 (Uxbridge)*, pages 143–162. Elsevier, Oxford, 2000. doi: 10.1016/B978-008043568-8/50008-0. URL http://dx.doi.org/10.1016/B978-008043568-8/50008-0.

B. Szabó and I. Babuška. *Finite element analysis*. A Wiley-Interscience Publication. John Wiley & Sons Inc., New York, 1991.

U. Trottenberg, C. W. Oosterlee, and A. Schüller. *Multigrid*. Academic Press, Inc., San Diego, CA, 2001. With contributions by A. Brandt, P. Oswald and K. Stüben.

R. Verfürth. *A posteriori error estimation techniques for finite element methods*. Numerical Mathematics and Scientific Computation. Oxford University Press, Oxford, 2013. doi: 10.1093/acprof:oso/9780199679423.001.

0001. URL http://dx.doi.org/10.1093/acprof:oso/9780199679423.001.0001.

M. Vohralík. Unified primal formulation-based a priori and a posteriori error analysis of mixed finite element methods. *Math. Comp.*, 79(272):2001–2032, 2010. doi: 10.1090/S0025-5718-2010-02375-0. URL http://dx.doi.org/10.1090/S0025-5718-2010-02375-0.

T. P. Wihler. An *hp*-adaptive strategy based on continuous Sobolev embeddings. *J. Comput. Appl. Math.*, 235(8):2731–2739, 2011. doi: 10.1016/j.cam.2010.11.023. URL https://doi.org/10.1016/j.cam.2010.11.023.

H. Wu and Z. Chen. Uniform convergence of multigrid V-cycle on adaptively refined finite element meshes for second order elliptic problems. *Sci. China Ser. A*, 49(10):1405–1429, 2006. doi: 10.1007/s11425-006-2005-5. URL http://dx.doi.org/10.1007/s11425-006-2005-5.

O. C. Zienkiewicz and J. Z. Zhu. A simple error estimator and adaptive procedure for practical engineering analysis. *Internat. J. Numer. Methods Engrg.*, 24(2):337–357, 1987.

O. C. Zienkiewicz and J. Z. Zhu. Adaptivity and mesh generation. *International Journal for Numerical Methods in Engineering*, 32(4):783–810, 1991. doi: 10.1002/nme.1620320409. URL https://onlinelibrary.wiley.com/doi/abs/10.1002/nme.1620320409.